PNC TJ201 84-09TR

NOT FOR PUBLICATION

分 置

Inpile Experiments on Fission Product Behavior in Sodium Loop Using FPL-II

March, 1985

POWER REACTOR AND NUCLEAR FUEL DEVELOPMENT CORPORATION

:e

[illegible] reactor

and Nuclear Fuel Development Corporation.

Not for publication
PNC SJ 201 84-09 TR
March , 1985

Inpile Experiments on Fission Product Behavior in Sodium Loop Using FPL-II

Authors: Takuhiko SAKAI** Seietsu HARA** Shigeo SUMIYOSHI**
Kiyoshi ONO** Norihiko HANDA*** Nobuyoshi MIYAJI**
Editor : Kazuo HAGA*

Abstract

Inpile experiments have been carried out using the Fission Product Behavior Test Loop (FPL-II) to study the behavior of fission products released from failed fuel in a primary cooling system of LMFBR.

FPL-II was installed in the Toshiba Training Reactor (TTR) at the Toshiba R&D Center. In an inpile plug, 100 grams of uranium dioxide fuel (20% enriched) was irradiated in flowing sodium at an average thermal neutron flux of 7×10^9 n/cm^2/sec. The fuel consists of numerous small sintered spheres with an about 0.5 mm diameter, held in a stainless steel basket. The total fuel surface directly touching the sodium is about 1000 cm^2. Fission products, released from the fuel surface to the coolant by recoil during neutron irradiation, were transported by the flowing sodium through a delay line made of a stainless steel tube (SUS 304). The dimension of the delay line piping is about 25 m long and 9.4 mm inner diameter.

The deposition distribution of non-volatile fission products was measured with gamma ray detectors along the delay line during irradiation and after sodium drainage. Deposition behavior for several non-volatile fission products, such as Sr, Y, Zr, Nb, Ba and La, were as follows:

---

* FBR Project, Power Reactor and Nuclear Fuel Development Corporation.
** Research and Development Center, Toshiba Corporation.
*** Nuclear Energy Group, Toshiba Corporation.

1) The deposition of Sr nuclides is very rapid and irreversible. The deposition rate constants are obtained for Sr-92, Sr-93 and Sr-94 by analyzing the deposition distribution patterns. The activation energy for the deposition process was found to be -13±1 (KJ/g-atom). It is concluded that the Sr deposition rate on a stainless steel surface is controlled by the Sr nuclide diffusion through the boundary layer.

2) The deposition rate of Y nuclides is similar to that of Sr between 200 and 500°C sodium temperature.

3) The deposition rate of Zr nuclides is smaller than the Sr deposition at 500°C sodium temperature and shows no dependence on the sodium temperature between 200 and 500°C.

4) The deposition rate of Ba nuclides is almost identical with that of Sr at 400°C sodium temperature, but the temperature dependence is smaller than Sr.

5) The deposition rate of La nuclides is similar to that of Ba between 350 and 500°C sodium temperature.

6) Nb nuclides show no deposition behavior in sodium.

The k factor (roughness factor), for an irradiation sample loaded in the FPL-II, was calculated using the volatile fission products gamma ray spectra and the thermal neutron flux at the irradiation section. About 0.4 in average was obtained by this method.

On the other hand, the delayed neutron precursor nuclides behavior was studied by measuring the delayed neutron with He-3 proportional counters at two positions on the delay line. The k factor was also calculated by using the delayed neutron counting data. The obtained value was 0.59. It is necessary to study the reason why different k factors were obtained.

Contents

List of Tables

List of Figures

1. INTRODUCTION

When fuel failure occurs in a fast breeder reactor (FBR), fission products (FPs) accumulated in the fuel pin will be released into sodium of primary coolant, then circulate through the primary cooling system together with the flowing sodium and deposit on the piping and inner wall of apparatus. Especially, non-volatile nuclides, such as Zr, Ru, La and Ce, have a strong tendency to deposit on surface of stainless steel wall and have long half life, resulting in the increase to the dose rate during maintenance and examination of reactor. In the experimental reactor of BOR-60 (in USSR), it is reported[1] that radiation level due to FPs, such as Zr-95/Nb-95, Ba-140/La-140, etc. in the primary system is almost same with that of Mn-54, a radioactive corrosion product (CP). However, quantitative study on the deposition behavior of non-volatile FP is very rare[2]. So, the Inpile Fission Product Behavior Test Loop (FPL-II) was built at the Toshiba Training Reactor (TTR) in 1981 and irradiation test was started from 1982[3] in order to study mainly deposition behavior of non-volatile FP. In the fiscal year (April 1983 through March 1984) succeeding previous year, many irradiation tests and analysis of the deposition behavior of non-volatile FP were continued.

In FPL-II, 20% enriched uranium dioxide, was loaded as irradiation specimen, which produces recoil FP. The released FP in to sodium transfers in the loop together with the flowing sodium. A delay line, which is made of stainless steel pipe with 25 m length and is 1/4 inch (9.4 mm) inner diameter, is equipped in FPL-II. During the non-volatile FP transfers from the irradiated fuel through the delay line, it deposits inside of the piping. The deposition distribution of non-volatile FP is measured with gamma ray detectors along the delay line piping.

In 1982, irradiation tests were conducted changing sodium temperature and flow. In this fiscal year, irradiation tests were conducted during 12 cycles of TTR operation. A cycle is composed of 4 hrs irradiation under 100 kW reactor power. The main

experimental items are as follows; i) the temperature dependence of non-volatile FP deposition behavior at low sodium temperature, ii) the elimination of precursor nuclides influence by the method of stopping the sodium flow during irradiation which is followed by the resuming flow 1 hr after irradiation, iii) FP deposition behavior by producing temperature gradient on the delay line by means of switching off the heater on it, and iv) FP deposition behavior in sodium with high oxygen concentration. Gamma ray peaks were measured at various detection positions during irradiation, after irradiation and after draining sodium.

As to analysis in this fiscal year, the deposition distribution of non-volatile FP in the delay line piping were obtained from the experimental results performed in 1982. The deposition behavior was analyzed by using a model by M.H. Cooper et al.[4] and the deposition rate constants of FP nuclides were obtained as a function of temperature and flow velocity.

Although many peaks of volatile FP, such as Br, Kr, Te, I and Xe, were detected in the gamma ray measurement of FPL-II, it is known that these volatile FP nuclides show small adsorption on the surface of piping in sodium at high temperature[5]. From these measured gamma ray of volatile FP, release fraction of FP from irradiated fuel surface to sodium was calculated. The k factor (ratio of measured release fraction to calculated one from recoil model), which is very important for the evaluation of fuel failure detection system responce in FBR, was calculated using the measured release fraction.

Transition behavior of released delayed neutron (DN) nuclides in sodium, together with the k factor, is important for evaluation of fuel failure detection system in FBR. Two neutron detectors were installed on the delay line of FPL-II, in order to detect DN and to measure the transition behavior of DN release nuclides under various transient conditions, flow change, flow stop and reactor (TTR) shut down (test scram). The k factor was calculated from the count rate.

2. INPILE FISSION PRODUCT BEHAVIOR TEST LOOP (FPL-II)

2.1 Outline of Test Loop

As the detail of FPL-II has been reported already[3], the outline only is described here.

2.1.1 Component diagram

An inpile plug, which loads 20% enrichment UO_2 of 100 g was installed at the horizontal irradiation hole of TTR. FPL-II is composed of a sodium system, argon cover gas system and control system, etc. and its sodium inventory is 4.8 kg. The FPL-II schematic diagram is shown in Fig. 2-1.

The sodium system is composed of inpile plug, where FP nuclides are produced, a circulation loop, dump tank, and purification loop.

2.1.2 Sodium system

A FPL-II flow diagram is shown in Fig. 2-2, and a photograph of the sodium system is in Fig. 2-3. The main specifications of FPL-II is given in Table 2-1.

The inpile plug has a quadruple structure with about 4 m length composed of uranium capsule, sodium pipe and outer triple tube. In the uranium capsule at the end of sodium pipe, the irradiation specimen (20% enriched uranium dioxide) is loaded into a mesh basket so as to contact with sodium directly. FP is produced by thermal neutron irradiation, and a part of FP is released in sodium by recoil phenomenon. Specifications of irradiation sample are indicated in Table 2-2. The uranium dioxide irradiation samples is shown in Fig. 2-4 and the uranium capsule is in Fig. 2-5.

The sodium purified at the cold trap temperature of 120°C in the purification system, is loaded in the experimental system, where the delay line piping (25 m total length, 13.8 mm outer diameter and 2.2 mm thickness) is equipped. FP is transferred from inpile plug by flowing sodium forced by an electromagnetic pump and deposits on the delay line piping. The delay line is arranged along the wall of container in spiral for reliable and easy to measure the gamma ray emitted from FP. An by-pass line for the inpile plug is also attached.

2.2 Outline of Gamma-Ray Detection Apparatus

2.2.1 Gamma-ray detection apparatus and detection method

1) Gamma-ray detection system

Gamma-ray emission from loop piping was detected by using a high purity Ge diode detectors made by Princeton Gamma Tech Co. (PGT) and Canberra Co. The Gamma-ray detection system diagram is indicated in Fig. 2-6. The output of gamma-ray detector, after being amplified and rectified by pre- and main-amplifiers, is analyzed by using an spectro-analyzer.

Measured spectra were memorized in a magnetic disk by using floppy disk apparatus. The results of photoelectron peak analysis are recorded by a printer and gamma-ray spectra are by X-Y plotter. Components of gamma-ray detection system module are indicated in Table 2-3.

Gamma-ray detection was performed simultaneously with two detectors at the two detection positions along the loop piping. The peak height analyzer used in the present experiment has two 4K memory capability: the two gamma-ray spectra were recorded simultaneously separately in the 4K memoray.

2) Gamma-ray detection position

In order to examine the deposition behavior of FP in sodium, 11 positions were decided at the same intervals on the delay line for gamma-ray detection. The gamma-ray detection positions (D-1 to D-11) are shown in Fig. 2-7. Distance from the uranium capsule, as the starting point, to each detection positions, sodium volume and internal surface area of piping which contacts with sodium are indicated in Table 2-4. Gamma-ray was measured through collimator allocated at outside of 14 cm-thick carbon steel shielding, as shown in Fig. 2-8.

3) Collimator

Center axis of gamma-ray detector should be consistent with the delay line piping through collimator, as shown in Fig. 2-8. However, the loop and the carbon steel shielding are on different bases, which elevations are different each other, so that the collimator position can not be decided correctly at the designing stage. Therefore, the collimator was allocated at an ellipsoidal hole of 10 cm × 25 cm on the carbon steel shielding, in order to be traversable for 10 cm vertically, as shown in Fig. 2-9. A slit of 64 mm × 20 mm is holed through lead block as collimator. For adjustment of the positions between collimator and piping, Na-24 gamma-ray was used[3] and after determing the optimum position, the front cover was fixed on the shield by bolts. Space between the shielding hole and the collimator was filled with lead granules. The packing density of lead granules is about 60% and the granules shows almost the same shielding effect with carbon steel.

4) Lead shielding

In order to obtain the reliable FP deposition behavior in the delay line piping, gamma-ray from remote loop piping and apparatus should be shielded. Marked interference gamma-ray at each detection position comes from the electromagnetic pump with large amount of sodium inventory and from the delay line

which located behind the measuring point. For shielding of gamma-ray, a lead shielding was allocated behind the piping at each detection position: a lead plate with 5 cm thick and 25 cm × 20 cm size against the electromagnetic pump and a lead plate with 2 cm thick and 50 cm × 15 cm size against the behind delay line. By the provision of lead shielding, gamma-ray radiation from background was reduced to less than 5% at every detection position.

5) Gamma-ray detector driving apparatus

A gamma-ray detector is of about 35 kg weight including a liquid nitrogen Dewar's vessel and a lead shield covering detector-head. In order to move the detector to the desired detection positions in a short time, a manual driving apparatus was manufactured as shown in Fig. 2-10.

2.2.2 Delayed neutron detection system

Two detectors for delayed neutron released from the fission products of iodine and bromine are equipped on the delay line at the distances of 700 cm (DND-1) and 2848 cm (DND-2) from the uranium capsule, with a neutron shielding and a neutron moderator as shown in Fig. 2-11. The layout of inner neutron shielding is shown in Fig. 2-12 and that of neutron moderator and outer neutron shielding is shown in Fig. 2-13.

Delayed neutron is detected by inserting a He-3 proportional counter into a hole of neutron moderator that is placed outside a container. The diagram is indicated in Fig. 2-14. Output pulse of He-3 proportional counter is amplified and rectified by pre- and linear amplifiers, then background noises were rejected by using single channel peak height analyzer. The remainded pulses are counted by using a linear ratemeter and a preset scalor timer.

The output of linear ratemeter is recorded by a 2-pen recorder. At preset scalor timer, two output pulses of DND-1 and DND-2 detectors are counted alternately and printed out. The output pulse of DND-1 detector is, if necessary, counted by a

multichannel scalor with 4K memory and printed out. Specifications of components of the delayed neutron detection system module are indicated in Table 2-5.

Table 2-1 Main Specifications of Inpile Fission Product Behavior Test Loop (FPL-II)

Sodium Inventory	4.8kg
Main Structural Materials	SUS 304
Main Pipe	1/4B Sch 40 (Outer diametor 13.8 mm, Thickness 2.2 mm
Maximum Temperature	
Inpile Plug	550℃
Experimental Loop System	600℃
Purification Loop System	350℃
Maximum Sodium Flow Rate	5 ℓ/min
Cover Gas	Argon
Cover Gas Pressure	−1 ~ 1.9kg/cm^{2}G
Container Size	2.6m^W× 2m^L× 2.5m^H

Table 2-2 Irradiation Samples Specifications

Irradiation Samples	UO_2
Enrichment	20%
Total Weight	100g
Size	0.5 ~ 0.6mmφ ∅ granular

Table 2-3 Components of γ-ray detection system module

Module	Model
Detector-1	PGT. Pure Ge Detection Efficiency 10%
High Voltage Power Supply-1	CANBERRA Model 3105
High Voltage Buffer-1	NAIG Model D-133S
Pre Amplifier-1	PGT
Main Amplifier-1	CANBERRA Model 2010
BIN-1	NAIG Model D-101A
Detector-2	CANBERRA Pure Ge Detection Efficiency 10%
High Voltage Power Supply-2	CANBERRA Model 3105
High Voltage Buffer-2	NAIG Model D-133
Pre Amplifier	CANBERRA
Main Amplifier	CANBERRA Model 1413
BIN-2	ORTEC Model 401A
Peak Hight Analyzer	CANBERRA Series 80
Floppy Disk	CANBERRA Model 8662
Printer	TI Silent 700 Model 745
X-Y Plotter	YHP. 7004B

Table 2-4 Length, Sodium Volume and Surface Area between Detector Positions and FPL-II Main Loop

	Length (cm)	cumlative	Volume (cm^3)	cumlative	Surface area(cm^2)	cumulative
Uranium Capsule	10	10	30	30	306	306
Uranium Capsule~VA-3	440	450	298	328	1298	1604
VA-3	14	464	7	335	36	1640
VA-3~D-1	30	494	21	356	89	1729
D-1~D-2	133	627	92	448	393	2122
D-2~DND-1	73	700	51	499	215	2337
DND-1~D-3	190	890	131	630	561	2898
D-3~D-4	403	1293	280	910	1189	4087
D-4~D-5	338	1631	234	1144	998	5085
D-5~D-6	403	2034	280	1424	1189	6274
D-6~D-7	338	2372	234	1658	998	7272
D-7~D-8	403	2775	280	1938	1189	8461
D-8~DND-2	73	2848	51	1989	215	8676
DND-2~D-9	185	3033	128	2117	547	9223
D-9~EMP-1	160	3193	111	2228	472	9695
EMP-1	79	3272	862	3090	2457	12152
VA-4	14	3286	7	3097	36	12188
VA-4~D-10	143	3429	99	3196	422	12610
D-10~H-1	104	3533	72	3268	307	12917
H-1	100	3633	185	3453	478	13395
H-1~D-11	187	3820	130	3583	552	13947
D-11~VA-2	131	3951	91	3674	387	14334
VA-2	14	3965	7	3681	36	14370
VA-2~Uranium Capsule	440	4405	298	3979	1298	15668
A~VA-5	40	40	28	28	118	118
VA-5	14	54	7	35	36	154
VA-5~B	209	263	145	180	617	771
E T	——		480~1500		364~899	

Table 2-5 Components of Delayed Neutron Detection System Module

Module	Model
^{3}He Proportional Counter	LND Type 2521 Resolution FWHM 10% Power Supply 2,500V
Pre Amplifier	OSAKA DENPA Model PA-5PC
High Voltage Power Supply	ORTEC Model 459
Linear Amplifier	OSAKA DENPA Model MPS-1221A
Single Channel Peak Hight Analyzer	OSAKA DENPA Model MPS-1233
Linear Rate Meter	ORTEC Model 449(DND-1) OSAKA DENPA Model MPS-1252A (DND-2)
Pre Amplifier Power Supply	OSAKA DENPA Model PS-5D
Recorder	YOKOGAWA
Preset Scalor Timer	OSAKA DENPA Model PST-11
Multichannel Scalor	NAIG Process Memory D-172 〃 Readout Controller D-167 〃 CRT Display CRT-2 HP Digital Recorder HP-5055A

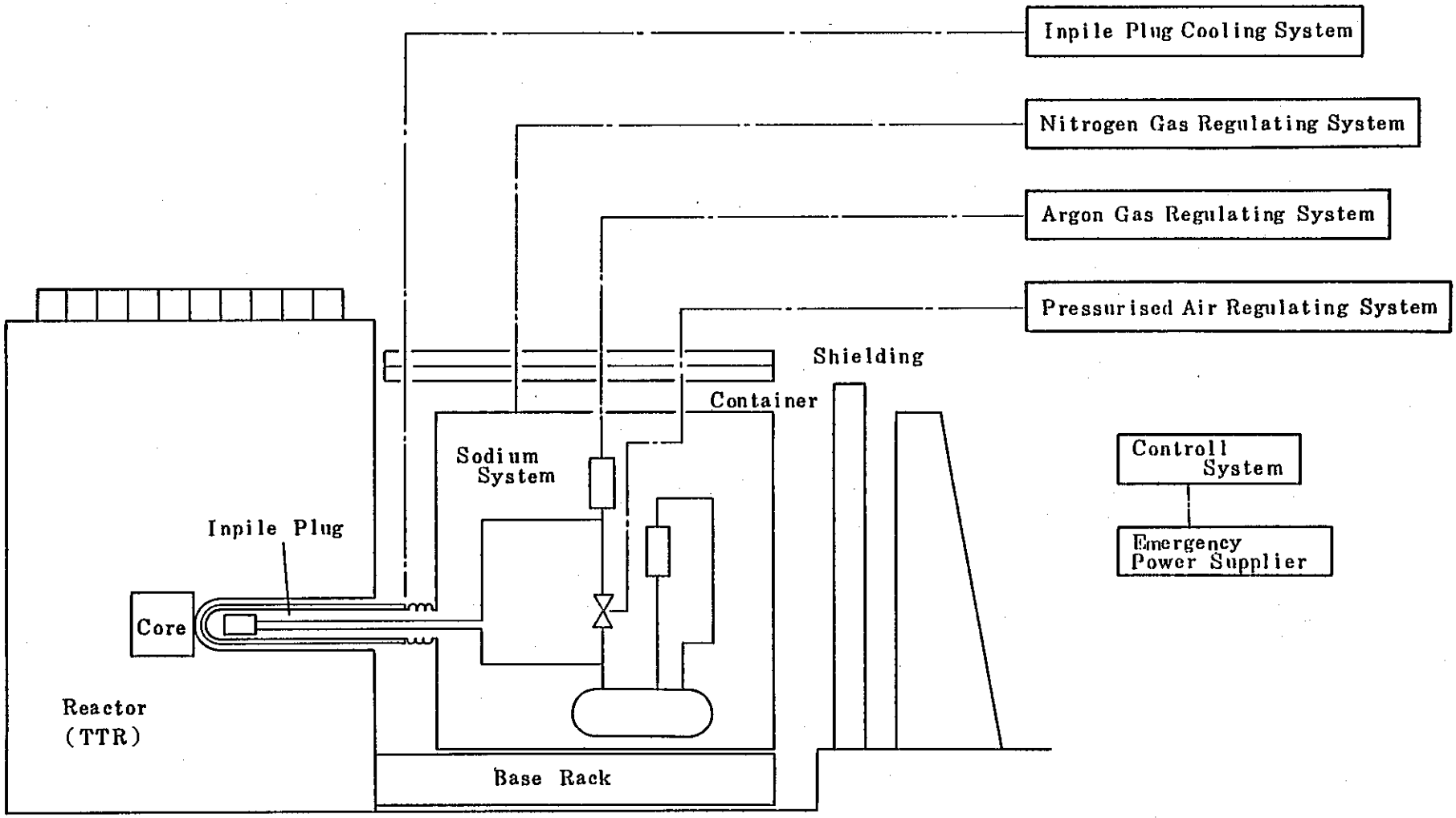

Fig. 2-1 Inpile Fission Product Behavior Test Loop (FPL-II) Diagram

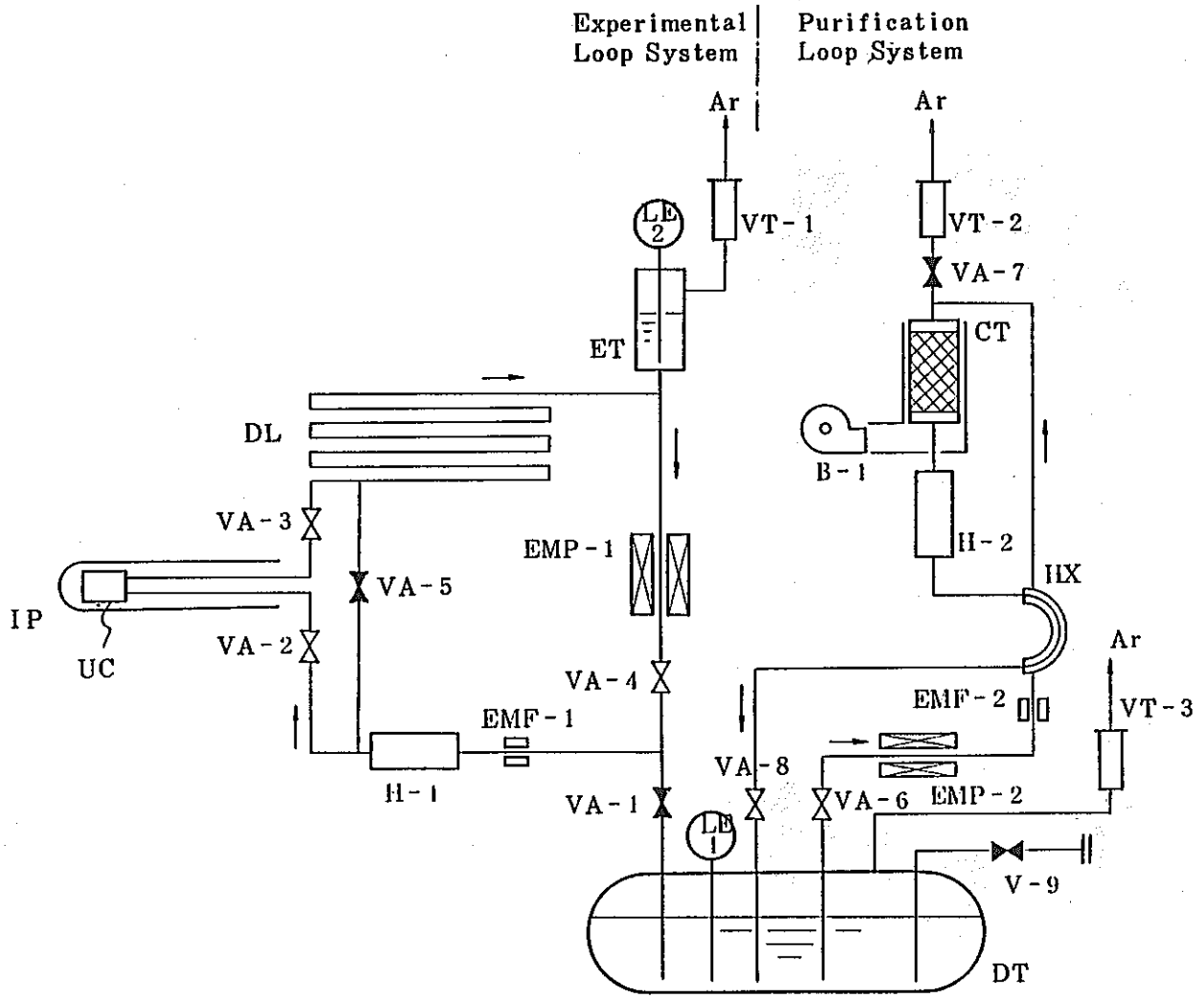

Symbol	Component
DT	Dump Tank
ET	Expansion Tank
CT	Cold Trap
H	Heater
HX	Economizer
EMP	Electro-magnetic Pump
EMF	Electro-magnetic Flow Meter
VT	Vapor Trap
IP	Inpile Plug
VA	Na Valve (Air Drive)
V	Na Valve (Manual)
B	Blower
LE	Induced Type Level Meter
DL	Delay Line
UC	Uranium Capsule

Fig. 2-2 Inpile Fission Product Behavior Test Loop (FPL-II) Flow Diagram

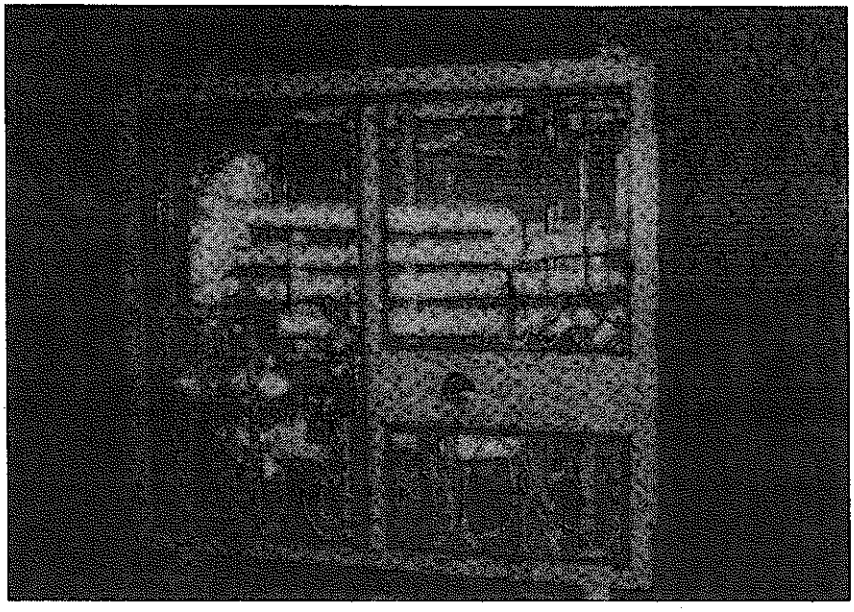

Fig. 2-3 Inpile Fission Product Behavior Test Loop

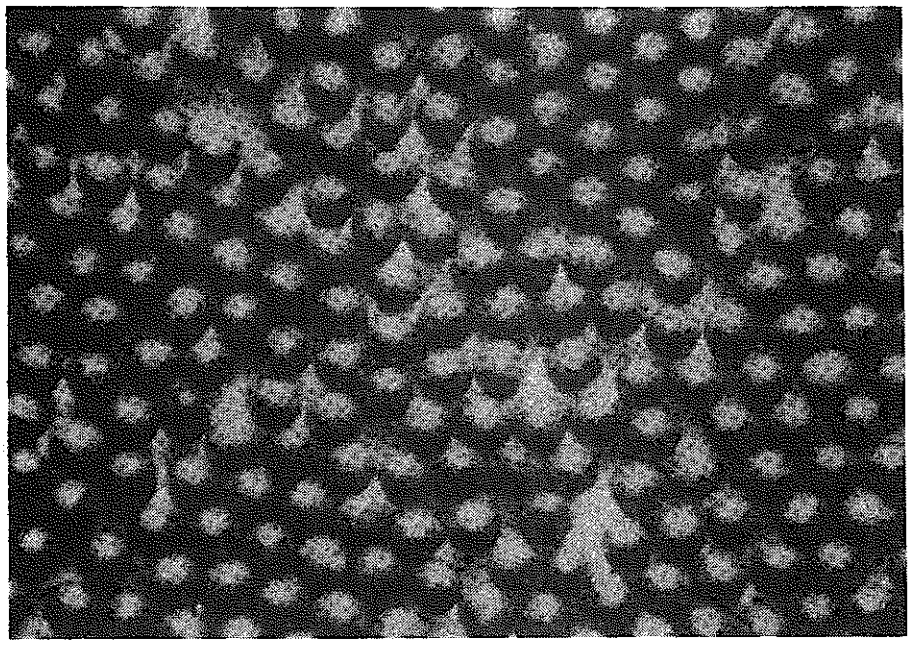

Fig. 2-4 Uranium Dioxide Irradiation Samples

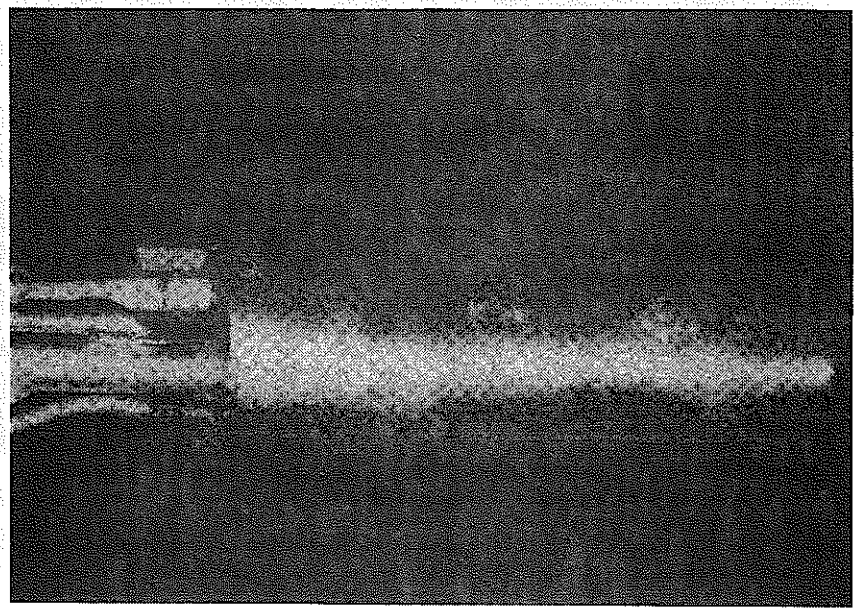

Fig. 2-5 Uranium Capsule

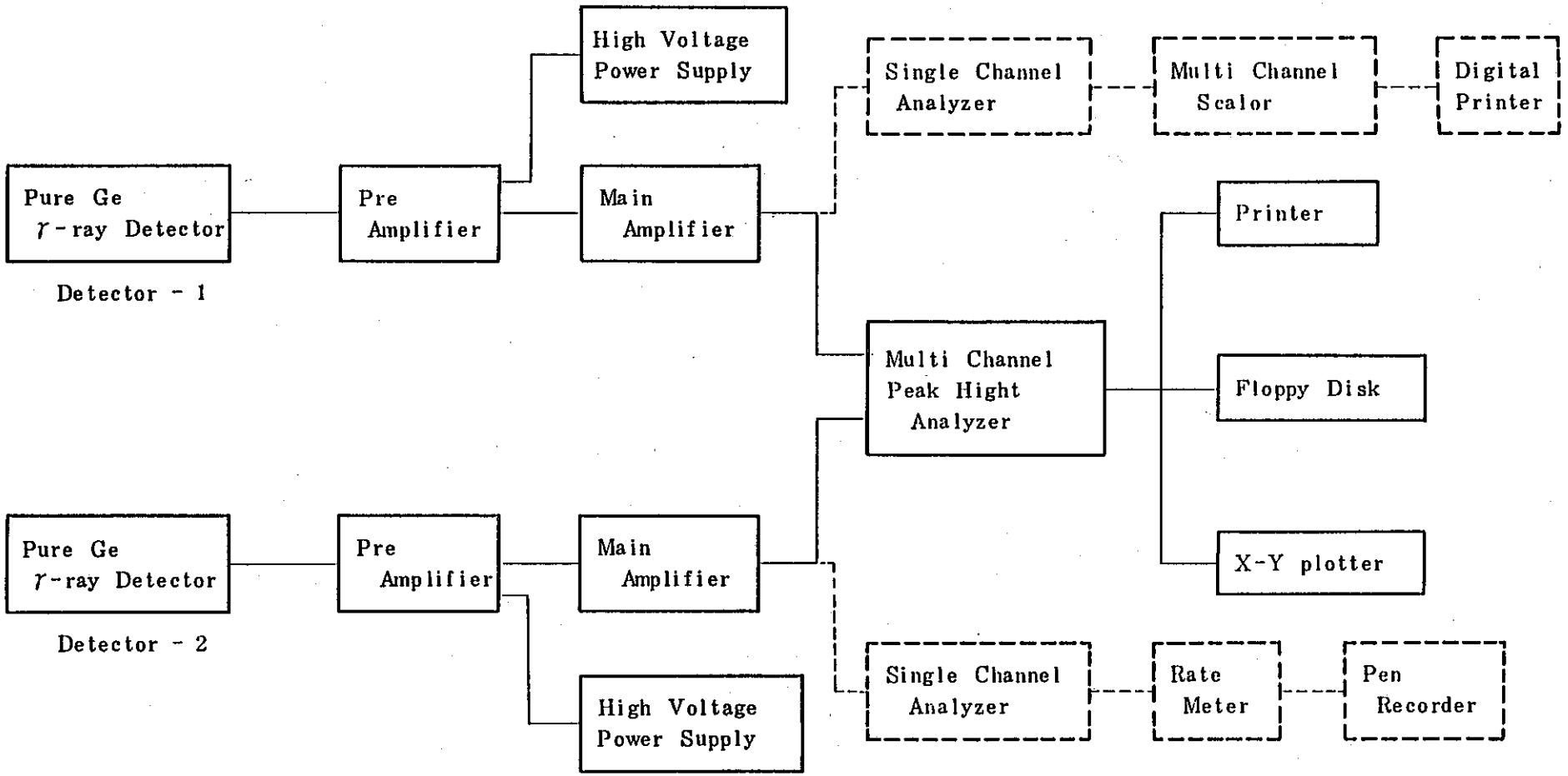

Fig. 2-6 γ-ray detection system diagram

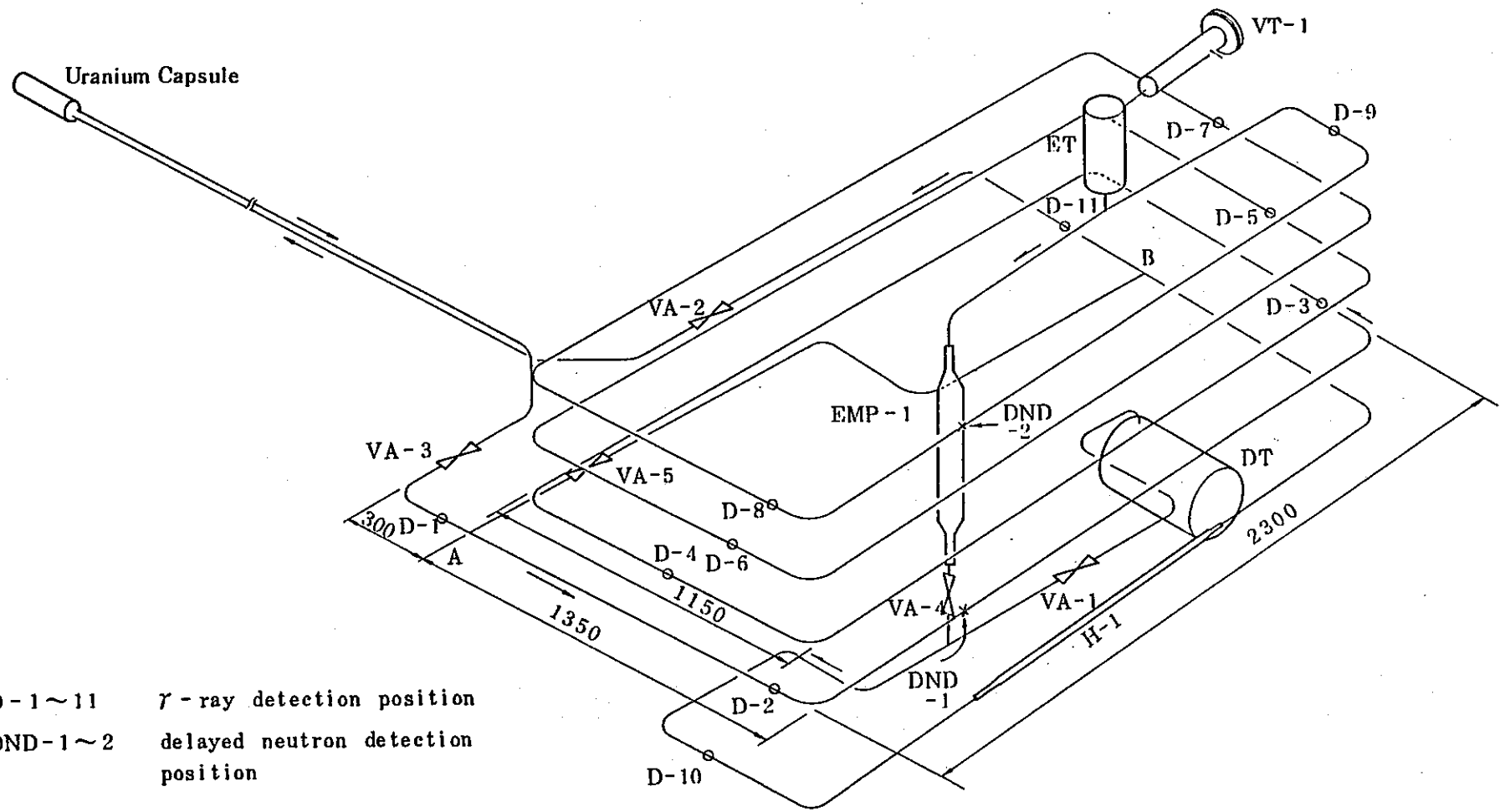

Fig. 2-7 Y-ray Detection Positions and Delayed Neutron Detection Positions

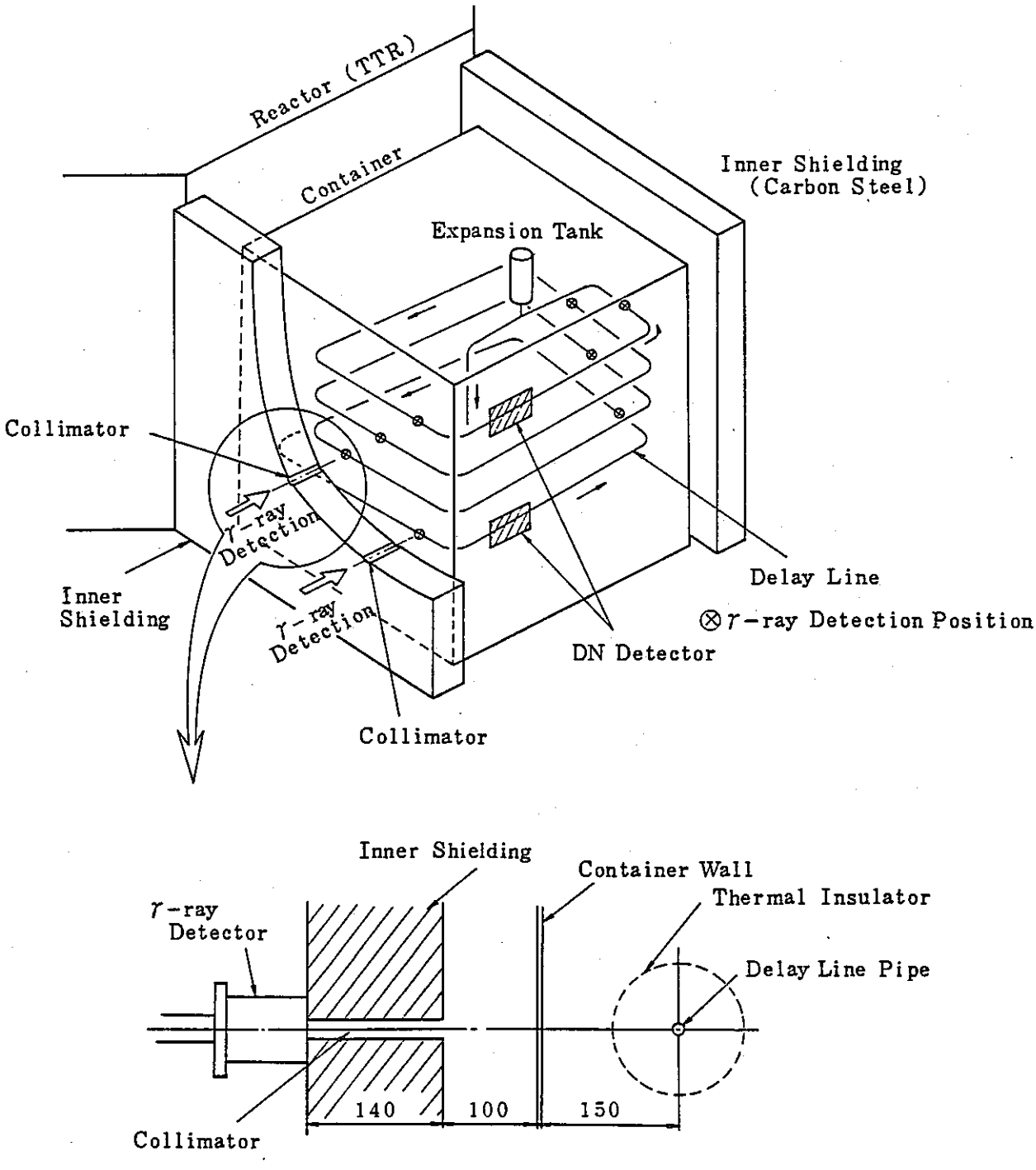

Fig. 2-8 Arrangement of γ-ray and DN Detectors

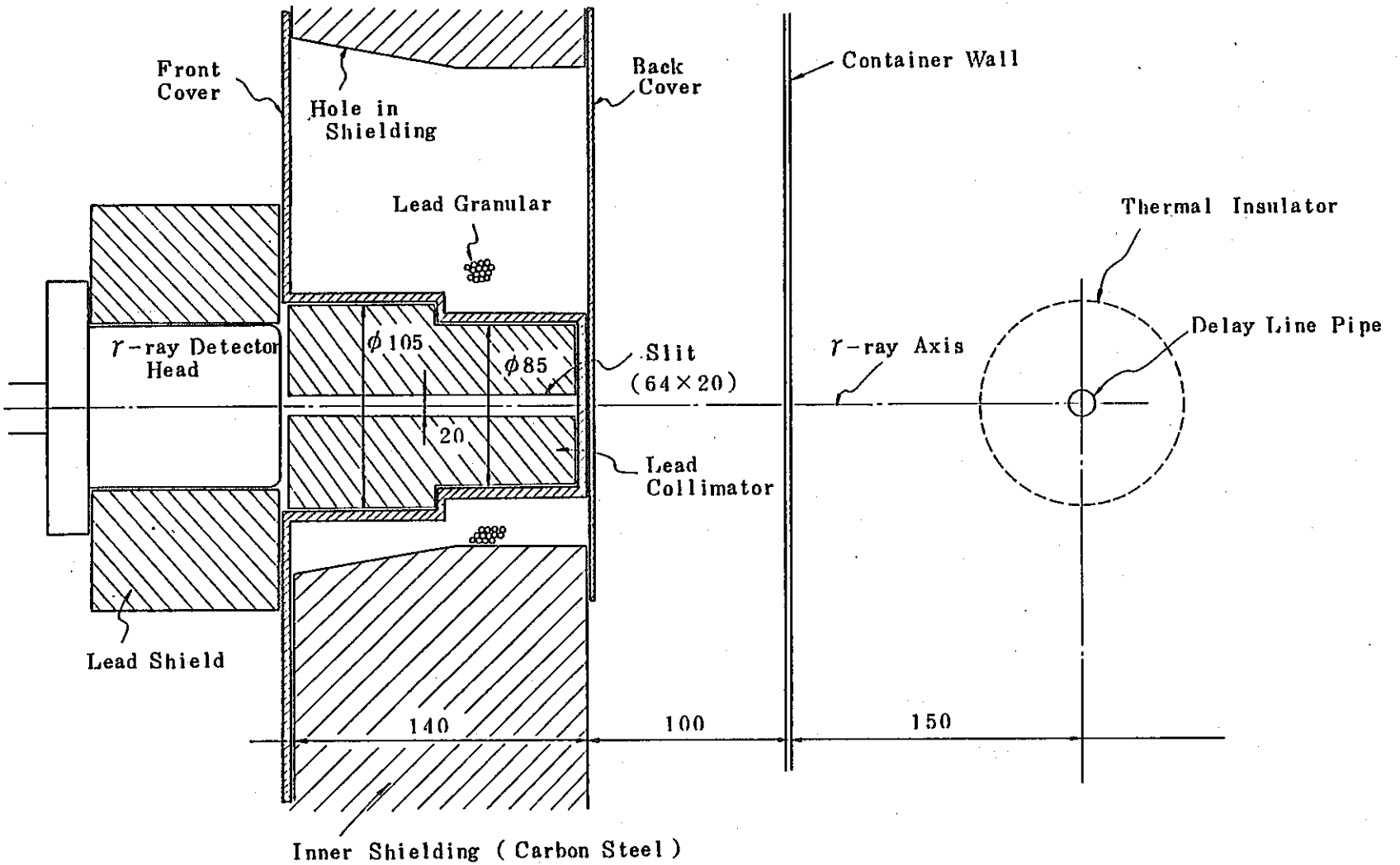

Fig. 2-9 γ-ray Collimator

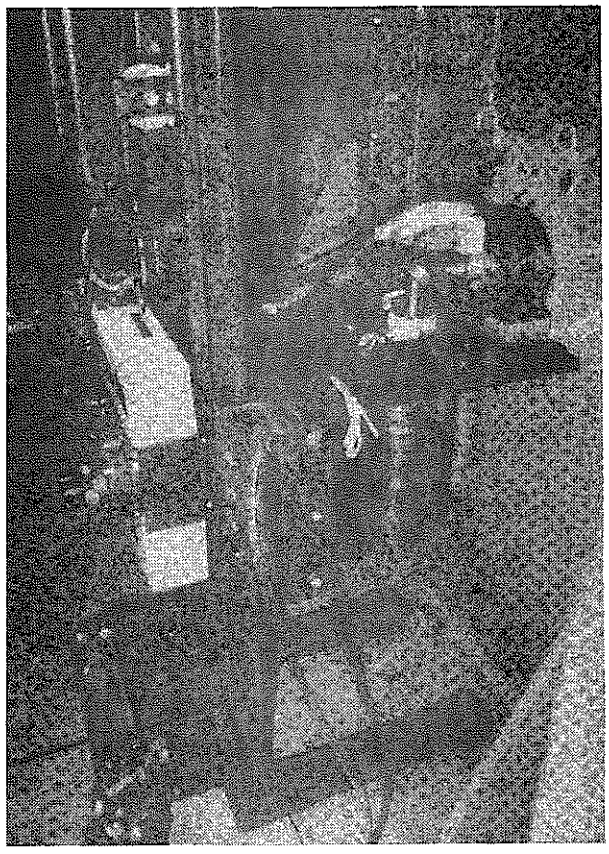

Fig. 2-10 γ-ray Detector Lifter

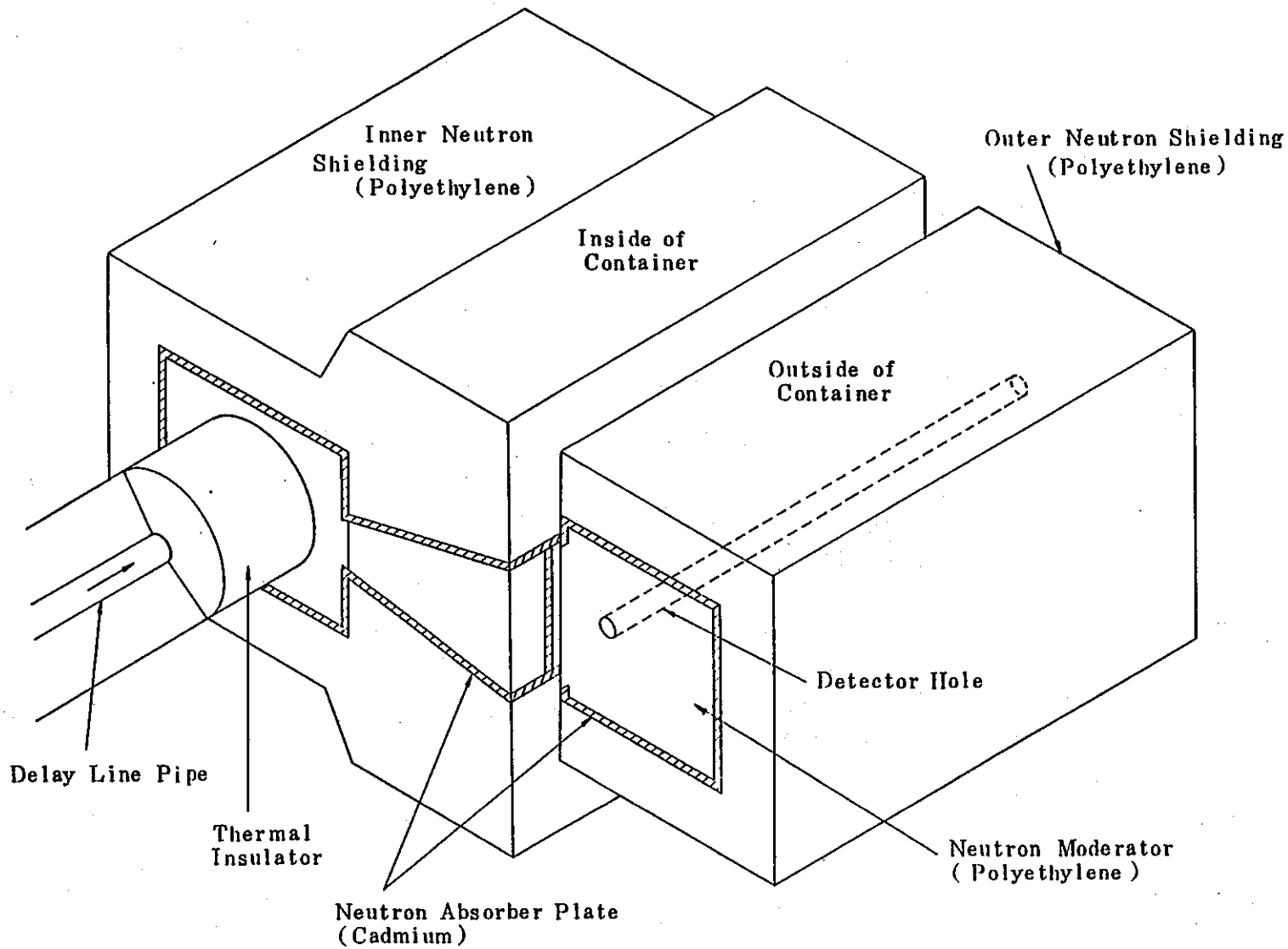

Fig. 2-11 Neutron Shielding and Neutron Moderator for DN Counter

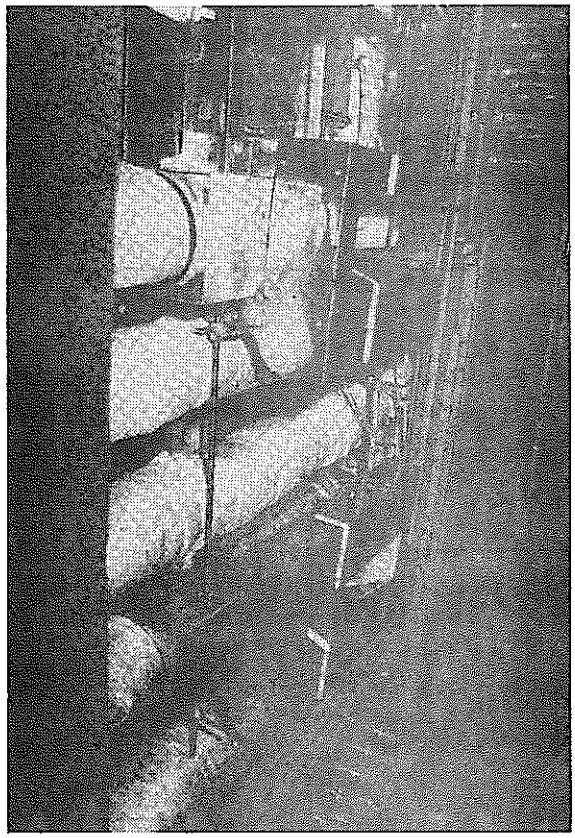

Fig. 2-12 Inner Neutron Shielding

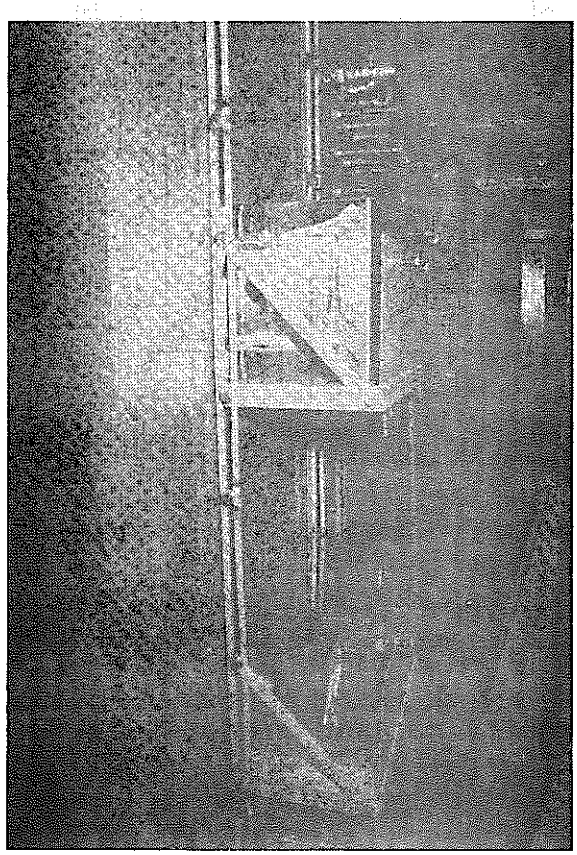

Fig. 2-13 Neutron Moderator and Outer Neutron Shielding

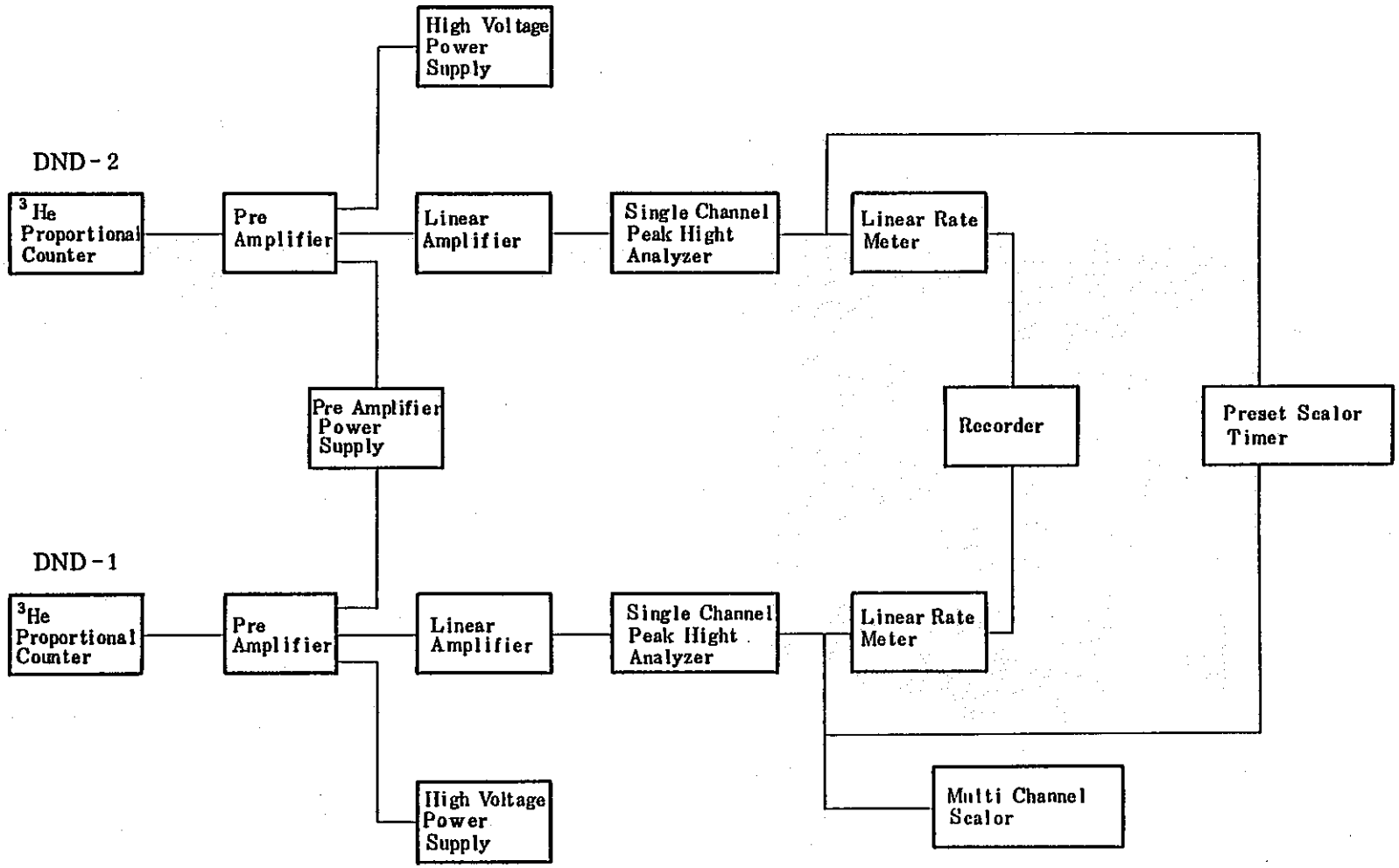

Fig. 2-14 Delayed Neutron Detection System Diagram

3. PRELIMINARY TEST

3.1 Mock-up Test

A DN counter system is, as shown in Fig. 2-11, composed of an inner neutron shielding surrounding the delay line piping, an outer neutron shielding allocated at outside of container and a neutron moderator. The neutron moderator is made of polyethylene of 50 mm thickness (thinnest value in the used inner neutron shielding) and a cadmium plate of 1 mm thickness is used for absorbant for thermal neutron. However, exceptionally no shielding exists at both ends of the outer neutron shielding and the neutron moderator.

The analytical result of DN measurement data in 1982 clarified that two DN detectors equipped in the loop have insufficient neutron shielding ability, because DN radiation is also detected from other places than detection positions (corresponding to DND-1 and DND-2 in Fig. 2-7 respectively), especially from the delay line located at upper and lower places of detection positions. So, mock-up tests were performed using Am-Be neutron source to obtain quantitative detection efficiency to each DN detector from the detection position and its upper and lower pipings.

Furthermore, another mock-up tests for other positions than above mentioned were performed as following procedure: after setting a standard neutron source was settled at the location corresponds to the same relative location to the actual detector in FPL-II, the neutron counts were measured. Next, after transferring the neutron source to another location corresponds, neutron measurement was performed. Thus these operation was repeated. In Fig. 3-1, positions correspond to the loop piping where neutron detection efficiency was measured are indicated by black circles, and for reference, the loop piping are indicated by dotted lines where DL-A to DL-D and E represent the mock-up test apparatus. Thus, detection efficiencies were measured at the upper and lower pipings of the delay line and at places corresponding to the corner places and the electromagnetic pump (T1 $\sim$ T3).

3.1.1 Experiment

1) Mock-up test equipment for piping

The mock-up test equipment for piping is shown in Fig. 3-2 and its photo is in Fig. 3-3. In the mock-up test, piping was set at 1.2 m length in order to detect neutron in the range of 50 cm right and left from the center of detector along the piping. Piping is surrounded by insulation material (Fineflex) of 50 mm thick similarly with FPL-II. Though piping of FPL-II is 13.8 mmϕ outer diameter and 2.2 mm thickness, piping of the mock-up test is designed as 21.7 mmϕ outer diameter and 2.8 mm thickness because neutron source (12.7 mm outer diameter) can be inserted into the piping possessing the similar thickness with that of FPL-II. The inner neutron shielding, the outer neutron shielding and the neutron moderator of DND-1 and DND-2 detectors were removed from FPL-II. Then, the shielding of DND-1 was equipped on piping DL-A of the mock-up and that of DND-2 was on piping DL-D, as shown in Fig. 3-2. Although FPL-II has container wall (material: curbon steel, thickness 3.2 mm) between inner and outer neutron shieldings, the mock-up has no steel plate corresponds to it.

2) Neutron source

Am-Be radiation source of following specification was used:

radioactivity	332.6 mCi
release rate	7.47×10^5 n/sec
average energy	ca. 700 keV
geometry	cylindrical
dimension	12.7 mm dia. × 25.4 mm length

3) Measurement of detection efficiency

Measurement using the mock-up piping was performed as follows:

To begin with, a He-3 proportional counter is set on DND-1 only. In piping DL-A, neutron counting (30 sec) of the neutron source was set at the Position No. 1 (500 mm left from the center of the detector, refer Fig. 3-2) and measured for 30 sec. Following that, by successively transferring the neutron source by 50 mm to the right side direction, Position No. 2 to Position neutron counting were conducted for 30 sec at each position. Subsequently, the same procedures were taken for piping DL-B to DL-D and E (see, Fig. 3-2).

Next, the He-3 proportional counter was set on DND-2 instead of DND-1, and counting measurement similar with DND-1 was conducted.

Following that, the detection efficiencies at 19 positions from O1 to V0 shown in Fig. 3-1 were measured as follows: placing neutron source in sequence at locations that correspond to O1 to V0 and setting He-3 counter on DND-1 and DND-2 alternately, neutron was counted for 30 sec.

From the obtained count number, the detection efficiency was calculated as follows:

$$\text{Detection efficiency (Count/n)} = \frac{\text{Count number (Count)}}{\text{Measuring time (sec)} \times \text{Release rate of neutron (n/sec)}}$$

3.1.2 Result of experiment

The detection efficiencies of DND-1 at selected positions (DL-A to DL-D and E) on the delay line shown in Fig. 3-4, and those of DND-2 at the same positions are shown in Fig. 3-5.

The detection efficiency distributions of DND-1 and DND-2 on the delay line are symmetrical against the center line of the mock-up (neutron source set position of No. 11, ref. Fig. 3-2), as shown in Figs. 3-4 and 3-5.

The detection efficiency of DND-1 at detection position DL-D shows comparative decrease at the central region owing to shielding of inner neutron shield (polyethylene 50 mm thick, cadmium 1 mm thick) of DND-2 detector. The detection efficiency of DND-1 to position DL-A is 4.7×10^{-3} Count/n (peak value), to DL-B is 19%, to DL-C is 9.5%, to DL-D is 3.1% and E is 11.4% of that of DL-A.

As for detection efficiency of DND-2, since positions DL-A and E are shielded by the inner neutron shielding of DND-1 detector, small values of detection efficiency were observed, especially the effect is remarkable owing to the shielding of 100 mm-thick polyethylene and 2 mm-thick cadmium. The detection efficiency of DND-2 to position DL-D is 4.7×10^{-3} Count/n (peak value), to DL-C is 17.6%, to DL-A is 3.0%, to E is 0.8% of the that of DL-D. Here, the detection efficiency of DND-1 to the position DL-A and that of DND-2 to position DL-D show, as stated above, approximately equal value. Furthermore, the detection efficiencies to pipings that correspond to relatively equivalent positions to detectors (for example, piping DL-C corresponds to DND-1 and piping DL-B corresponds to DND-2) were clarified to be in good agreement with both detectors.

The detection efficiencies of DND-1 and DND-2 to 19 positions (from O1 to VO) are shown in Fig. 3-6. Both efficiencies show little difference to the detection positions except to the elecromagnetic pump part ($T_1 \sim T_3$) and around its outlet (U_0). The detection efficiency vaties approximately 2 times from 3×10^{-5} to 6×10^{-5} Count/n depending on the detection positions. The detection efficiencies of DND-1 to positions T_1 and U_0 are approximately 2 times larger than those of DND-2 at the same positions, respectively, owing to large difference of distances from each positions to each detector.

The detection efficiency distribution to the whole part of FPL-II loop piping are shown in Fig. 3-7 for DND-1 and in Fig. 3-8 for DND-2. Here, the abscissa in figures shows distance from the uranium capsule. It is clear from these figures that the detection

efficiency of DND-1 is high to the detection positions DL-B to D, E and to electromagnetic pump as well as DL-A on which the detector is set. Similarly, as for DND-2, the detection efficiency to DL-A, DL-B, DL-C and the electromagnetic pump is high as well as DL-D. However, at the position E, a small value of detection efficiency is obtained as explained above. Since sodium volume per unit length at electromagnetic pump is approximately 15 times higher than that of piping, actual detection efficiency is approximately 15 times higher, and it is estimated that the electromagnetic pump part is rather influential.

3.1.3 Conclusion

Using the FPL-II piping mock-up and a uranium source, neutron detection efficiencies of DND-1 and DND-2 to delayed neutron detectors were measured to the experimental system loop. Results are as follows:

(1) Despite of lack of neutron shielding at the both side ends of outer neutron shielding and neutron moderator, the leaked neuron from the ends could be neglected.

(2) The detection efficiency of DND-1 to the piping DL-A is 4.7×10^{-3} Count/n (peak value) and to DL-B is 19%, to DL-C is 9.5%, to DL-D is 3.1% and to E is 11.4% of the peak value.

(3) The detection efficiency of DND-2 to the piping DL-D is 4.7×10^{-3} Count/n (peak value) and to DL-C is 17.6%, to DL-B is 9.0%, to DL-A is 3.0% and to E is 0.8% of the peak value.

From these results, detection efficiencies of DND-1 and DND-2 to various positions in the experimental loop were estimated.

3.2 Calibration Test of Delayed Neutron Detectors

Calibration test of measuring instrument, which are used routinely for long period, is necessary before the start of experiment in order to confirm the normal function and the

reproducibility of these apparatus. Calibration test of DN measuring instrument was conducted before every irradiation test using a standard neutron source.

The neutron source of Ra-Be (radioactivity 3 mCi) is placed inside the hole of a cylindrical moderator (50 cm dia. × 45 cm high) and He-3 counters of DND-1 and DND-2 are inserted through an experimental hole perforated through the side wall of the moderator, and the neutron count rate was measured using the same detection system shown in Fig. 2-14. Actually a single channel peak height analyzer and a multi channel peak height analyzer (MCA) were connected in parallel to the linear amplifier in order to measure the neutron spectrum. Procedures of calibration test are as follows:

① At no neutron source state, confirm that no large variation occurs in the noise level by changing discrete level of the single channel peak height analyzer.

② The variation of count level of counter is measured with neutron source by similar procedure to ①, and confirm that no variation of DN count rate occurs around discrete level settled.

③ During measurement of ②, neutron spectra are measured by the multi channel peak height analyzer, and confirms that no large variation occurs between them.

Results of calibration tests performed before irradiation tests of Exp. Nos. 18 to 28 are shown in Table 3-1 and Fig. 3-9. Measured neutron count rates showed little variation, and it was confirmed that the DN detection system functioned normally during the tests.

Table 3-1 Delayed Neutron Detectors Calibration Test before Each Irradiation Test

Exp. No	Date	Count rate (cps)	
		DND-1	DND-2
18	83/9/16	6208.1	6211.8
19	10/15	6180.9	6274.8
20	11/05	6148.6	6202.9
21	11/26	6146.6	6241.4
22, 23	12/09	6160.2	6154.4
24	84/1/23	6094.8	6198.7
25, 26	1/27	6091.6	6049.3
〃	1/30	6147.0	6245.4
27	2/10 13	6055.3	6163.4
28	2/24	6070.4	6041.1

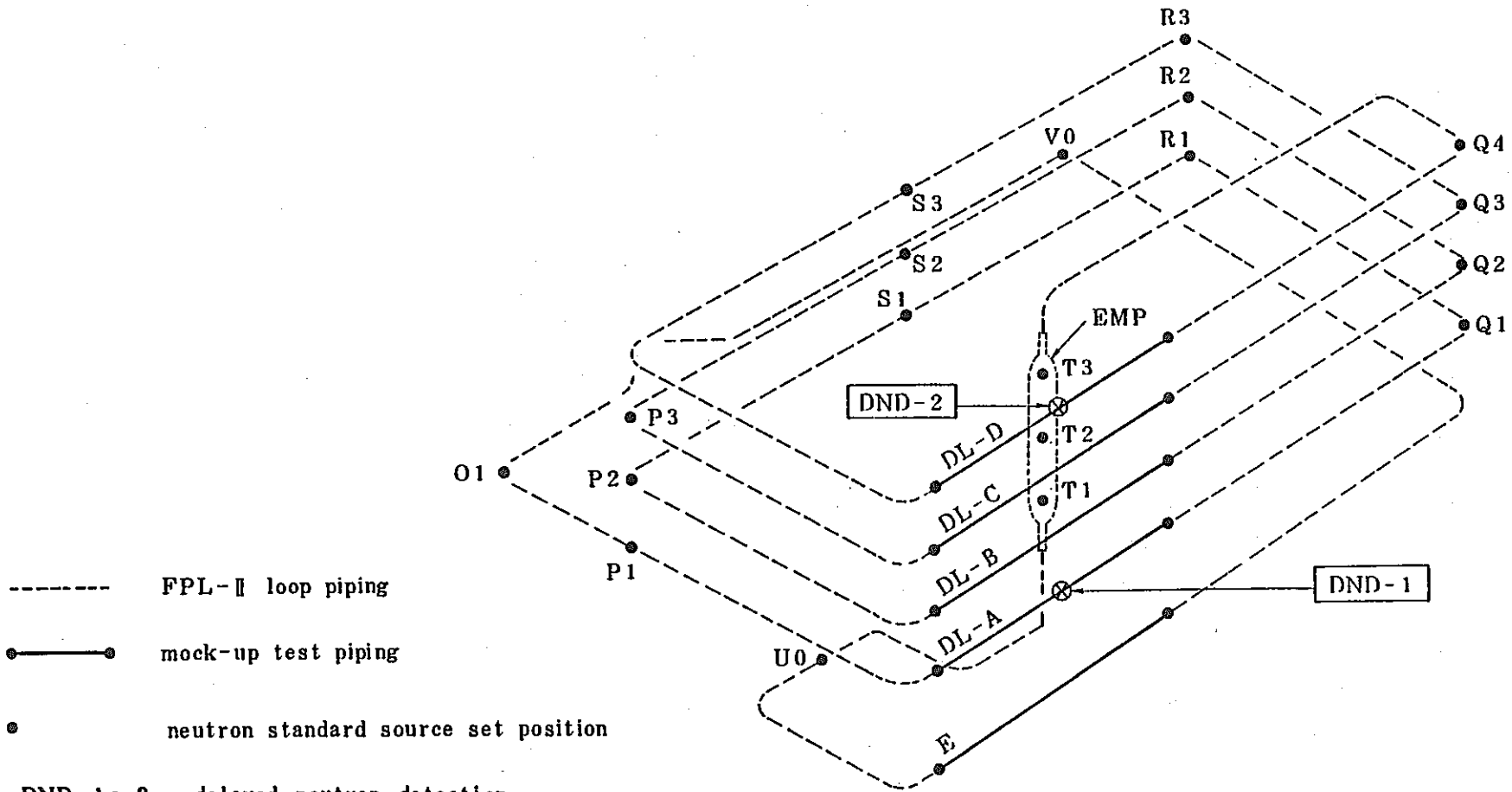

Fig. 3-1 The Positions where Neutron Detection Efficiency was Measured in the Mock-up Test

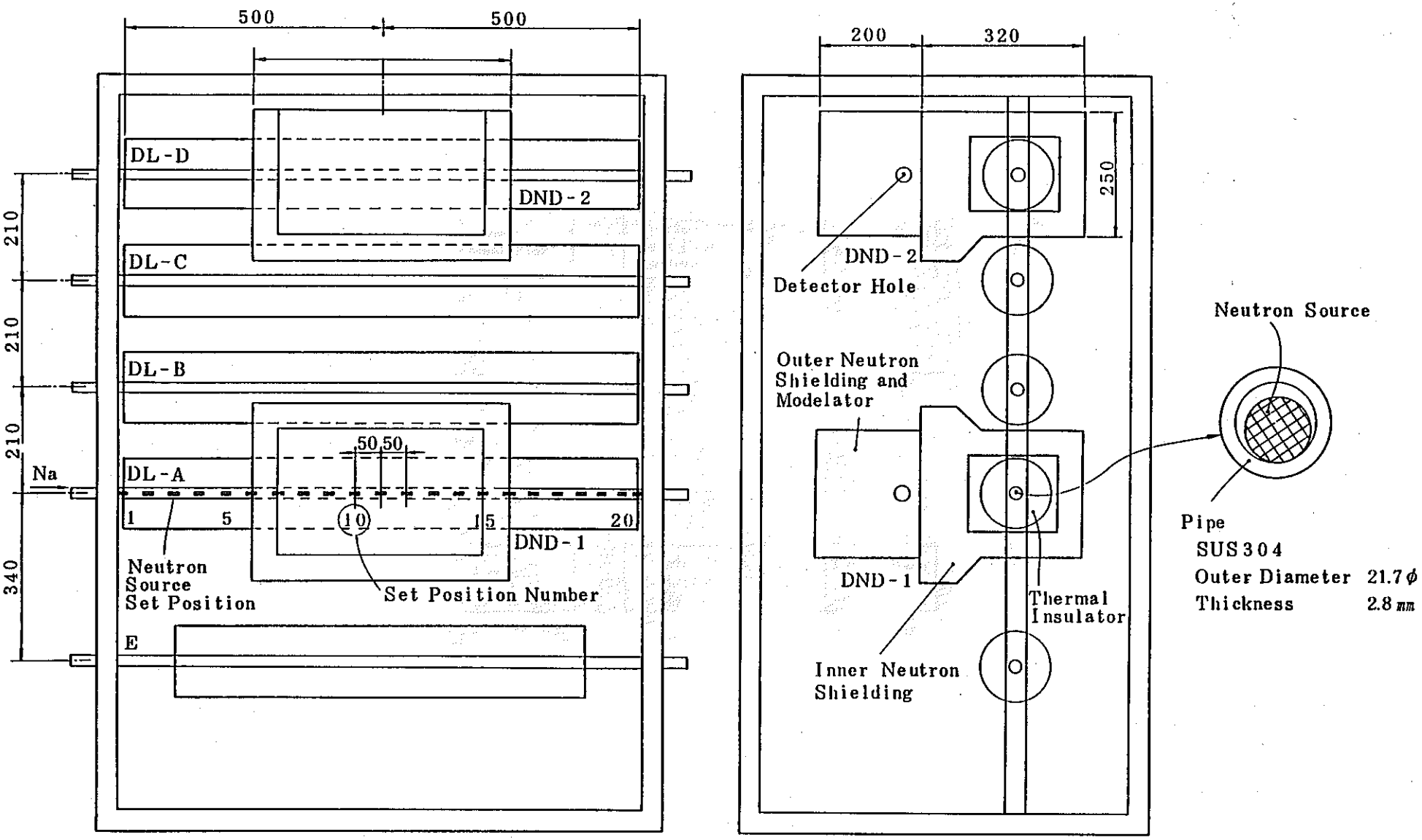

Fig. 3-2 Mock-up Test Equipment

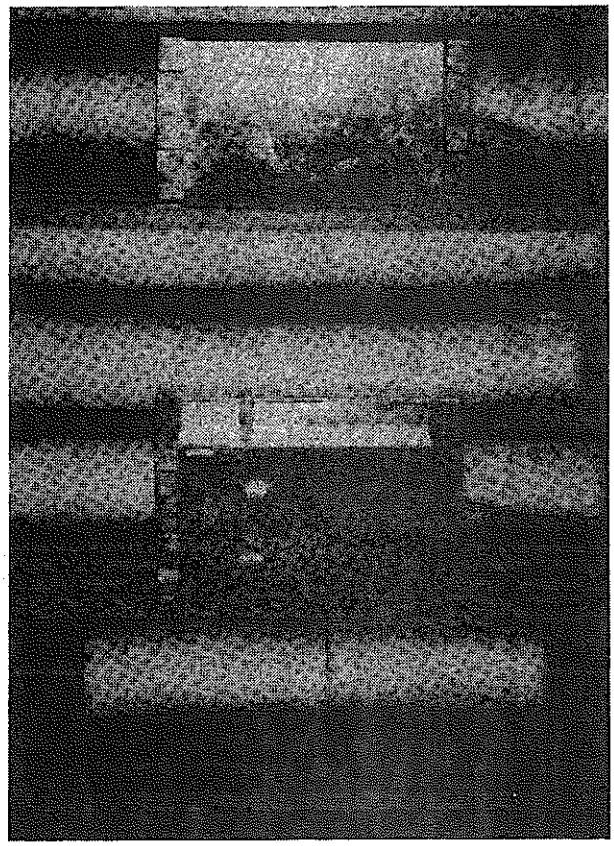

Fig. 3-3 Photograph of the Mock-up Test Equipment

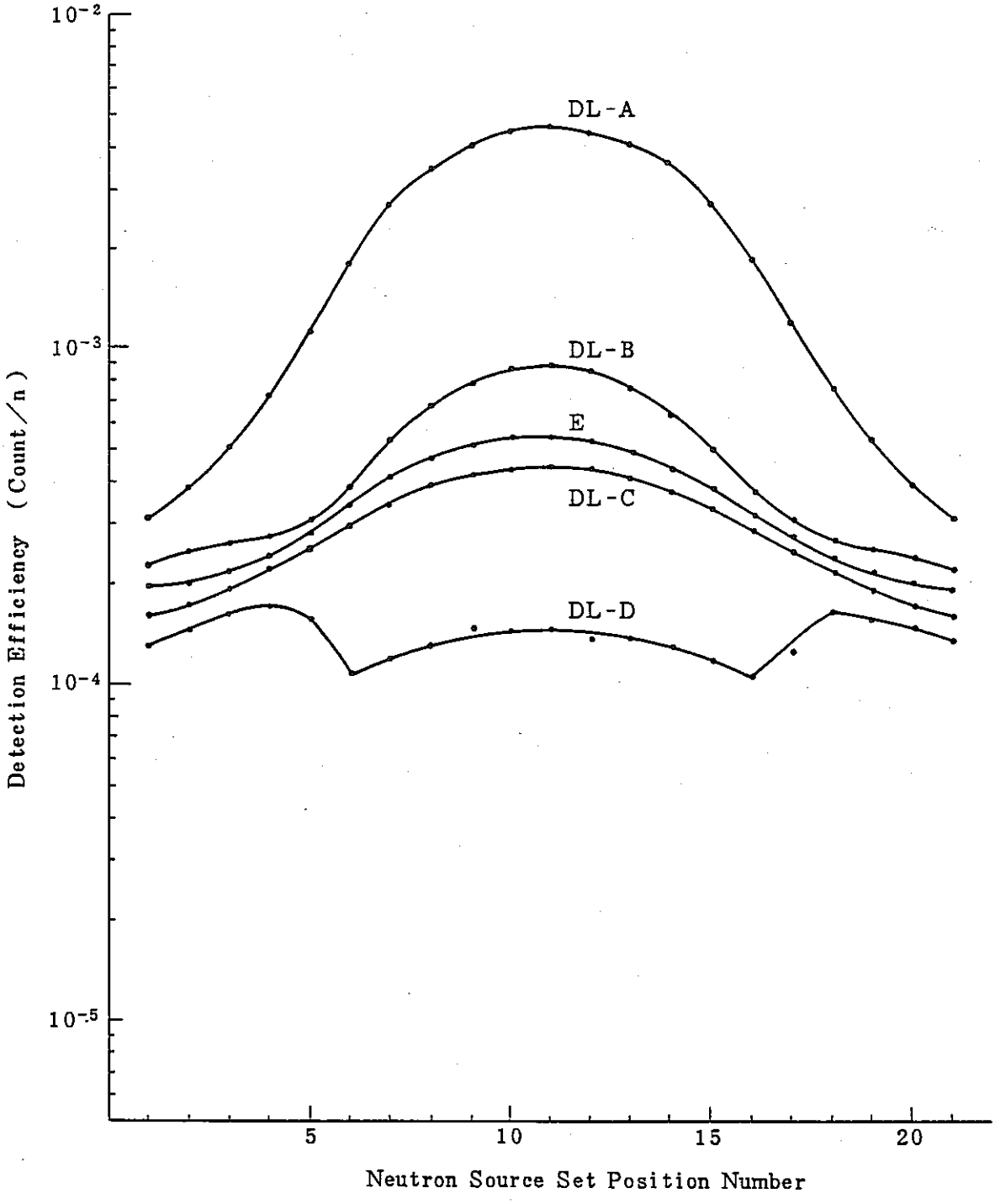

Fig. 3-4 Detection Efficiency at the DND-1 Delayed Neutron Detector from the Delay Line Piping

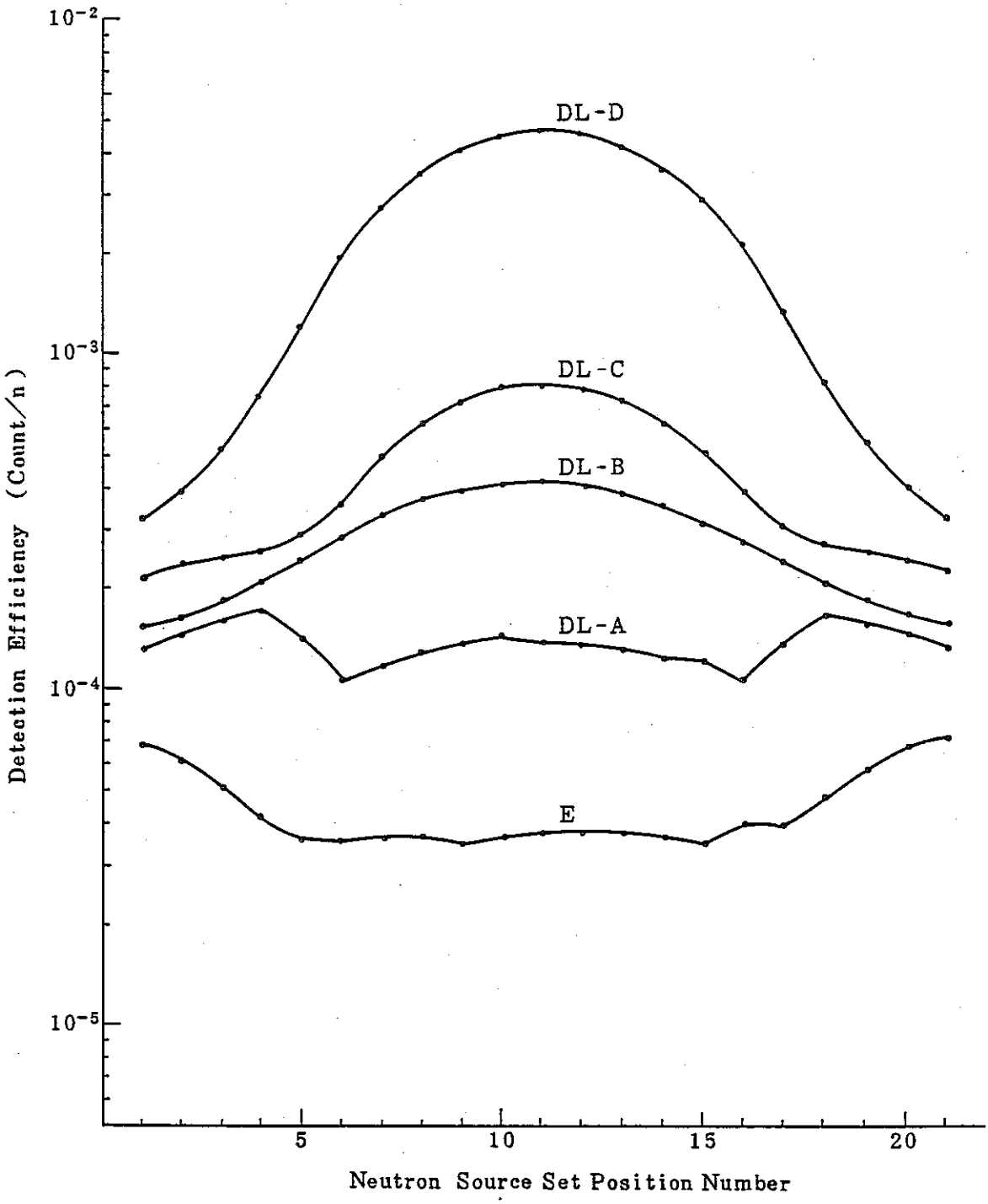

Fig. 3-5 Detection Efficiency at the DND-2 Delayed Neutron Detector from the Delay Line Piping

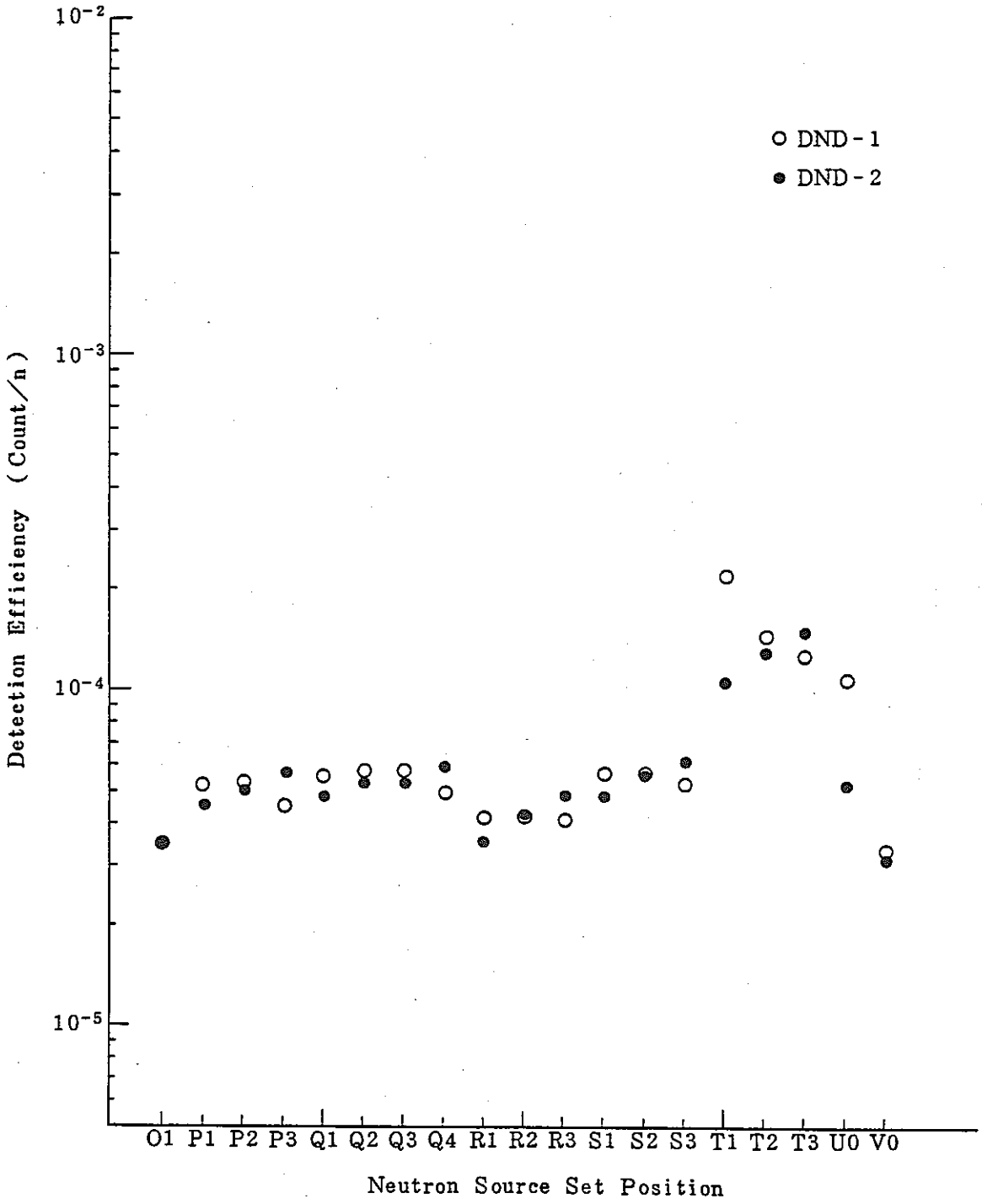

Fig. 3-6 Detection Efficiency at Each Delayed Neutron Detector from the Various Part of FPL-II Loop Piping (from O1 to V0)

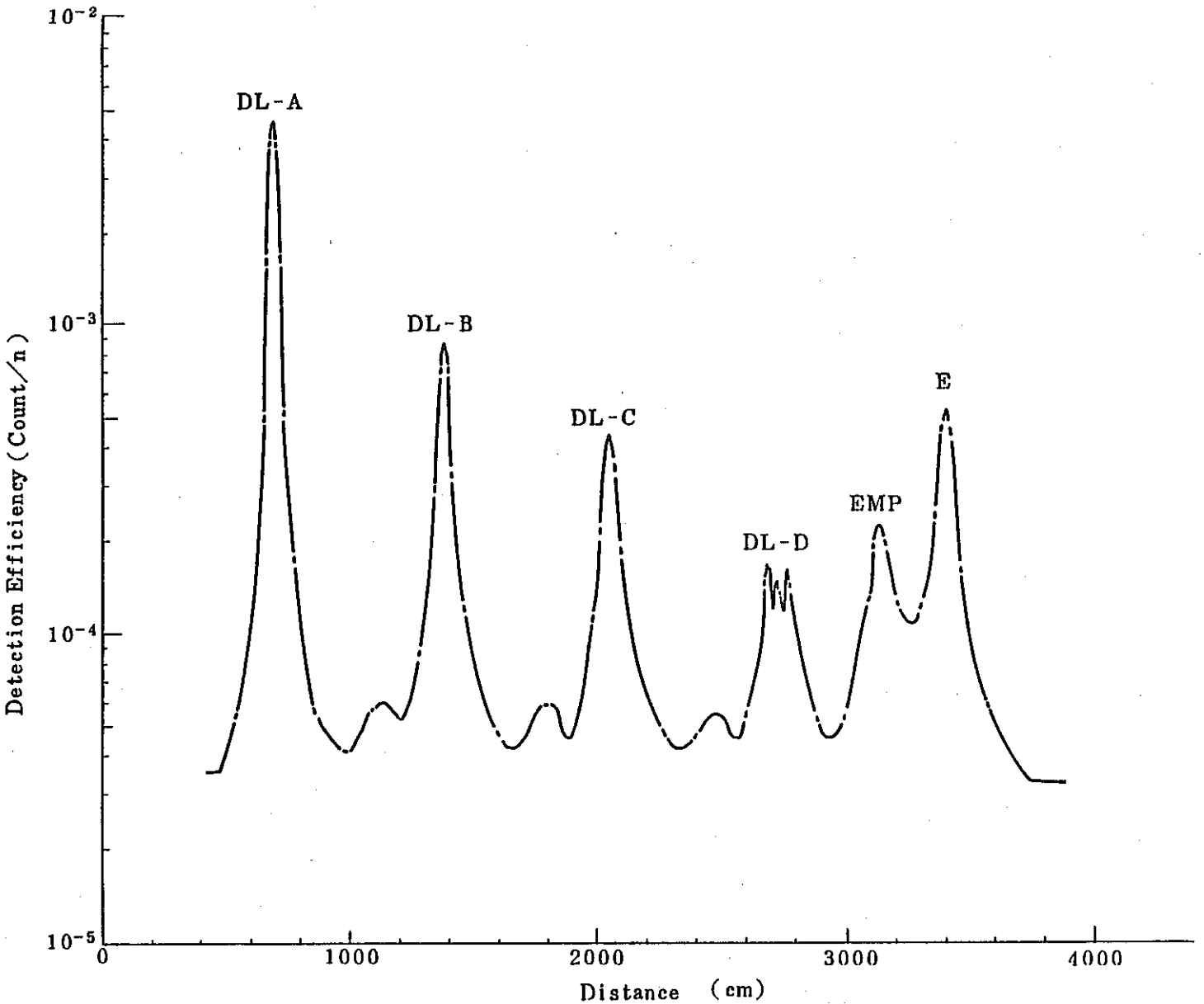

Fig. 3-7 Detection Efficiency at DND-1 Delayed Neutron Detector from the Whole Part of FPL-II Loop Piping

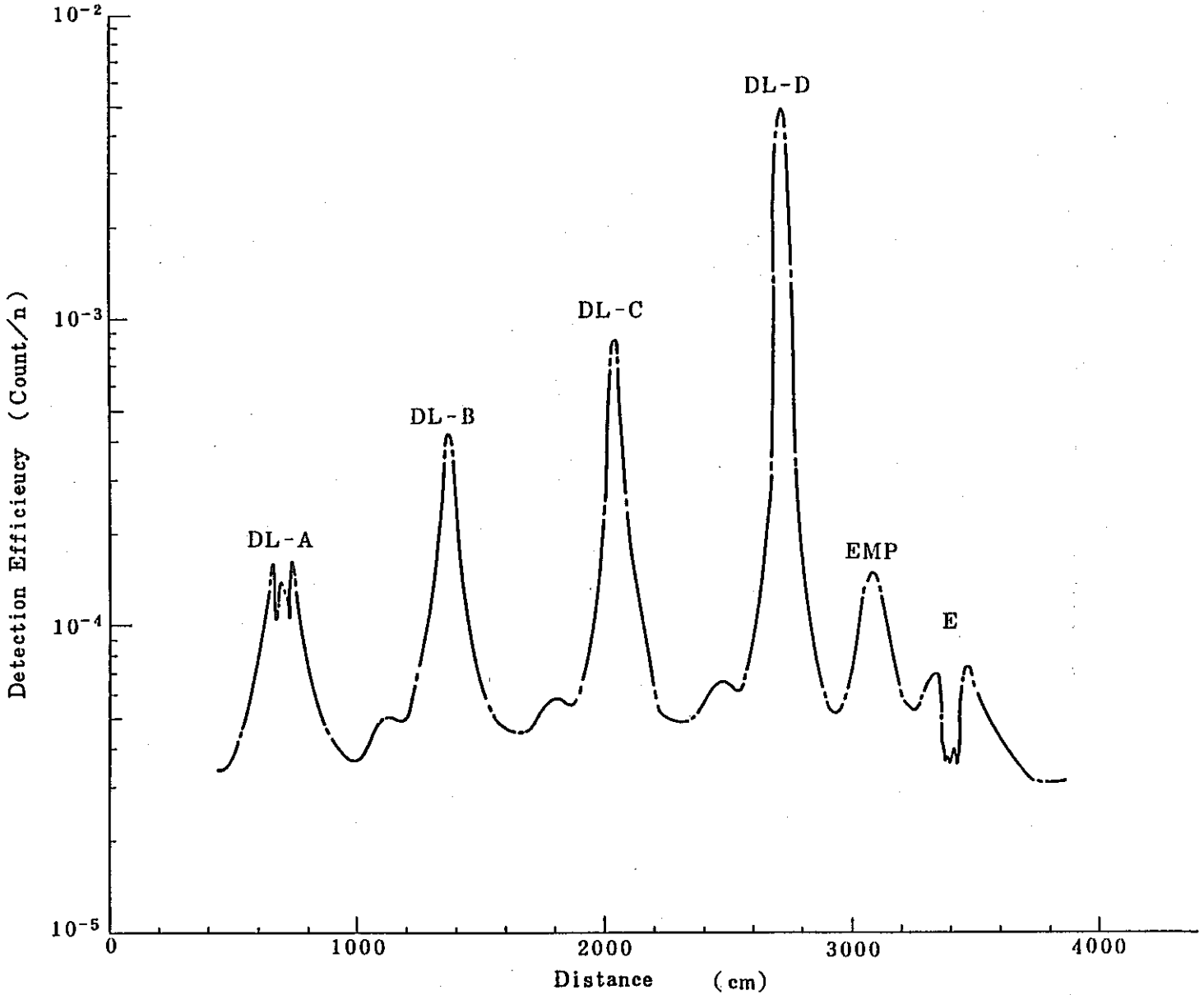

Fig. 3-8 Detection Efficiency at DND-2 Delayed Neutron Detector from the Whole Part of FPL-II Loop Piping

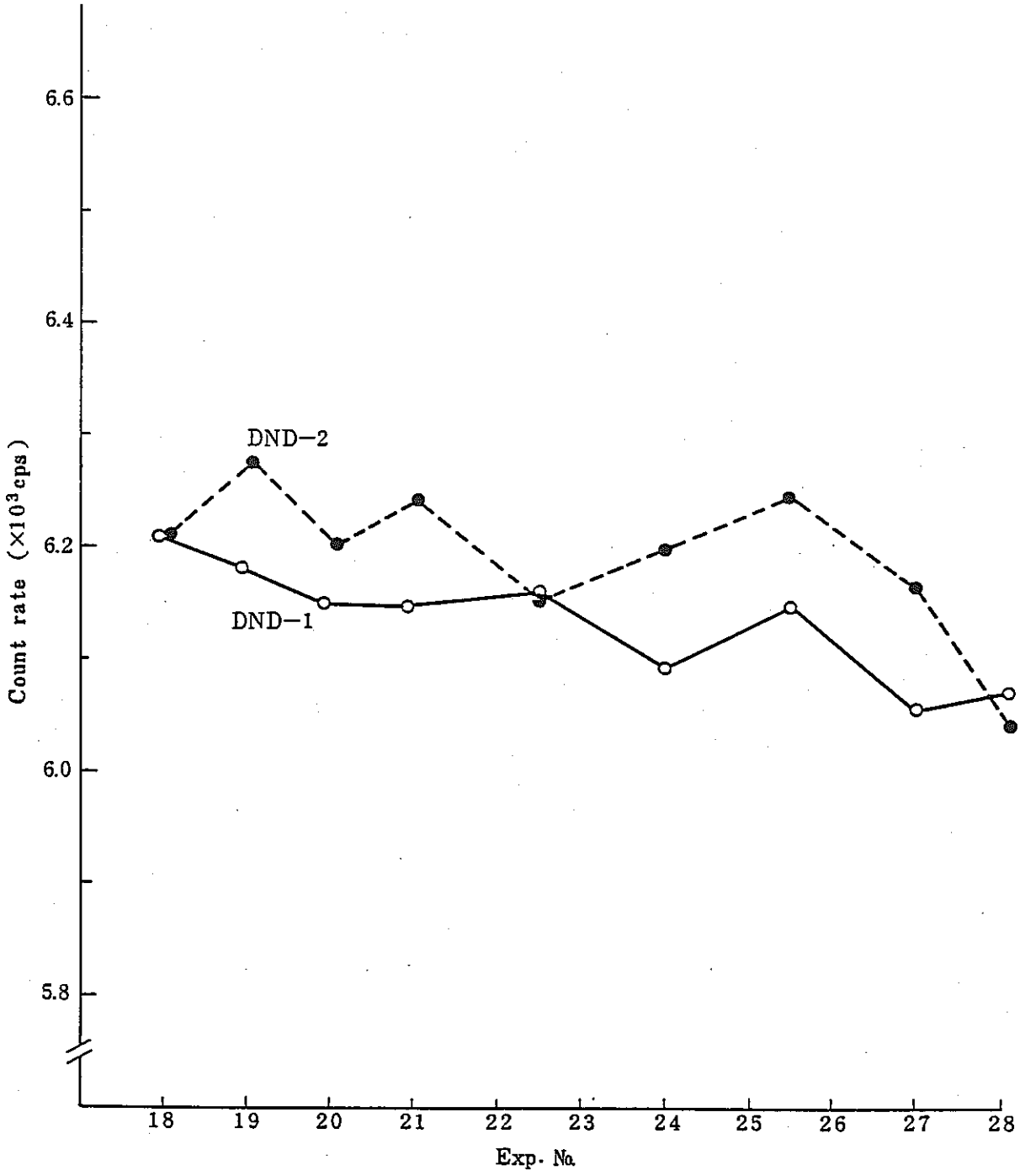

Fig. 3-9 Delayed Neutron Detectors Calibration Test Results Performed before Each Irradiation Test

4. IRRADIATION TESTS

4.1 Procedure of FPL-II Operation

An irradiation test of FPL-II started after purification of sodium, cleaning of test system and repurification of sodium were performed. Sodium was purified by cooling a cold trap to 120°C. Cleaning of the experimental loop system was performed by circulating purified sodium at 300°C through the system except the inpile plug, in order to dissolve impurities in sodium. Operation procedure of FPL-II is shown in Fig. 4-1 and explained as follows:

1) Gas substitution in the loop

   (1) The gas inside the test system and purification system is substituted 3 times with fresh argon gas.

2) Sodium purification

   (1) Temperature of the purification system is elevated up to 300°C with rate of ca. 50°C/30 min.

   (2) Passing through test of the purification system is done.

   (3) After the purification system is evacuated to vacuum state, sodium is charged in the purification system by pressurizing dump tank.

   (4) Temperature of the purification system is elevated up to 350°C by circulating sodium with 3 liters/min flow rate.

   (5) Heaters equipped on cold trap (CT), inlet and outlet piping of CT are cut off.

   (6) CT is cooled by operating the CT blower.

   (7) Flow rate of sodium is lowered stepwise until 0.4 liter/min.

(8) Temperature of main heater (H-2) in the purification system is lowered at the rate of 10°C/10 min until temperature of CT lower part attains 120±5°C.

(9) After temperature of CT lower part attains 120±5°C and is kept constant, sodium is circulated for more than 1 hr, then drained.

3) Cleaning of the experimental loop system

(1) The experimental loop system excluding inpile plug is preheated up to 300°C with rate of ca. 50°C/30 min.

(2) Sodium valves VA-2 and VA-3 are closed.

(3) Passing through test in the experimental loop system is done.

(4) After evacuating dump tank and the experimental loop system to vacuum state, sodium is charged in the experimental loop system excluding the inpile plug by pressurizing the dump tank.

(5) Sodium is circulated for more than 2 hrs with flow rate of 3 liters/min at 300°C.

(6) Sodium is drained.

(7) Passing through test in the experimental loop system is done.

4) Irradiation test

(1) The inpile plug is cooled by using the inpile plug cooling system.

(2) Temperature of the experimental loop system including inpile plug is raised to 300°C (200°C for inpile plug) with rate of ca. 50°C/30 min.

(3) After evacuation of the dump tank and the experimental loop system to vacuum state, sodium is charged in the experimental loop system including the inpile plug by pressurizing the dump tank.

(4) Sodium is circulated with test flow rate through the main circulation loop.

(5) Temperature of loop is raised or lowered to a test temperature with rate of 50°C/30 min, the temperature of dump tank is raised or lowered to the same level of the loop.

(6) Irradiation test is performed after the test temperature is attained.

(7) Sodium is drained after a test is completed.

(8) Passing through test in the experimental loop system is done.

(9) Uranium capsule is cooled down to 95°C by blowing argon gas through the inpile plug.

4.2 Outline of Irradiation Test

Irradiation tests have been conducted 15 times from September 7, 1982 through March 1, 1983. The objective and the result of the test have been already reported in detail[1]. A summary of test conditions is indicated in Table 4-1.

During this fiscal year, irradiation tests have been conducted 11 times from September 20, 1983 to February 28, 1984. These conditions are summarized in Table 4-1 including the previously performed tests. Time charts of sodium temperature, sodium flow rate and TTR power regarding to Exp. No. 16 and hereafter experiments are shown in Fig. 4-2, where Exp. No. 17 is eliminated because of no FPL-II operation.

As stated in Section 4.1, after purifying sodium by using the purification system, sodium was charged in the experimental loop system in order to dissolve the sodium oxide deposited on the inner wall of the loop piping, and then drained to the dump tank. After that, sodium was purified again by using the purification system and charged in the experimental loop system, then after sodium temperature and flow rate were set to the test condition. The temperature was kept constant during irradiation for 4 hrs at the 100 kW power. Usually, the loop was operated in the isothermal condition and was kept at the same temperature to the inpile plug, excluding few irradiation test cases. However, the electromagnetic pump was cooled by blower to suppress coil heating and, therefore, kept at a lower temperature (80°C maximum) than other loop parts.

Gamma-ray measurements were performed at various detection positions during and after irradiation. Two detectors were used simultaneously at two detection positions, transferring along the delay line piping. Lists of magnetic disks recording gamma-ray measurement data are shown in Appendix B.

Delayed neutron (DN) measurement was conducted for 1 ∿ 5 min counting time during normal loop operation. In the case of measurement of DN count rate variation with elapsed time after sodium flow stop or TTR output decrease, DND-1 and DND-2 detectors were counted alternately setting the preset scaler timer at 1 sec, the output DND-1 was also connected to the multi-channel scaler and the signal was measured with counting time of 1 sec.

The main features of each test run is introduced below.

1) Exp. No. 16

With objective to measure deposition behavior of non-volatile FP in sodium, Exp. No. 14 was repeated in Exp. No. 16 with the sodium temperature of 530°C and the flow rate of 1 ℓ/min. Contrary to Exp. No. 14 where sodium was drained immediately after irradiation, sodium circulation was continued still for approximately 20 hrs after irradiation in Exp. No. 16 and the

redistribution possibility of non-volatile FP which deposited once on the wall surface was measured. It is clarified that redistribution of Zr may have occurred, but not for Sr and Y after sodium circulation for at least 20 hrs.

2) Exp. No. 17

The deposition distribution of long lived non-volatile FP released in the irradiation tests up to Exp. No. 16, was measured in Exp. No 17. The gamma-ray counting time is ca. 22 hrs at each detection position. The gamma-rays of Zr-95/Nb-95, Ru-103, Ce-141 were detected.

3) Exp. No. 18

Many kinds of non-volatile FP nuclides are released into sodium by irradiation of uranium fuel: most of them are produced from the beta-decay of precursor nuclides and some of them are directly produced by fission influenced. The deposition behavior of non-volatile FP is readily to the behaviors of precursor nuclides, therefore, direct measurement of deposition behavior of non-volatile FP is difficult. In order to eliminate the influence of precursor nuclides, the circulation of sodium started after decay of precursor nuclides, and the deposition behavior of non-volatile FP was measured. Change of values with elapsed time is shown in Fig. 4-2.(2).

At first stage, the whole loop was kept at 500°C by circulating sodium before irradiation. Immediate before irradiation, the sodium flow was by-passed and the sodium flow inside uranium capsule was stopped. As the preheater capacity of capsule is small, capsule temperature began to drop rapidly but was kept at 280°C constantly after ca. 1 hr, while temperature at other parts of the loop was lowered accompanying with the capsule temperature. The irradiation condition of TTR was at 100 kW power for 2 hrs. Waiting for complete decay of precursor nuclides for 1 hr after

irradiation, then the sodium flow was resumed. The flow suspending time of 1 hr after irradiation was decided considering the half lives of precursor nuclides of non-volatile FP (for example, Ru-103, Ru-105, La-142, Ce-143, etc.) Conditions of resumed sodium flow was the temperature of 280°C and the flow rate of 2 ℓ/min. Gamma-ray measurement was started after restart of sodium flow, but gamma-ray peaks of non-volatile FP that was expected to accumulate in the sodium inside of uranium capsule by irradiation for 2 hrs, was not detected. (Only gamma-ray peaks of Na-24 and of volatile FP, such as Te and I, etc. of long lived, were detected.) As the reason it is conceivable that non-volatile FP nuclides deposit on the surface of irradiation specimen (the surface area of the irradiation specimen is very large) and on the inner surface of uranium capsule, so that they do not transfer up to the gamma-ray detector position. Another reason is that they have small transfer rate. After 17 hrs since the sodium flow had restarted, the flow rate was changed to 5 ℓ/min, but no change was observed in the gamma-ray spectrum. Very weak several gamma-ray peaks of non-volatile FP were detected as a result of the sodium temperature change from 280°C to 500°C another 8 hrs. after. Two reasons are considered why these peaks were observed. One is due to the easier transfer of non-volatile FP from accumulated place in capsule to loop piping by increasing sodium temperature to 500°C. The other reason is that almost all Na-24, which causes the Compton scattering with the gamma-rays, decayed resulting relatively intensified gamma-ray peak of non-volatile FP. The total sodium flow time after irradiation was ca. 40 hrs.

4) Exp. Nos. 19 ∿ 21

Irradiation tests in 1982 were performed taking sodium temperature as parameter and keeping sodium flow at constant rate[1)], but in Exp. Nos. 19-21, the deposition behavior of non-volatile FP was measured mainly taking flow rate as parameter: 530°C and 2 ℓ/min in Exp. No. 19, 170°C and 1 ℓ/min in Exp. No. 20 and 170°C and 5 ℓ/min in Exp. No. 21.

5) Exp. No. 22 and No. 25

Variation of deposition behavior of non-volatile FP owing to temperature gradient produced on the delay line piping was measured. The temperature gradient is produced by switching off all of preheater on the delay line piping. Sodium flow is 1 ℓ/min in both of Exp. No. 22 and No. 25, and the sodium temperature at uranium capsule is 400°C in Exp. No. 22 and 300°C in Exp. No. 25. The temperature difference between inlet and outlet of the delay line piping is 130°C in Exp. No. 22 and 100°C in Exp. No. 25.

Regarding the effect of temperature gradient on deposition behavior of non-volatile FP, further detailed study of each nuclides would be necessary, but little effect was observed for Sr-92 and Sr-94.

6) Exp. No. 23

Correlation between the DN count rate and the TTR power was studied: the DN count rate was measured by increasing the TTR power from 0.1 to 100 kW stepwise, and a good linear relation was obtained (refer Fig. 7-2). It was confirmed that recoil is the main mechanism of FP release and the DN counting system showed linear relationship in wide range.

7) Exp. No. 24

In order to confirm the reproducibility of the test result in 1982, an irradiation test of the same sodium temperature with Exp. No. 11 was conducted. The sodium temperature is 270°C and the flow rate is 5 ℓ/min. In this experiment sodium was drained immediately after irradiation, and adsorbed amount of DN on the inner wall of the delay line piping was tried to measure directly. However, this trial was in failure (refer Sec. 7.5), because much time (ca. 1 min) was necessary to drain sodium completely from the loop piping and DN signals were decayed out.

8) Exp. No. 26

With objective to measure the dependence of DN count rate on sodium flow rate, Exp. No. 10 and No. 13 in 1982 were repeated by changing sodium flow rate stepwise during irradiation. Among the results of tests, DN count rate was the same with the result of previous tests (refer. Sec. 7.2 and Table 7-2 and 7-4), and therefore, it was certified indirectly that no change occurred on the surface of the irradiation specimen loaded in the loop between irradiation test periods (the change of FP release rate from the surface is obtained if any change occurs on the surface). Immediately after the irradiation and the sodium draining, adsorbed amount of DN precousors on the inner wall of piping at high temperature (500°C) was tried to measure directly, but failed for the same reason with Exp. No. 24 (refer Sec. 7.5).

9) Exp. No. 27 and No. 28

They are conducted with objective to measure the deposition behavior of non-volatile FP in sodium with high oxygen concentration. Oxygen concentration in sodium was controlled to ca. 12 ppm (using sodium with cold trap temperature of 200°C)[6]. To the contrary of Exp. No. 27 where sodium was drained immediately after irradiation and the non-volatile FP adsorbed on the inner wall of the loop piping was measured, in Exp. No. 28 the possibility of redistribution of the non-volatile FP, i.e., desorption of FP, which once adsorbed on the inner wall was checked, in high oxygen concentration during sodium circulation for 40 hrs after irradiation, was checked.

Although regarding the dependence of the deposition behavior of non-volatile FP on the oxygen concentration, further detailed study of each nuclides would be necessary, no effect of oxygen concentration was observed for Sr-92 and Sr-94.

Table 4-1 FPL-II Experiments List

Exp. No.	Date	Na Temp (°C)	Na Flow Rate (l/min)	TTR Power (KW)	Duration Time *
1	7. Sep '82	500	5.0	100x4h	0.08 h
2	9. Sep '82	200	5.0	100x4h	0.17 h
3	19. Oct '82	350	5.0	100x4h	0.08 h
4	21. Oct '82	350	5.0	100x4h	0.10 h
5	16. Nov '82	420	5.0	100x4h	0.18 h
6	25. Nov '82	420	5.0	100x4h	0.10 h
7	30. Nov '82	500	5.0	100x4h	0.10 h
8	7. Dec '82	530	5.0	100x4h	0.08 h
9	14. Dec '82	170	5.0/2.0/5.0/0/ 5.0	100x4.38h	19.97 h
10	15. Dec '82	500	5.3/2.5/1.0/ 0.5/1.0/2.5/ 5.0/0/2.5/0/ 1.0/0/4.2/3.6/ 5.0	100x4h	19.72 h
11	16. Dec '82	270	5.0/2.0/5.0	100x4h	1.38 h
12	25. Jan '83	225	5.0/2.0/5.0	100x4h	19.52 h
13	27. Jan '83	500	5.3/4.2/3.6/ 2.5/1.0/0.5/ 1.0/2.5/3.6/ 4.2/5.0/0/2.5/ 0/1.0/0/5.0	100x4h	2.98 h
14	22. Feb '83	530	1.0	100x4h	0.43 h
15	1. Mar '83	300	5.0/2.0/5.0 (IP bypass flow)	100x4h	1.63 h
16	12. Apr '83	530	1.0	100x3.5h	18.47 h
18	20. Sep '83	280 - 500	2.0 - 5.0	100x2h	47.18 h
19	18. Oct '83	530	2.0	100x4h	0.17 h
20	8. Nov '83	170	1.0	100x4h	42.65 h
21	29. Nov '83	170	5.0	100x4h	19.00 h
22	13. Dec '83	400	1.0	100x4h	44.92 h
23	15. Dec '83	500	5.0	0.1/0.2/0.5/1.0 /2.0/5.0/10/20/ 50/70/100x1.58h	- 0.90 h **
24	26. Jan '84	270	5.0	100x4h	0.00 h
25	31. Jan '84	300	1.0	100x4h	19.92 h
26	1. Feb '84	500	5.0/0/2.5/0/ 1.0/0/5.0	100x4h	- 0.07 h **
27	14. Feb '84	500	5.0	100x4h	0.10 h
28	28. Feb '84	500	5.0/0/5.0	100x4h	37.22 h

* Duration time of sodium circulation after TTR shut down

** Sodium drain before TTR shut down

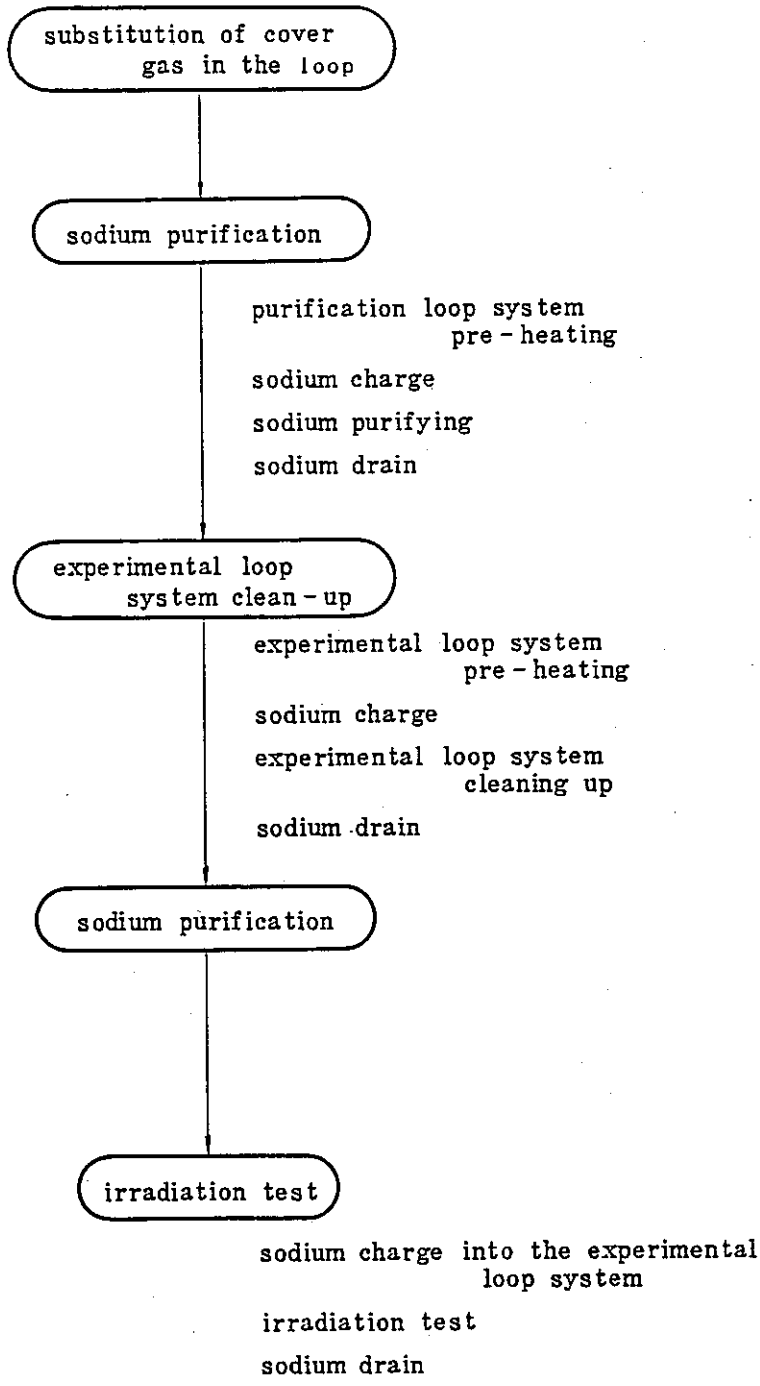

Fig. 4-1 FPL-II Operation Sequence

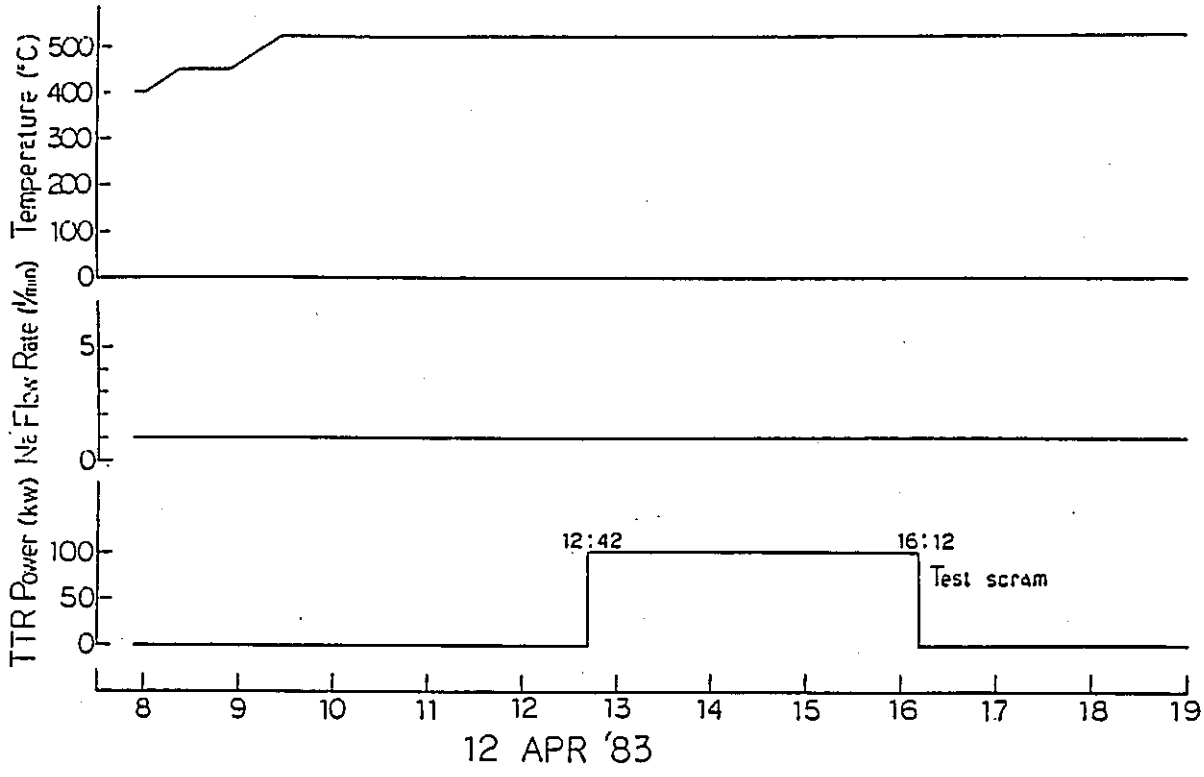

(1) Exp. No. 16

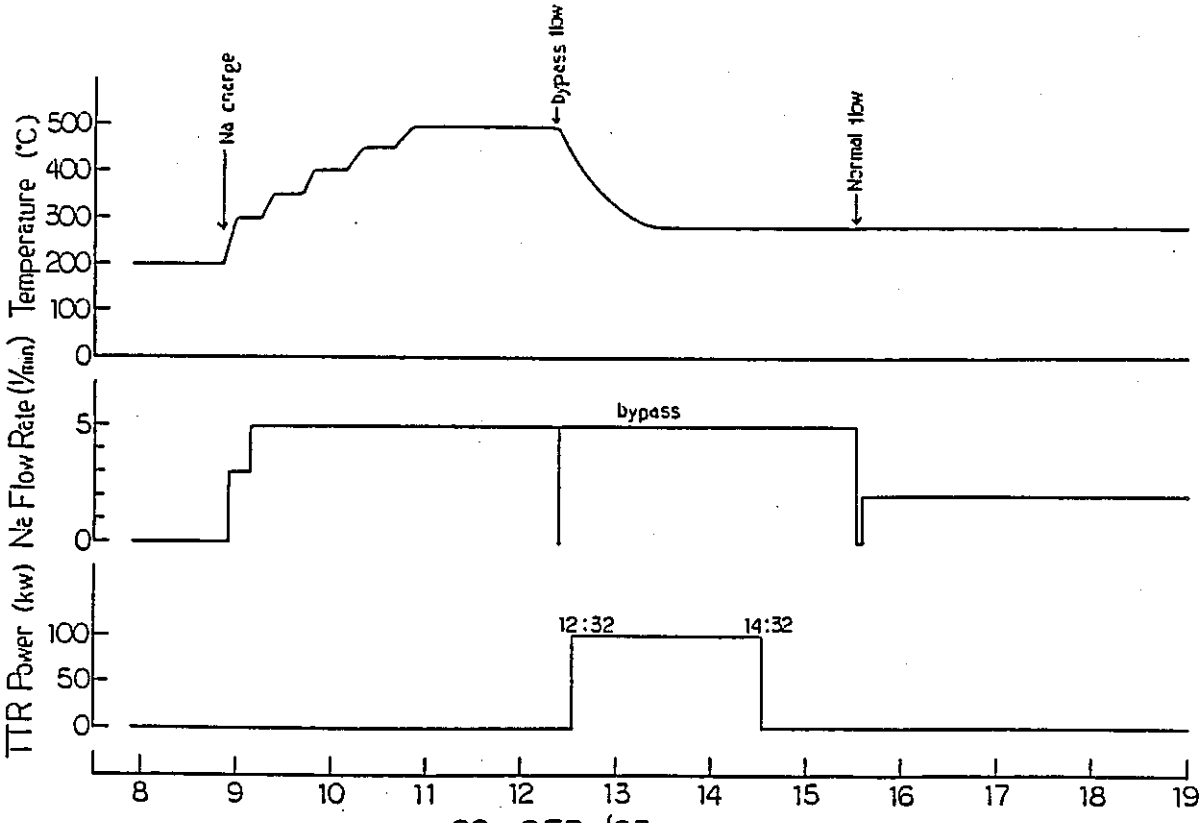

(2) Exp. No. 18

Fig. 4-2 Experimental Condition for Each Experiment

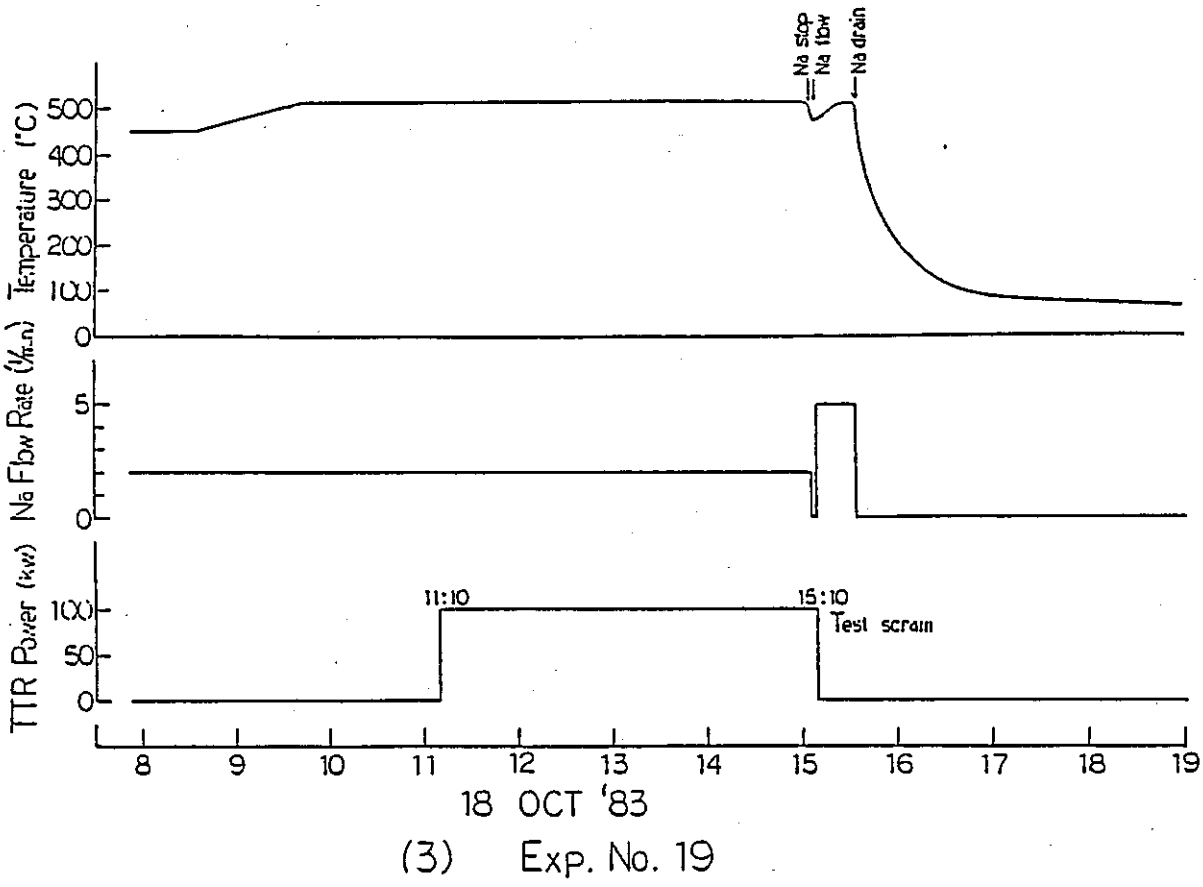

(3) Exp. No. 19

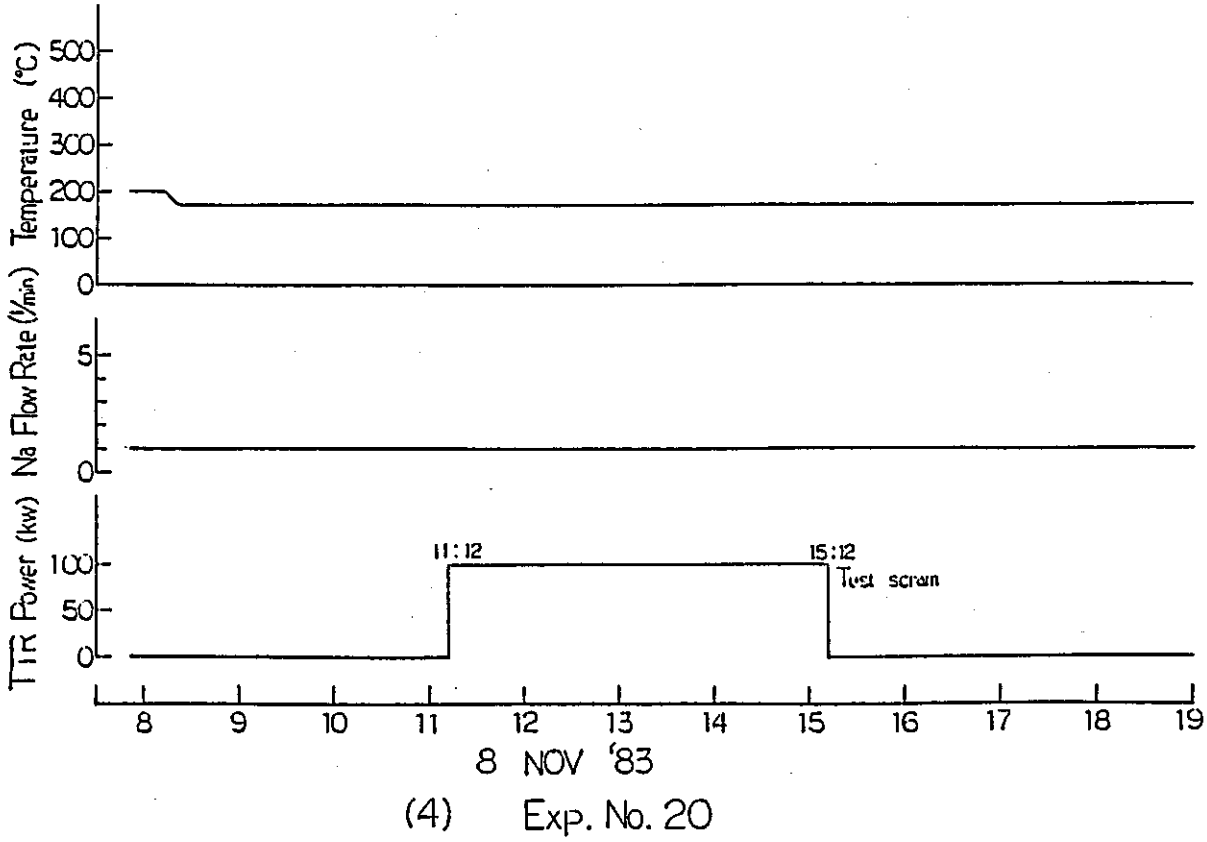

(4) Exp. No. 20

Fig. 4-2 (continued)

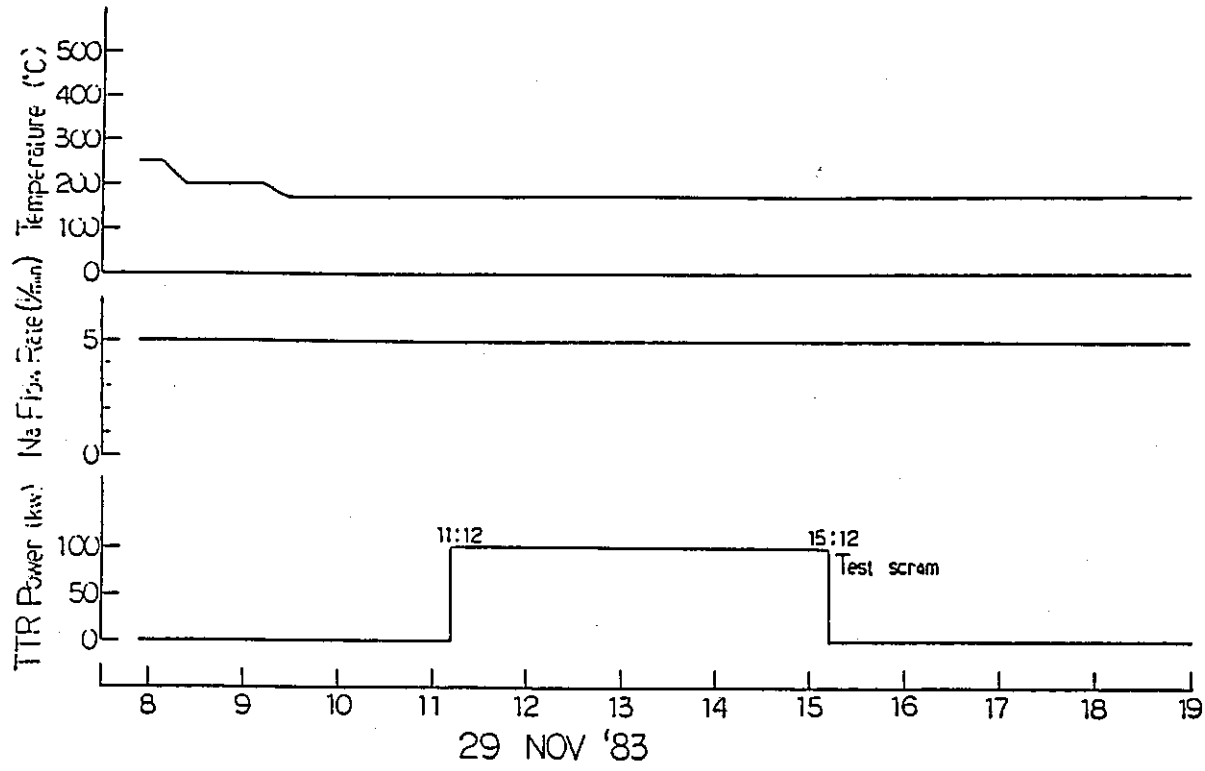

29 NOV '83

(5) Exp. No. 21

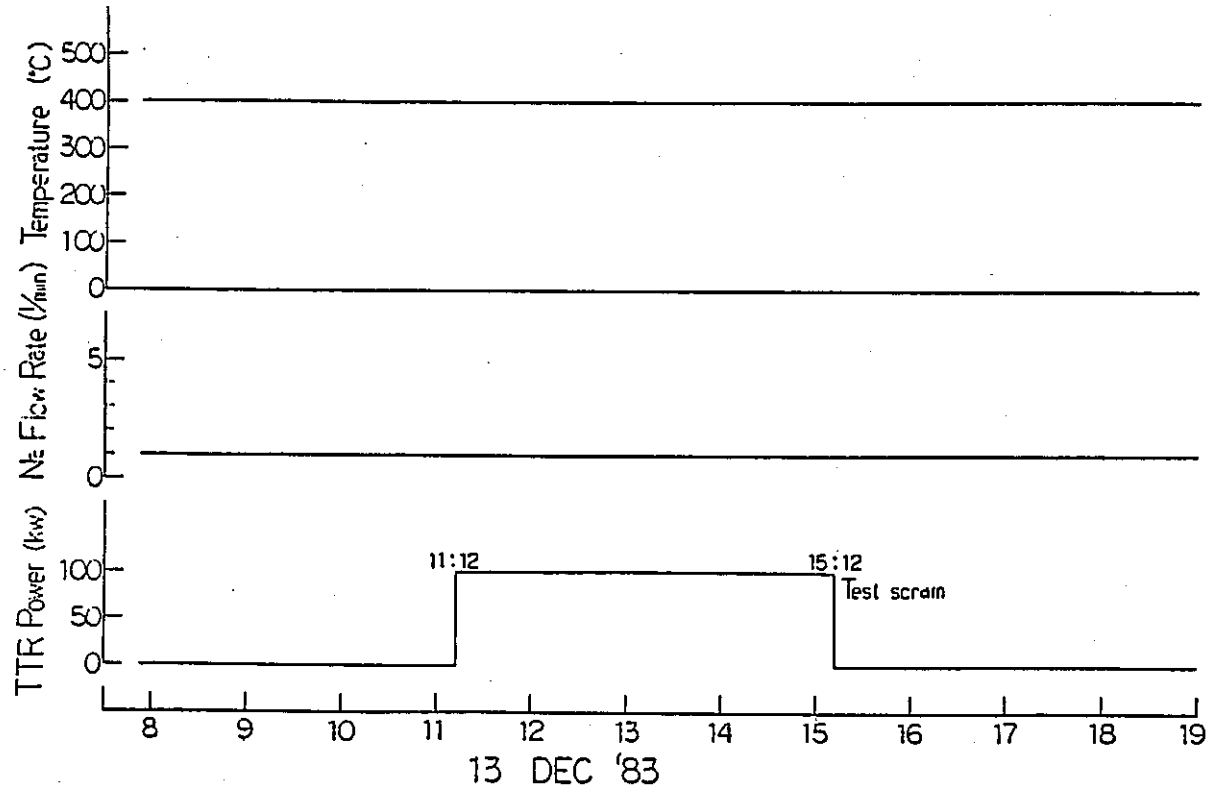

13 DEC '83

(6) Exp. No. 22

Fig. 4-2 (continued)

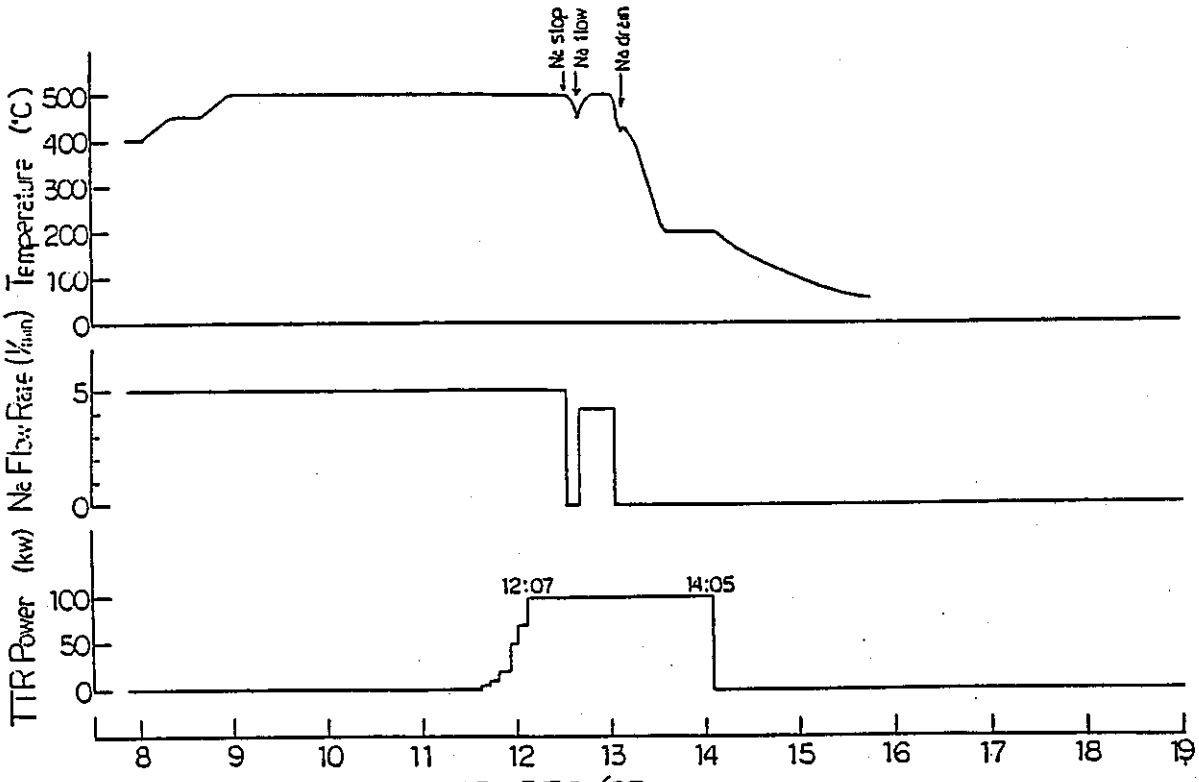

(7) Exp. No. 23

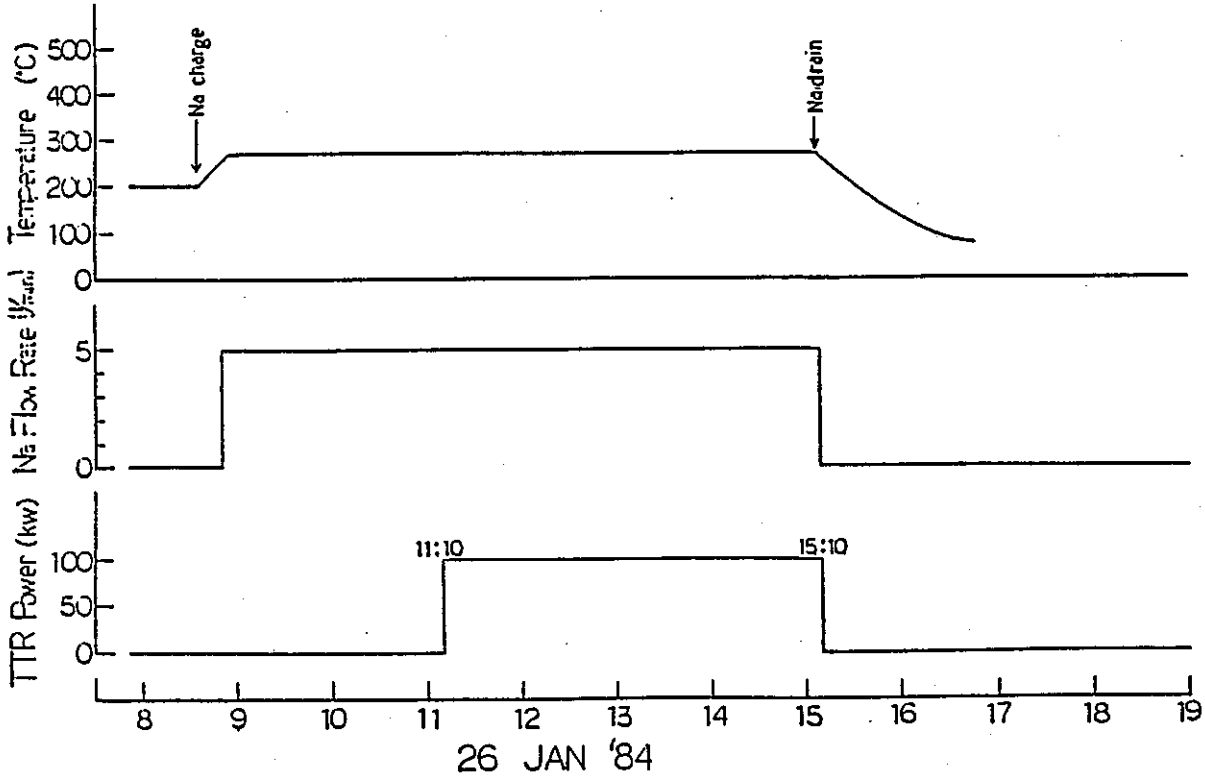

(8) Exp. No. 24

Fig. 4-2 (continued)

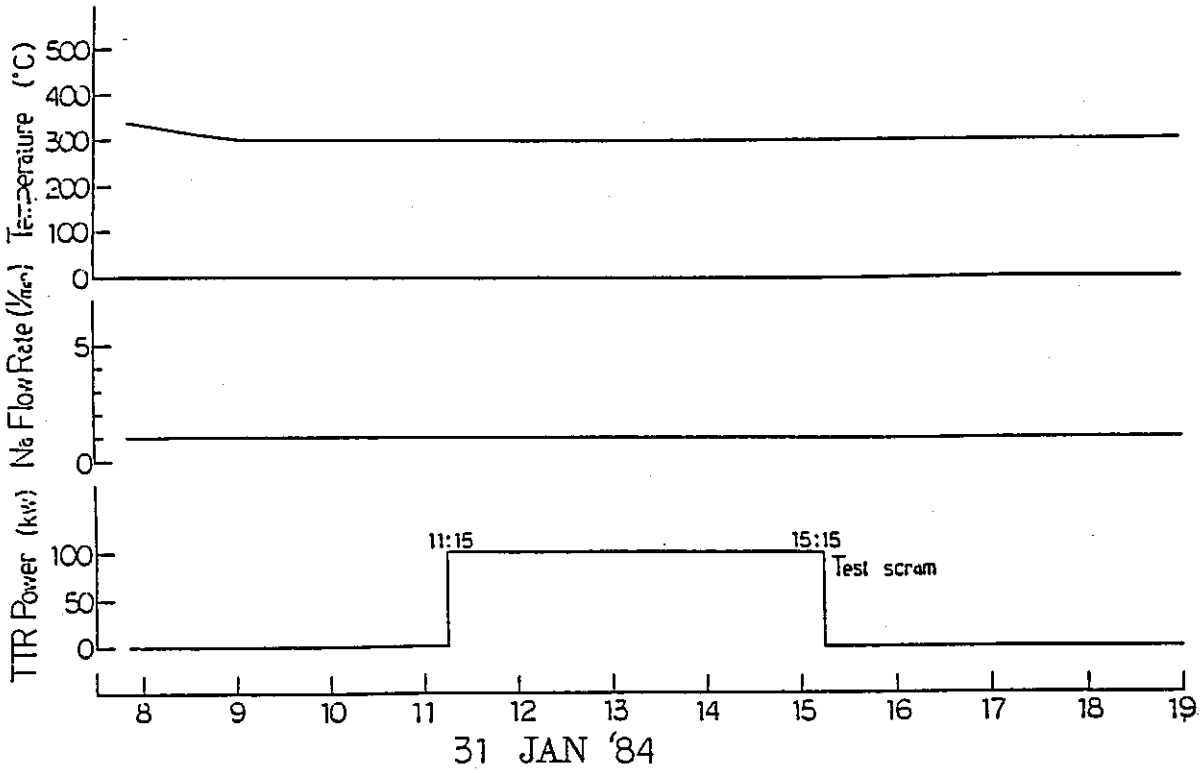

31 JAN '84

(9) Exp. No. 25

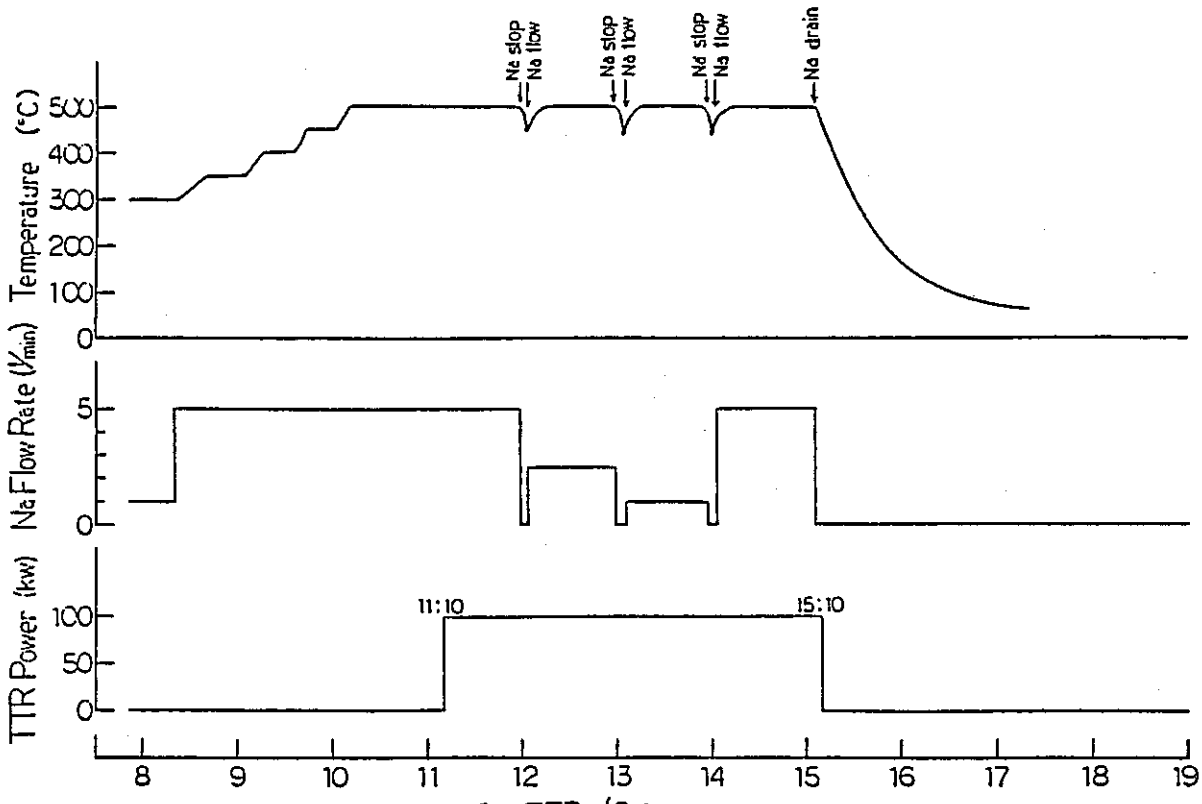

1 FEB '84

(10) Exp. No. 26

Fig. 4-2 (continued)

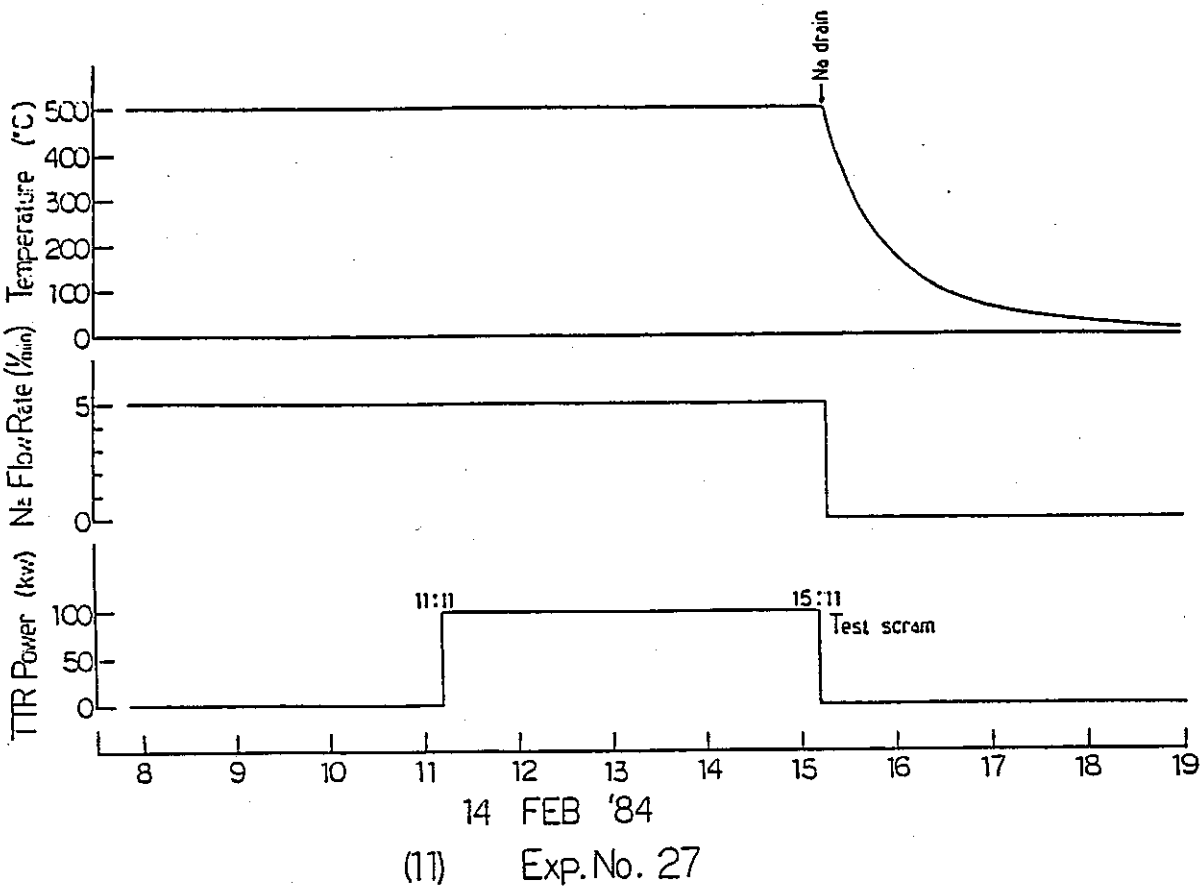

14 FEB '84

(11) Exp. No. 27

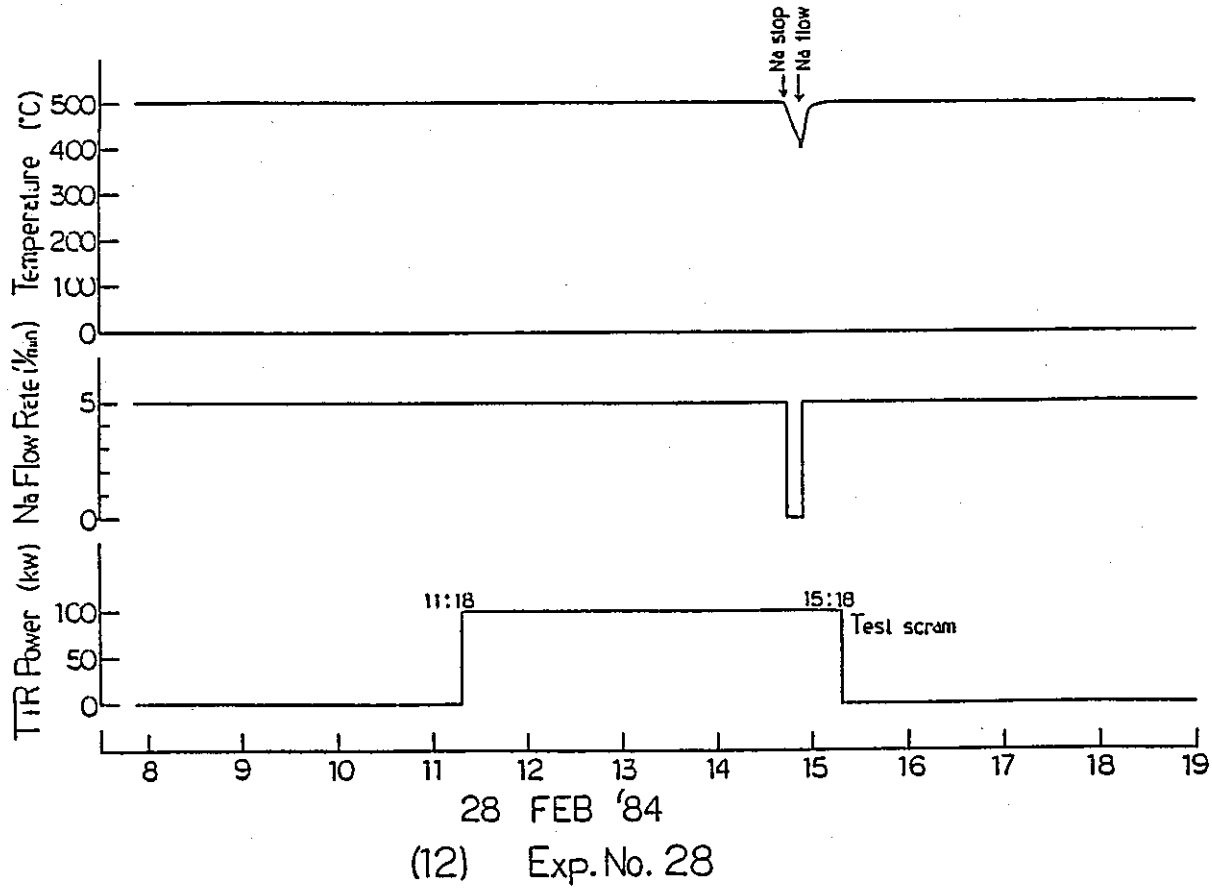

28 FEB '84

(12) Exp. No. 28

Fig. 4-2 (continued)

5. ANALYSIS OF DEPOSITION BEHAVIOR OF NON-VOLATILE FP

5.1 Measurement of Gamma-Ray Spectra

The gamma-ray spectra were measured along the delay line during and after irradiation. The gamma-ray spectra of 800 to 1500 keV measured at two cases, i.e. (i) during irradiation and (ii) immediately after sodium drain which was conducted 10 min after irradiation, are shown in Fig. 5-1.

The experimental conditions: sodium temperature is 500°C, flow velocity is 1.2 m/sec and the detection position is D-2. Range of gamma-ray spectrum measurement is 0 to 2000 keV.

In the spectra shown in Fig. 5-1(a), peaks of Na-24 at 1368.5 keV and 2753.9 keV are clearly recognized. Though the background is relatively high owing to the Compton scattering, the gamma-ray peaks of volatile FP nuclides, such as Br-88 (775.2 keV), Rb-89 (1031.9, 1248.1 keV), Kr-90 (1118.7 keV), Rb-90 (831.7 keV), Rb-94 (836.9 keV), Sb-132 (973.9 keV), I-134 (847.0, 884.1 keV), I-136m (1313.0 keV), I-137 (1218.6 keV) and Cs-138 (1453.9 keV) and peaks of non-volatile FP nuclides, such as Sr-92 (1383.9 keV), Sr-93 (875.9 keV), Sr-94 (1428.3 keV) and Y-94 (918.8 keV) are clearly detected (7).

On the other hand, in the specra shown in Fig. 5-1(b), FP nuclides of short half life is not detected because of the radioactive decay. The gamma-ray peaks of volatile FP with long half lived, such as I-134 (half life 52.5 min) and Cs-138 (half life 32.2 min), also disappear completely as same as Na-24. However, peaks of non-volatile FP nuclides, such as Sr-91 (1024.3 keV), Sr-93 (876.3, 888.3 keV), Y-94 (918.8 keV), Ba-142 (1078.5 keV) and La-142 (894.9 keV), as well as the strong peak of Sr-92 (1383.9 keV) are clearly detected. It means that non-volatile FP nuclides remain depositing on the inner wall of piping after sodium was drained at high sodium temperature of 500°C. The deposition behavior of non-volatile FP was an analyzed using analytical model and the deposition distribution data.

5.2 Analytical Model for Deposition Behavior of Non-Volatile FP

To obtain the deposition behavior of non-volatile FP on the surface of inner wall of stainless steel piping, gamma-ray measurement was conducted at various detection positions along the delay line. In this section, deposition behavior of non-volatile FP in sodium is analyzed by using CP transfer model (4) applied by M. H. Cooper et al.

It is assumed that once FP nuclides deposit on the stainless steel surface, they do not desorb into sodium. Then, the change of FP concentration in sodium C_p (atoms/cm^3) along the direction of flow is expressed as follows.

$$\frac{dC_p(x)}{dx} = -\frac{K_p \cdot (\ell/a) + \lambda_p}{v} C_p(x) \qquad (5\text{-}1)$$

where,

x : distance of sodium flow from irradiated specimen (cm)
v : flow velocity of sodium (cm/sec)
ℓ : inner circumference length of piping ($2\pi r$) (cm)
r : inner radius of piping (cm)
a : flow area (πr^2) (cm^2)
λ_p : radioactive decay constant of nuclide p (sec^{-1})
K_p : deposition velocity constant (cm/sec)

Integrating Eq. (5-1) yields

$$C_p(x) = C_{po} \cdot e^{-\alpha_p \cdot x} \qquad (5\text{-}2)$$

where,

$$\alpha_p = \frac{K_p \cdot (\ell/a) + \lambda_p}{v} \qquad (5\text{-}2a)$$

C_{po} : initial concentration of nuclide p at irradiation section (atoms/cm^3)

After sodium circulates several times in the loop,

$$C_{po} = \frac{P_p}{F \cdot (1 - e^{-\alpha_p \cdot L})}$$

where,

L : total length of loop (cm)

P_p : release velocity from irradiated specimen of nuclide p per unit time (atoms/sec)

F : sodium flow rate (cm^3/sec)

The concentration of nuclide p at wall surface $C_p^W(x,t)$ (atoms/cm^2) is

$$\frac{\partial C_p^W(x,t)}{\partial t} = K_p \cdot C_p(x) - \lambda_p \cdot C_p^W(x,t) \qquad (5\text{-}3)$$

Integrating Eq. (5-3) yields

$$C_p^W(x,t) = \frac{K_p \cdot C_p(x)}{\lambda_p}(1 - e^{-\lambda_p \cdot t}) \qquad (5\text{-}4)$$

where, t is the irradiation time (sec).

As seen in Eq. (5-4), the concentration $C_p^W(x,t)$ is proportional to the concentration in sodium $C_p(x)$. Therefore, the distribution of non-volatile FP in the loop is the expressed by exponential functions against x (distance from irradiated specimen) given by Eqs. (5-2) and (5-4).

α_p is obtained from the gradient of deposition distribution in the loop, and the deposition velocity constant K_p of nuclide p is obtained from Eq. (5-2a).

By the way, because FP nuclides usually contain excess

neutrons compared with stable nuclide, they make beta-decay fission chain. Example stated above is an ideal case of deposition behavior of non-volatile FP where radioactive decay of parent nuclides is negligible and, therefore, it is very rare case. In almost all cases of deposition behavior, the analysis of FP nuclides should be taken into account the decay chain.

However, when the chain is long, the behavior of FP at the last position of the chain is complicately influenced by the precursor nuclides behavior in sodium, and consequently it is difficult to analyze separately. In this section, the decay chains of two nuclides (parent and daughter) only are considered.

When the daughter nuclide is a non-volatile FP, the decay chain is allowable to be separated in two cases depending on that the parent nuclide is volatile or non-volatile.

1) When the parent nuclide is a volatile FP and the sodium temperature is high:

It is the case of Rb-Sr or Cs-Ba. When the half life of parent nuclides is short enough (less than 5 min) compared with the irradiation time, the parent nuclide concentration in sodium attains a radiation equilibrium immediately after irradiation starts. Therefore, when the sodium temperature is high, the parent nuclide, whose adsorption on the stainless steel surface can be neglected, decreases only by the radioactive decay along sodium flow and the following equation is obtained. Where parent and daughter nuclides are expressed by p and d, respectively.

$$\frac{d\,C_p(x)}{d\,x} = -\frac{\lambda_p}{v} C_p(x)$$

where,

$$C_p(x) = C_{po} \cdot e^{-\beta_p \cdot x}$$

where,

$$\beta_p = \lambda_p / v$$

$$C_{po} = \frac{P_p}{F \cdot (1 - e^{-\beta_p \cdot L})}$$

For the daughter nuclide, the following equation is obtained,

$$\frac{dC_d(x)}{dx} = -\frac{K_d \cdot (\ell/a) + \lambda_d}{v} C_d(x) + \frac{\lambda_p}{v} C_p(x) \qquad (5\text{-}5)$$

Solving the equation,

$$C_d(x) = \frac{C_{po} \cdot \beta_p}{\alpha_d - \beta_p} (e^{-\beta_p \cdot x} - e^{-\alpha_d \cdot x}) + C_{do} \cdot e^{-\alpha_d \cdot x} \qquad (5\text{-}6)$$

where,

$$\alpha_d = \frac{K_d \cdot (\ell/a) + \lambda_d}{v}$$

$$C_{do} = \left\{ \frac{C_{po} \cdot \beta_p}{\alpha_d - \beta_p} (e^{-\beta_p \cdot L} - e^{-\alpha_d \cdot L}) + \frac{P_d}{F} \right\} / (1 - e^{-\alpha_d \cdot L})$$

Pd: release velocity from irradiated specimen of nuclide d per unit time (atoms/sec)

The concentration of daughter d at wall surface $C_d^W(x,t)$ (atoms/cm^2) is

$$\frac{\partial C_d^W(x,t)}{\partial t} = K_d \cdot C_d(x) - \lambda_d \cdot C_d^W(x,t) \qquad (5\text{-}7)$$

Integrating Eq. (5-7) yields

$$C_d^W(x,t) = \frac{K_d \cdot C_d(x)}{\lambda_d} \left(1 - e^{-\lambda_d \cdot t}\right) \tag{5-8}$$

This indicates that the $C_d^W(x,t)$ is proportional to $C_d(x)$, but the distribution of daughter nuclide in the loop does become exponential.

2) When the parent nuclide is a non-volatile FP:

The behavior of daughter nuclide is more complicated, because the deposition behavior of parent nuclide can not be neglected. The distribution of parent nuclide in the loop is, according to Eqs. (5-2) and (5-4)

$$C_p(x) = C_{po} \cdot e^{-\alpha_p \cdot x} \tag{5-2b}$$

$$C_p^W(x,t) = \frac{K_p \cdot C_p(x)}{\lambda_p} \left(1 - e^{-\lambda_p \cdot t}\right) \tag{5-4b}$$

As for daughter nuclide, according to Eqs. (5-5) and (5-7)

$$\frac{dC_d(x)}{dx} = -\frac{K_d \cdot (\ell/a) + \lambda_d}{v} C_d(x) + \frac{\lambda_p}{v} C_p(x) \tag{5-9}$$

$$\frac{\partial C_d^W(x,t)}{\partial t} = K_d \cdot C_d(x) - \lambda_d \cdot C_d^W(x,t) + \lambda_p \cdot C_p^W(x,t) \tag{5-10}$$

Integrating these equations yields,

$$C_d(x) = \frac{C_{po} \cdot \beta_p}{\alpha_d - \alpha_p} \left(e^{-\alpha_p \cdot x} - e^{-\alpha_d \cdot x} \right) + C_{do} \cdot e^{-\alpha_d \cdot x} \qquad (5\text{-}11)$$

$$C_d^W(x,t) = \frac{K_p \cdot C_p(x) + K_d \cdot C_d(x)}{\lambda_d} \left(1 - e^{-\lambda_d \cdot t} \right) + \frac{K_p \cdot C_p(x)}{\lambda_p - \lambda_d} \times \left(e^{-\lambda_p \cdot t} - e^{-\lambda_d \cdot t} \right) \qquad (5\text{-}12)$$

When the parent nuclide is non-volatile FP, the concentration of daughter nuclide in sodium is not proportional to that on wall surface.

However, when the parent nuclide is non-volatile FP which half life is more than 1 min, and the independent fission yield of daughter nuclide is very small compared to that of parent nuclide, such as less than 5%, the deposition distribution of daughter nuclide is concluded as almost same with that of parent nuclide. The conclusion holds only in the case that the deposited FP on wall surface is never desorbed and the daughter nuclide also remains on the wall surface being not desorbed. FP chains composed of Sr-92/Y-92, Sr-94/Y-94, Zr-97/Nb-97, Ba-142/La-142 etc. are belong to this case.
In the case of Sr-94/Y-94, for instance, though the behavior of Sr-94 alone can be obtained, being assumed that Y does not desorb from the wall surface, the deposition behavior of parent nuclide Sr-94 can be also obtained from the deposition distribution of Y-94 in the loop.

For the following explanation, the case of Ba-142/La-142 is selected. Even if K_d=0 (means that the nuclide does not deposit), it was assumed that the daughter nuclide on wall surface does not dissolve into sodium and remains on wall surface.

In order to estimate the deposition distribution of daughter nuclide for K_d value, putting K_p=0.04 (the deposition rate constants of Sr and Ba are in this order) and the irradiation

time of 4 hrs (same value to the irradiation test), the $C_d^W(x,t)$ value after irradiation was calculated from Eq. (5-12) taking K_d as parameter for the decay chain of Br-142 and La-142. The result together with $C_p^W(x,t)$ value of parent nuclide is shown in Fig. 5-2.

In Table 5-1, $C_d^W(x,t)$ values are indicated at x=500, 1500 and 3000 in the region of gamma-ray detection (x=627 ∿ 3033 cm) and at x=5734 cm of the loop end position

Consequently, it was clarified as follows:

① At $K_d=0$, the deposition gradient of C_d^W is in good agreement with gradient of C_p^W (ratio of C_d^W/C_p^W is constant and independent of x).

② At $K_d \geqq K_p$ (where $K_d=0.04$ and 0.1), the ratio of C_d^W/C_p^W varies within 2% through the whole loop.

③ The ratio of C_d^W/C_p^W at x=500 varies within 2% for the K_d value variation of 0 ∿ 0.1

④ The ratio of C_d^W/C_p^W at x=1500 varies within 4% for the K_d value variation

⑤ The ratio of C_d^W/C_p^W at x=3000, taking $K_d=0.04$ ($=K_p$) as standard, varies by 18% (max.) for $K_d=0.001$ and varies by 8% for $K_d=0.02$.

For reference, similar calculation was conducted, varying $K_p=0.03$, 0.02 and 0.01. The obtained conclusions are as follows.

⑥ The variation width of C_p^W/C_d^W ratio at x=500, that tends to increase as K_p decreases, shows 6% max for K_d variation ($K_d=0$∿0.1) at $K_p=0.01$.

⑦ The variation width of C_p^W/C_d^W ratio at x=1500 is within 4%, independent of K_p value.

⑧ The variation width of C_p^W/C_d^W ratio at x=3000, that tends to decrease as K_p decreases, shows 10% max at K_p=0.03 and decreases to 5% at K_p=0.01

From the analytical results, C_p^W/C_d^W ratio shows almost constant value independent of K_d value in the region of gamma-ray detection positions in the case of Ba-La decay chain.

When conditions from (i) through (iii) are satisfied,

(i) the parent nuclide is non-volatile FP which half life is longer than 1 min

(ii) the independent nuclear fission yield of daughter nuclide is less than 5% that of parent nuclide, and

(iii) the daughter nuclide, which was produced by radiation decay of parent nuclide deposited, does not desorb,

the deposition distribution of daughter nuclide represents that of parent nuclide.

5.3 Analysis of Deposition Behavior of Sr

1) Discussion of measurable Sr isotope

The radioactive isotopes of Sr are Sr-87m, Sr-89, Sr-90, Sr-91, Sr-92, Sr-93, Sr-94, Sr-95, Sr-96, Sr-97, Sr-98, Sr-99.

Among them, since Sr-87m, Sr-89 and Sr-90 have long half lives and do not emit gamma-ray or have low gamma branch ratio, gamma-ray is not detectable. Since Sr-91, Sr-92, Sr-93 and Sr-94 have high nuclear fission yield and emit gamma-ray with high branch ratio and no other strong gamma-ray peak of other

FP exist around there, the deposition behavior of Sr is easily detected. Since Sr-95, Sr-96, Sr-97, Sr-98 and Sr-99 have low nuclear fission yield and short half lives, gamma-ray is difficult to detect. Therefore, the deposition behaviors of Sr-91, Sr-92, Sr-93, and Sr-94 were analyzed, especially Sr-94 is readily analyzed being little influenced by precursor nuclides. So, the deposition behavior of Sr-94 is described at first.

2) Deposition behavior of Sr-94

Sr-94 emits very strong gamma-ray of 1428.3 keV.[2] Using this peak, the deposition behavior of Sr-94 was analyzed.

As Sr-94 has the half life of 74.1 sec, it decays in a little more than 10 min after irradiation. For the analysis of the deposition behavior of Sr-94, the gamma-ray spectrum during irradiation was used, where 12 irradiation tests (Exp. Nos. 2, 3, 4, 5, 6, 7, 8, 9, 11, 12, 14 and 16) were applied. Exp. Nos. 10, 13, 15 were excluded from the test, because in these tests the sodium flow rate change in short time interval during irradiation. The Sr-94 distribution along the loop obtained by 12 irradiation tests are shown in Fig. 5-3 together with the statistic error. In abscissa, x shows distance from the uranium capsule. In ordinate, count rate (cps) is expressed, where the count rate is corrected by the geometric correction at positions D-2 to D-9 in Table 5-2 and by the correction of gamma-ray detection efficiency.

However, the correction of radioactive decay is not necessary, because Sr-94 has such a short half life of 74.1 sec that the count rate attains a saturated level after ca. 10 min of irradiation.

In Fig. 5-3 the Sr-94 distribution clearly shows an exponential function against the distance. The half lives and fission yields of FP nuclides with mass number of 94 fission chain are indicated below:[7, 8]

	Kr-94 ⟶	Rb-94 ⟶	Sr-94 ⟶	Y-94 ⟶	Zr-94
half life:	0.20 sec	2.73 sec	74.1 sec	19.0 min	(stable)
fission yield (%):	0.26	1.60	4.15	0.39	

From these FP chain data, it is clear that K-94 and Rb-94, which are precursor nuclides of Sr-94, have short half lives and low fission yields; therefore the deposition behavior of Sr-94 is little influenced by these precursor nuclides and Sr-94 has an exponential distribution.

After fitting the deposition distribution of Fig. 5-3 by least square method, from the gradient, deposition rate constant K (cm/sec), that had been unknown value of analytical model stated in the previous section, was obtained.

A straight line fitted by least square method is also shown in Fig. 5-3, where only 2 detection positions are shown in each Exp. Nos. 2, 9, 11 and 12. But as shown in Exp. No. 3 ∿ No. 8, the Sr-94 distribution indicates an exponential function, so the straight line connecting 2 positions is meaningful and the deposition rate constant K can be obtained from the gradient of the line.

Values of Sr-94 deposition rate constant K at various sodium temperatures and flow velocities are indicated in Table 5-3. Sodium flow velocities were 1.2 m/sec (flow rate 5.0 ℓ/min) in Exp. Nos. 2 ∿ 8, 1.2 m/sec and 0.48 m/sec (2.0 ℓ/min) in Exp. Nos. 9, 11 and 12 and 0.24 m/sec (1.0 ℓ/min) in Exp. Nos. 14 and 16.

Following results were obtained from the analysis:

(i) At constant flow velocity, Sr-94 deposition rate increases with increasing temperature

(ii) At constant temperature, Sr-94 deposition rate increases with increasing flow velocity,

where result (i) is also estimated from the fact that the gradient of deposition distribution increases with increasing temperature in Fig. 5-3 and the result (ii) suggests that the deposition rate constant K is a function of flow velocity. (described in detail in Sec. 5.9). The steeper gradient of the deposition distribution with lowing flow velocity is observed in Fig. 5-3, because the flow velocity v is contained in the denominator of α, which expresses the gradient of deposition distribution. (defined by Eq. (5-2a))

3) Deposition behavior of Sr-92

Sr-92 emits strong gamma-ray with 1383.9 keV. Using the peak, the deposition behavior of Sr-92 was analyzed.

As the half life of Sr-92 is 2.7 hrs, the gamma-ray is detectable for a long time even after irradiation. The data of high S/N ratio is obtained on Sr-92 after irradiation because of the decay of FP nuclides with short half lives. Therefore, the gamma-ray spectra used for the analysis of deposition behavior of Sr-92 were measured when sodium was drained after irradiation. Exceptional cases are Exp. Nos. 14 and 16, where the gamma-ray spectra was measured during irradiation, because the sodium flow velocity was low as 0.24 m/sec (flow rate 1 ℓ/min) and little influence of FP with short half life was expected. The deposition distribution of Sr-92 was calculated using the data of 9 irradiation tests (Exp. Nos. 2, 3, 4, 5, 6, 7, 8, 14 and 16). Exp. Nos. 9, 10, 11, 12, 13 and 15 were excluded from the calculation, because the sodium flow velocity was changed during irradiation. The Sr-92 distribution data of 9 irradiation tests are shown in Fig. 5-4 with statistic error. The abscissa and ordinate are same in Fig. 5-3. The count rate is corrected considering the detection efficiency. Furthermore, since Sr-92 has the long half life, all count rates are subject to correction of decay at the moment just irradiation stop.

As shown in Fig. 5-4, the Sr-92 deposition distribution in the loop at sodium flow velocity of 1.2 m/sec (excluding Exp. Nos. 14 and 16) do not show a linear distribution (exponential function) as Sr-94 shows. (But linear distribution was obtained at sodium flow velocity 0.24 m/sec.) That is owing probably to strong influence of precursor nuclide of Sr-92.

The FP chains mass number of 92 are indicated with half lives and fission yield of FP nuclides.[7, 8]

	Br-92 →	Kr-92 →	Rb-92 →	SR-92 →	Y-92 →	Zr-92
half life:	0.365sec	1.84sec	4.54sec	2.71 hr	3.53 hr	(stable)
fission yield (%):	0.02	1.52	3.31	1.10	0.01	

As seen from the above FP chain data, Sr-92 is produced by direct fission and by radioactive decay from volatile FP of Br-92, Kr-92 and Rb-92, in which nuclide Rb-92 contributes mostly (ca. 81%). When the sodium flow velocity is 1.2 m/sec, Rb-92 (half life: 4.54 sec) decays only 1/2.2 during its transfer of 5.2 sec from uranium capsule to the nearest gamma-ray detection position (D-2), so Rb-92 has large influence on the deposition behavior of Sr-92.

Fitting of experimental data to an analytical model has been done by non-linear least square method using Eqs. (5-6) and (5-8) with K_d as a parameter.

The result was indicated by a solid line in Fig. 5-4, and the values of deposition rate constant K at various sodium temperatures and flow velocities obtained by the analysis are indicated in Table 5-4. The result is in good agreement with experimental data, it is clarified that the analytical model fits with the deposition behavior of Sr-92 in the loop. The K values indicated in Table 5-4 express the deposition behavior of Sr-92 alone entirely eliminating the effect of precursor nuclides. Comparing these values with those of Sr-94 in Table 5-3, good agreements are observed at every sodium temperature

and flow velocity. It is concluded that the deposition behavior of Sr has no isotope effect.

4) Deposition behavior of Sr-93

Though Sr-93 emits many gamma-ray peaks, the deposition behavior of Sr-93 is analyzed by using 2 peaks of 590.2 and 875.9 keV that are hard to be influenced from other FP peaks[7].

As the half life of Sr-93 is 7.5 min, the distribution in the loop is difficult to be measured after irradiation, so the gamma-ray spectra measured during irradiation were used for the analysis of deposition behavior of Sr-93. Exp. Nos. 9, 10, 11, 12, 13 and 15 were conducted varying sodium flow velocity during irradiation, so the deposition behavior of Sr-93 is considered to be influenced by the flow velocity variation. Furthermore, the detection positions are fixed at two places. That the reason why the data of these experiments are not available for the analysis of non-volatile FP, except for the case like Sr-94 where the half life is short and the effect of precursor is negligible.

Exp. No. 2 was also eliminated, because the detection positions are only two fixed places. So, the deposition distribution of Sr-93 in the loop was analyzed using 8 irradiation tests (Exp. Nos. 3, 4, 5, 6, 7, 8, 14 and 18). The results are shown in Fig. 5-5 together with statistic error, where the count rate in ordinate is corrected with detection efficiency and decay.

The deposition distribution of Sr-93 is, similar with that of Sr-92, not exponential function being subject to effect of precursors. The FP chain of mass number 93 is indicated with the half life and the fission yield of FP nuclides[7, 8]:

	Kr-93 ⟶	Rb-93 ⟶	Sr-93 ⟶	Y-93 ⟶	Zr-93
half life:	1.29 sec	5.85 sec	7.5 min	10.2 hr	1.5×10^{6} y
fission yield (%):	0.52	2.97	2.78	0.10	0.0003

As seen above, Sr-93 is mainly produced by the radioactive decay of Rb-93 with the ratio of 3.49:2.78. Fitting of experimental data to the analytical model by the non-linear least square method has been done using Eqs. (5-6) and (5-8) with K_d as a parameter. The result was indicated by the solid line in Fig. 5-5 and the value of deposition rate constant K at various sodium temperatures and flow velocities obtained by the analysis are indicated in Table 5-5. The result is in good agreement with experimental data, though data of 875.9 keV indicate some lower values as a whole. Comparing K values of Sr-93 in Table 5-5 with those of other Sr isotopes, it is found that they are in good agreement mutually at sodium temperatures of 500 and 530°C, both but those of Sr-93 show some higher values at 350 and 420°C.

It is probably due to the interferences of 10∿20% from other FP nuclides gamma-ray peaks to 590.2 and 875.9 keV Sr-93 peaks. When the flow velocity is 0.24 m/sec, the analytical result of 590.2 keV peak is in good agreement with cases of Sr-92 and Sr-94 at the same flow velocity.

5) Deposition behavior of Sr-91

As Sr-91 has the long half life of 9.48 hrs, though its gamma-ray is not clearly detectable during irradiation, many strong peaks are detected after sodium drain or after decay of FPs of short half lives during sodium circulation, after irradiation.

The distribution of Sr-91 in the loop was measured after irradiation using two gamma-ray peaks at 749.8 and 1024.3 keV with high intensity[7]. Distributions in the loop for 749.8 and 1024.3 keV at sodium temperature of 350°C and flow

velocity of 1.2 m/sec (flow rate 5 ℓ/min) in Exp. No. 3 are shown in Fig. 5-6 1) and 2), respectively.

Sr-91 distributes almost homogeneously throughout the loop because of the influence of Rb-91 precursor.

The half life and fission yield of nuclides for mass number 91 in the FP chain are indicated as follows:[7, 8]

	Br-91 ⟶	Kr-91 ⟶	Rb-91 ⟶	Sr-91
half life:	0.54 sec	8.57 sec	58.7 sec	9.84 hr
fission yield (%):	0.42	3.09	2.23	0.17

As seen from these data, Sr-91 is mostly produced by radioactive decay of Rb-91 with ratio of 5.74:0.17. As Rb-91 has a half life of 58.7 sec and does not be adsorbed in piping, a homogeneous distribution of Sr-91 is formed in the loop. When the sodium flow velocity is 1.2 m/sec, the same distribution with Exp. No. 3 was obtained independent of the sodium temperature. Fitting experimental data with the analytical model of non-linear least square method was tried using Eqs. (5-6) and (5-8) with K_d as a parameter, but the solution did not converge.

On the other hand, in the case of Exp. Nos. 14 and 16 where sodium flow velocity is 0.24 m/sec, Rb-91 decays to ca. 1/16 during the time of 239 sec in which sodium circulates through the whole loop (57.4 m length), and therefore Rb-91 has little influence on the system.

Distributions of Sr-91 in the loop obtained in Exp. Nos. 14 and 16 are shown in Figs. 5-6 3), 4), 5) and 6), in which the adopted gamma-ray peak is different. The distributions are similar with those of Sr-92 and Sr-93 at flow velocity of 1.2 m/sec.

By analyzing the deposition behavior using Eqs. (5-6) and (5-8), analytical results are shown in Figs. 5-6 3), 4), 5) and 6) by solid lines, and obtained values of deposition rate constant K of Sr-91 at sodium flow velocity of 0.24 m/sec are described in Table 5-6. Though the measured values show some scattering to the analytical results, the fitting seems in a tolerable range. Despite some higher values in Exp. No. 14 than those in Exp. No. 16, the K value of Sr-91 at flow velocity of 0.24 m/sec is in good agreement with those of Sr-92, Sr-93 and Sr-94 at the same condition; therefore, no difference of deposition behaviors are indicated among isotopes.

The present analytical model has an assumption that the deposited non-volatile FP nuclides on stainless steel surface never desorb again. In order to confirm if desorption occurs, Exp. No. 16 was conducted and measured variation of count rate (corrected value by the decay factor) of gamma-ray peak during sodium circulation for ca. 20 hrs after irradiation. No variation of count rate with elapsed time was observed. (refer Fig. 5-6)

Count rate of Sr-91 in Exp. No. 14 was compared with that in Exp. No. 16. The experimental condition of Exp. No. 14 is identical with that of Exp. No. 16 except that sodium was drained right after the irradiation. After correction of difference of irradiation time in both experiments, almost same count rate were obtained. Thus, it is concluded that no desorption of Sr-91 occurred at least during sodium circulation of 20 hrs.

5.4 Analysis of Deposition Behavior of Y

1) Discussion of measurable Y isotope

What are mentioned as radioactive isotopes of Y are Y-89m, Y-90m, Y-90, Y-91m, Y-91, Y-92, Y-93, Y-94, Y-95, Y-96, Y-97m, Y-97, Y-98, Y-99 etc. Among them, Y-89m to Y-91 are not

suitable for the analysis of deposition behavior, because they do not emit gamma-ray or emit gamma-ray only with low branch ratio and have low independent fission yield owing to their late location in the FP chain.

Y-92 to Y-95 nuclides have long half lives and emit gamma-ray with high branch ratio. However, because Y nuclides are daughter nuclides of Sr that have strong deposition affinity and Y nuclides themselves also indicates the same trend, the deposition distribution obtained by using their gamma-ray peaks is probable to be that of parent nuclide instead.

In order to confirm the probability, an analysis was tried using gamma-ray data of Y-92 and Y-94, which show clear gamma-ray peaks. The result is stated in the following sections.

On the other hand, Y-96 appeared to be suitable to measure the deposition behavior of Y, because it locates at the head of FP chain showing high independent nuclear fission yield and having a peak at 1750.7 keV with high branch ratio[7]. But experimentally, the gamma-ray peak at 1750.7 keV was too weak to detect, so the distribution was not analyzed. Regarding Y-97m to Y-99, owing to their location at the top of FP chain, nuclear fission yields decrease again and the production is suppressed and, furthermore, the half life is short as less than 4 sec, no peak was detected in the gamma-ray measurement.

As a conclusion, the deposition behavior of Y alone is difficult to analyze. As explained above, results of gamma-ray measurements of Y-92 and Y-94 are shown as follows for reference.

2) Result of gamma-ray measurement of Y-92

Y-92 has, as shown in FP chain data of Sr-92 paragraph, very low fission yield as 0.01%. Since Sr-92, the parent nuclide of Y-92, has a long half life of 2.7 hrs, the distribution of

Y-92 obtained by the gamma-ray measurement represents the distribution behavior of Sr-92. As Y-92 emits strong gamma-ray at 934.5 keV and has a long half life of 3.5 hrs, the distribution of Y-92 in the loop was measured using the gamma-ray spectrum with high S/N ratio after irradiation. 9 irradiation tests (Exp. Nos. 2, 3, 4, 5, 6, 7, 8, 14 and 16) were adopted for the analysis.

The distribution of Y-92 obtained by the gamma-ray measurement together with the statistic error is shown in Fig. 5-7. The error is considerably large compared with the case of Sr-92, but the distribution in the loop is very similar to that of Sr-92. Here, the count rate is corrected by considering the produced amount of Sr-92 and decreased amount of Y-92 due to the radiation decay, besides by the detection efficiency due to the position.

When the distribution of Y-92 obtained by the gamma-ray measurement is regarded as the distribution of Sr-92 in the loop, the deposition rate constant was obtained by the analytical method mentioned above. Result of fitting is expressed by solid lines in Fig. 5-7 and K values are in Table 5-7.

By comparing these K values and those obtained from the distribution of Sr-92, it was found that the former values (K values obtained from Y-92) indicate 10% higher at the flow velocity of 1.2 m/sec than those of Sr-92. Reversely the K values become lower at flow velocity of 0.24 m/sec. But within 10% of experimental error, both values are in good agreements and it was concluded that the distribution of Y-92 represents deposition distribution of Sr-92.

One of other important things in estimating the deposition behavior of non-volatile FP, is the probability of redistribution of FP, i.e. whether once deposited FPs on stainless steel surface would desorb again or not. Having relatively high half life of 3.5 hrs and being influenced by

production from Sr-92 with half life of 2.7 hrs, the gamma-ray peaks of Y-92 are detectable for considerable time even after irradiation.

In Exp. No. 16, the variation of count rate of Y-92 with elapsed time was measured during sodium circulation for 20 hrs after irradiation. No variation was observed. And the count rates were compared between Exp. No. 14 and Exp. No. 16, as did in the case of Sr-91, and consistence of both experimental results was observed. From these facts it was concluded that Y-92 does not desorb during sodium circulation for 20 hrs at least.

3) Result of gamma-ray measurement of Y-94

By the same reason with Y-92, it is explained that the distribution of Y-94 in the loop represents that of Sr-94, precursor of Y-94, by experimental data.

In the experiment, using the strong gamma-ray peak of Y-94 at 918.8 keV,[7] the distribution of Y-94 in the loop was measured in 9 irradiation tests (Exp. Nos. 2, 3, 4, 5, 6, 7, 8, 14 and 16).

The distribution of Y-94 in the loop obtained by gamma-ray measurement is shown in Fig. 5-8 together with the statistic error. Though some fluctuations of data are observed, a distribution with exponential function is recognized.

Regarding the distribution of Y-94 obtained by the gamma-ray measurement is identical with that of Sr-94, the deposition rate constant was obtained by the above mentioned method, as shown in Table 5-8. Comparing these K values with those measured from deposition distribution of Sr-94, good agreement within 10% was obtained. From these results, it was concluded that the deposition distribution of Y-94 represents that of Sr-94. Here, the desorption of Y-94 during sodium circulation for long time after irradiation was not confirmed.

5.5 Analysis of Deposition Behavior of Zr

1) Discussion of measurable Zr isotope

Among FP nuclides, as Zr isotope Zr-93, Zr-95, Zr-97, Zr-98, Zr-99, Zr-100, Zr-101 etc. exist. Among them, having very long half life of 66.5 days, Zr-95 gamma-ray with strong intensity was detected in FBR experimental reactors such as EBR-II and BOR-60.[2]

In FPL-II, a gamma-ray peak of Zr-95 was detected after draining sodium, but it was not used for the analysis of deposition behavior because of the low intensity. Regarding other radioactive isotopes, except Zr-97, owing to short half life and no gamma-ray emission or small gamma branch ratio, no data were obtained available for the analysis of deposition behavior.

2) Deposition behavior of Zr-97

Zr-97 is a daughter nuclide of Y-97. The half life and fission yield of nuclides of mass number 97 composing FP chain are indicated:[7, 8]

	Rb-97 ⟶	Sr-97 ⟶	Y-97 ⟶	Zr-97 ⟶	Nb-97
half life:	0.172sec	0.40sec	3.70sec	16.8hr	72.2min
fission yield (%):	0.03	1.73	3.18	1.00	0.01

As seen from these data, Zr-97 is mostly produced at the ratio of 4.94:1.00 by radioactive decay of Y-97, parent nuclide of Zr. Since the half life of Y-97 is comparatively short as 3.7 sec, a certain amount of Zr-97 is produced until sodium arrives at a gamma-ray detection position from the irradiation specimen. Therefore, being different from cases of Y-92 and Y-94, the distribution of Zr-97 in the loop is a combination of deposition behaviors of parent nuclides of Y-97 and Zr-97. From the distribution, using Eqs. (5-11) and (5-12), fitting of analytical model has been done with K_p and K_d parameters by

non-linear least square method, and the deposition rate constants of Y-97 and Zr-97 are obtained at the same time.

From above described data of FP chain, Zr-97 deposition distribution in the loop was obtained using the gamma-ray spectrum, which was obtained at sodium drainage immediately after irradiation with good S/N ratio due to its half life of 16.8 hrs. The deposition distribution of Zr-97 was measured in 9 irradiation tests (Exp. Nos. 2, 3, 4, 5, 6, 7, 8, 14 and 16). The results are shown with statistic error in Fig. 5-9. Values of deposition rate constants of Y-97 and Zr-97 are indicated in Table 5-9. The statistic error is not so high.

Result of fitting was in good agreement with experimental data. Comparing obtained K values of Y-97 and Zr-97 with the value of Sr, followings are clarified:

(1) Deposition rate constant of Y-97 is in fairly good agreement with that of Sr, except at 200°C,

(2) Deposition rate constant of Zr-97 is almost independent of temperature in the range of 200 and 530°C and indicates 2.2×10^{-2} cm/sec at sodium flow velocity of 1.2 m/sec.

As seen from these results, Y deposits on stainless steel surface with the same mechanism of Sr. However the deposition mechanism of Zr is different from that of Sr and Y.

As described in Paragraphs of Sr-91 and Y-92, in the case of non-volatiles FP of long half life, the desorption from the stainless steel surface can be checked by the sodium circulation for a long time even after irradiation. Now we discuss the test results of Zr-97 in Exp. No. 16, which gamma-ray peak of 743.4 keV incidentally overlaps with the gamma-ray peak of volatile FP nuclides such as Te-134, so the variation of count rate of Zr-97 gamma-ray peak with time was not measured during dissolved volatile FPs are circulating

with sodium. Consequently, the results of Exp. No. 14 and No. 16 were compared, which were performed at the same irradiation conditions except irradiation time and sodium circulation time after irradiation. Exp. No. 16 showed higher value of count rate by 50% than Exp. No. 14, but the irradiation time was lower by 13%.

It was speculated from these results that a part of Zr-97, having deposited on the inner surface upstreamside of the piping, might desorb and flow to downstreamside along with sodium circulation after irradiation and possibly might deposit again. Here, the deposition rate constant defined in Eq. (5-1) is considered to express the resultant of elementary reactions, such as diffusion, adsorption and desorption, in the deposition process of FP on the inner wall surface.

Because the effect of desorption is already contained in the Zr-97 deposition rate constant, the estimation of Zr deposition amount on piping in FBR plant can be made by using the Zr-97 deposition rate constant obtained by FPL-II irradiation test. Also, because the effect of desorption on deposition rate constant is large, the temperature dependency of rate constant of Zr-97 shows a quite different trend from that of Sr.

5.6 Analysis of Deposition Behavior of Nb

1) Discussion of measurable Nb isotope

Nb radioactive isotope for FP nuclides are Nb-93m, Nb-95, Nb-95m, Nb-97m, Nb-97, Nb-98m, Nb-98, Nb-99m, Nb-99, Nb-100, Nb-101, Nb-102, Nb-104, Nb-105 etc.

Among them, Nb-95 nuclide has a long half life as 36.5 days and is a decay product from Zr-95 with long half life, so it is detected with high intensity in the experimental reactor stated above. In FPL-II, the peak of Nb-95 is detected at long counting time measurement after irradiation but too weak

to use it for the analysis of deposition behavior. Regarding other isotopes, except Nb-97, distributions in the loop were not observed because of their short half life, no gamma-ray emission or low gamma branch ratio. Regarding Nb-97, owing to its high gamma branch ratio, gamma-ray emission was detected with high intensity after irradiation. So, result of gamma-ray measurement of Nb-97 is described below.

2) Result of gamma-ray measurement of Nb-97

Nb-97 emits a strong gamma-ray at 657.9 keV.[7] As Nb-97 has half life of 72.2 min and is produced mostly by decay of Zr-97, using gamma-ray spectrum with good S/N ratio obtained after draining sodium after irradiation, the distribution of Nb-97 in the loop was measured in 9 irradiation tests (Exp. Nos. 2, 3, 4, 5, 6, 7, 8, 14 and 16). Distribution of Nb-97 together with statistic error is shown in Fig. 5-10.

As for Exp. No. 16, the Nb-97 distribution in the loop was obtained based on result of gamma-ray measurement during sodium circulation after irradiation, but Nb-97 was distributed homogeneously in the loop (Fig. 5-10) and any distinct deposition behavior was not indicated. No volatile FP nuclides which interfere Nb-97 peaks exist in flowing sodium and that the gamma-ray peak at 657.9 keV comes from Nb-97. Therefore it is concluded that Nb is dissolved in sodium and distributed homogeneously in the loop.[7]

But as seen from Fig. 5-10, Nb-97 shows the similar deposition distribution in loop to Zr-97 in tests except Exp. No. 16. It comes from the fact that the sodium in the loop was drained immediately after irradiation in these tests and the radiation equilibrium of Nb-97 with Zr-97 is attainable in a short time (ca. 3 hrs after draining sodium) because of the short half life of Nb-97 compared to that of Zr-97. Therefore, in Exp. Nos. 2 to 14, the deposition rate constants of Y-97 and Zr-97 were obtained by using the analytical method for Zr-97 and using Nb-97 distribution data along the loop. Result is

indicated in Table 5-10 and result of fitting is shown by solid lines in Fig. 5-10 in which a good agreement with experimental value is indicated.

Comparing K values of Y-97 and Zr-97 obtained from Zr-97 and Nb-97 deposition distribution respectively, they were in good agreement except for Y-97 at 200°C.

5.7 Analysis of Deposition Behavior of Ba

1) Discussion of measurable Ba isotope

Ba radioactive isotopes in FP nuclides are Ba-137m, Ba-139, Ba-140, Ba-141, Ba-142, Ba-143, Ba-144, Ba-145, Ba-146 etc. Among them, Ba-140 has long half life of 12.8 days and is detected with relatively high intensity in BOR-60 experimental reactor.[2]

In FPL-II, gamma-ray peaks of Ba-140 and its daughter nuclide La-140 are detected at long counting time measurement after sodium drainage, but the intensity is too low to use for the analysis. Ba-139 emits a high intensity gamma-ray at 165.8 keV, but it is difficult to obtain deposition behavior of Ba alone because Ba-139 is allocated at the last position of FP chain and is strongly influenced by precursor volatile FPs behavior in sodium. Since Ba-142 emits many gamma-ray peaks with high gamma branch ratio and has high nuclear fission yield, its deposition behavior was analyzed.

2) Analysis of deposition behavior of Ba-142

Among many gamma-ray peaks of Ba-142, the peak at 255.1 keV[7] is not so strongly interfered by other nuclides. Thus the deposition behavior of Ba-142 was analyzed using this peak at 7 irradiation tests (Exp. Nos. 3, 4, 5, 6, 7, 8 and 16). The half life of Ba-142 is 10.65 min. As it decays in a short time after irradiation, gamma-ray spectrum during irradiation was used for analysis of deposition behavior. The result and

its statistic error are shown in Fig. 5-11. As recognized in the figure, Ba-142 shows the distribution of a approximate exponential function in the loop being little influenced by precursor nuclides.

Half life and fission yield of nuclides with mass number 142 composing FP chain are indicated as follows: (7, 8)

	Xe-142 ⟶	Cs-142 ⟶	Ba-142 ⟶	La-142 ⟶	Ce-142
half life:	1.24sec	1.68sec	10.65min	92.5min	(stable)
fission yield (%):	0.38	2.38	3.07	0.10	

Exponential function distribution of Ba-142 deposition shown in these data is owing to its high independent fission yield and short half life (Maximum of 2 sec.) of its precursor.

By fitting the distribution in the loop by least square method, the deposition rate constant K (cm/sec) was obtained from the gradient. The result of least square method fitting is shown by straight line in the figure, and K values at various sodium temperatures and flow velocities are indicated in Table 5-11.

By comparing K values of Ba and Sr, followings are clarified:

① Ba-142 deposition rate constant shows little dependence on temperature between 350 and 530°C, and is ca. 3.5×10^{-2} cm/sec at sodium flow velocity of 1.2 m/sec, and

② K values of Sr and Ba are in fairly good agreement at 400°C.

Thus the deposition behavior of Ba is found to be a little different from that of Sr.

5.8 Analysis of Deposition Behavior of La

1) Discussion of measurable La isotope

La radioactive isotopes in FP nuclides are La-140, La-141, LA-142, La-143, La-144, La-145, La-146, La-147, La-148 etc.. Among them, La-140 is a daughter nuclide of Ba-140 and it is detected with high intensity in FBR experimental reactor, such as EBR-II and BOR-60 etc. La-142 is detected with high intensity after irradiation, and that is the same with La-144. Results of gamma-ray measurement of these two nuclides are described as follows.

2) Result of gamma-ray measurement of La-142

La-142 is mostly produced by radioactive decay of Ba-142 with a half life of 10.7 min. Therefore, La-142 distribution in the loop is conceivably expressing Ba-142 distribution. As La-142 emits a strong gamma-ray at 641.2 keV[7] and have a half life of 92.2 min, using gamma-ray remaining after irradiation with good S/N ratio, the La-142 distribution in the loop was measured in 9 irradiation tests (Exp. Nos, 2, 3, 4, 5, 6, 7, 8, 14 and 16). The result with statistic error is shown in Fig. 5-12.

Assuming La-142 distribution obtained in the loop is regarded as that of Ba-142, the Ba-142 deposition rate constant is obtained, as indicated in Table 5-12. In Fig. 5-12, the result of fitting is shown by solid lines. Experimental values are obtained with smaller error than those of Ba-142. Hence the accuracy of experimental data are improved and the result of fitting is in good agreement with experimental values.

A good agreement is observed between the Ba-142 deposition rate constant obtained by La-142 gamma-ray measurement and that obtained by Ba-142 deposition distribution. Consequently, in the case that the deposition behavior of

parent nuclide, is not determined correctly, the deposition behavior of parent nuclide is obtained utilizing the result of gamma-ray measurement of daughter nuclide.

3) Analysis of deposition behavior of La-144

La-144 emits a gamma-ray with considerably high intensity at 397.3 keV[7]. Moreover, as no other gamma-ray peaks exist around there to interfare it, La-144 deposition behavior is analyzed using the peak. As La-144 has a short half life of 39.9 sec, the gamma-ray peak decays to be undetectable in 2 min after irradiation. Therefore, gamma-ray spectrum during irradiation was used for the analysis of La-144 deposition behavior.

For the analysis of La-144 deposition behavior, the gamma-ray spectra in 7 irradiation tests (Exp. Nos. 3, 4, 5, 6, 7, 8 and 16) were examined.

In Exp. No. 2, though gamma-ray spectrum was measured at only 2 detection positions, the distribution in the loop was obtained with some statistic error, as shown in Fig. 5-13.

Half lives and fission yields of nuclides of mass number 144 FP chains are indicated.[7, 8]

	Xe-144 ⟶	Cs-144 ⟶	Ba-144 ⟶	La-144 ⟶	Ce-144
half life:	1.15sec	1.00sec	11.9sec	39.9sec	284.5days
fission yield (%):	0.006	0.28	3.95	1.15	0.063

As seen from the data above, La-144 is mostly produced with rate of 4.24:1.15 by radioactive decay of Ba-144, parent nuclide of La. However, as Ba-144 has a short half life of 11.9 sec, ca. 3/4 of the nuclide decays and La-144 is produced instead after 25.3 sec when sodium arrives at the detection position D-9 located at the end of the delay line under the sodium flow velocity of 1.2 m/sec.

A calculation of the deposition rate constants of Ba-144 and the La-144 was tried from the La-144 deposition distribution by fitting of Eqs. (5-11) and (5-12) with non-linear least square method. However, the result was found to be erroneous as 50% because of the non-convergent solution of the least square method of calculation and the experimental data of La-144 containing a large statistic error. Moreover, as seen in Fig. 5-13, La-144 has a mostly linear distribution. Thus it was clarified that the fitting by the non-linear least square method was not available to the case of La-144.

When deposition behaviors of parent and daughter nuclides are similar, the deposition distribution of daughter nuclide is in fairly good agreement with that of parent nuclide, as seen in Fig. 5-2. Cs-144, parent nuclide of Ba-144, has such a short half life of 1 sec that Ba-144 seems to show a exponential distribution without being affected by Cs.

The deposition rate constant of La-144, which is a daughter nuclide of Ba-144, is calculated by approximating these experimental data to the distribution of exponential function. The results are indicated in Table 5-13. By comparing these values with those of Table 5-12, a fairly good agreement is obtained between the results shown in Table 5-13 and in Table 5-12.

Strictly speaking, though values in Table 5-13 indicate overlapped deposition behaviors of Ba-144 and La-144, because half life of Ba-144 is short as explained previously, the deposition behavior of La-144 appears to be fully reflected in these values and similar deposition behaviors between La and Ba are concluded.

5.9 Summary of Deposition Behavior of non-volatile FP

1) Temperature dependence of deposition behavior and deposition mechanism of Sr

Temperature dependence of deposition rate constant K of Sr isotope was studied. Average values of deposition rate constants of Sr-92, Sr-93, and Sr-94 are indicated in Table 5-14 and the Arrhenius plot of these K values are shown in Fig. 5-14. A linear relationship between ℓn K and reciprocal absolute temperature 1/T is observed. From the gradient of the line, activation energy of -13±1 (KJ/g-atom) was obtained under sodium flow velocity of 1.2 and 0.48 m/sec. The deposition rate constant K can be directly compared with the mass transfer coefficient K_L (cm/sec) in cylindrical tube. The mass transfer coefficient K controlled by diffusion through boundary layer in cylindrical tube is given by Treybal[9] as follows,

$$k_L = 0.023 \cdot Re^{0.83} \cdot Sc^{0.33} \cdot D/d \qquad (5\text{-}13)$$

where,

Re, Sc: Reynolds number (—) and Schmidt number (—), respectively
D : diffusion coefficient (cm^2/sec)
d : inner diameter of cylindrical tube (cm)

To compare K and K_L of Sr, the value of diffusion coefficient D of Sr in sodium is necessary to know, but there is no report regarding D value. Self-diffusion coefficient of sodium and diffusion coefficient of Ba in sodium have been reported by Nachtrieb[10] and Cooper[11], respectively.

Also the diffusion coefficient can be estimated by using Stokes-Einstein's equation

$$D = k \cdot T/6\pi\mu r \qquad (5\text{-}14)$$

where,

r : molecular radius (cm)
k : Boltzman constant (erg/K)
T : absolute temperature (K)
M : viscosity ($g/cm^3/sec$)

Assuming that Sr is ionic Sr^{2+} in sodium, the diffusion coefficient of Sr is calculated by using Eq. (5-14) from Sr^{2+} ion radius of 1.3×10^{-8} cm. Temperature dependence of Sr deposition rate constant K (cm/sec) and mass transfer coefficient K_L (cm/sec) is shown in Fig. 5-15, where sodium flow velocity is 1.2 m/sec, and mass transfer coefficients are calculated by Eq. (5-13) from diffusion coefficients obtained by 3 methods described above. A fairly good agreement is observed. Especially, temperature dependence of mass transfer coefficient calculated by using self-diffusion coefficient of sodium agreed well with that by using diffusion coefficient obtained from Stokes-Einstein's equation in the temperature dependence of deposition rate constant.

From these results, the deposition of Sr on stainless steel surface is well explained by the diffusion-controlled mass transfer mechanism in liquid sodium and is concluded that its velocity is controlled by the diffusion of Sr nuclide passing through boundary layer between piping and sodium.

In order to be consistent the diffusion-controlled model described above with the deposition rate constant obtained by experiments, the sticking coefficient S (dimensionless), which is used to correct the mass transfer coefficient, was calculated. The mass transfer coefficient K_L is calculated using Eq. (5-13) and the diffusion coefficient D obtained by the calculation of Sr^{2+} radius. Values of sticking coefficient S thus calculated are indicated in Table 5-15 summarized at each sodium temperature and flow velocity. They show consistent values within a range of 0.4 and 0.6, independent of sodium temperature and flow velocity. It is

concluded that the present analytical model is useful to estimate the Sr deposition behavior in large-scale FBR plant.

2) Temperature dependence of deposition behavior of Y

Y-97 deposition behavior was obtained from Zr-97 and Nb-97 deposition distributions. The temperature dependence of Y deposition rate constant was examined. An Arrhenius plot of K is indicated in Fig. 5-16, where a linear relationship between ℓn (K) and reciprocal absolute temperature 1/T is hold. In the figure, the temperature dependence of Sr deposition rate constant, shown by dotted line, is in good agreement with that of Y between 200 and 530°C. Y is the daughter nuclide of Sr and has the similar deposition mechanism to Sr.

3) Temperature dependence of Zr deposition rate constant

Temperature dependence of Zr deposition rate constant K was examined, where the deposition rate constant is defined as an apparent deposition rate including desorption phenomenon. Arrhenius plot of K is indicated in Fig. 5-17, where values have no temperature dependence between 200 and 530°C and the recurrence line of Zr deposition rate constant obtained by least square method is expressed by solid line and that of Sr is by dotted line for reference.

As seen in the figure, deposition behaviors of Sr and Zr are different: the deposition rate of Sr is higher at high sodium temperature than that of Zr, and adversely at lower temperature (200°C). Different mechanism between them is probably due to the redistribution by desorption in case of Zr.

4) Temperature dependence of deposition behavior of Ba

Temperature dependence of Ba deposition rate constant K was examined. Arrhenius plot of deposition rate constant obtained from Ba-142 deposition and also obtained from La-142

deposition is shown in Fig. 5-18. The deposition rate of Ba shows little temperature dependence between 350 and 530°C and looks to decrease at low temperature region. However, the decreasing tendency is not clear, because of the lack of analytical data below 200°C. For reference, a recurrence line of Ba deposition rate constant obtained by least square method is expressed by a solid line and that of Sr is by a dotted line in the figure.

The deposition rate of Ba at around 400°C shows similar value to that of Sr that belongs to the same periodic table group of Ba, but at low sodium temperature (200°C), Ba shows higher rate than Sr. To check possibility of Ba desorption, variation of deposition distribution of FP nuclides having long half life such as Ba-140 should be analyzed during sodium circulation.

Regarding La, as similar deposition behavior to Ba is assumed, a detailed discussion is not done here.

5.10 Conclusion

Deposition behaviors of various FP nuclides, such as Sr, Y, Zr, Nb, Ba and La have been clarified as follows:

1) Sr deposition is rapid and irreversible, and the rate is accelerated at higher sodium temperature. Deposition rate constants are obtained for Sr-92, Sr-93 and Sr-94 as function of temperature, and show good agreements with each other. Activation energy for the deposition process is -13 ± 1 (KJ/g-atom). The deposition rate of Sr nuclide on stainless steel surface is controlled by Sr nuclide diffusion through the boundary layer.

2) Y nuclides show similar deposition behavior to Sr nuclides between 200 and 530°C.

3) Redistribution probably occurs for Zr nuclides; i.e. deposited Zr nuclides will desorb during sodium circulation for long time after irradiation. The deposition rate constant of Zr including desorption phenomenon is smaller than Sr at sodium temperature of 500°C and shows no temperature dependence between 200 and 530°C.

4) Nb nuclides show no deposition behavior and dissolve in sodium.

5) The deposition rate of Ba nuclide shows nearly the same value as that of Sr at sodium temperature of 400°C, but it has smaller temperature dependence compared with Sr deposition rate.

6) The deposition rate of La nuclide is similar to that of Ba nuclide between 350 and 530°C.

Another important point to estimate the deposition behavior of non-volatile FP is, as described at paragraph of Zr, to confirm if redistribution occurs by desorption. Further analyses are necessary on the probability of redistribution of non-volatile FPs in sodium as well as the effect of the oxygen concentration in sodium.

Table 5-1 Calculated value of C_d^W as a function of K_d

K_d (cm/sec)	C_d^W (atoms/cm²)			
	x=500	x=1500	x=3000	x=5734
0	3.29×10^{-3}	7.87×10^{-4}	9.23×10^{-5}	1.86×10^{-6}
1.0×10^{-5}	3.29×10^{-3}	7.93×10^{-4}	9.74×10^{-5}	6.92×10^{-6}
1.0×10^{-4}	3.30×10^{-3}	8.03×10^{-4}	1.08×10^{-4}	1.71×10^{-5}
1.0×10^{-3}	3.31×10^{-3}	8.08×10^{-4}	1.12×10^{-4}	1.94×10^{-5}
1.0×10^{-2}	3.32×10^{-3}	8.16×10^{-4}	1.10×10^{-4}	8.46×10^{-6}
2.0×10^{-2}	3.34×10^{-3}	8.18×10^{-4}	1.04×10^{-4}	3.62×10^{-6}
4.0×10^{-2}	3.36×10^{-3}	8.13×10^{-4}	9.66×10^{-5}	1.99×10^{-6}
1.0×10^{-1}	3.36×10^{-3}	7.97×10^{-4}	9.33×10^{-5}	1.88×10^{-6}

Table 5-2 Geometry correction factor for each detection position

Detection position	Correction factor
D-2	1.00 (normalize)
D-3	0.943
D-4	1.19
D-5	1.01
D-6	1.27
D-7	0.980
D-8	0.917
D-9	0.880

Table 5-3 Sr-94 deposition rate constant

Na Temp (℃)	Exp. No.	Na Flow Velocity (m/sec)	Deposition Rate Constant (cm/sec)
170	9	1.20	8.25×10^{-3}
200	2	1.20	1.57×10^{-2}
225	12	1.20	1.42×10^{-2}
270	11	1.20	1.52×10^{-2}
350	3	1.20	2.75×10^{-2}
	4	1.20	2.94×10^{-2}
420	5	1.20	3.62×10^{-2}
	6	1.20	3.38×10^{-2}
500	7	1.20	3.81×10^{-2}
530	8	1.20	4.42×10^{-2}
170	9	0.48	4.82×10^{-3}
225	11	0.48	6.98×10^{-3}
270	12	0.48	9.64×10^{-3}
530	14	0.24	1.08×10^{-2}
	16	0.24	1.02×10^{-2}

Table 5-4 Sr-92 deposition rate constant

Na Temp (℃)	Exp. No.	Na Flow Velocity (m/sec)	Deposition Rate Constant (cm/sec)
200	2	1.20	1.41×10^{-2}
350	3	1.20	2.63×10^{-2}
	4	1.20	2.84×10^{-2}
420	5	1.20	3.48×10^{-2}
	6	1.20	3.29×10^{-2}
500	7	1.20	3.76×10^{-2}
530	8	1.20	4.25×10^{-2}
	14	0.24	1.30×10^{-2}
	16 *1	0.24	1.37×10^{-2}
	16 *2	0.24	1.12×10^{-2}

*1 during irradiation

*2 after irradiation

Table 5-5 Sr-93 deposition rate constant

Na Temp (℃)	Exp. No.	Na Flow Velocity (m/sec)	Deposition Rate Constant (cm/sec)	
			590.2 KeV	875.9 KeV
350	3	1.20	3.39×10^{-2}	2.80×10^{-2}
	4	1.20	3.68×10^{-2}	3.05×10^{-2}
420	5	1.20	3.70×10^{-2}	3.67×10^{-2}
	6	1.20	3.75×10^{-2}	3.48×10^{-2}
500	7	1.20	4.20×10^{-2}	3.76×10^{-2}
530	8	1.20	4.27×10^{-2}	3.95×10^{-2}
	14	0.24	1.19×10^{-2}	9.40×10^{-3}
	16	0.24	1.21×10^{-2}	8.84×10^{-3}

Table 5-6 Sr-91 deposition rate constant

Na Temp (℃)	Exp. No.	Na Flow Velocity (m/sec)	Deposition Rate Constant (cm/sec)	
			749.8 KeV	1024.3 KeV
530	14	0.24	1.03×10^{-2}	1.01×10^{-2}
	16	0.24	9.75×10^{-3}	8.64×10^{-3}

Table 5-7 Sr-92 deposition rate constant obtained by using Y-92 deposition distribution pattern along the delay line

Na Temp (℃)	Exp. №	Na Flow Velocity (m/sec)	Deposition Rate Constant (cm/sec)
200	2	1.20	1.87×10^{-2}
350	3	1.20	2.90×10^{-2}
	4	1.20	3.34×10^{-2}
420	5	1.20	3.75×10^{-2}
	6	1.20	3.70×10^{-2}
500	7	1.20	4.27×10^{-2}
530	8	1.20	4.55×10^{-2}
	14	0.24	1.02×10^{-2}
	16	0.24	9.80×10^{-3}

Table 5-8 Sr-94 deposition rate constant obtained by using Y-94 deposition distribution pattern along the delay line

Ne Temp (℃)	Exp. №	Na Flow Velocity (m/sec)	Deposition Rate Constant (cm/sec)
200	2	1.20	1.66×10^{-2}
350	3	1.20	2.30×10^{-2}
	4	1.20	2.41×10^{-2}
420	5	1.20	2.95×10^{-2}
	6	1.20	2.75×10^{-2}
500	7	1.20	3.27×10^{-2}
530	8	1.20	3.78×10^{-2}
	14	0.24	9.38×10^{-3}
	16	0.24	8.81×10^{-3}

Table 5-9 Y-97 and Zr-97 deposition rate constant obtained by using Zr-97 deposition distribution pattern along the delay line

Na Temp (℃)	Exp. №	Na Flow Velocity (m/sec)	Deposition Rate Constant (cm/sec)	
			^{97}Y	^{97}Zr
200	2	1.20	4.75×10^{-3}	2.01×10^{-2}
350	3	1.20	2.11×10^{-2}	2.17×10^{-2}
	4	1.20	1.96×10^{-2}	2.18×10^{-2}
420	5	1.20	3.01×10^{-2}	2.11×10^{-2}
	6	1.20	3.85×10^{-2}	2.01×10^{-2}
500	7	1.20	3.20×10^{-2}	2.39×10^{-2}
530	8	1.20	4.60×10^{-2}	2.19×10^{-2}
	14	0.24	1.70×10^{-2}	6.11×10^{-3}
	16	0.24	1.57×10^{-2}	5.51×10^{-3}

Table 5-10 Y-97 and Zr-97 deposition rate constant obtained by using Nb-97 distribution pattern along the delay line

Na Temp (℃)	Exp. No.	Na Flow Velocity (m/sec)	Deposition Rate Constant (cm/sec)	
			^{97}Y	^{97}Zr
200	2	1.20	1.15×10^{-2}	1.61×10^{-2}
350	3	1.20	2.16×10^{-2}	2.04×10^{-2}
	4	1.20	2.40×10^{-2}	2.07×10^{-2}
420	5	1.20	3.12×10^{-2}	1.97×10^{-2}
	6	1.20	4.20×10^{-2}	1.91×10^{-2}
500	7	1.20	3.70×10^{-2}	1.96×10^{-2}
530	8	1.20	4.86×10^{-2}	1.68×10^{-2}
	14	0.24	———	7.76×10^{-3}

Table 5-11 Ba-142 deposition rate constant

Na Temp (℃)	Exp. No.	Na Flow Velocity (m/sec)	Deposition Rate Constant (cm/sec)
350	3	1.20	4.02×10^{-2}
	4	1.20	2.96×10^{-2}
420	5	1.20	2.84×10^{-2}
	6	1.20	3.49×10^{-2}
500	7	1.20	3.97×10^{-2}
530	8	1.20	3.15×10^{-2}
	16	0.24	1.31×10^{-2}

Table 5-12 Ba-142 deposition rate constant obtained by using La-142 deposition distribution pattern along the delay line

Na Temp (℃)	Exp. №	Na Flow Velocity (m/sec)	Deposition Rate Constant (cm/sec)
200	2	1.20	1.79×10^{-2}
350	3	1.20	2.70×10^{-2}
	4	1.20	2.86×10^{-2}
420	5	1.20	3.28×10^{-2}
	6	1.20	3.18×10^{-2}
500	7	1.20	2.92×10^{-2}
530	8	1.20	2.99×10^{-2}
	14	0.24	9.78×10^{-3}
	16	0.24	6.79×10^{-3}

Table 5-13 La-144 deposition rate constant

Na Temp (℃)	Exp. No	Na Flow Velocity (m/sec)	Deposition Rate Constant (cm/sec)
200	2	1.20	1.59×10^{-2}
350	3	1.20	2.26×10^{-2}
	4	1.20	2.10×10^{-2}
420	5	1.20	3.48×10^{-2}
	6	1.20	2.68×10^{-2}
500	7	1.20	2.87×10^{-2}
530	8	1.20	2.95×10^{-2}
	16	0.24	6.64×10^{-3}

Table 5-14 Deposition rate constant of Sr isotopes

(x 10^{-2} cm/sec)

Flow Velocity / Temperature	1.2 m/sec			0.48 m/sec
	Sr-92	Sr-93	Sr-94	Sr-94
170℃	—	—	0.83	0.48
200	1.4	—	1.6	—
225	—	—	1.4	0.70
270	—	—	1.5	0.96
350	2.7	3.4	2.9	—
420	3.4	3.7	3.5	—
500	3.8	4.2	3.8	—
530	4.3	4.3	4.4	—

Table 5-15 Sticking coefficient of Sr isotopes calculated by using modified mass transfer model (dimensionless)

Flow Velocity / Temperature	1.2 m/sec			0.48 m/sec
	Sr-92	Sr-93	Sr-94	Sr-94
170℃	—	—	0.38	0.47
200	0.55	—	0.61	—
225	—	—	0.49	0.52
270	—	—	0.43	0.58
350	0.58	0.71	0.60	—
420	0.57	0.63	0.59	—
500	0.52	0.58	0.52	—
530	0.54	0.54	0.56	—

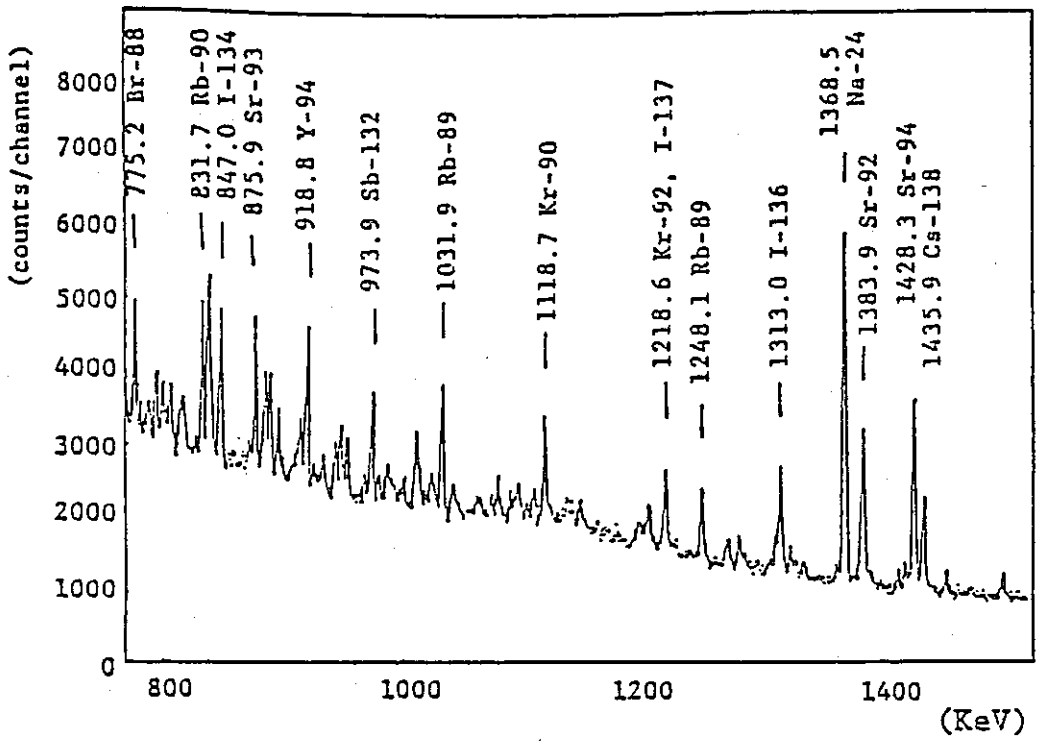

(a) During irradiation

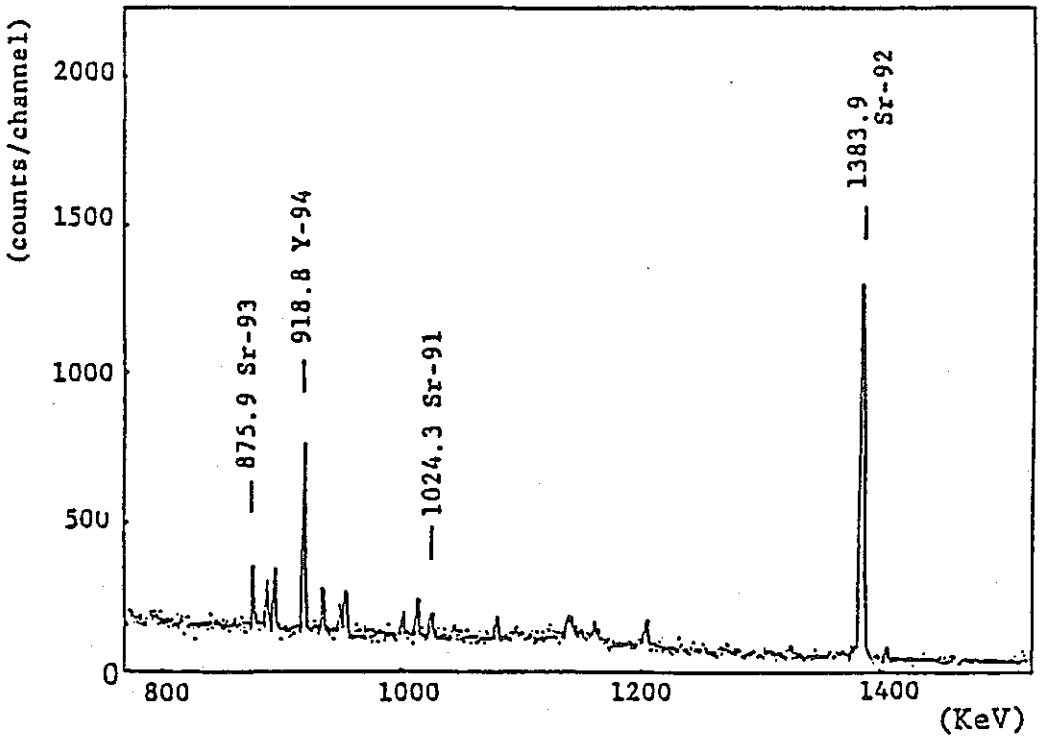

(b) After sodium drain

Fig. 5-1 Gamma ray spectra (Na temp. 500°C, Na flow velocity 1.2 m/sec)

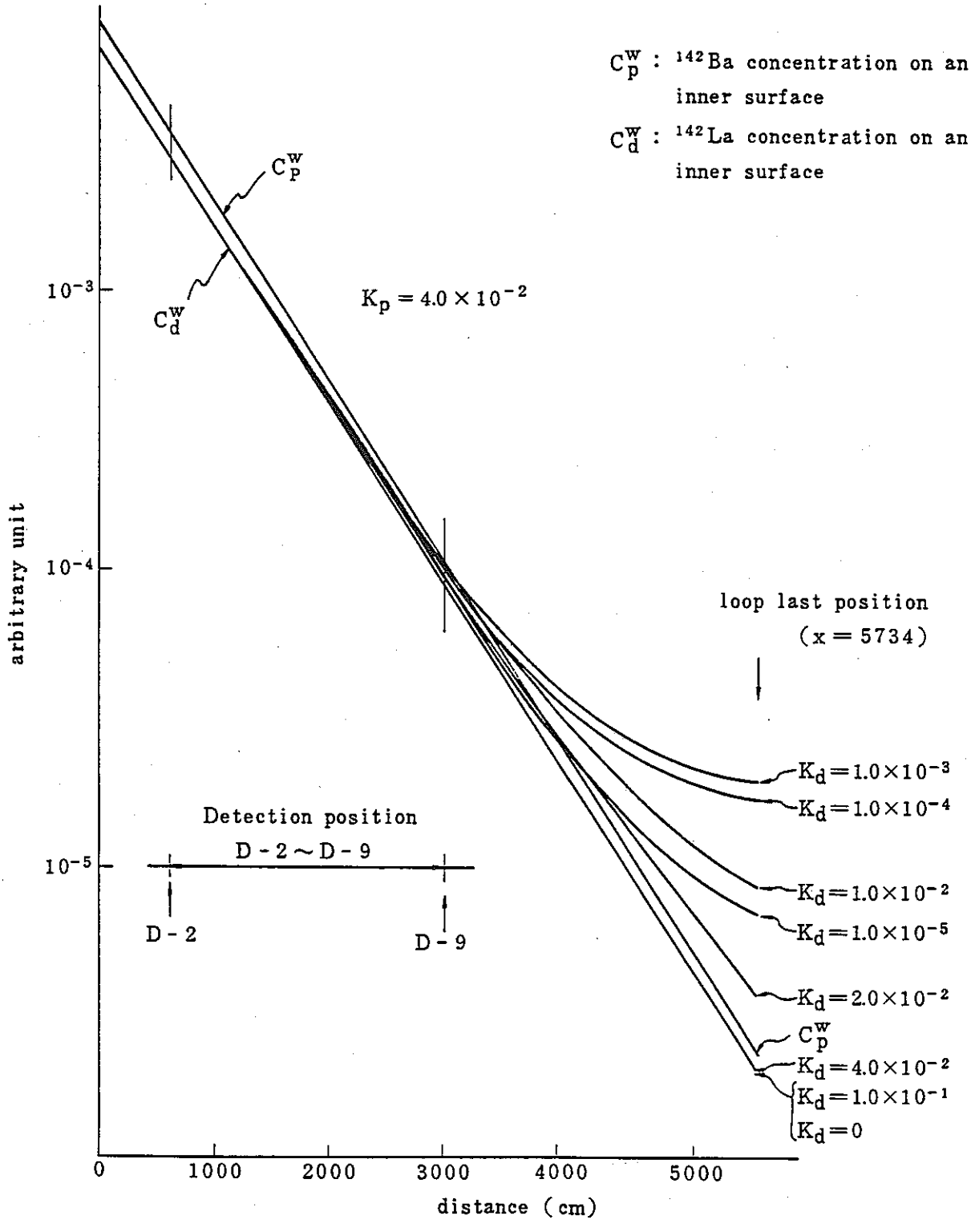

Fig. 5-2 Ba-142 and La-142 deposition distribution along the delay line calculated by using analytical model

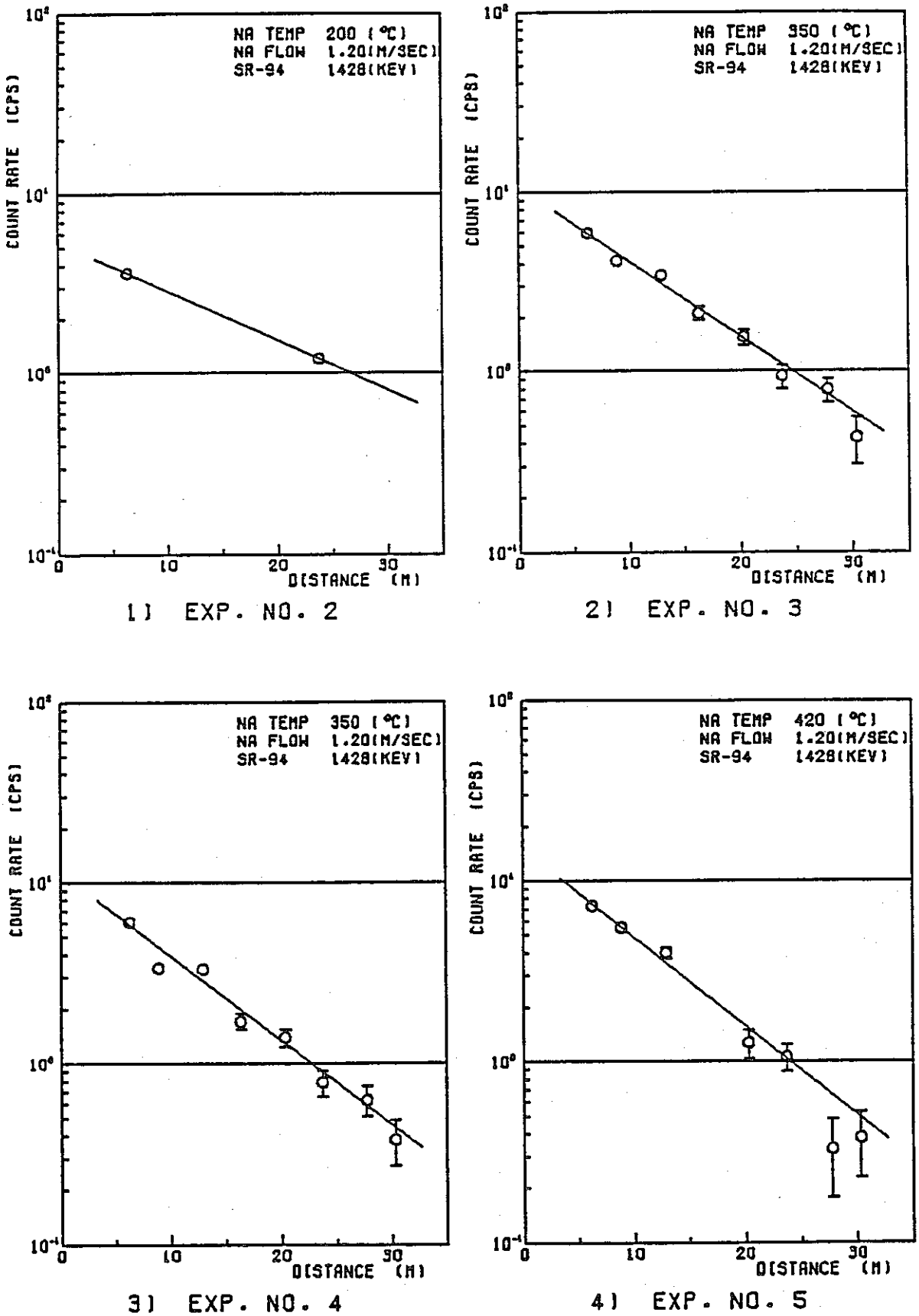

Fig. 5-3 Sr-94 distribution along the delay line

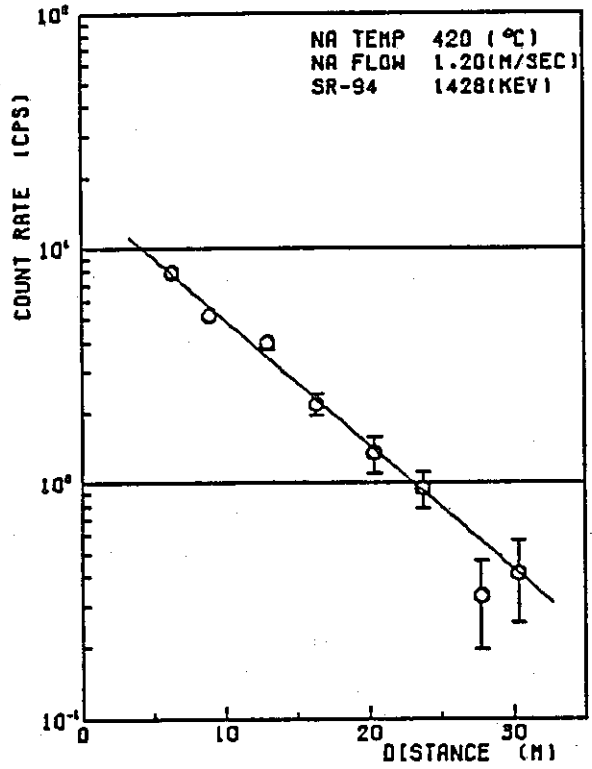

5) EXP. NO. 6

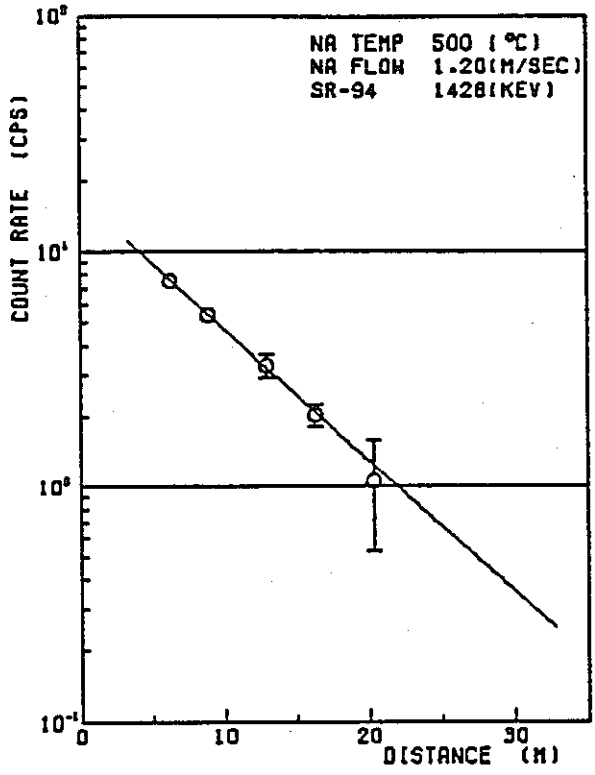

6) EXP. NO. 7

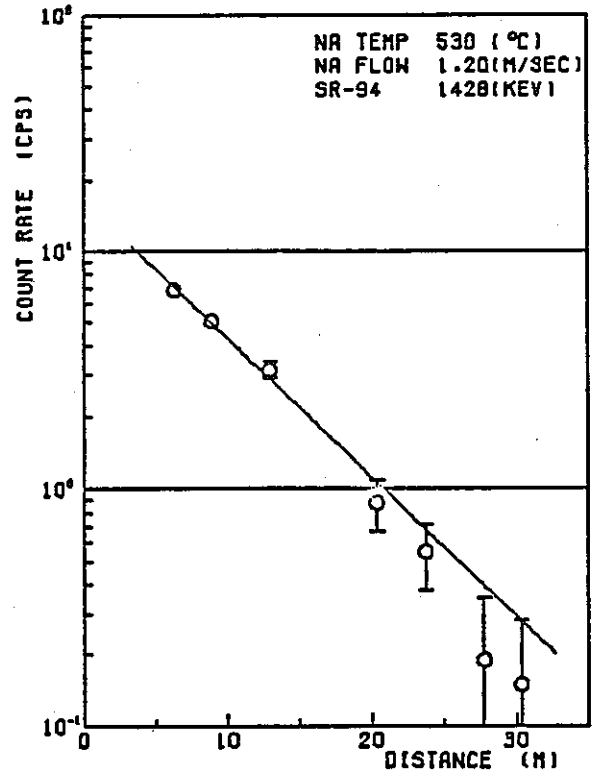

7) EXP. NO. 8

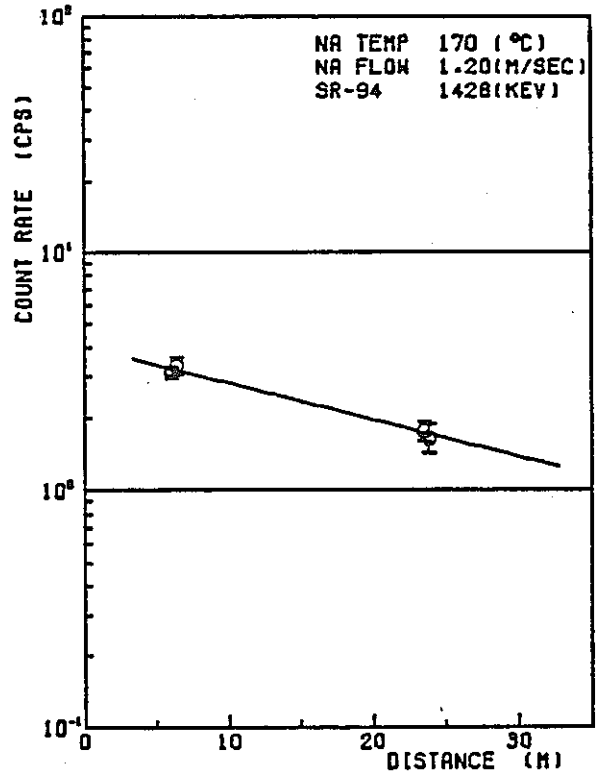

8) EXP. NO. 9

Fig. 5-3 (continued)

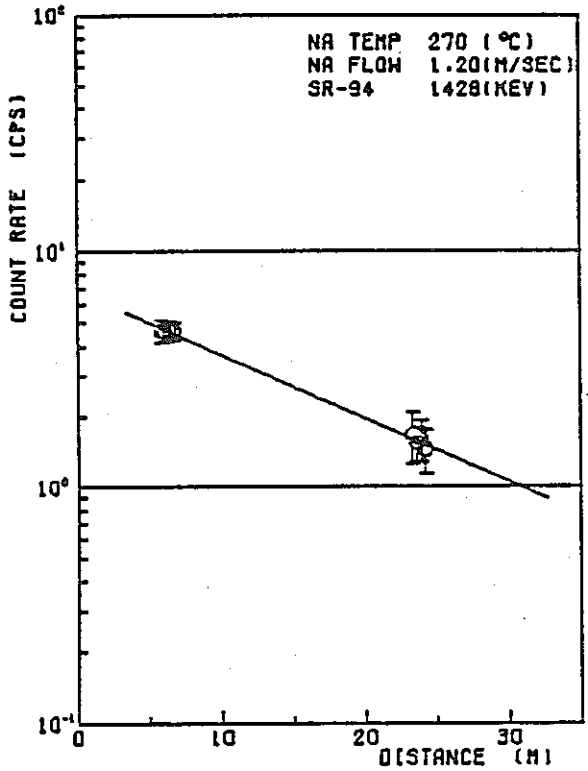

9) EXP. NO. 11

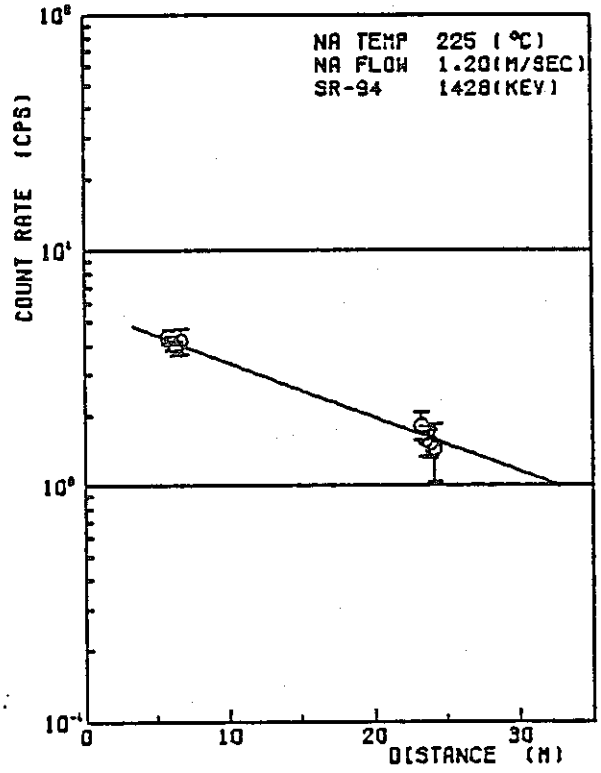

10) EXP. NO. 12

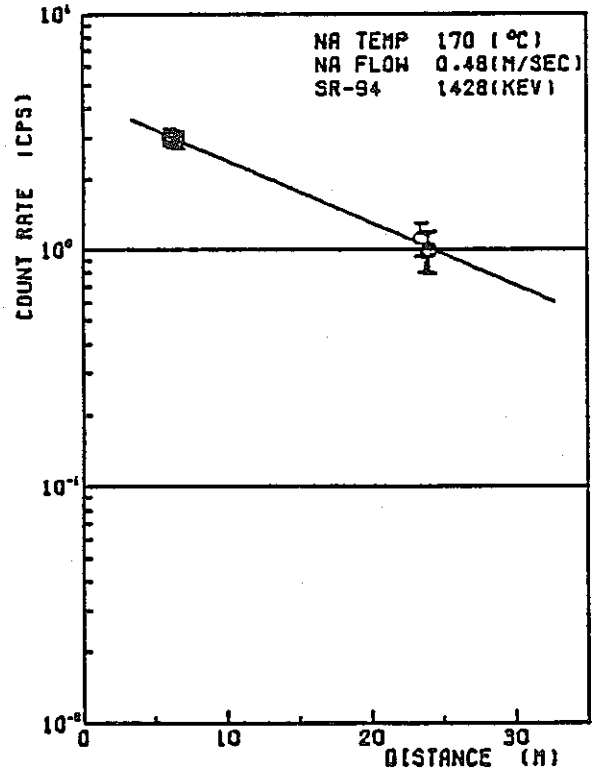

11) EXP. NO. 9

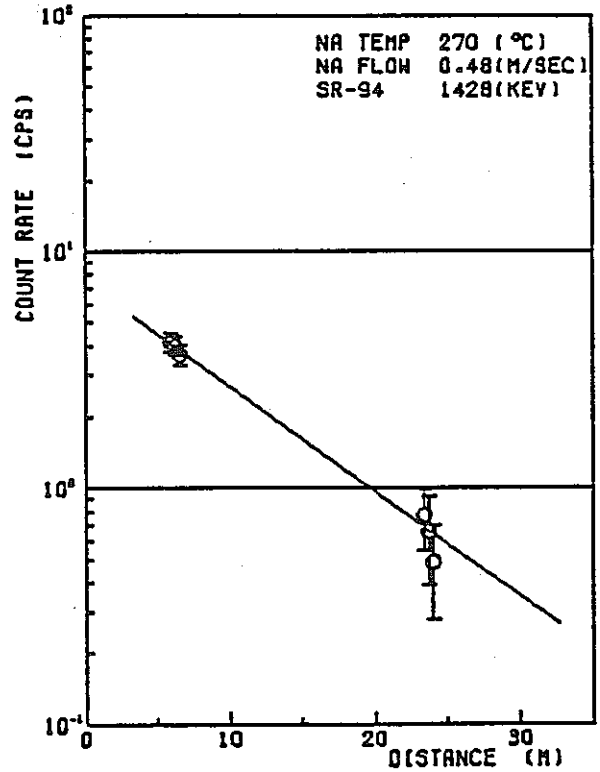

12) EXP. NO. 11

Fig. 5-3 (continued)

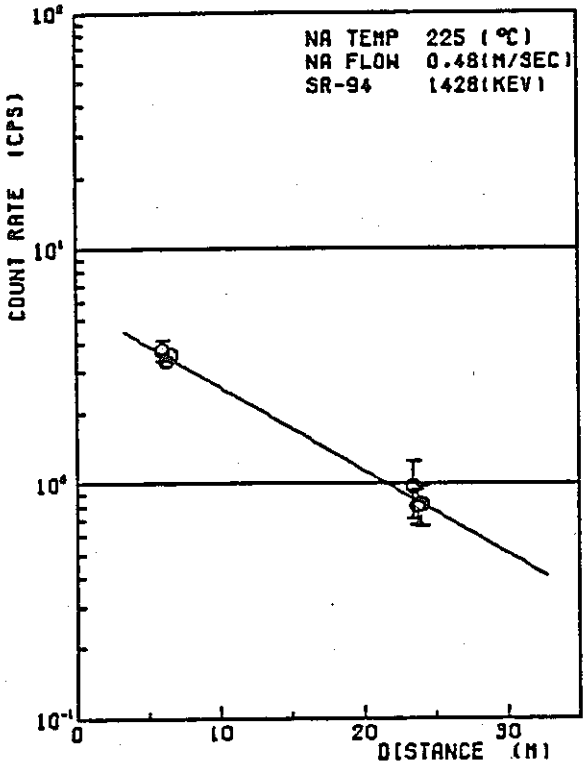

13) EXP. NO. 12

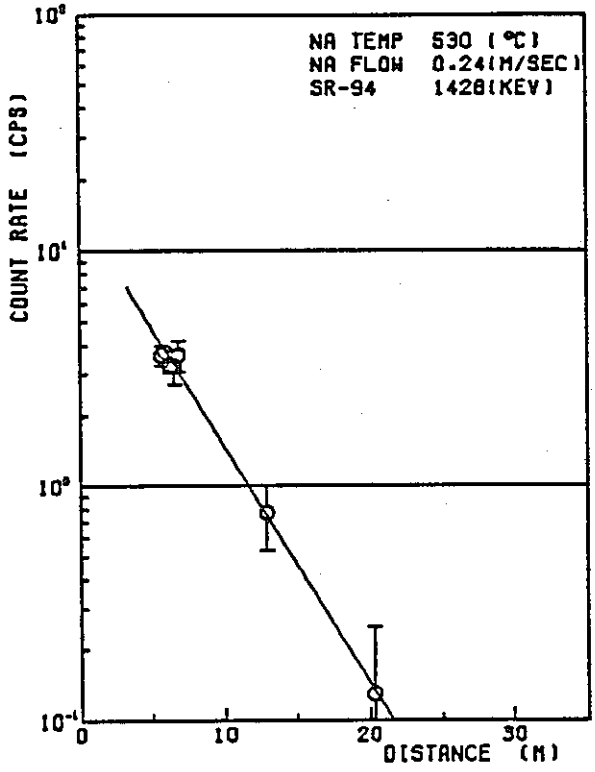

14) EXP. NO. 14

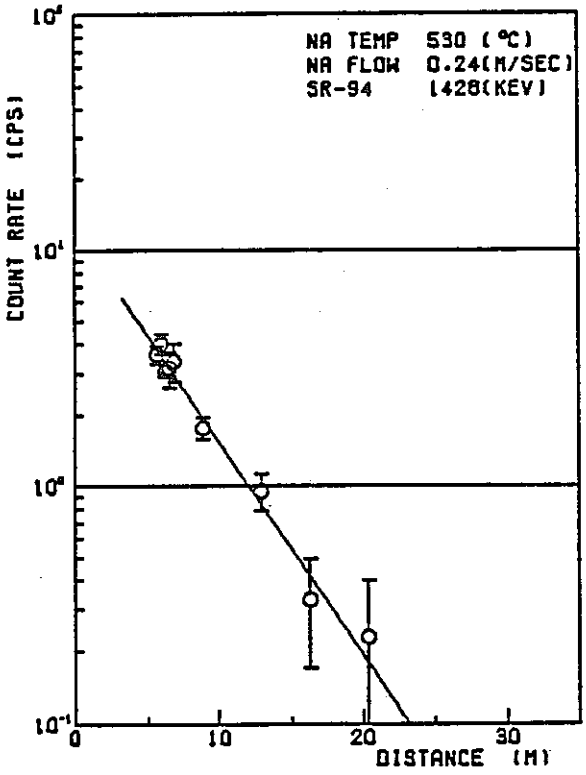

15) EXP. NO. 16

Fig. 5-3 (continued)

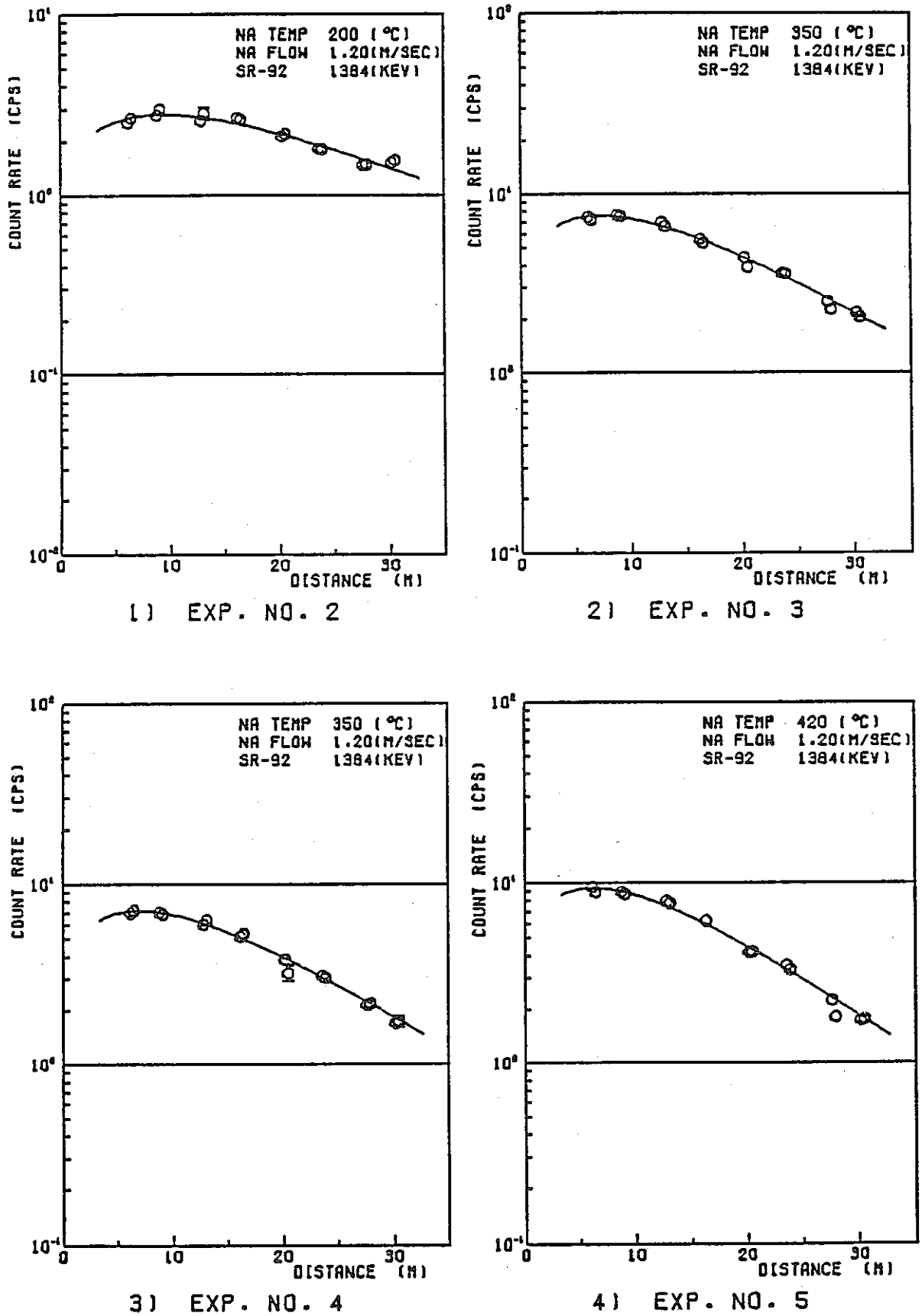

Fig. 5-4 Sr-92 deposition distribution along the delay line

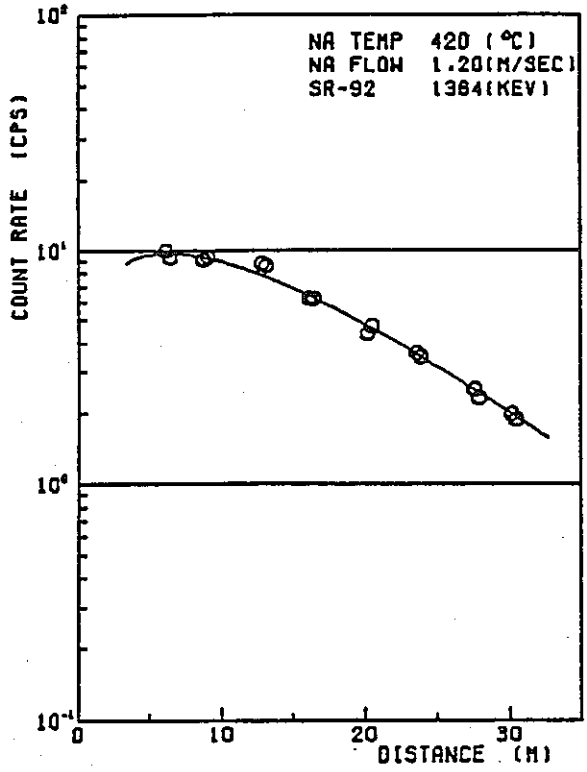

5) EXP. NO. 6

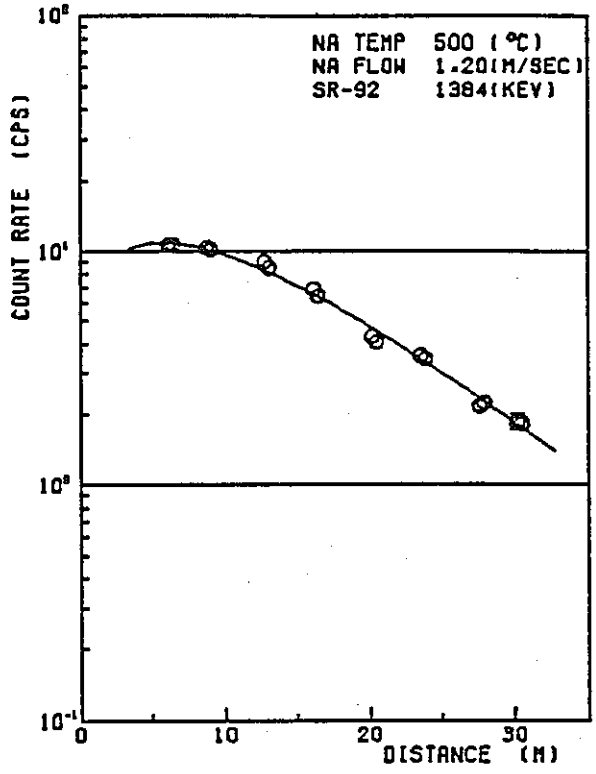

6) EXP. NO. 7

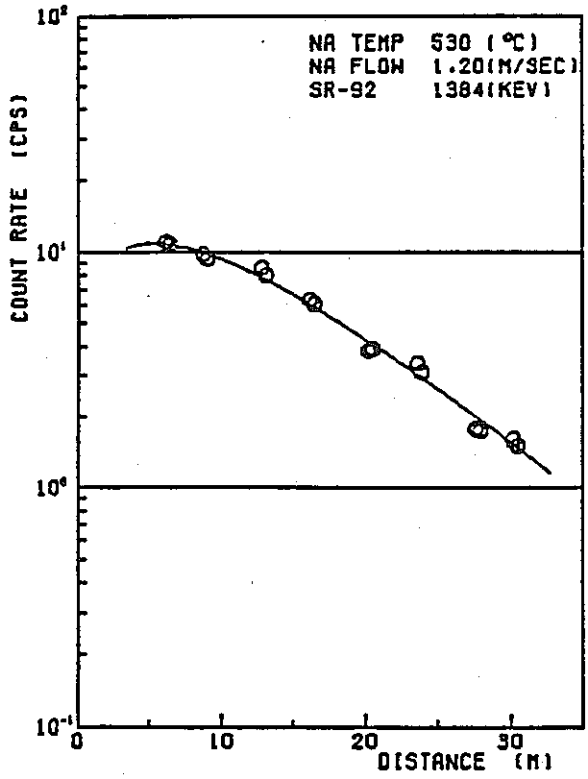

7) EXP. NO. 8

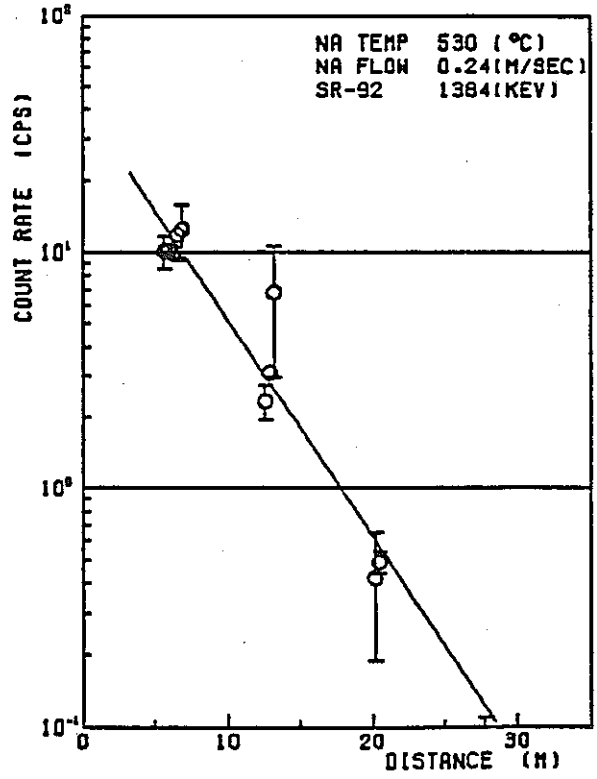

8) EXP. NO. 14

Fig. 5-4 (continued)

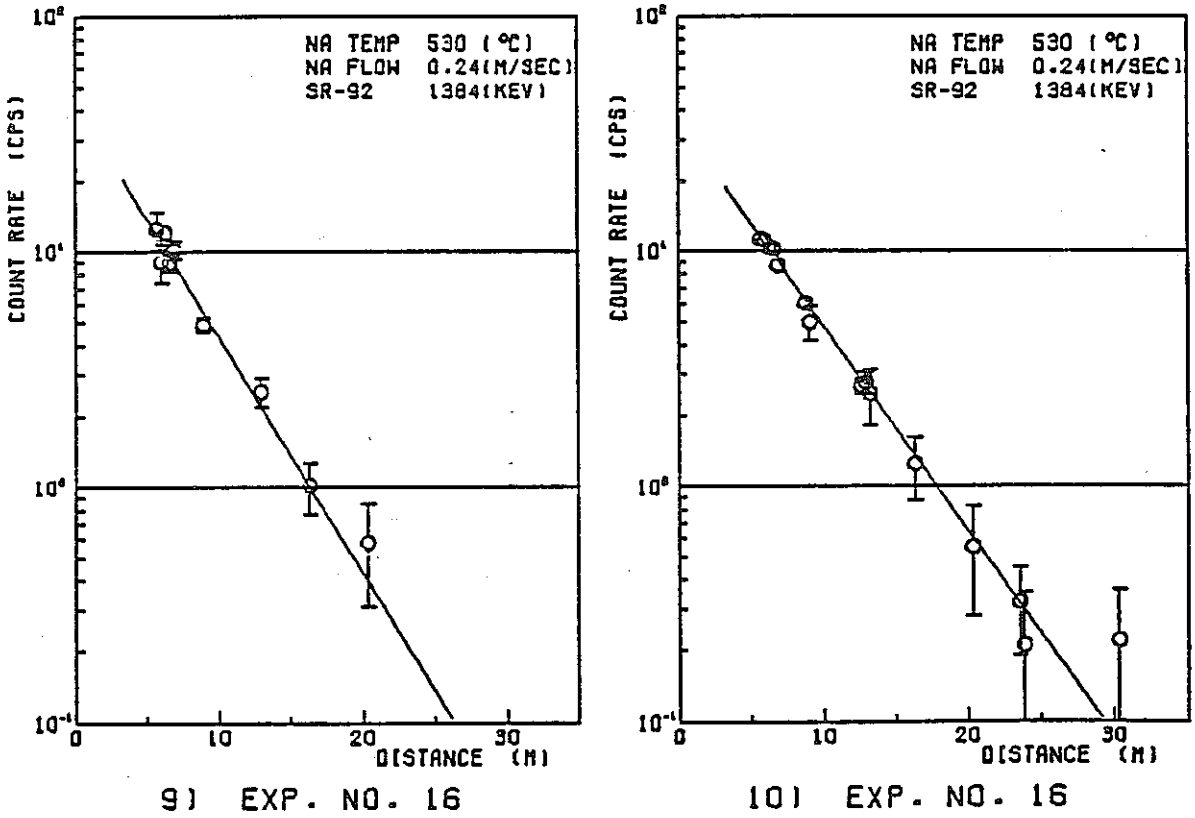

Fig. 5-4 (continued)

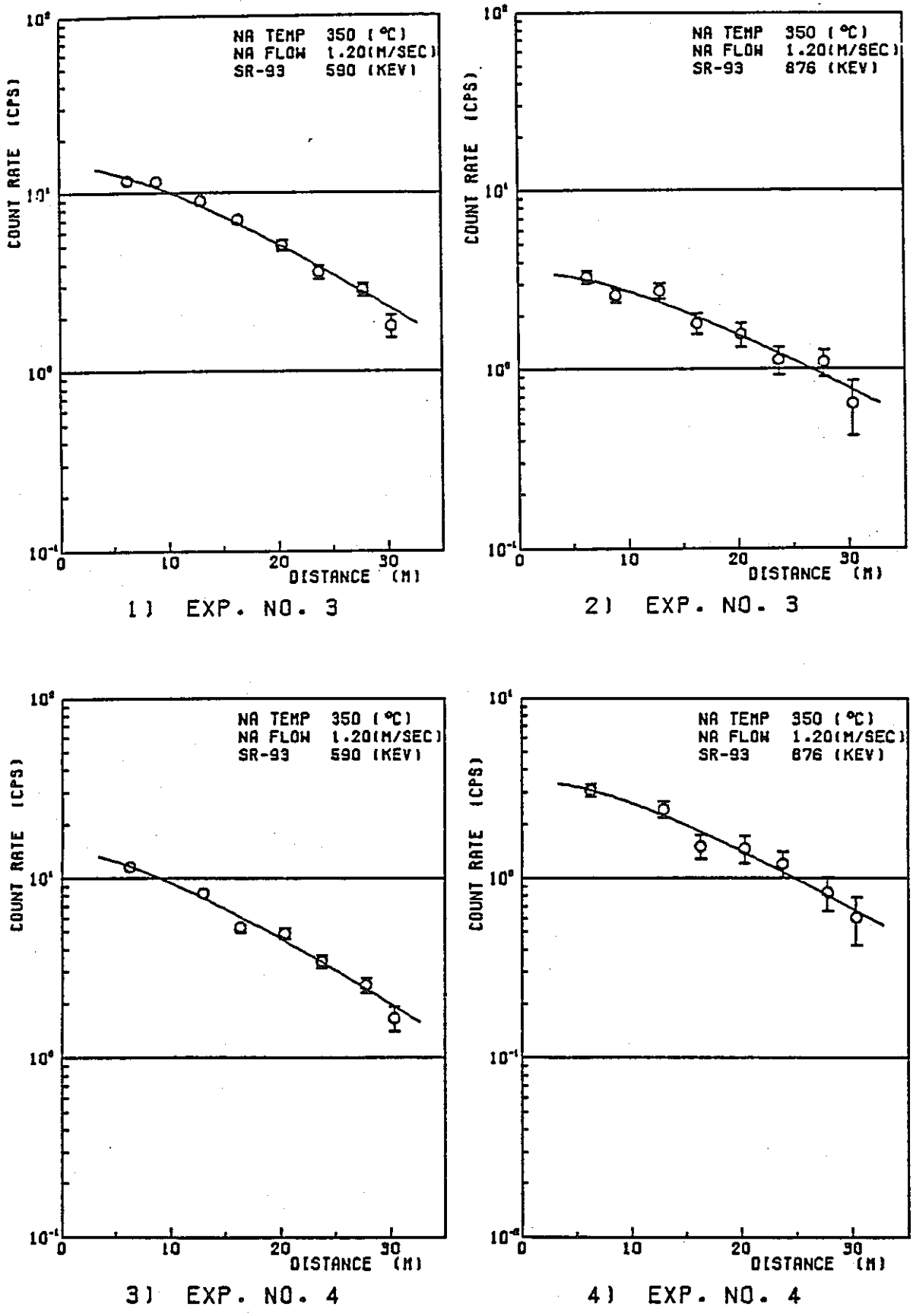

Fig. 5-5 Sr-93 distribution along the delay line

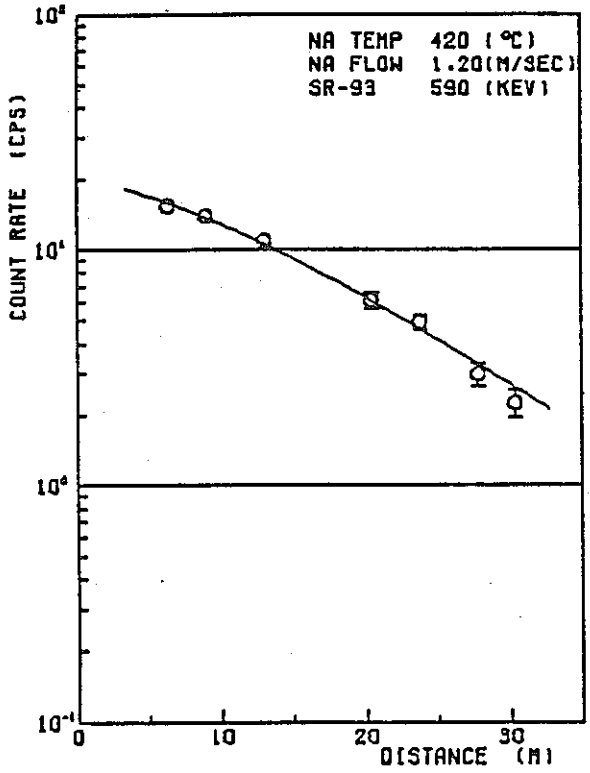

5) EXP. NO. 5

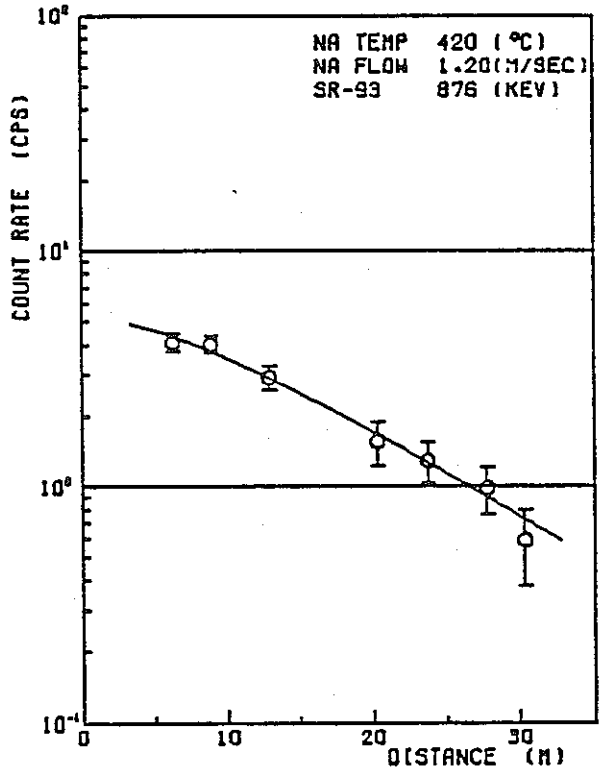

6) EXP. NO. 5

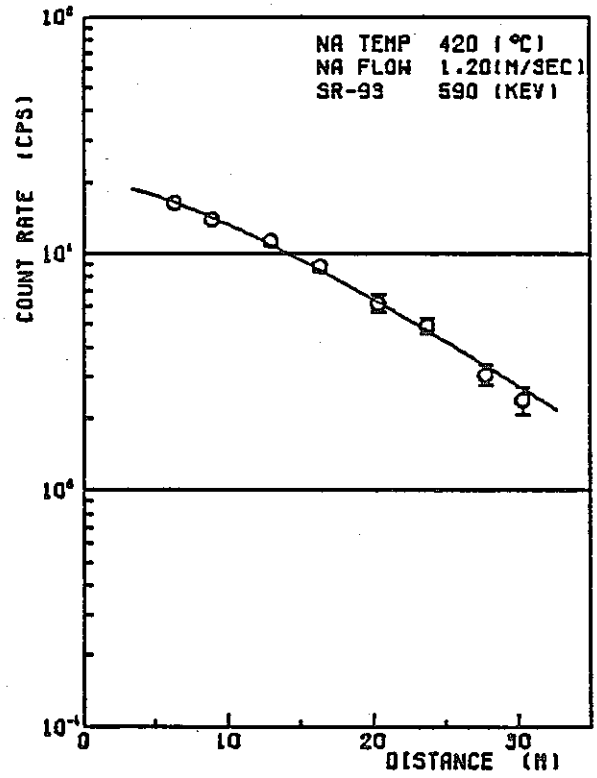

7) EXP. NO. 6

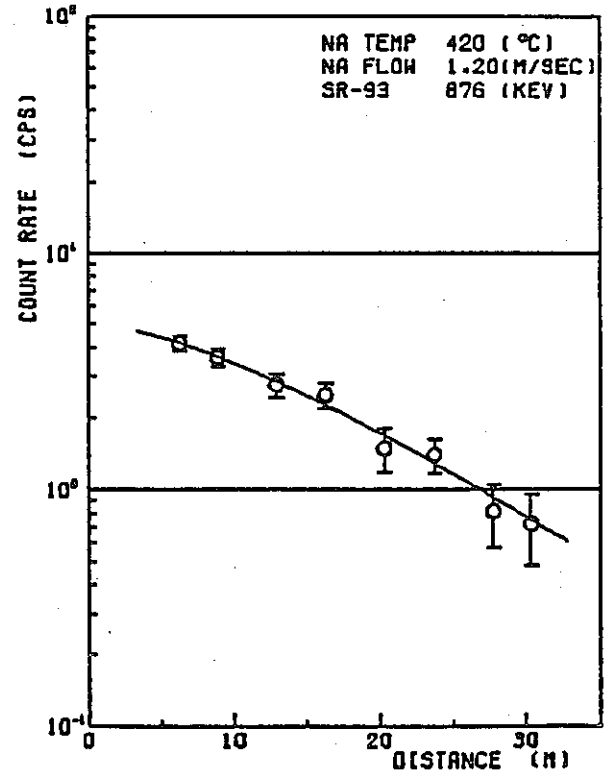

8) EXP. NO. 6

Fig. 5-5 (continued)

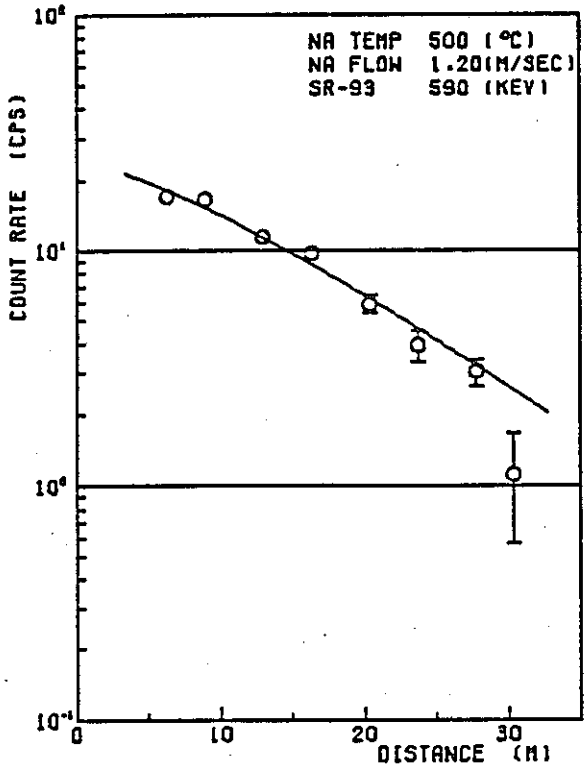

9) EXP. NO. 7

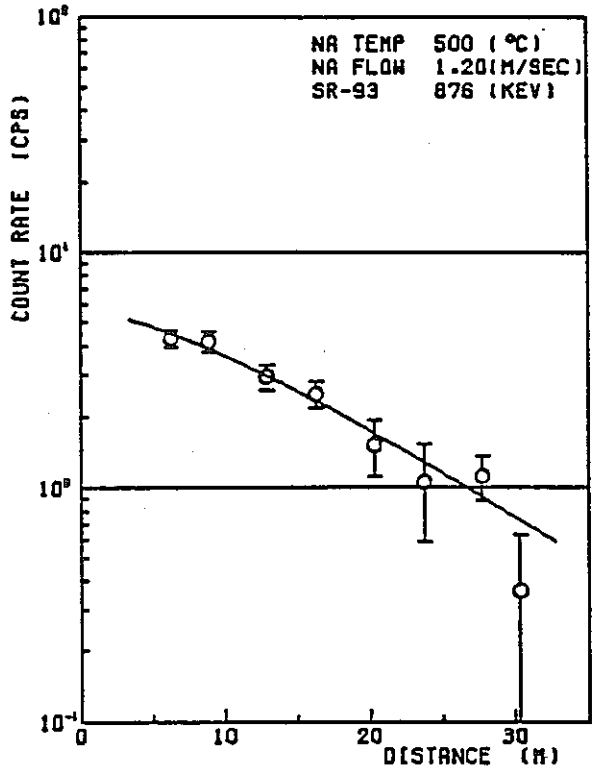

10) EXP. NO. 7

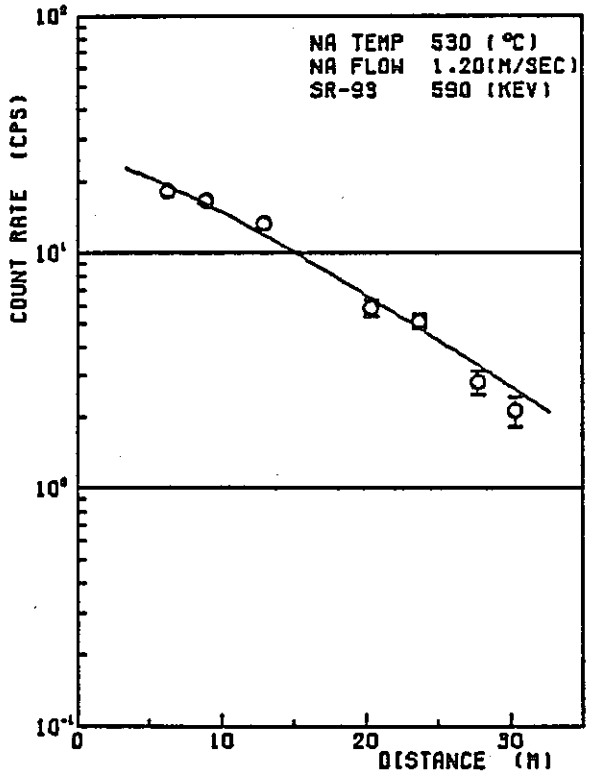

11) EXP. NO. 8

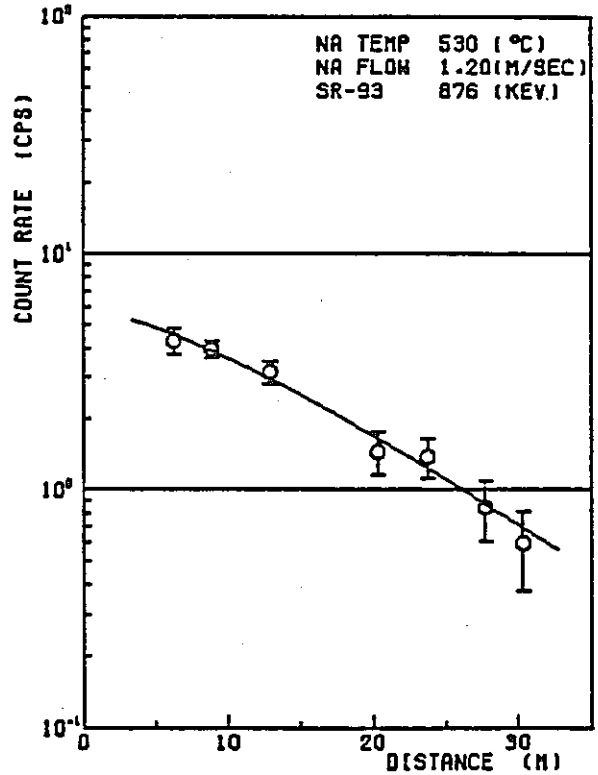

12) EXP. NO. 8

Fig. 5-5 (continued)

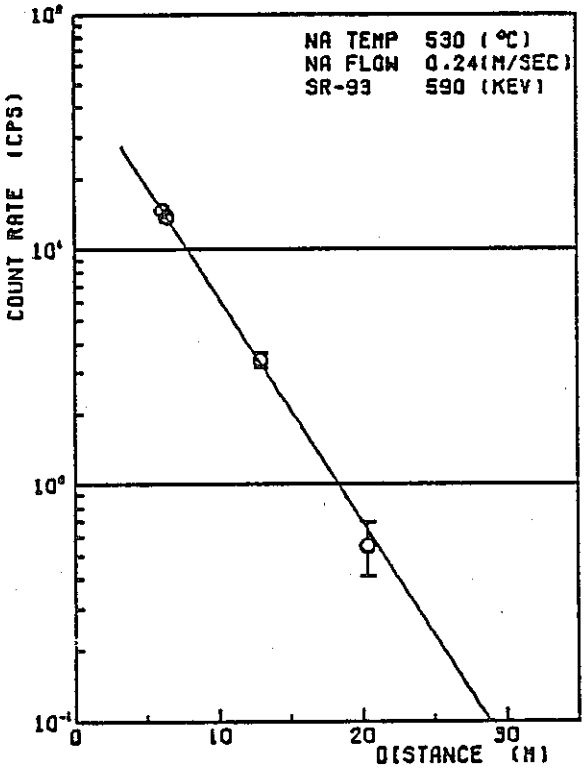

(3) EXP. NO. 14

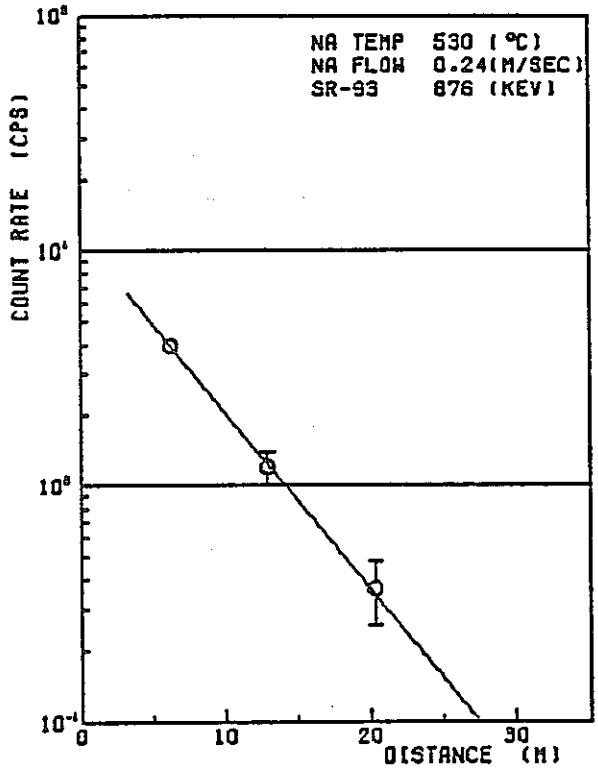

(4) EXP. NO. 14

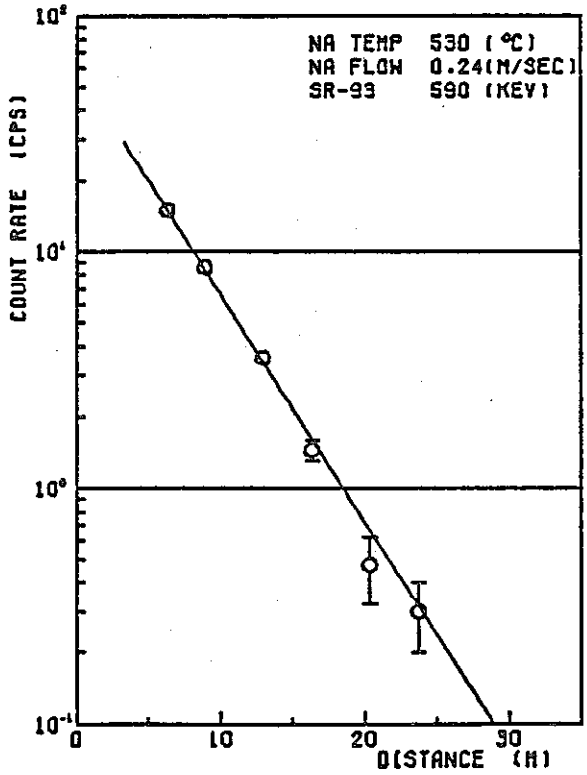

(5) EXP. NO. 16

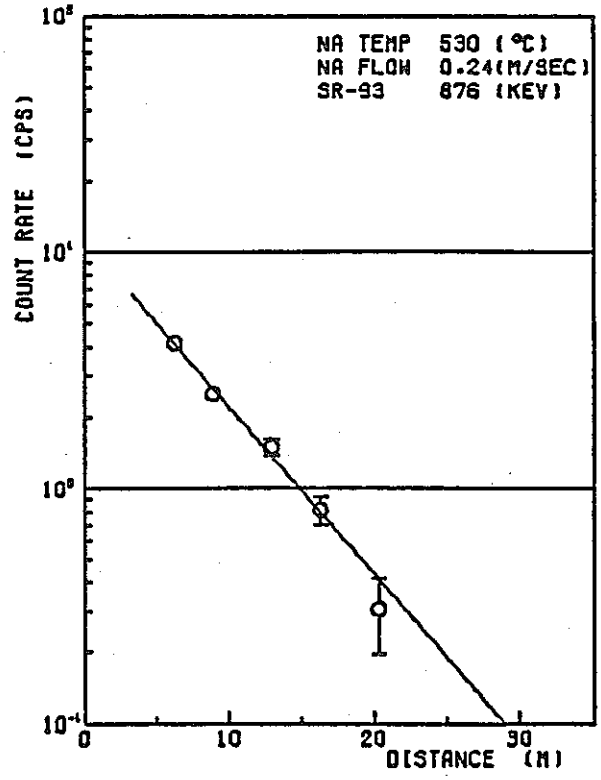

(6) EXP. NO. 16

Fig. 5-5 (continued)

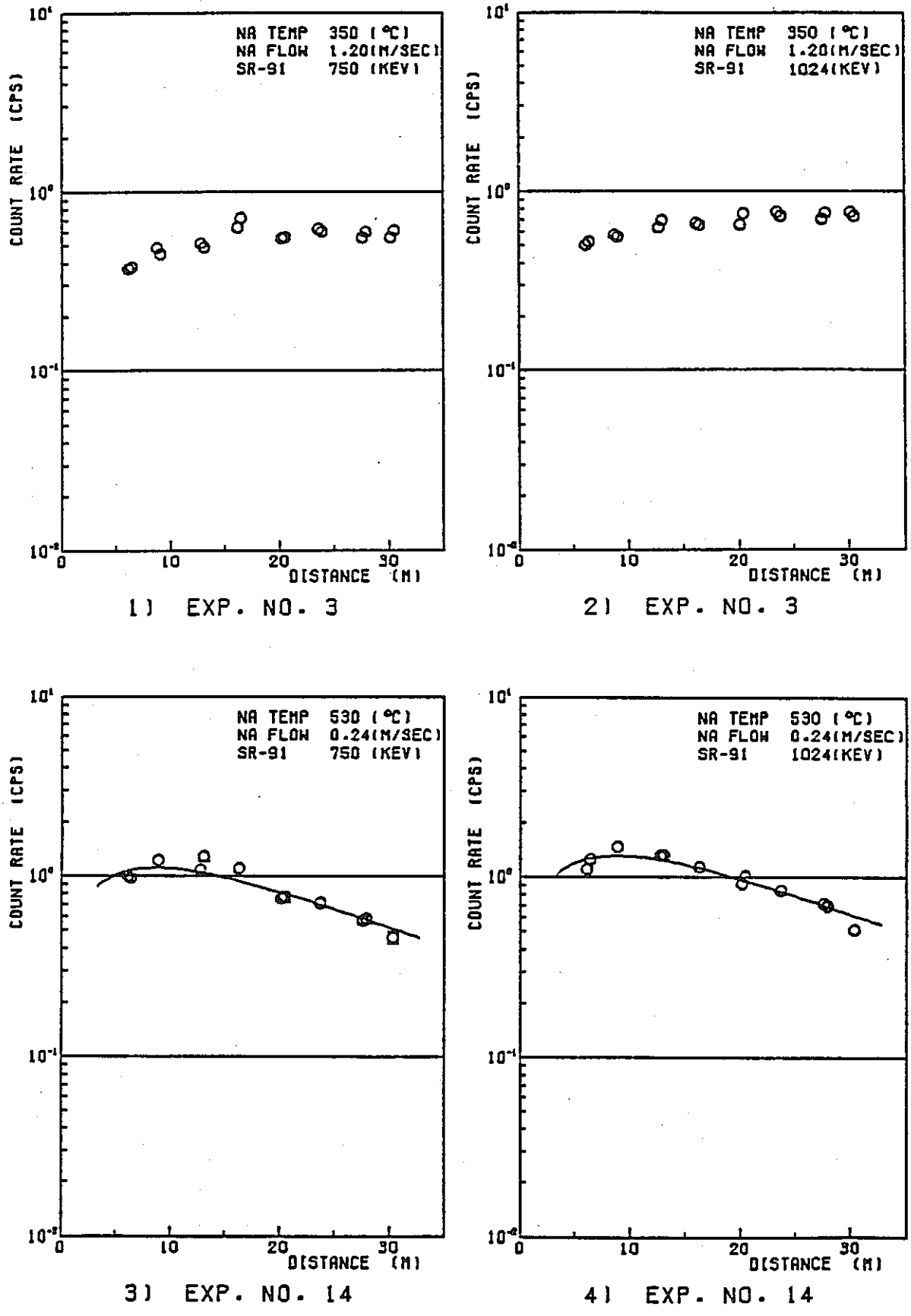

Fig. 5-6 Sr-91 deposition distribution along the delay line

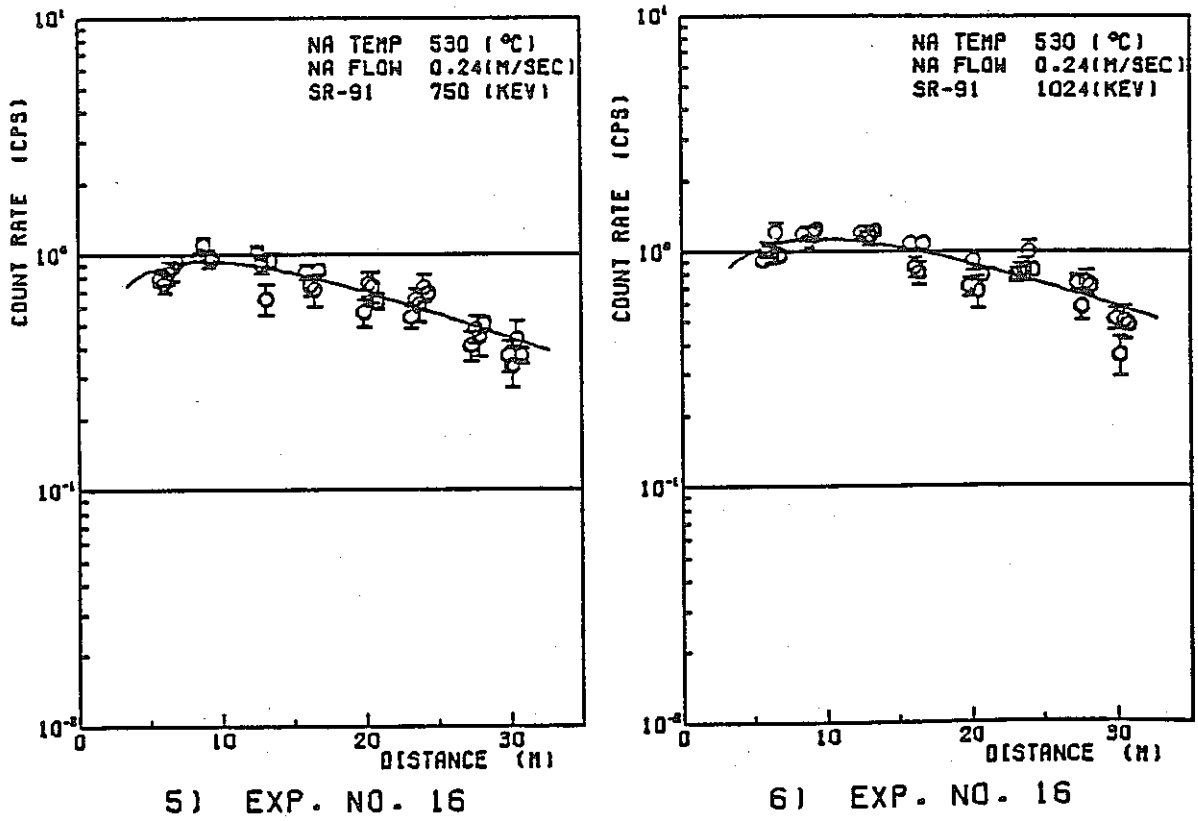

Fig. 5-6 (continued)

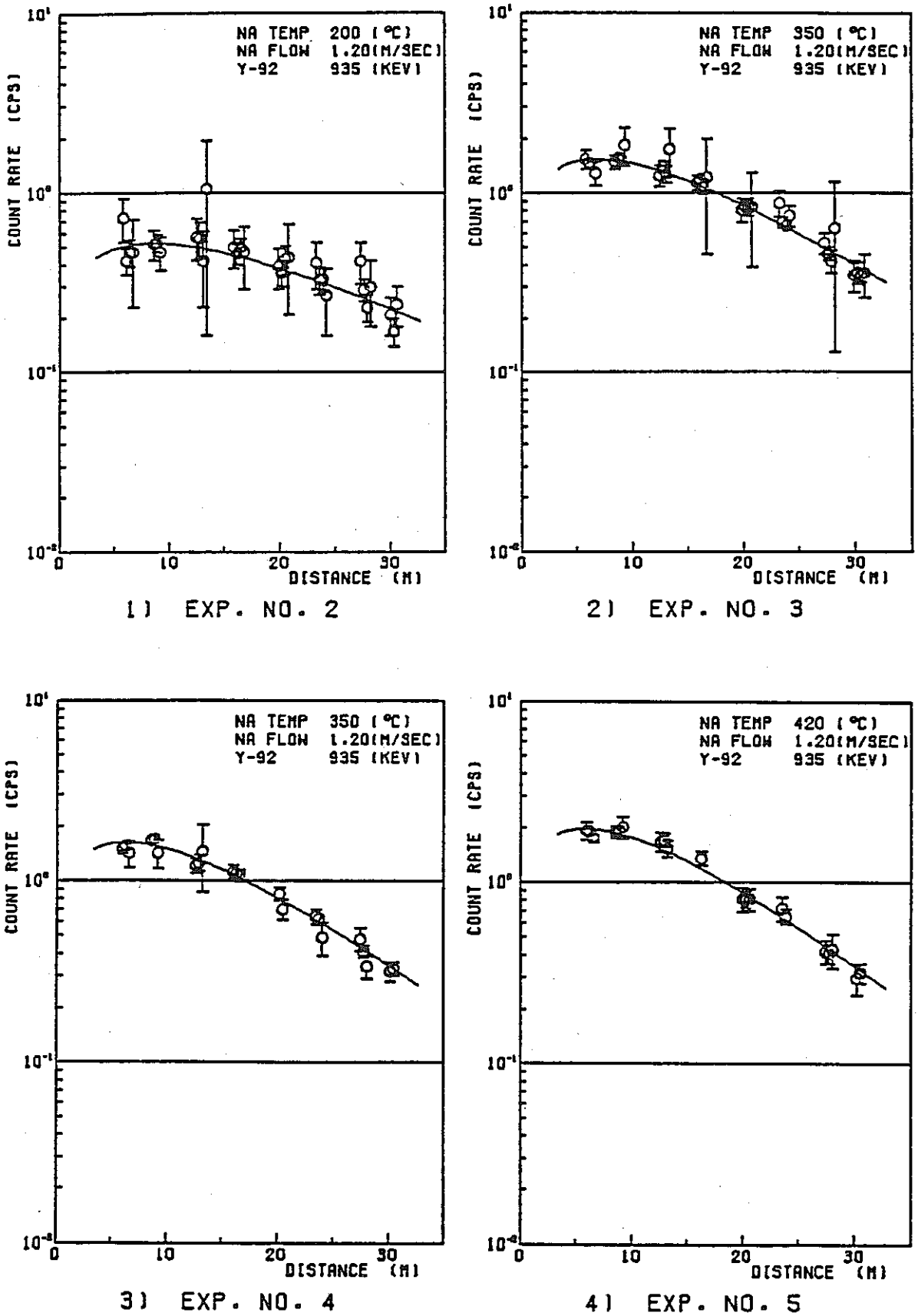

Fig. 5-7 Y-92 deposition distribution along the delay line

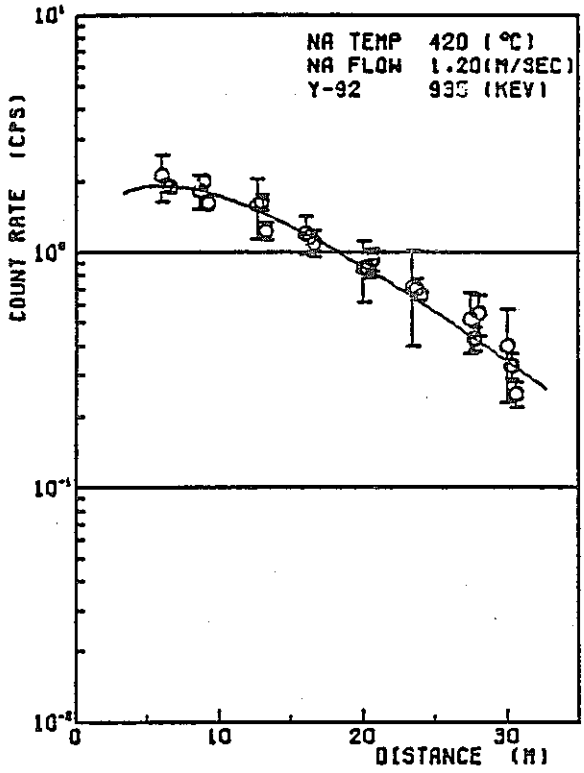

5) EXP. NO. 6

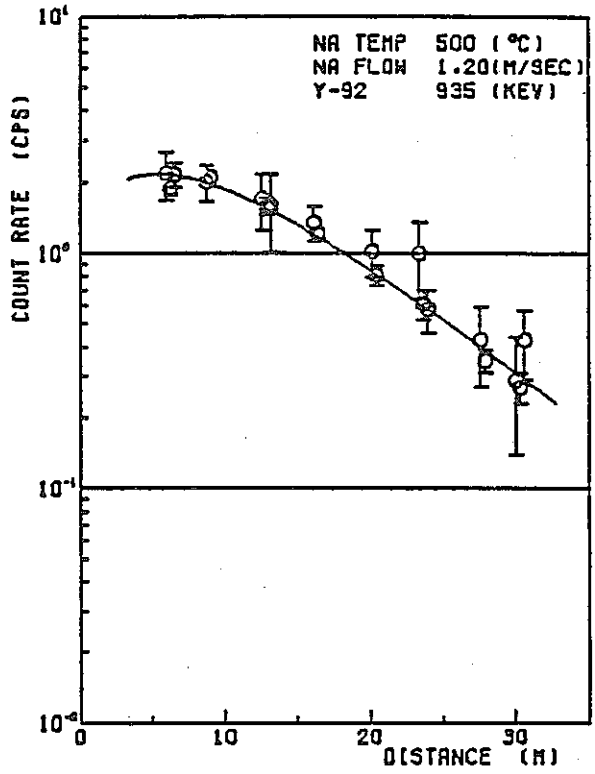

6) EXP. NO. 7

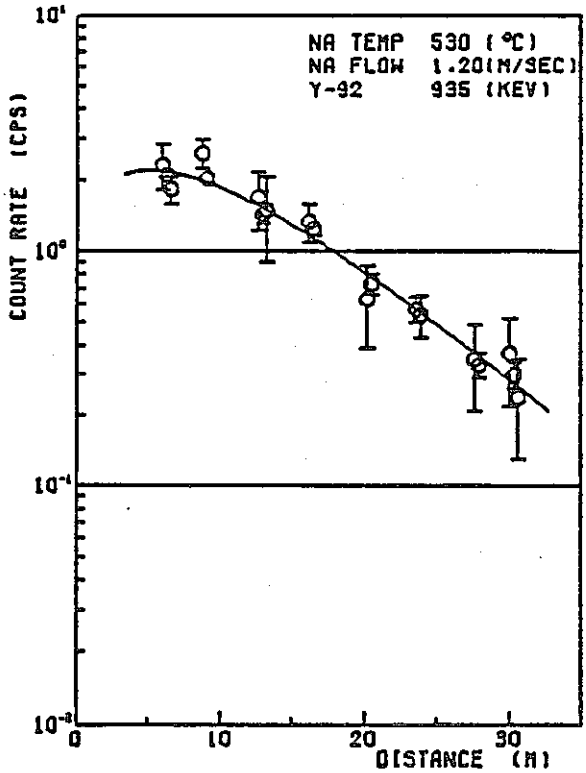

7) EXP. NO. 8

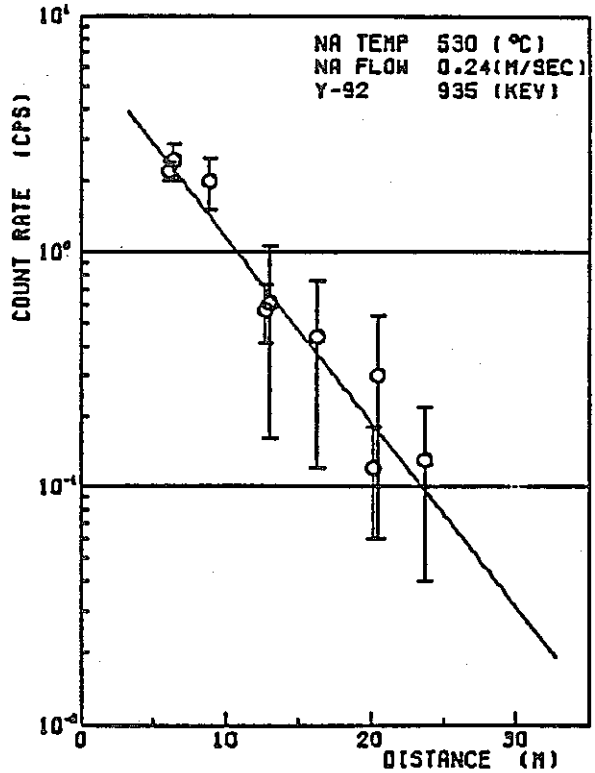

8) EXP. NO. 14

Fig. 5-7 (continued)

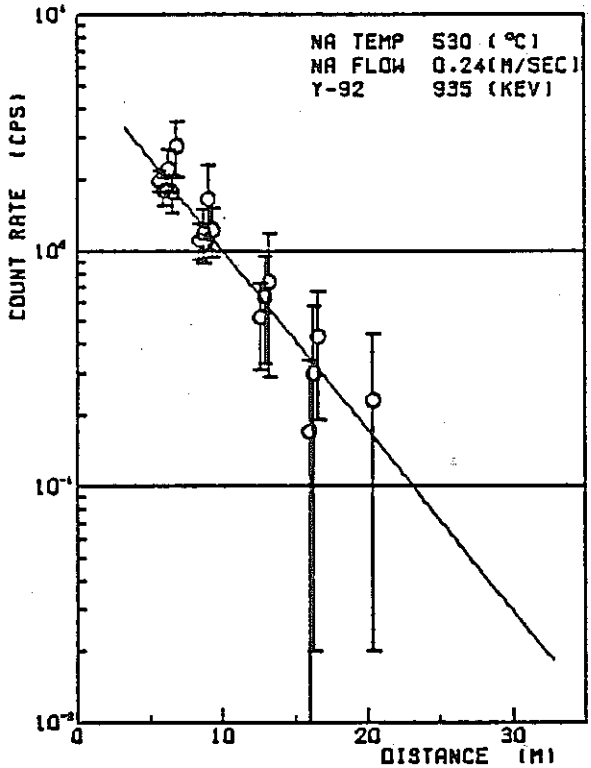

9) EXP. NO. 16

Fig. 5-7 (continued)

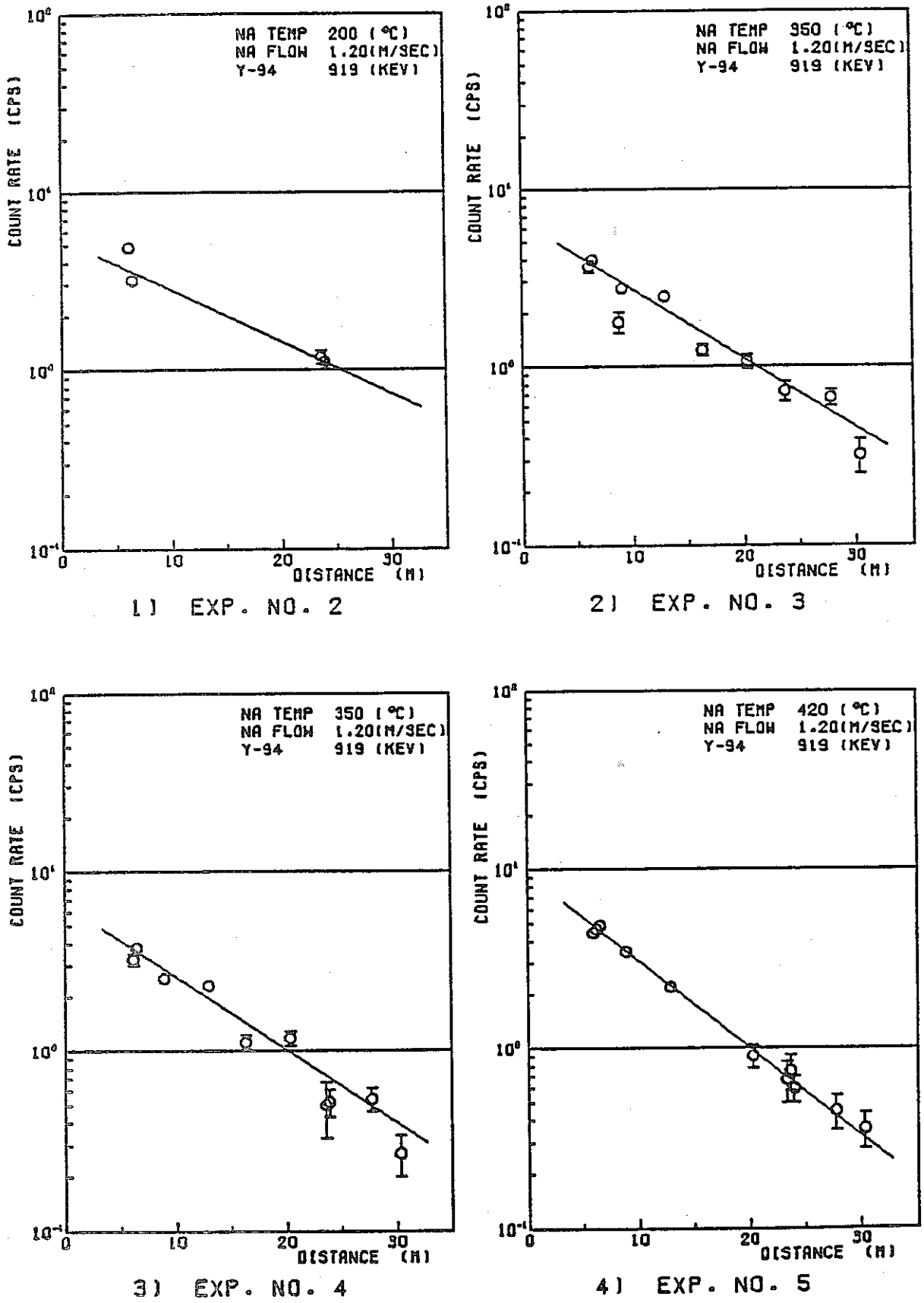

Fig. 5-8 Y-94 distribution along the delay line

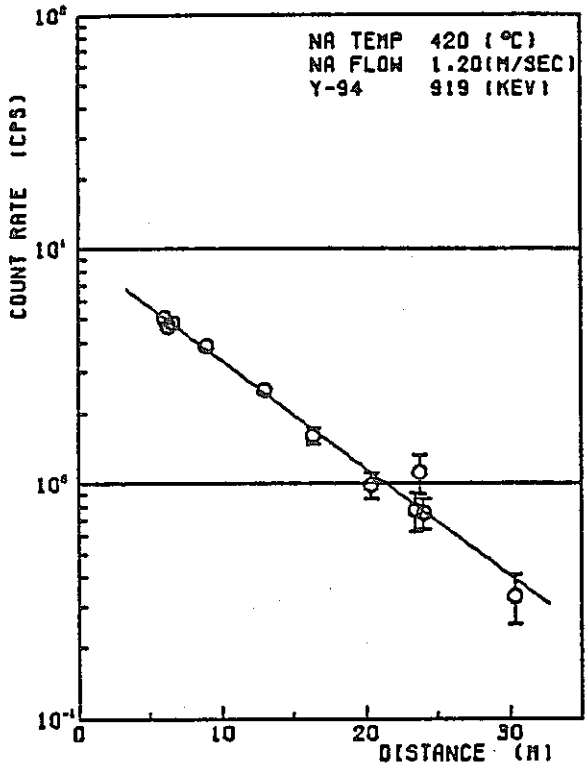

5) EXP. NO. 6

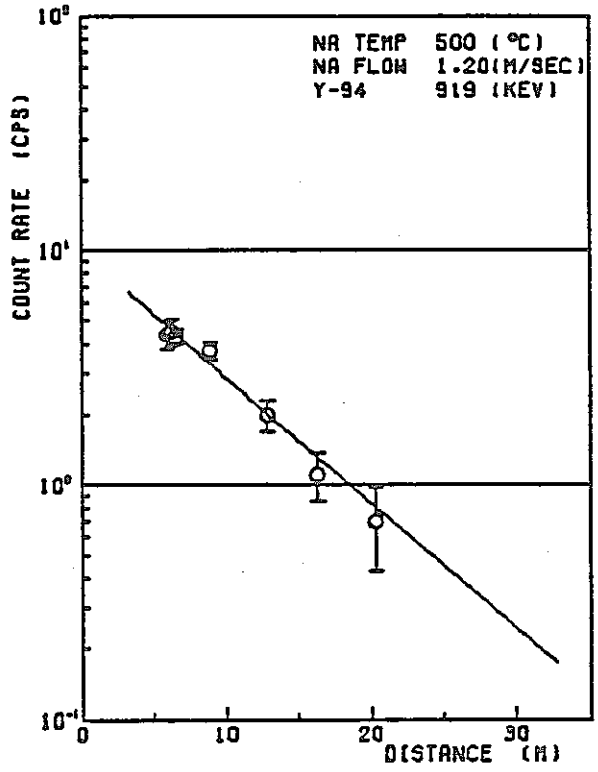

6) EXP. NO. 7

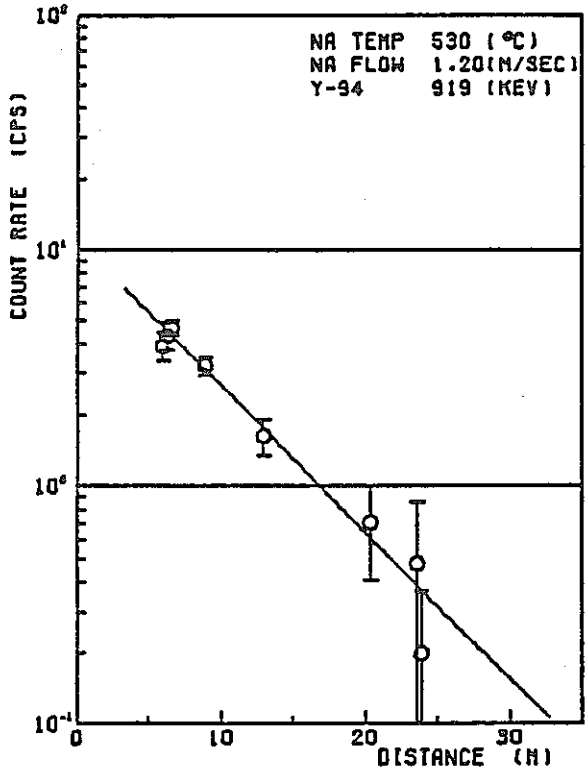

7) EXP. NO. 8

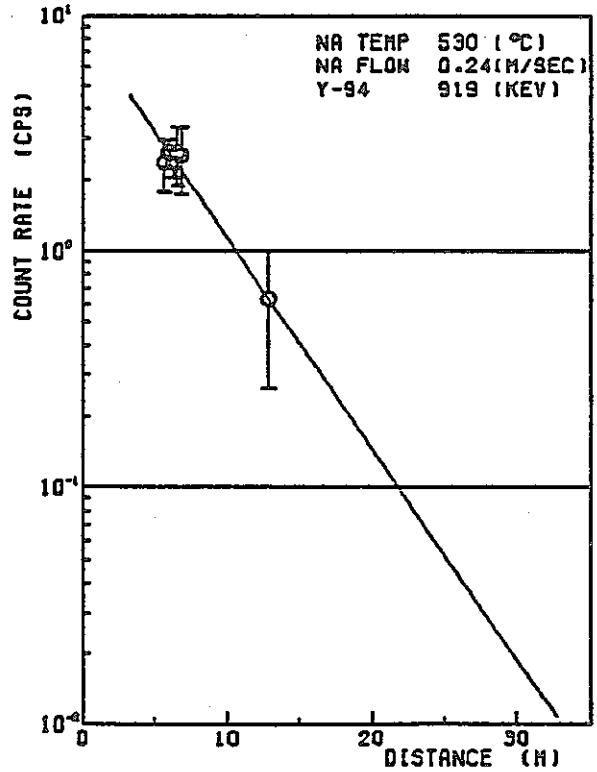

8) EXP. NO. 14

Fig. 5-8 (continued)

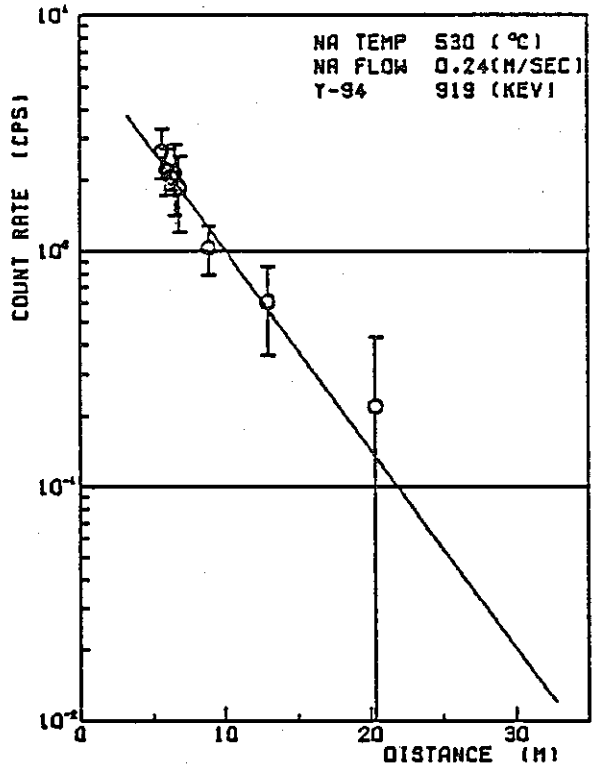

Fig. 5-8 (continued)

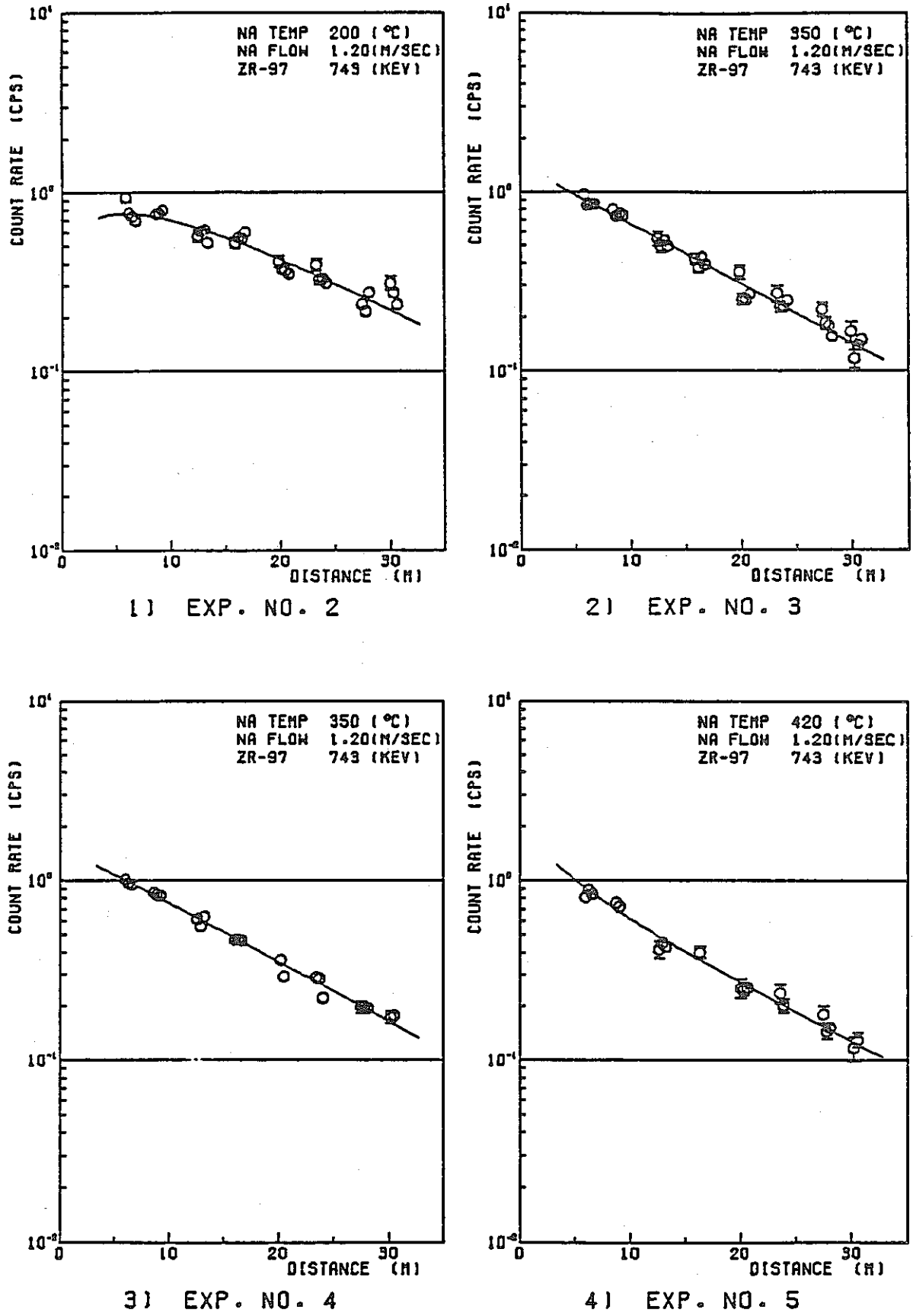

Fig. 5-9 Zr-97 deposition distribution along the delay line

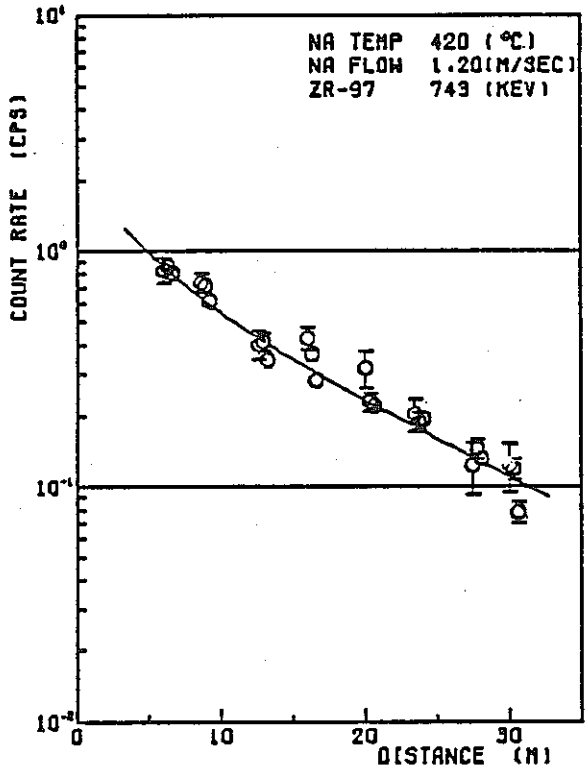

5) EXP. NO. 6

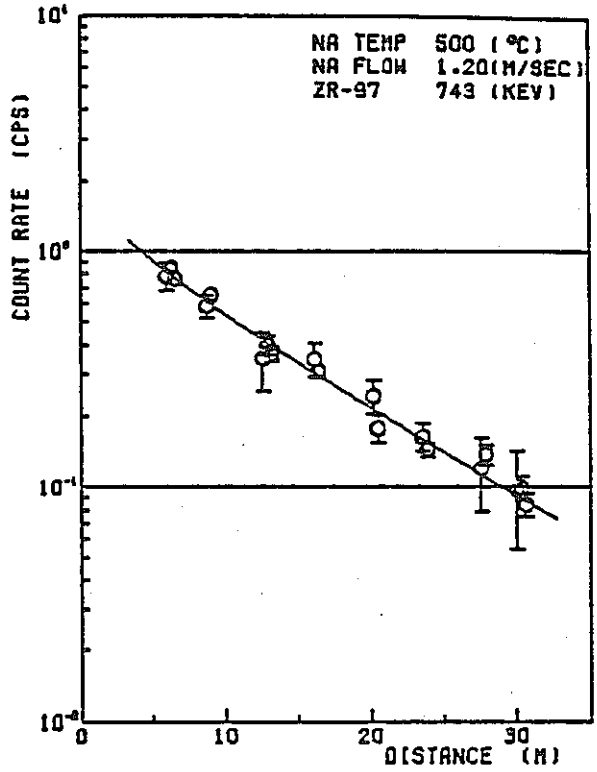

6) EXP. NO. 7

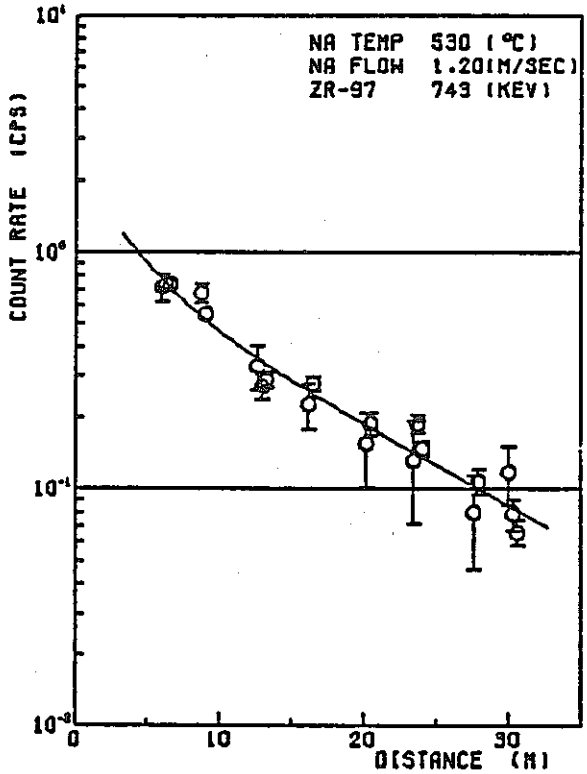

7) EXP. NO. 8

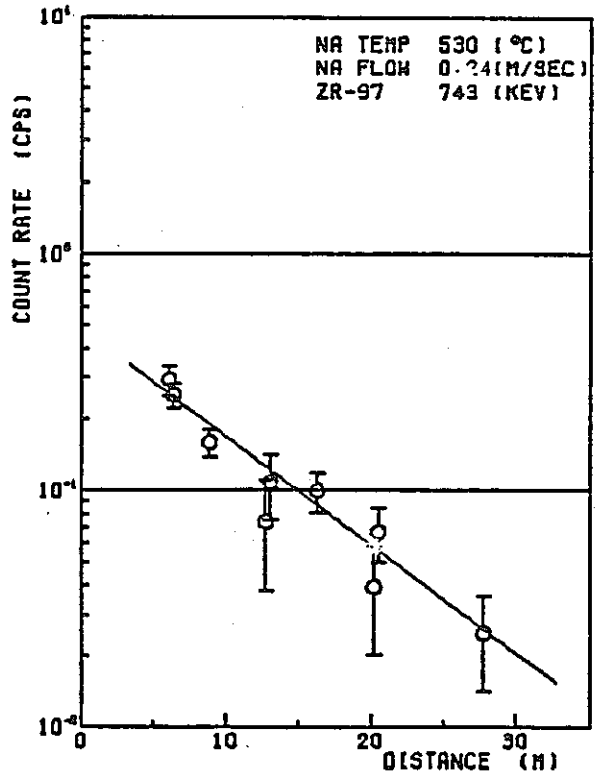

8) EXP. NO. 14

Fig. 5-9 (continued)

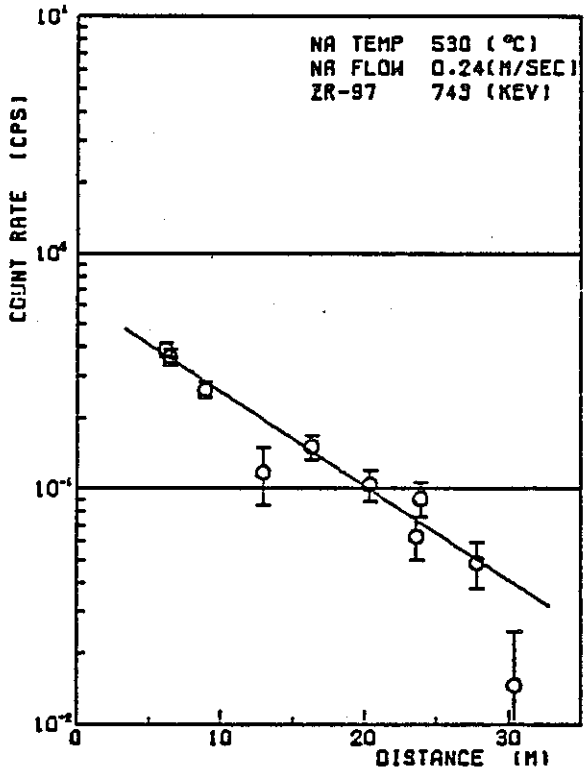

9) EXP. NO. 16

Fig. 5-9 (continued)

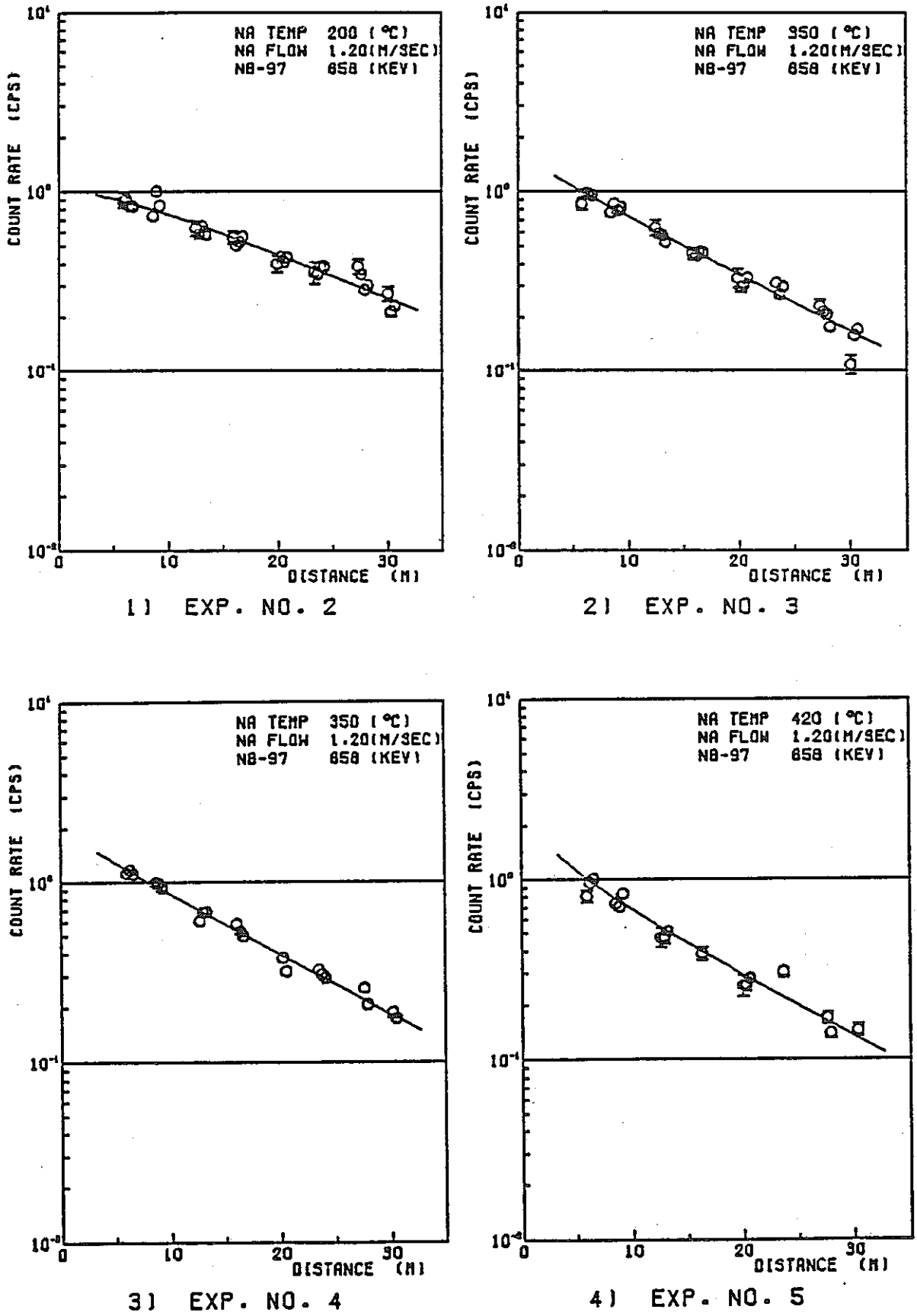

Fig. 5-10 Nb-97 distribution along the delay line

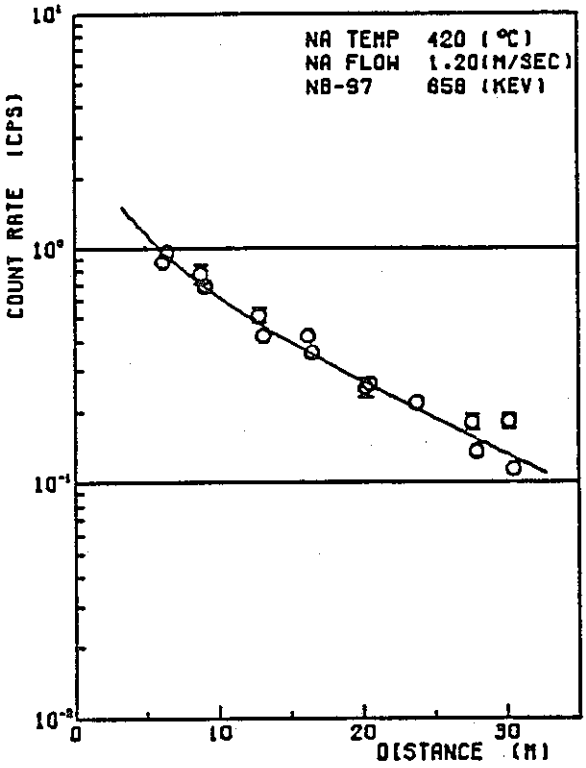

5) EXP. NO. 6

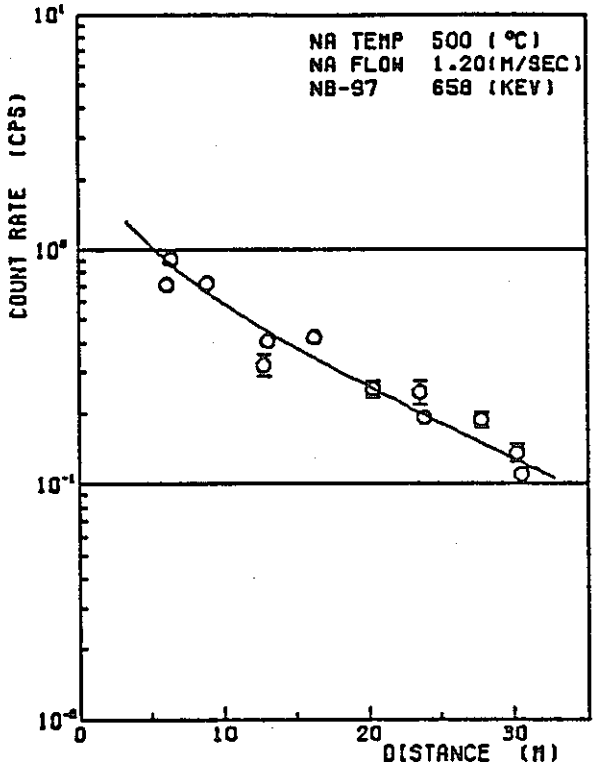

6) EXP. NO. 7

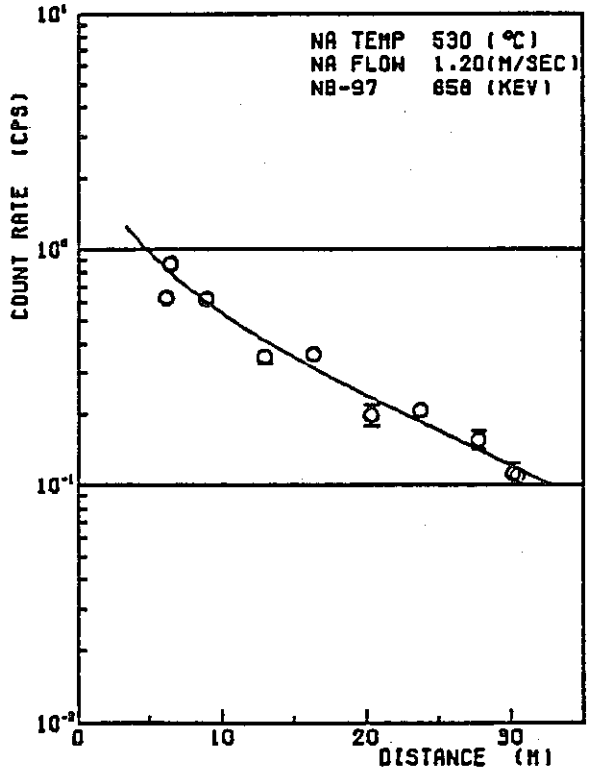

7) EXP. NO. 8

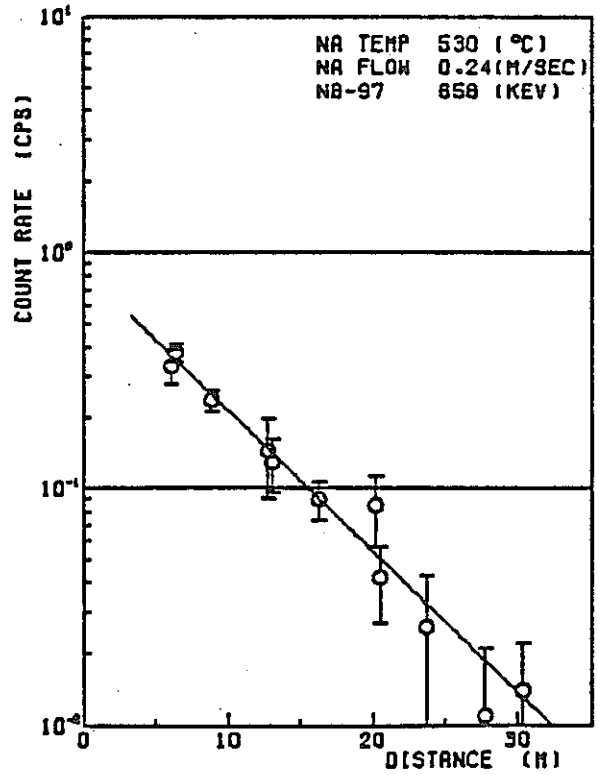

8) EXP. NO. 14

Fig. 5-10 (continued)

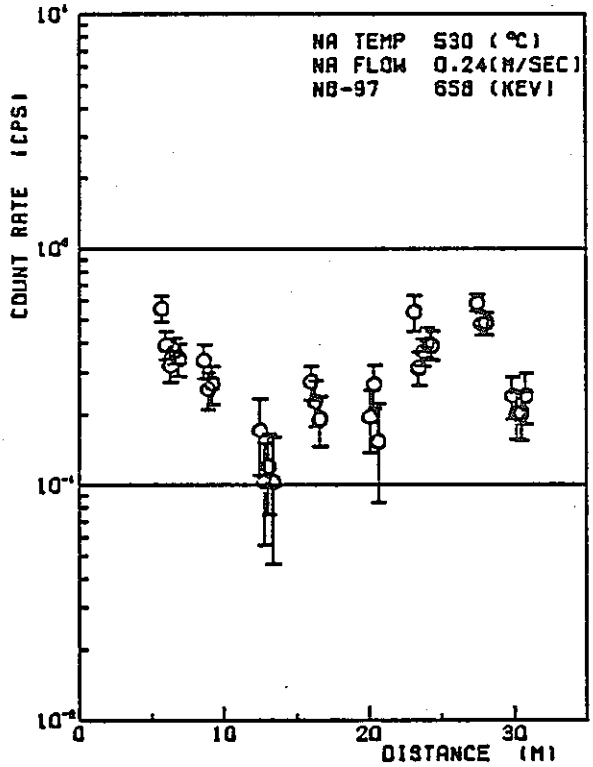

9) EXP. NO. 16

Fig. 5-10 (continued)

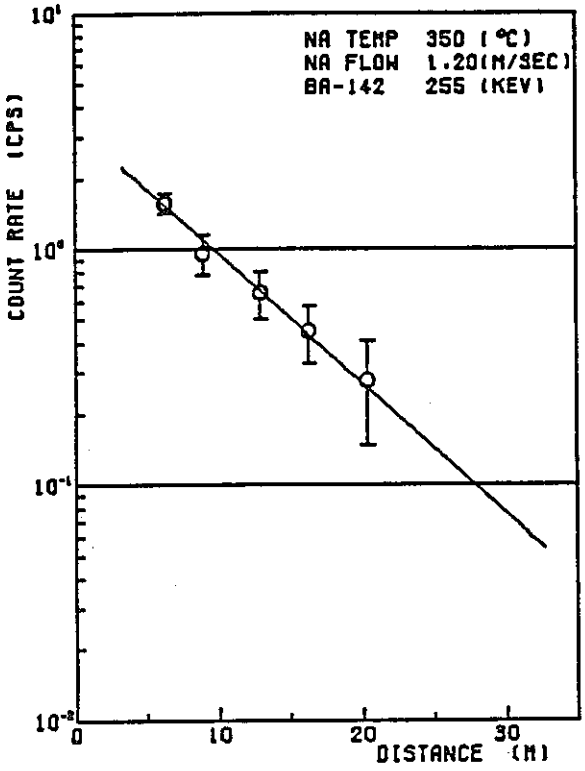

1) EXP. NO. 3

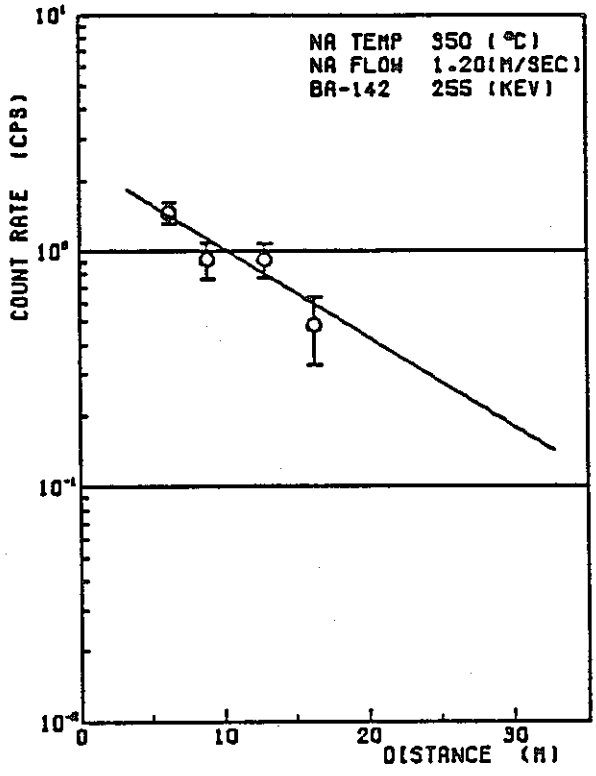

2) EXP. NO. 4

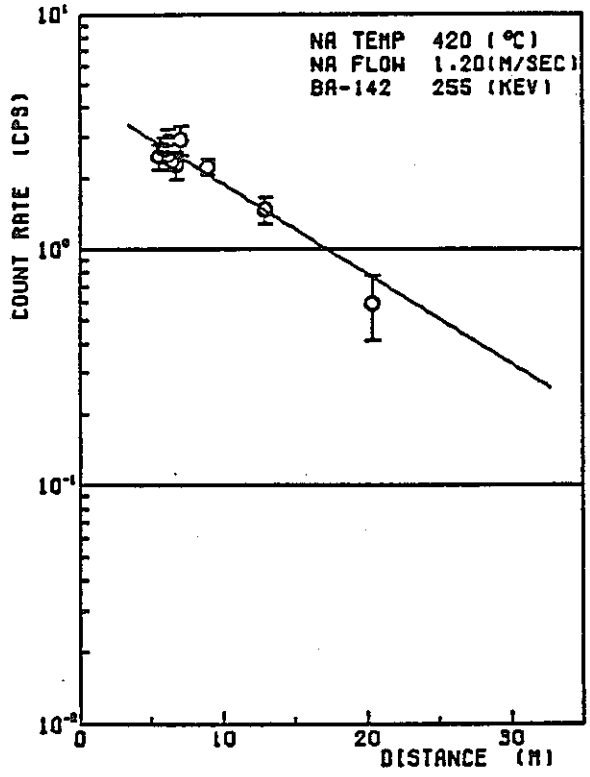

3) EXP. NO. 5

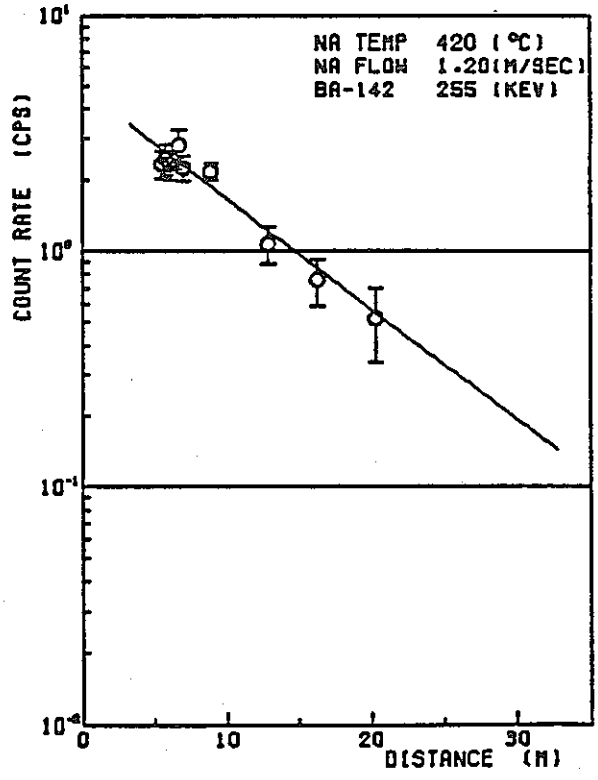

4) EXP. NO. 6

Fig. 5-11 Ba-142 distribution along the delay line

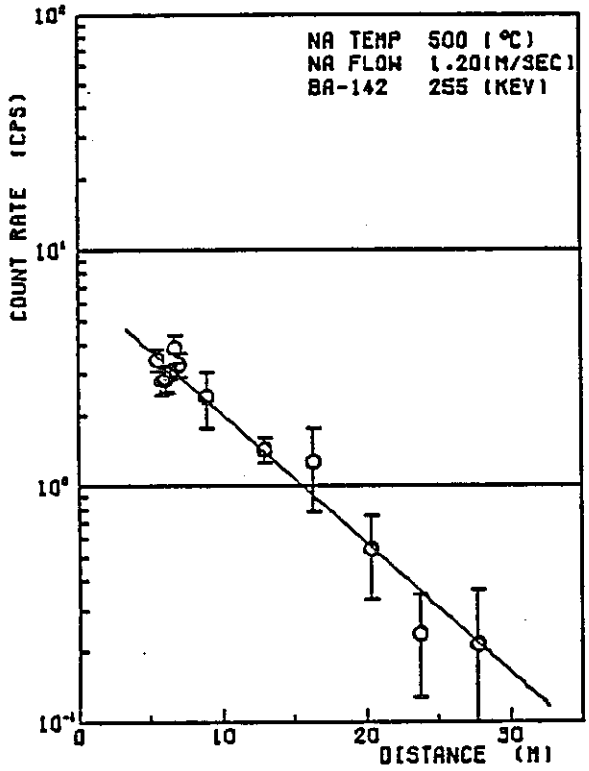

5) EXP. NO. 7

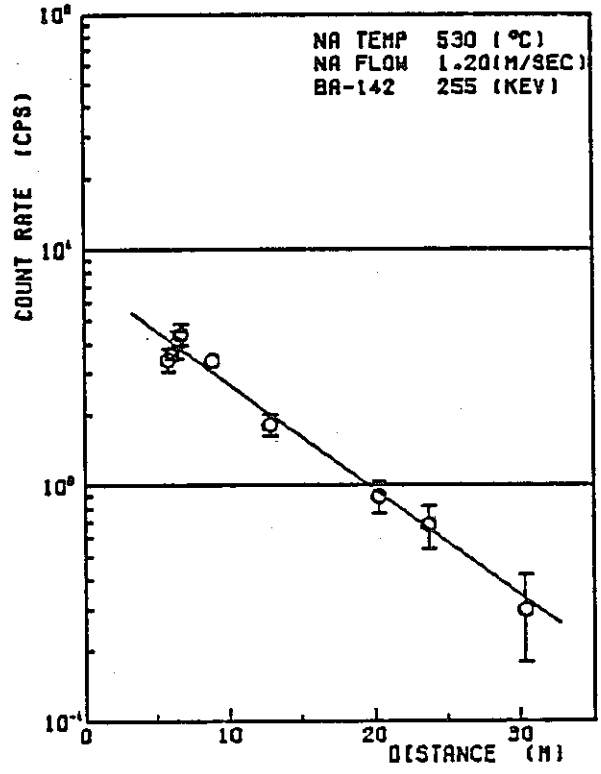

6) EXP. NO. 8

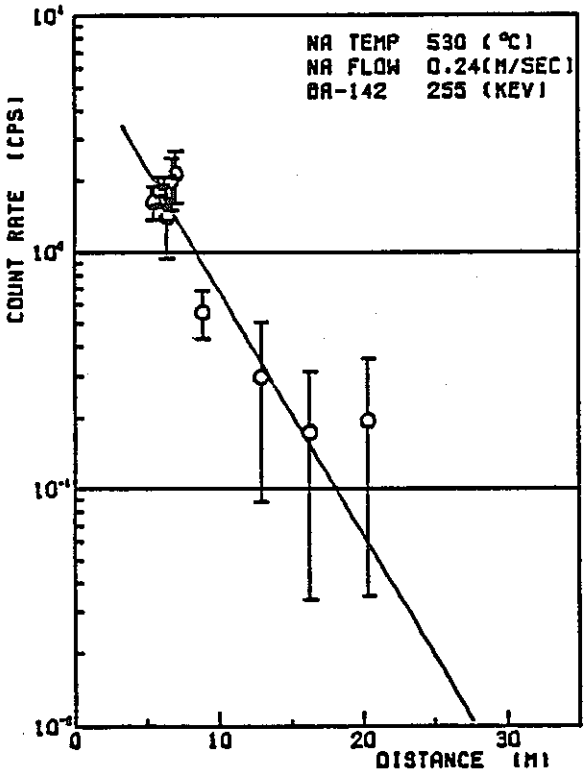

7) EXP. NO. 16

Fig. 5-11 (continued)

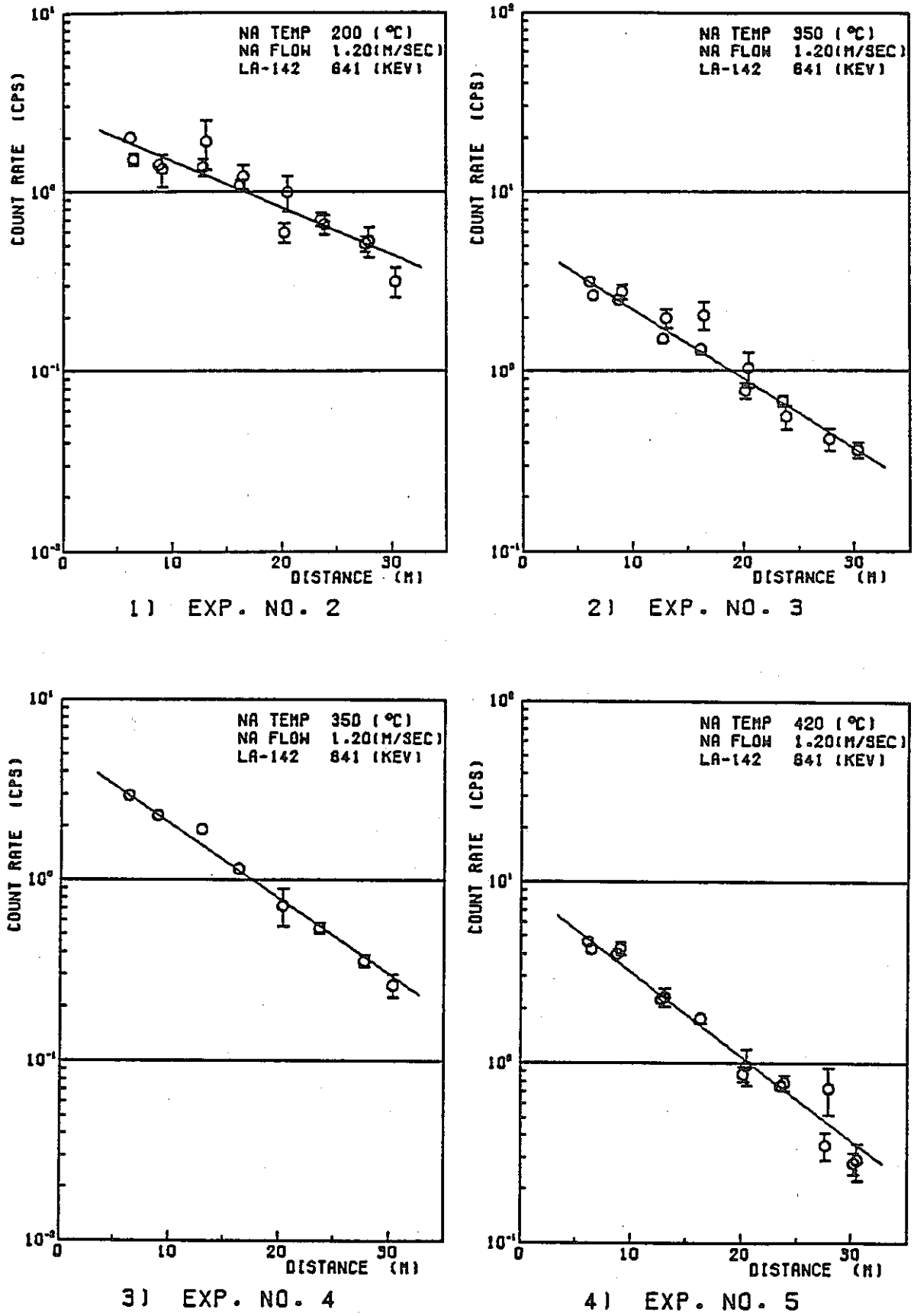

Fig. 5-12 La-142 deposition distribution along the delay line

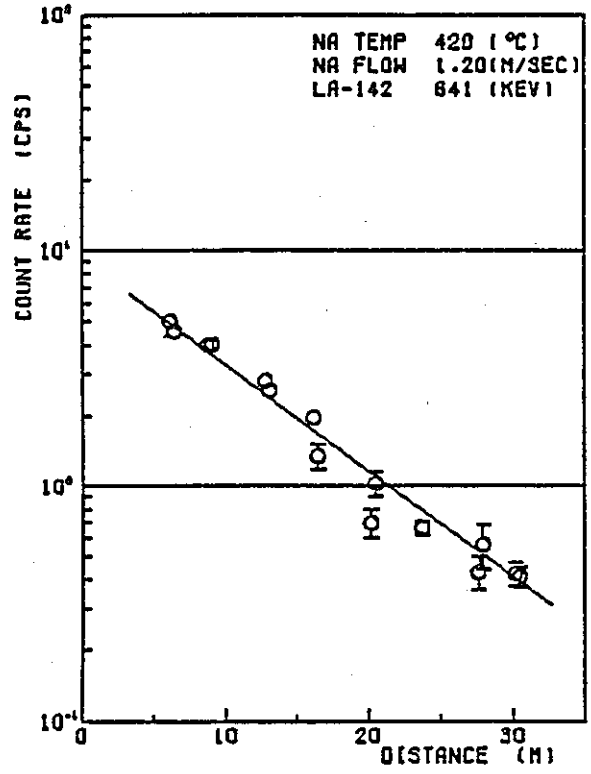

5) EXP. NO. 6

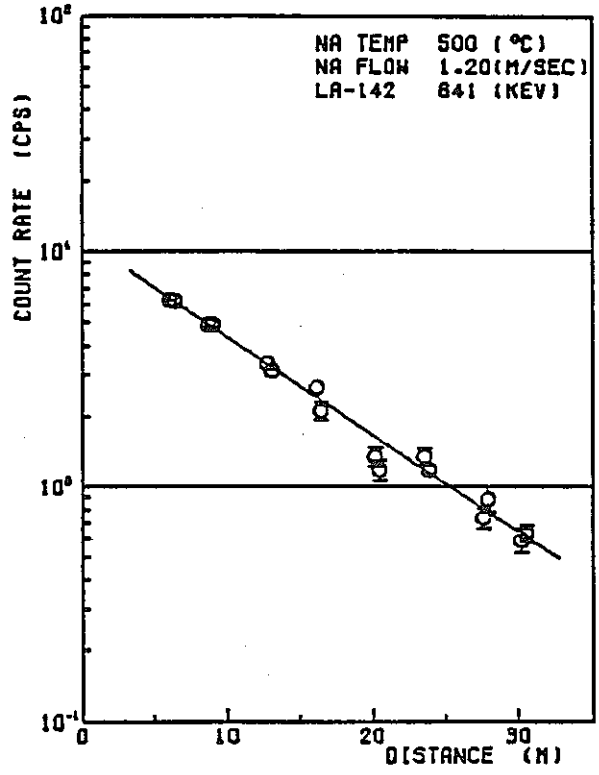

6) EXP. NO. 7

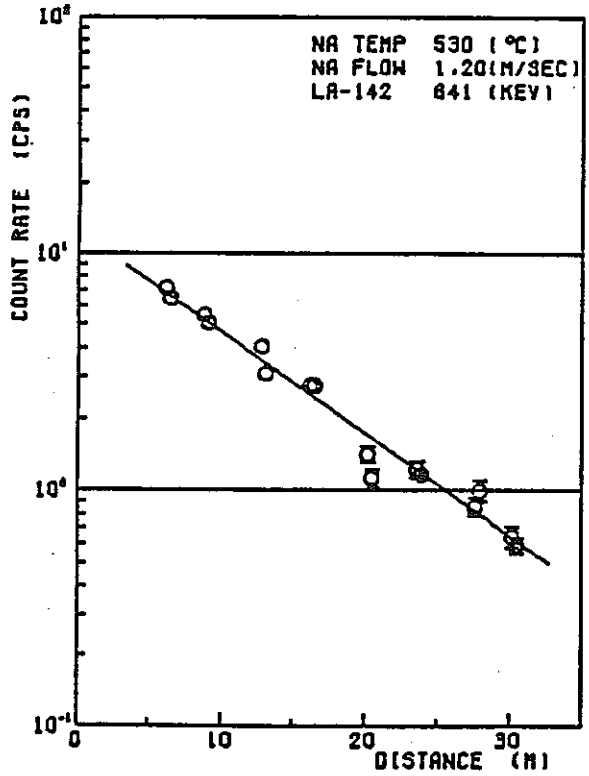

7) EXP. NO. 8

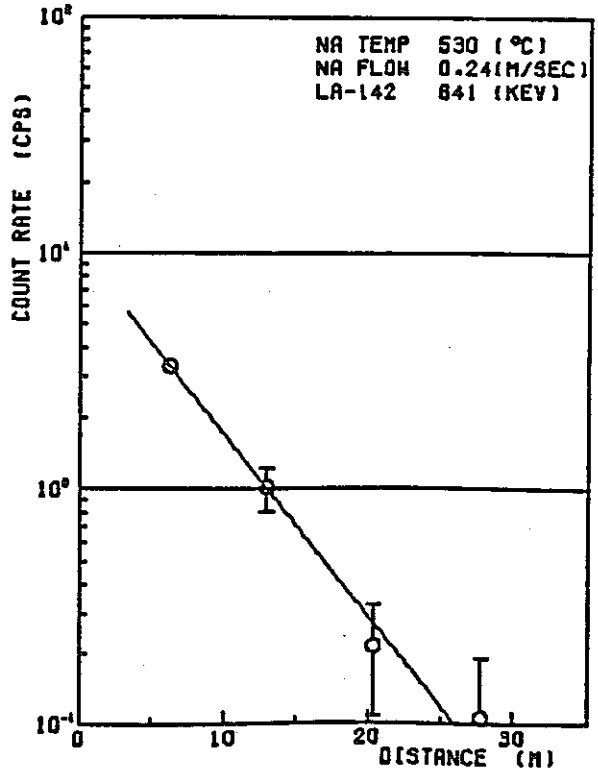

8) EXP. NO. 14

Fig. 5-12 (continued)

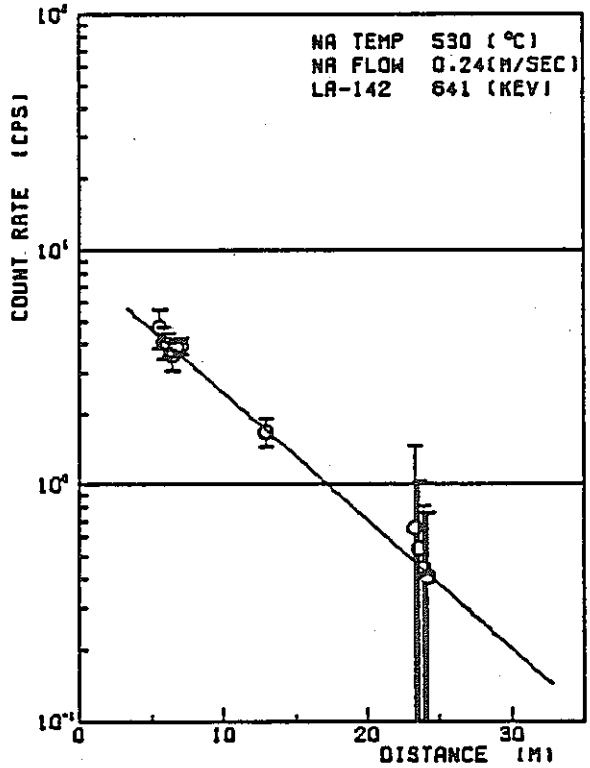

9) EXP. NO. 16

Fig. 5-12 (continued)

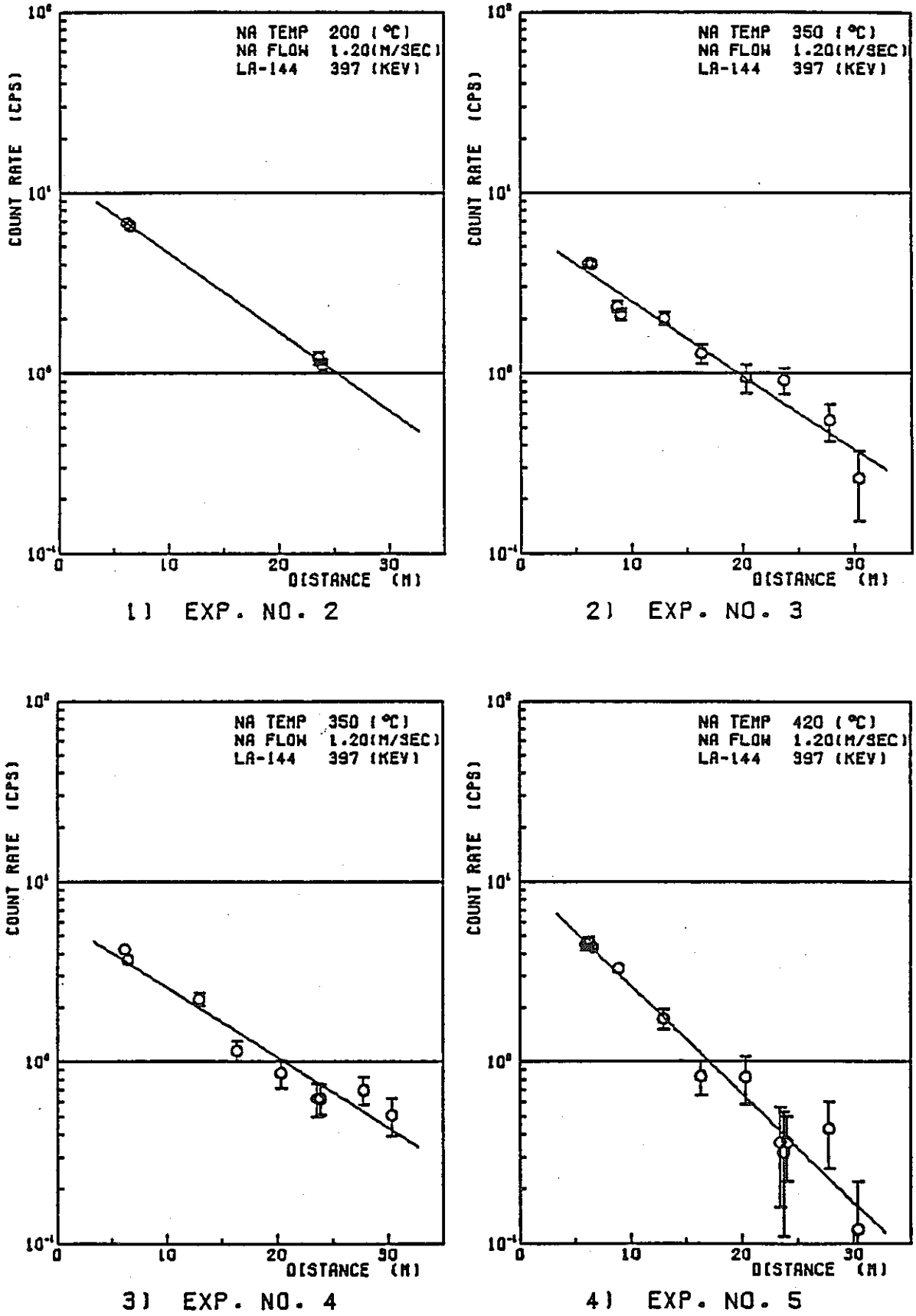

Fig. 5-13 La-144 distribution along the delay line

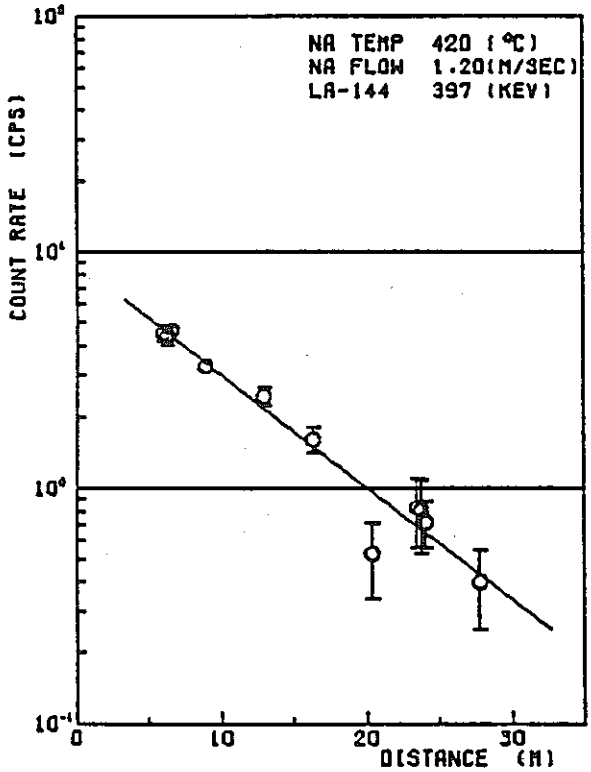

5) EXP. NO. 6

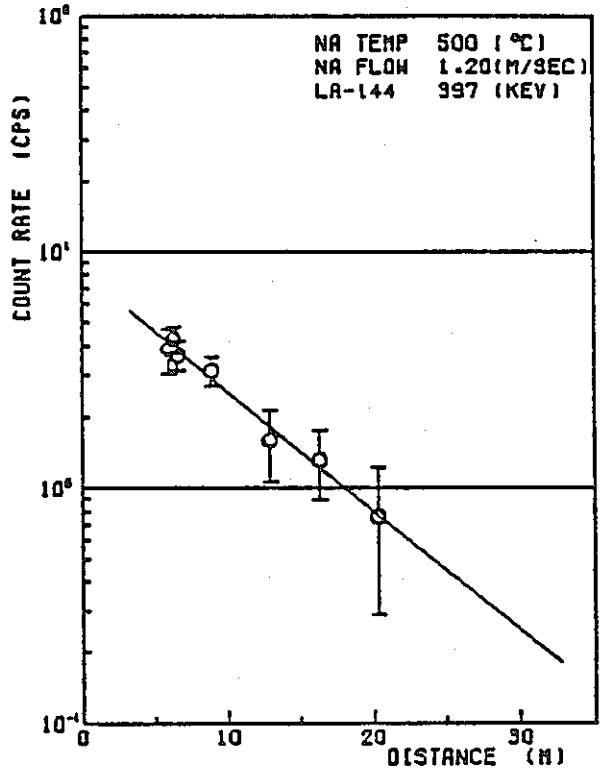

6) EXP. NO. 7

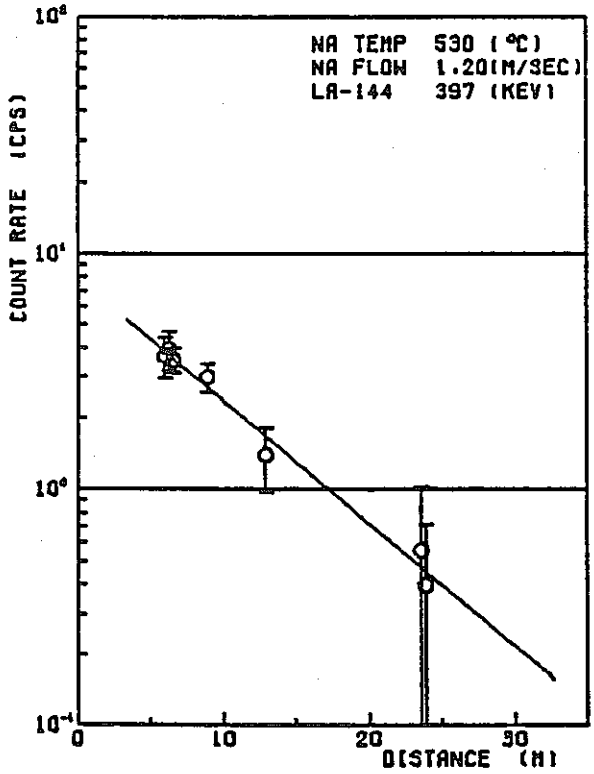

7) EXP. NO. 8

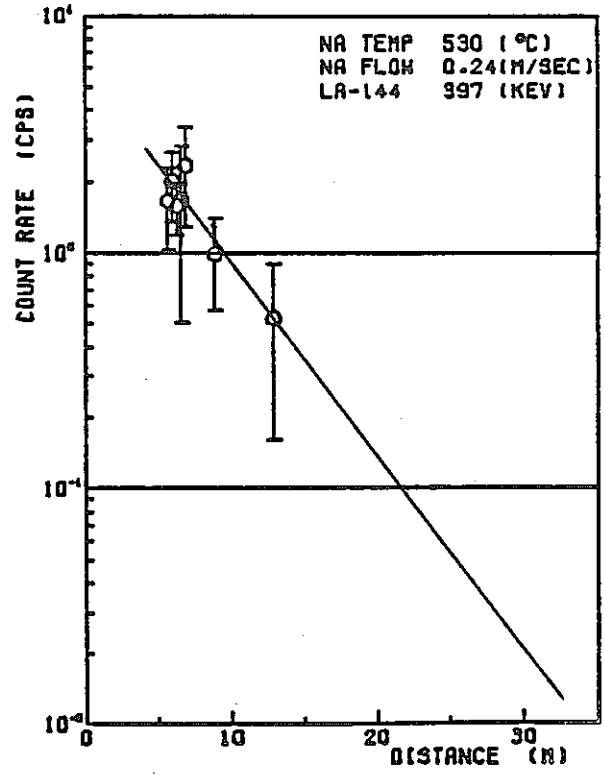

8) EXP. NO. 16

Fig. 5-13 (continued)

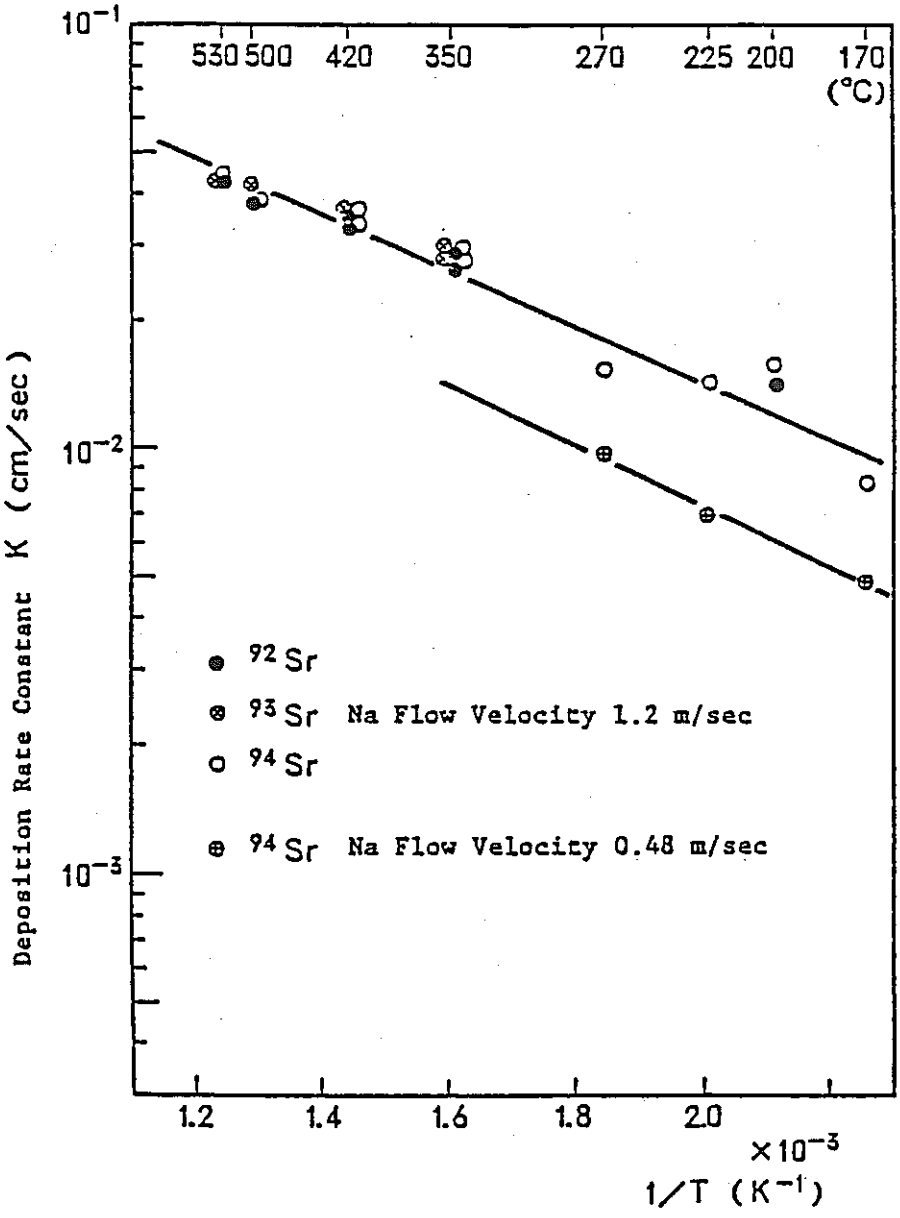

Fig. 5-14 Relationship between Sr deposition rate constant and reciprocal temperature

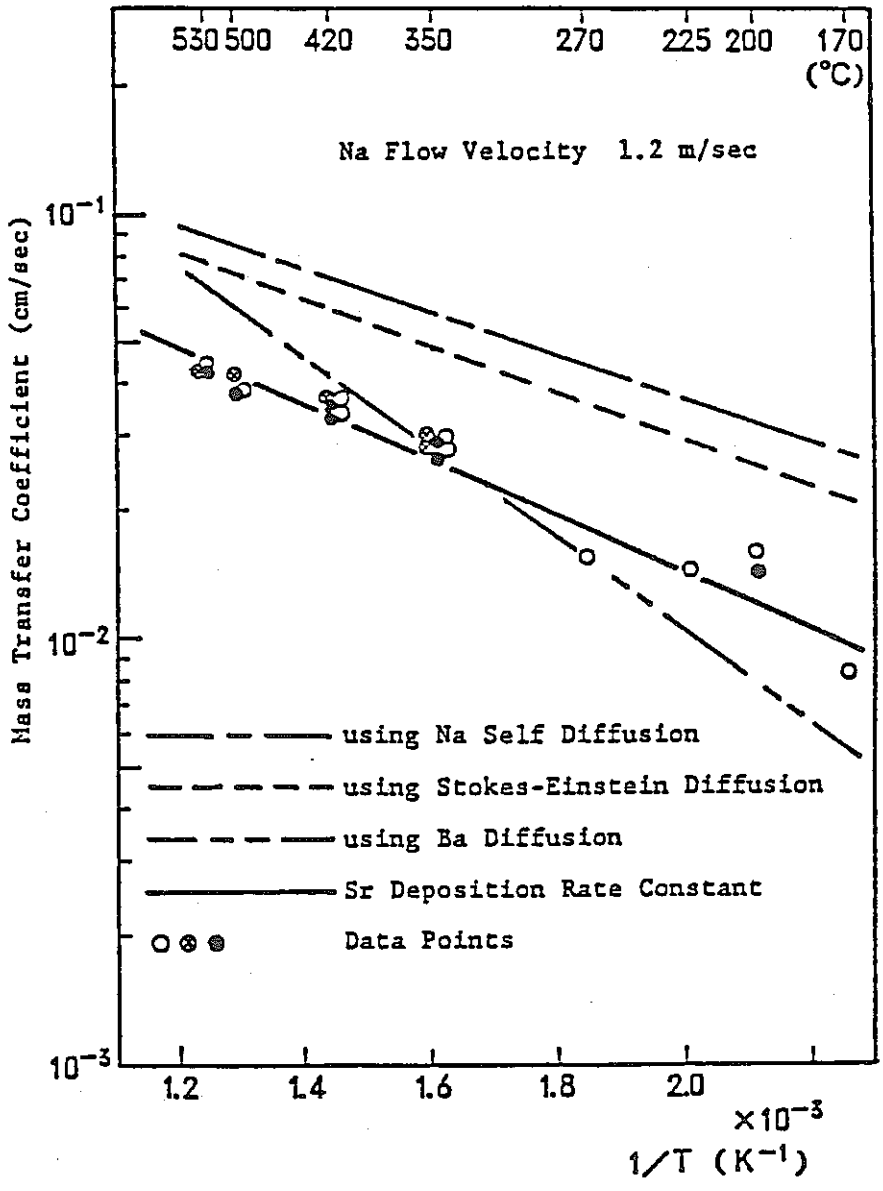

Fig. 5-15 Comparison between Sr deposition rate constant and mass transfer coefficients

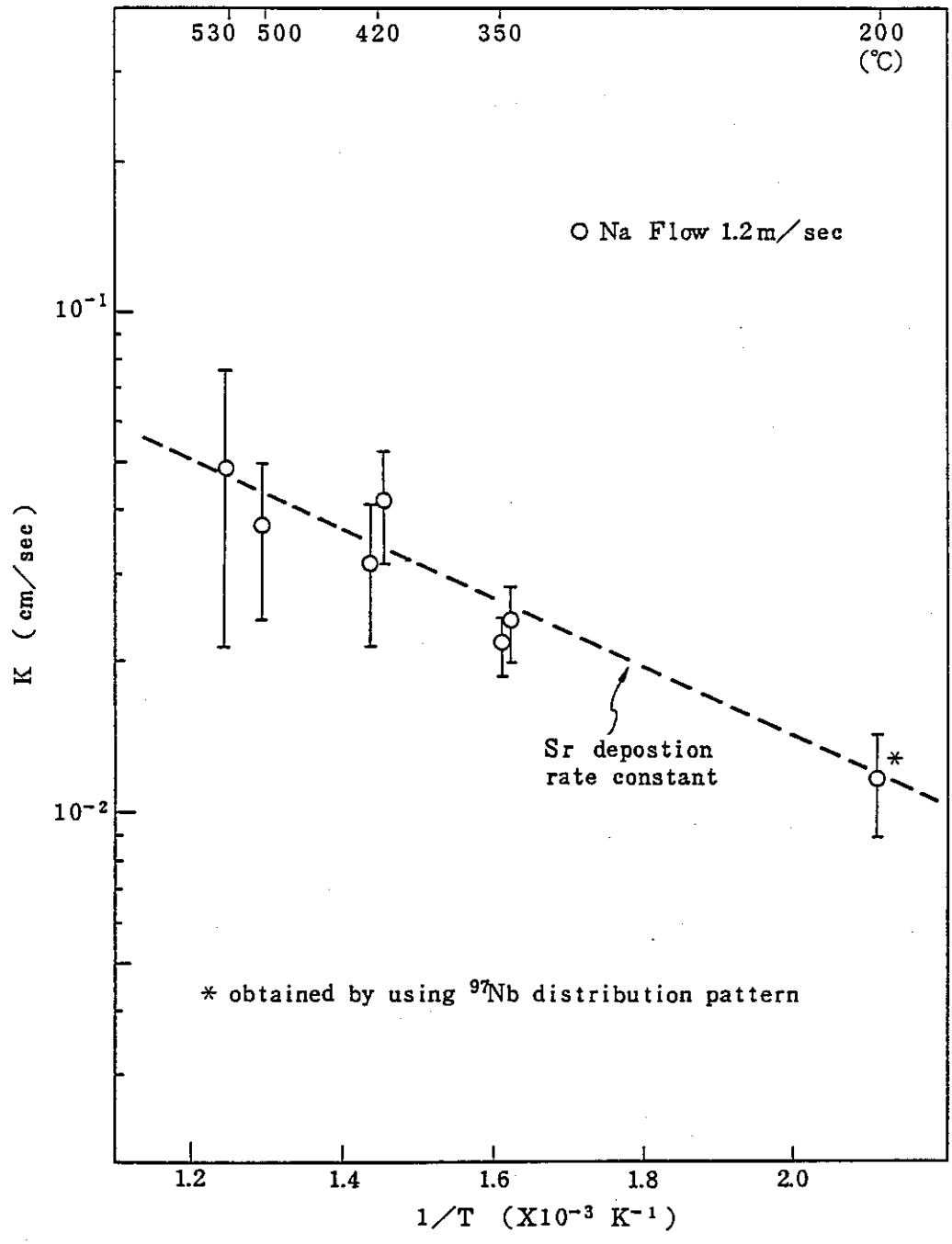

Fig. 5-16 Relationship between Y deposition rate constant and reciprocal temperature obtained by using Zr-97 deposition distribution pattern

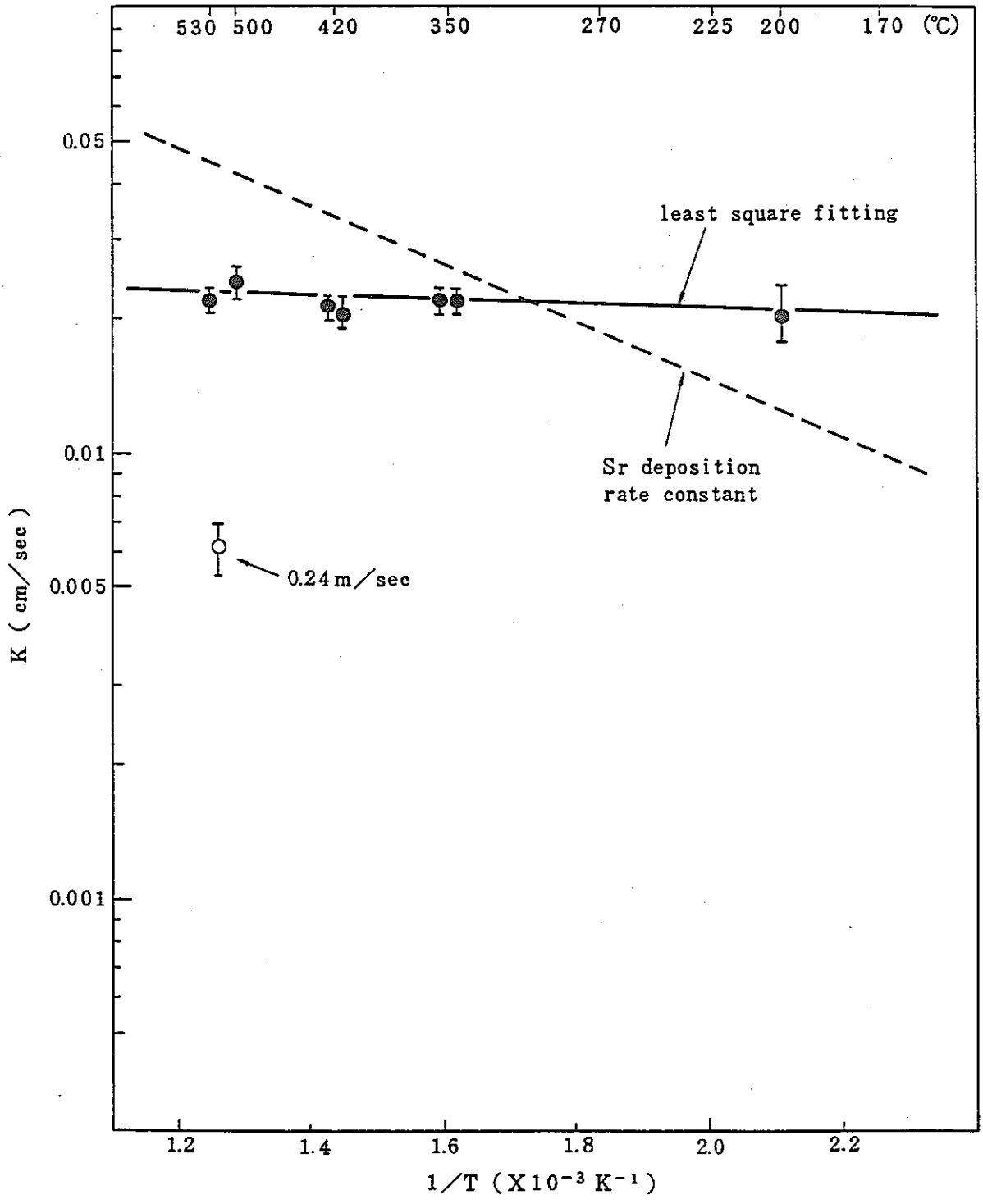

Fig. 5-17 Relationship between Zr deposition rate constant and reciprocal temperature obtained by using Zr-97 deposition distribution pattern

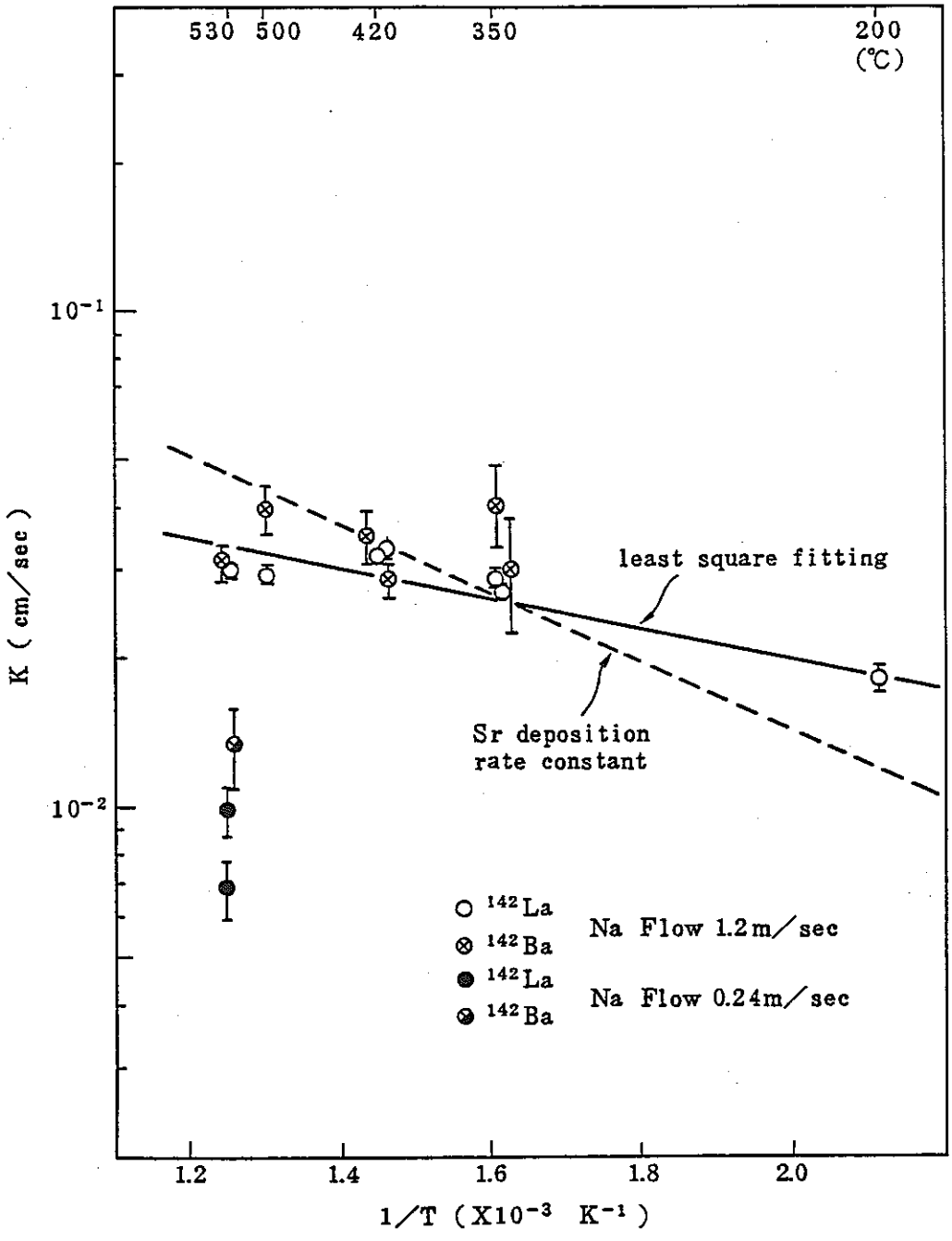

Fig. 5-18 Relationship between Ba deposition rate constant and reciprocal temperature obtained by using Ba-142 and La-142 deposition distribution pattern

6. K FACTOR BY GAMMA-RAY MEASUREMENT OF VOLATILE FP

6.1 Introduction

20% enriched uranium dioxide granules with 0.5 ∿ 0.6 mm diameter of 100g are used as the irradiation specimen in FPL-II. Irradiation of TTR thermal neutron produces fission product (FP) in the specimen. A part of FP nuclides is released in to sodium by recoil. The release fraction, i.e. ratio of release rate to production rate of FP nuclides, is useful to evaluate the data obtained by irradiation tests of FPL-II.

k factor (roughness factor), ratio of experimental release fraction to calculated one by recoil model, is required for the evaluation of released FP nuclides amount in coolant system at the case of fuel failure in FBR. Release fraction of FP was calculated on the basis of FP radioactivity in sodium obtained by irradiation test. 8 FP nuclides were applied to calculation: volatile products, such as Br-86, Br-88, Rb-89, Te-134, and I-136m were detected in irradiation tests at sodium temperature between 420 and 530°C, flow rate 5 and 1 ℓ/min and rare gas products, such as Kr-90, Xe-139 and Xe-140. As seen from these results, the release fraction of FP depends on mass number, i.e. the release fractions are 0.80 ± 0.02% for light FPs of mass number less than 90, and 0.48 ± 0.02% for heavy FPs of mass number around 140.

These values corresponds to 0.40 ± 0.01 times of release fraction values calculated from the recoil model.

6.2 Calculation of Release Fraction

6.2.1 FP nuclides applied

The release fraction of FP is calculated based on the FP concentration in the sodium at irradiation position obtained from the FP concentration in the delay line during irradiation. When the adsorption (*) of FP on the loop piping can be neglected, the FP concentration distribution in along

the sodium flow is dependent of radioactive decay only, so the FP concentration in sodium at irradiation specimen is readily calculated by considering its half life.

Note (*): Adsorption and desorption of volatile FP are reversible on sodium temperature. So, the word "adsorption" is used in the cases of volatile FPs, instead of the word "deposition" in the case of non-volatile FPs.

As adsorption of volatile- and rare gas FPs on inner wall of piping can be neglected at higher than 250°C sodium temperature (1), the release fraction was calculated by using irradiation tests at higher sodium temperatures than 250°C (Exp. Nos. 5, 6, 7 and 16) and volatile- and rare gas FPs.

FP nuclides repeat beta-decay and so-called "fission chain" is formed. Concentration of FP nuclides located latter half of the fission chain is affected complexly by the decay of precursors.

Therefore, requirements of experiments are:

(i) Nuclides should be located at the top of fission chain to minimize the affect of precursor nuclides,

(ii) The producted amount of the nuclide should be saturated during irradiation (with half life: less than 15 min) for simplification of calculation, and

(iii) Gamma-ray peaks of the test data should be interferenced little from gamma-rays of other FPs and have high intensity.

Consequently, Br-86, Br-88, Rb-89 and I-136m from volatile FPs and Kr-90, Xe-139 and Xe-140 from rare gases were selected for calculation of release fraction. Besides, Te-134, which half life is 42 min, was selected to examine the correlation of

release fraction and the half life of FP (stagnant flow at irradiation specimen). Fission chains of these 8 nuclides are shown in Figs. 6-1 and 6-2. Here, since the FP nuclides which half lives are less than 1 sec and cumulative fission yields are less than 0.05% can be eliminated in the calculation of release fraction, they are not shown in the fission chain.

6.2.2 Calculation method of release fraction

1) Calculation method of FP with short half life

Regarding 7 nuclides except Te-134, the calculation method of the release fraction is explained as follows:

In the calculation, a FP is regarded as a daughter nuclide, then the chain from parent nuclide to daughter one is considered.

The change of parent nuclide concentration in sodium (atoms/cm^3) along the flow C_p is expressed as,

$$\frac{dC_p(x)}{dx} = -\frac{\lambda_p}{v} C_p(x)$$

where,

λ_p : decay constant of parent nuclide (1/sec)
v : flow velocity of sodium (cm/sec)
x : distance from irradiation specimen (cm)

Concentration of parent nuclide in sodium $C_p(x)$ is obtained as,

$$C_p(x) = C_{po} \cdot e^{-\lambda_p \frac{x}{v}}$$

where

C_{po}: concentration at irradiation specimen

When the production is saturated,

$$C_{po} = \frac{P_p}{F \cdot (1 - e^{-\lambda_p \frac{L}{v}})}$$

where,

P_p : release rate of parent nuclide (atoms/sec)
F : sodium flow rate (cm^3/sec)
L : total length of the loop (cm)

The release rate P_p is,

$$P_p = F_r \cdot F_{Yp} \cdot R_f$$

where,

F_r : fission rate (atoms/sec)
F_{Yp} : cumulative fission yield of parent nuclide (-)
R_f : release fraction (-)

Change of the daughter nuclide concentration in sodium C_d ($atoms/cm^3$) along flow direction is,

$$\frac{dC_d(x)}{dx} = -\frac{\lambda_d}{v} C_d(x) + \frac{\lambda_p}{v} \varepsilon \cdot C_p(x)$$

where,

λ_d : decay constant of daughter nuclide (1/sec)
ε : decay branch ratio from parent- and daughter nuclides (-)

Concentration of daughter nuclide in sodium $C_d(x)$ is,

$$C_{d(x)} = \frac{\lambda_p \cdot \varepsilon \cdot C_{p0}}{\lambda_d - \lambda_p} \left(e^{-\lambda_p \frac{x}{v}} - e^{-\lambda_d \frac{x}{v}} \right) + C_{d0} \cdot e^{-\lambda_d \frac{x}{v}}$$

where C_{do} : concentration of daughter nuclide in irradiation specimen

$$C_{d0} = \frac{\frac{\lambda_p \cdot \varepsilon \cdot C_{p0}}{\lambda_d - \lambda_p}\left(e^{-\lambda_p \frac{L}{v}} - e^{-\lambda_d \frac{L}{v}} \right) + \frac{P_d}{F}}{1 - e^{-\lambda_d \frac{L}{v}}}$$

where,

P_d : release rate of daughter nuclide (atoms/sec)

Release rate P_d is,

$$P_d = F_r \cdot F_{Yd} \cdot R_f$$

where,

F_{Yd} : independent yield of daughter nuclide (-)

Assuming release fractions of parent- and daughter nuclides are equal,

$$C_d(x) = \frac{\lambda_p}{\lambda_d - \lambda_p} \cdot \frac{\varepsilon \frac{F_r \cdot F_{Yp} \cdot R_f}{F}}{1 - e^{-\lambda_p \frac{L}{v}}} \left\{ \left(e^{-\lambda_p \frac{x}{v}} - e^{-\lambda_d \frac{x}{v}} \right) + \frac{e^{-\lambda_p \frac{L}{v}} - e^{-\lambda_d \frac{L}{v}}}{1 - e^{-\lambda_d \frac{L}{v}}} e^{-\lambda_d \frac{x}{v}} \right\}$$

$$+ \frac{\frac{F_r \cdot F_{Yd} \cdot R_f}{F}}{1 - e^{-\lambda_d \frac{L}{v}}} e^{-\lambda_d \frac{x}{v}}$$

$$= C_{d1}(x) + C_{d2}(x) \qquad \cdots\cdots\cdots\cdots (6\text{-}1)$$

The first term $C_{d1}(x)$ is the concentration of daughter nuclide produced by decay of parent nuclide. The ratio of daughter nuclide concentration directly produced by fission to the whole daughter nuclide concentration is $C_{d2}(x)/C_d(x)$.

The concentration of daughter nuclide directly produced by

fission $A_F(x)$ (atoms/cm^3) is,

$$A_F(x) = A(x) \frac{C_{d_2}(x)}{C_d(x)} \qquad \cdots\cdots\cdots\cdots \quad (6\text{-}2)$$

where,

$A_F(x)$: concentration of daughter nuclide in sodium at distance x obtained by gamma-ray detection on the delay line (atoms/cm^3)

$$\chi^2 = \sum_i \frac{1}{\sigma_{x_i}^2} \left(A_F(x_i) - A_{F0}' \cdot e^{-\lambda_d \frac{x_i}{v}} \right)^2 \qquad (6\text{-}2a)$$

where,

$A_F(x_i)$: concentration of daughter nuclide directly produced by fission at x_i (atoms/cm^3)

A_{FO}' : concentration of daughter nuclide at irradiated specimen

When χ^2 is minimized, A_{FO} is used to express the concentration of daughter nuclide at irradiated specimen.

σ_{xi} : standard deviation of $A_F(x_i)$ (atoms/cm^3)

Since A_{Fo} corresponds to $C_{d2}(x)$ at x=0 of the second term in Eq. (6-1),

$$A_{F0} = \frac{\frac{F_r \cdot F_{Yd} \cdot R_f}{F}}{1 - e^{-\lambda_d \frac{L}{v}}}$$

The release fraction R_f is,

$$R_f = A_{F0} \left(1 - e^{-\lambda_d \frac{L}{v}} \right) \frac{F}{F_r \cdot F_{Yd}} \qquad \cdots\cdots\cdots\cdots \quad (6\text{-}3)$$

Here, the release fraction of I-136m located at the top of chain can be calculated by the same method, putting concentration of parent nuclide is zero.

2) Calculation method of FP with long half life

The calculation method of release fraction of Te-134 with relatively long half life of 42 min is explained. The precursor nuclide of Te-134, as shown in Fig. 6-2, is Sb-134, which has a short half life as 10.4 sec compared with Te-134 and is small cumulative fission yield as 0.469% compared with the independent yield of Te-134 as 6.299%, i.e. less than 1/13, therefore the accumulation amount of Te-134 in sodium Nc(dps) is expressed approximately by the following equation.

The accumulation amount N_c (dps) is,

$$Nc = F_r \cdot F_{Yc} \cdot R_f \cdot (1 - e^{-\lambda \cdot t})$$

where,

F_r : nuclear fission rate (atoms/sec)
F_{Yc}: cumulative fission yield of Te-134 (-)
R_f : release fraction (-)
λ : decay constant of Te-134 (1/sec)
t : irradiation time (sec)

On the other hand, the half life of Te-134 (42 min) is very long compared with one circulation time (48 ∿ 240 sec) of sodium, so Te-134 distributes homogeneously along the delay line.

Te-134 amount in sodium N_e (dps) is,

$$Ne = \overline{C}_r \cdot \frac{3.7 \times 10^4}{f_r(E) \cdot f_e(E) \cdot V} \cdot V_T$$

where,

Cr : average count rate of gamma-ray at energy E (keV) (cps)

$f_r(E)$: gamma-ray branch ratio with energy E (-)

$f_e(E)$: detection efficiency with energy E (cps. cm/μCi)

V : sodium volume per unit delay line (cm^3/cm)

V_T : sodium volume at main circulation part (cm^3)

Nc obtained by calculation and Ne obtained by experiment should be primarily equal. Therefore, the release fraction R_f of Te-134 is,

$$R_f = \frac{\overline{C}_r \dfrac{3.7 \times 10^4}{f_r(E) \cdot f_e(E) \cdot V} V_T}{F_r \cdot F_{Yc}(1-e^{-\lambda \cdot t})} \qquad \cdots\cdots\cdots\cdots \quad (6\text{-}4)$$

6.3 Calculation of Release Fraction and k Factor

6.3.1 Release fraction of FP

Count rate of each FP nuclides was obtained by gamma-ray detection on the delay line, where the geometric detection efficiency between detection positions and difference in detection efficiency among Ge detectors (two Ge detectors were used for the measurement) were corrected, and the difference in production amount caused by the different start time for detection was corrected to the values at completion of irradiation for 4 hrs.

1) Release fraction of FP with short half life

Regarding 7 nuclides except Te-134, the concentration of daughter nuclide in sodium A (atoms/sec) is obtained from count rate,

$$A = C_r \times \frac{3.7 \times 10^4}{f_r(E) \cdot f_e(E) \cdot V \cdot \lambda_d}$$

where,

C_r : count rate of gamma-ray with energy E (keV)
$f_r(E)$: branch ratio of gamma-ray with energy E (keV)
$f_e(E)$: detection efficiency of gamma-ray with energy E (keV) (cps. cm/μC_i)
V : sodium volume per unit length of the delay line (cm^3/cm)
λ_d : decay constant of daughter nuclide (1/sec)

In the calculation,

$f_e(E)$: $\exp(8.25 - 0.914 \times \ell n\ E + 0.0211 \times \ell n\ E^2)$ (1)
V : 0.694

were used. In Eq. (6-3), the total length of loop L=5734 (cm), nuclear fission rate Fr = 2.05×10^{11} (atoms/sec) and thermal neutron flux = 7.9×10^9 (n/cm^2sec) (the calculation method is shown in Appendix A) were used.

Using A obtained above, concentration of daughter nuclide in sodium directly produced by nuclear fission A_F is calculated by Eqs. (6-1) and (6-2). Distribution of A_F in the delay line is shown in Figs. 6-3 to 9. No difference in distributions between Exp. Nos. 5, 7 and 8 at sodium flow rate of 1.2 m/sec was observed, but in Exp. No. 16 the gradient of distribution is longer due to the low sodium flow rate as 0.24 m/sec. Optimized result by selecting A_{Fo} so as to minimize χ^2-value defined Eq. (6-2a) based on A_F value distributed in the loop is shown in the figure, where Exp. No. 5 is expressed by solid line, Exp. No. 7 is by one point-dotted line, Exp. No. 8 is by two points-dotted line and Exp. No. 16 by discrete line.

Based on each A_{Fo} values obtained by above method, the release fraction of FP was calculated from Eq. (6-3), as

indicated in Table 6-1. Here, error of release fraction includes that of independent fission yield of daughter nuclide.

2) Release fraction of FP with long half life

The distribution of Te-134 count rate along the delay line is shown in Fig. 6-10. The half life of Te-134 is 42 min and being long enough compared with one circulation time of sodium in the loop, the distribution is homogeneous in every test and no difference is seen among these tests.

Average values $\bar{C}_r$ (*) of Te-134 count rate in each experiment are,

Exp. No.	C_r (cps)
5	1.76 ± 0.12
7	1.45 ± 0.13
8	1.66 ± 0.13
16	1.67 ± 0.11

Note (*) Average values are all obtained by the following equation.

$$\bar{x} \pm \sigma_{\bar{x}} = \frac{\Sigma(x_i/\sigma_i^2)}{\Sigma(1/\sigma_i^2)} \pm \sqrt{1/\Sigma(1/\sigma_i^2)}$$

Release fraction of Te-134 calculated by Eq. (6-4) from R_f values is indicated in Table 6-1, where

$F_r = 2.05 \times 10^{11}$, $F_{Yc} = 0.0694$, $f_r(E) = 0.191$, $f_e(E) = \mathrm{Exp}\,(8.25 - 0.914 \times \ell n(E) + 0.0211 \times \ell n(E)^2) = 27.23$, $V = 0.694$, $V_T = 3979$ were used in Eq. (6-4).

The release fraction of Te-134 is 0.42 to 0.51%.

3) Summary of release fraction of FP

Release fractions of FPs indicated in Table 6-1 are shown in Fig. 6-11, where release fractions of each FP are consistent within experimental error.

The relation between average value of release fraction and mass number of FP is shown in Fig. 6-12, where FP nuclides are divided into 2 groups, i.e. the light FPs with mass number about 90 and the heavy FP with mass number about 140, and release fraction values, except that of Br-88, are in good agreement within each group. Exceptionally only Br-88 showed small value approx. 1/1.5 of average release fraction of light FP group, but the reason is not clear yet.

Release fractions between the light FP group except Br-88 and the heavy FP group show some differences depending on mass number.

The average value of release fraction of light FP group (except Br-88) is 0.80 ± 0.02%, and that of heavy FP group is 0.48 ± 0.02%, and the ratio of release fractions between light- and heavy groups is 1.67. The dependence of release fraction on mass number is shown by solid line in Fig. 6-12.

On the other hand, release fraction of FP calculated theoretically by the recoil model is,

$$R_{fc} = \frac{S \cdot R}{4V} \qquad \cdots\cdots\cdots\cdots (6\text{-}5)$$

where,

S: geometrical surface area of irradiation specimen (cm^2)
V: volume of irradiation specimen (cm^3)
R: recoil range of FP (cm)

It shows that the release fraction of FP depends on the

recoil range of FP. Relation between R and mass number of FP is shown in Fig. 6-13, where higher recoil range with smaller mass number is observed. (12) It shows that recoil range is 8 μm and 4.5 μm for mass number of a little less than 90 and 140, respectively. This relation (recoil range vs. mass number) is plotted by dotted line in Fig. 6-12, where the relation of release fraction vs. mass number is plotted by a solid line. The same dependence of the release fraction and recoil range of FP on mass number indicates that release of FP from irradiation specimen in FPL-II is due to recoil phenomenon.

6.3.2 Calculation of k factor

Ratio of release fraction of FP obtained by gamma-ray detection vs. that obtained by calculation, i.e. (R_f/R_{fc}), k factor, is described in this section.

Practically irradiation specimen in FPL-II is granule with nearly spherical shape (average diameter 590 μm), but the release fraction from the specimen was calculated by assuming it as spherical shape with 590 μm in diameter. The release fraction from irradiation specimen that is a sphere with radius r (cm), is expressed by Eq. (6-5) as,

$$R_{fc} = \frac{3R}{4r}$$

By putting R = 8 μm for light FP and R = 4.5 μm for heavy FP, R_{fc} = 2.03% and 1.14% are obtained, respectively. The k factor for each FP nuclide obtained from the release fraction is indicated in Table 6-2.

k factor are 0.23 to 0.41 and 0.30 to 0.57 for light- and heavy FP groups, respectively. The plot of k factor against decay constant for each FP is shown in Fig. 6-14. According to the figure, difference in k factor is not observed for various decay constants. Plot of k factor against mass number is shown in Fig. 6-15. Difference in k factor due to different mass numbers is

not observed between light FPs (except Br-88) and heavy FPs. The average value of k factor for light FP group except Br-88 is 0.40 ± 0.01 that for heavy FP group is 0.43 ± 0.02 and that for 7 nuclides except Br-88 is 0.40 ± 0.01.

6.3.3 Discussion

Release fraction of FP obtained from gamma-ray detection depends on FP mass number, and the trend is in fairly good agreement with that calculated from recoil model.

From the fact that it is conceivable that the release of FP from irradiation specimen loaded in FPL-II is due to recoil phenomenon of fission fragment.

However, it is generally said that k factor is usually higher than 1, because actual surface area is larger than geometrical one. For instance reported k factor is between 3.5 to 17 for sodium inpile loop (SIL) at the Japan Atomic Energy Institute. (13) On the other hand, the value obtained in this FPL-II is 0.41 ± 0.01.

Three reasons to explain why k factor is less than 1 are considered as follows:

(1) Production of FP is small, because

a) thermal neutron flux is small, and

b) a part of irradiation specimen leaked from uranium capsule mesh basket

c) self-shielding of irradiation specimen from thermal neutron

(2) Release of FP is small, because

a) a part of irrdiation specimen is solidified, so that

contact area between specimen and sodium is small, and

(3) Concentration of FP in sodium is underestimated, because

a) value of detection efficiency used is high.

Here, cases of (1) b. and (2) a. are unpractical. The detection efficiency used in case of (3) a. is not direct reason why k factor is less than 1, because effect of detection efficiency on k factor is canceled by using same equation in detection efficiency calculation in obtaining thermal neutron flux. Next, the thermal neutron flux used in case (1) a. is calculated from radioactive amount of Na-24 and, therefore, shows an average value at irradiation specimen. On the other hand, distribution of thermal neutron flux was measured at the position of uranium capsule (inner length 82 mm) and according to the measurement performed before installation of FPL, thermal neutron flux at the tail position of uranium capsule is small as 1/3 compared to that at the head position. Therefore, if irradiation specimen is located at a deviating position in tailward, thermal neutron flux is smaller resulting in the smaller production rate than expected.

As explained above, thermal neutron flux appears to be responsible as one of the reasons why k factor is smaller than 1, but further study is necessary to confirm it.

6.4 Conclusion

Release fraction of irradiation specimen in FPL-II was calculated based on the concentration of volatile- and rare gas FP in sodium obtained by gamma-ray detection, and results are as follows:

(1) Release fraction of each FP from irradiation specimen keeps constant value independent of sodium temperature (420 ∿ 530°C) and flow rate (1 ∿ 5 ℓ/min),

(2) Release fraction depends on mass number of FP and shows

0.80 ± 0.02% for light FP with mass number about 90 and
0.48 ± 0.02% for heavy FP with mass number about 140,

(3) Dependence of release fraction on mass number is in fairly good agreement with that of recoil range, and therefore, the release of FP from FPL-II is due to recoil phenomenon, and

(4) k factor, i.e. the ratio of release fraction of FP obtained by gamma-ray detection vs. the release fraction calculated by recoil model is 0.40 ± 0.01 for light FP, 0.43 ± 0.02 for heavy FP and 0.40 ± 0.01 for all FP nuclides concerned.

Further study is necessary to clarify why small k factor which is less than 1, is obtained.

Table 6-1 Fission product release fraction (%) calculated by using each FP nuclide concentration in sodium

Nuclide	Half life	Exp.No.5	7	8	16	Average
		420 ℃ 5 ℓ/min	500 ℃ 5 ℓ/min	530 ℃ 5 ℓ/min	530 ℃ 1 ℓ/min	
^{86}Br	55 s	0.99 ± 0.10	0.95 ± 0.09	0.96 ± 0.09	0.81 ± 0.07	0.91 ± 0.04
^{88}Br	16 s	0.54 ± 0.04	0.52 ± 0.04	0.57 ± 0.05	0.44 ± 0.04	0.51 ± 0.02
^{89}Rb	15.2 m	0.81 ± 0.05	0.75 ± 0.05	0.79 ± 0.05	0.75 ± 0.05	0.78 ± 0.03
^{90}Kr	32.3 s	0.78 ± 0.03	0.76 ± 0.03	0.74 ± 0.03	0.82 ± 0.03	0.78 ± 0.02
^{136m}I	46 s	0.75 ± 0.18	0.69 ± 0.16	0.72 ± 0.17	0.62 ± 0.14	0.69 ± 0.08
^{139}Xe	39.7 s	0.48 ± 0.03	0.49 ± 0.04	0.45 ± 0.03	0.58 ± 0.04	0.50 ± 0.02
^{140}Xe	13.6 s	0.49 ± 0.09	0.32 ± 0.07	0.40 ± 0.09	0.33 ± 0.06	0.37 ± 0.04
^{134}Te	42 m	0.51 ± 0.17	0.42 ± 0.14	0.49 ± 0.16	0.49 ± 0.16	0.47 ± 0.08

Table 6-2 k factor for each fission product nuclide

Nuclide	Release Fraction (%)		k factor (-)
	Measured	Calculated	
^{86}Br	0.91 ± 0.04	2.03	0.45 ± 0.02
^{88}Br	0.51 ± 0.02		0.25 ± 0.01
^{89}Rb	0.78 ± 0.03		0.38 ± 0.02
^{90}Kr	0.78 ± 0.02		0.38 ± 0.01
^{136m}I	0.69 ± 0.08	1.14	0.61 ± 0.07
^{139}Xe	0.50 ± 0.02		0.44 ± 0.02
^{140}Xe	0.37 ± 0.04		0.33 ± 0.04
^{134}Te	0.47 ± 0.08		0.41 ± 0.07

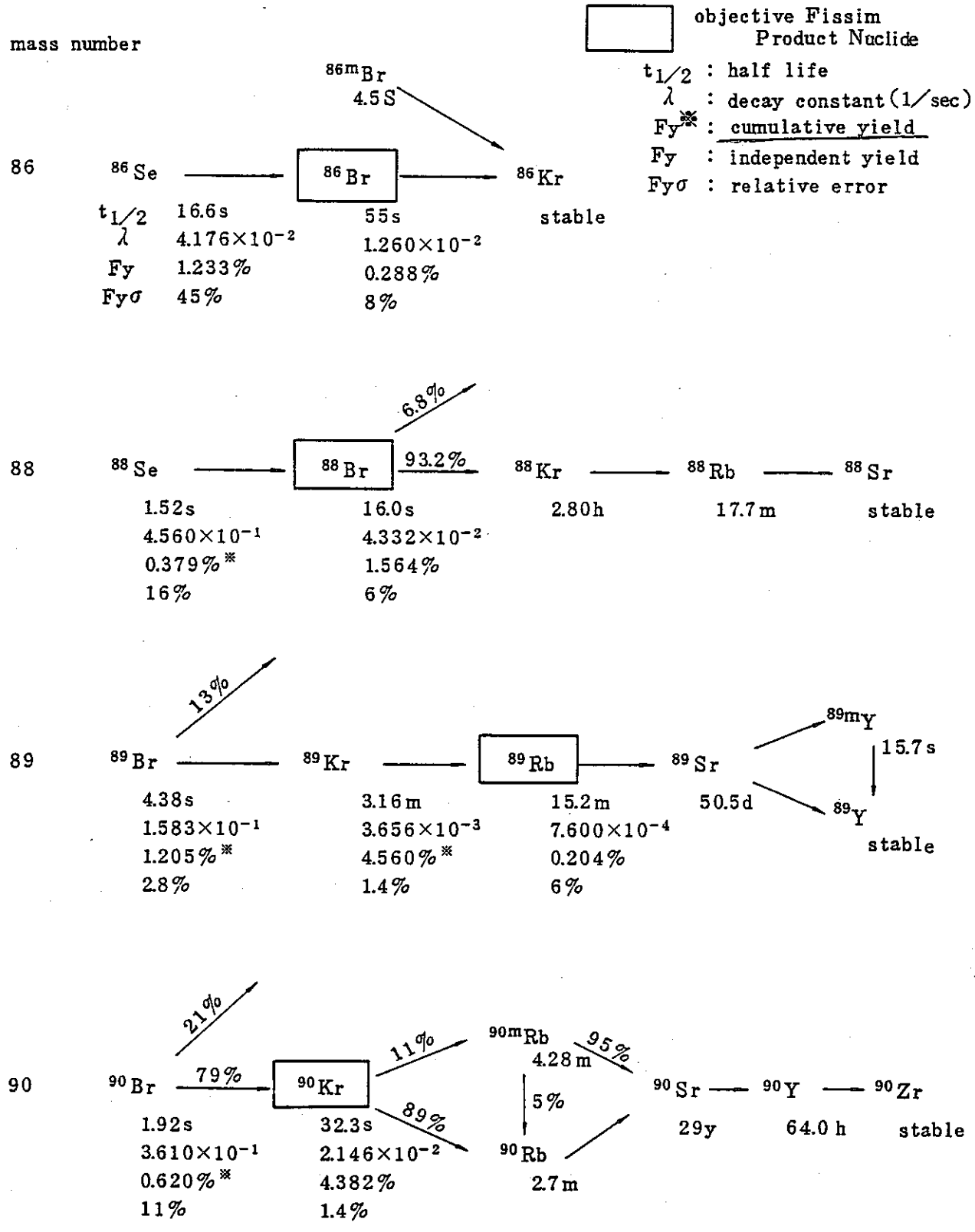

Fig. 6-1 Fission chain (1)

mass number

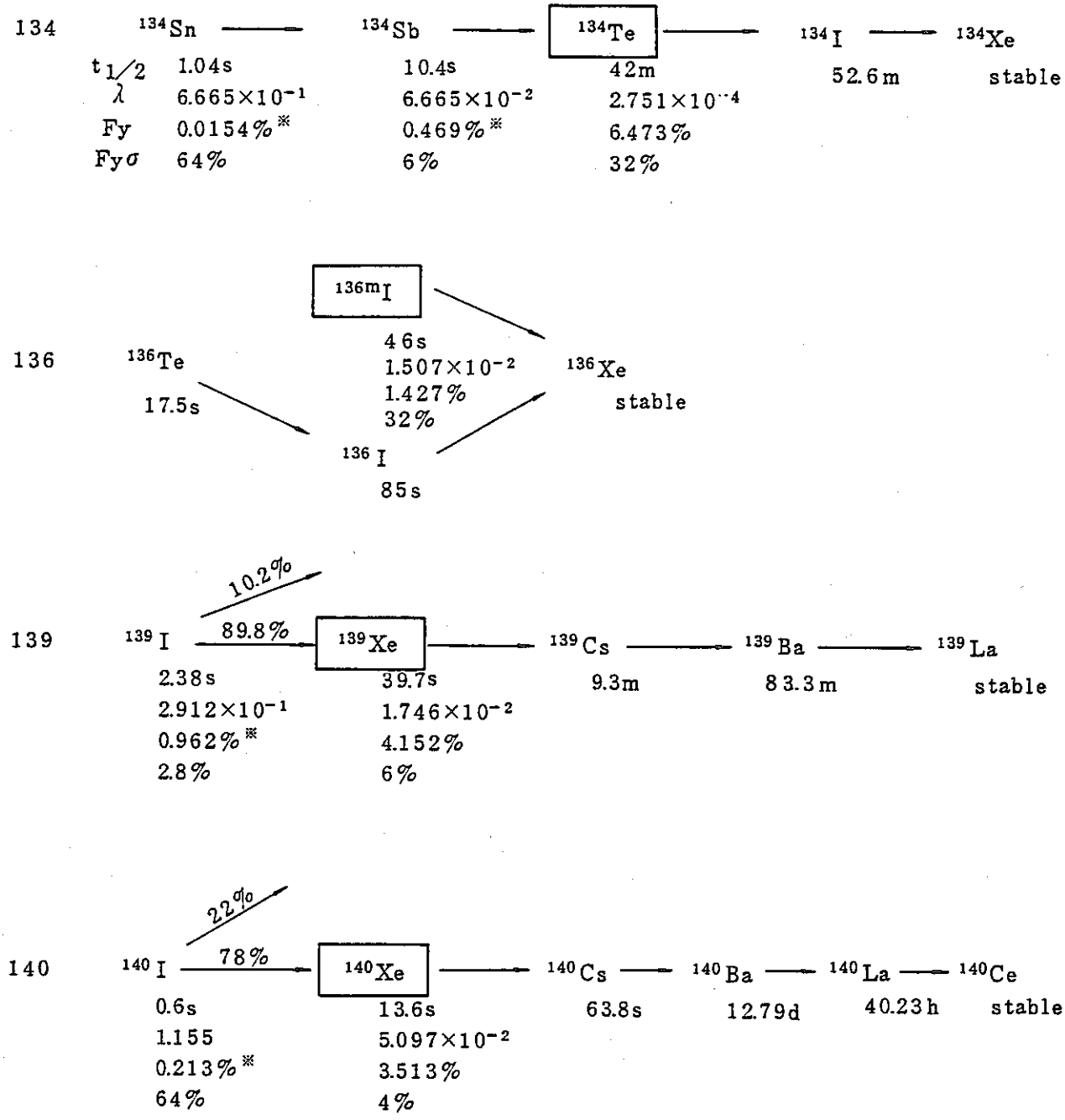

Fig. 6-2 Fission chain (2)

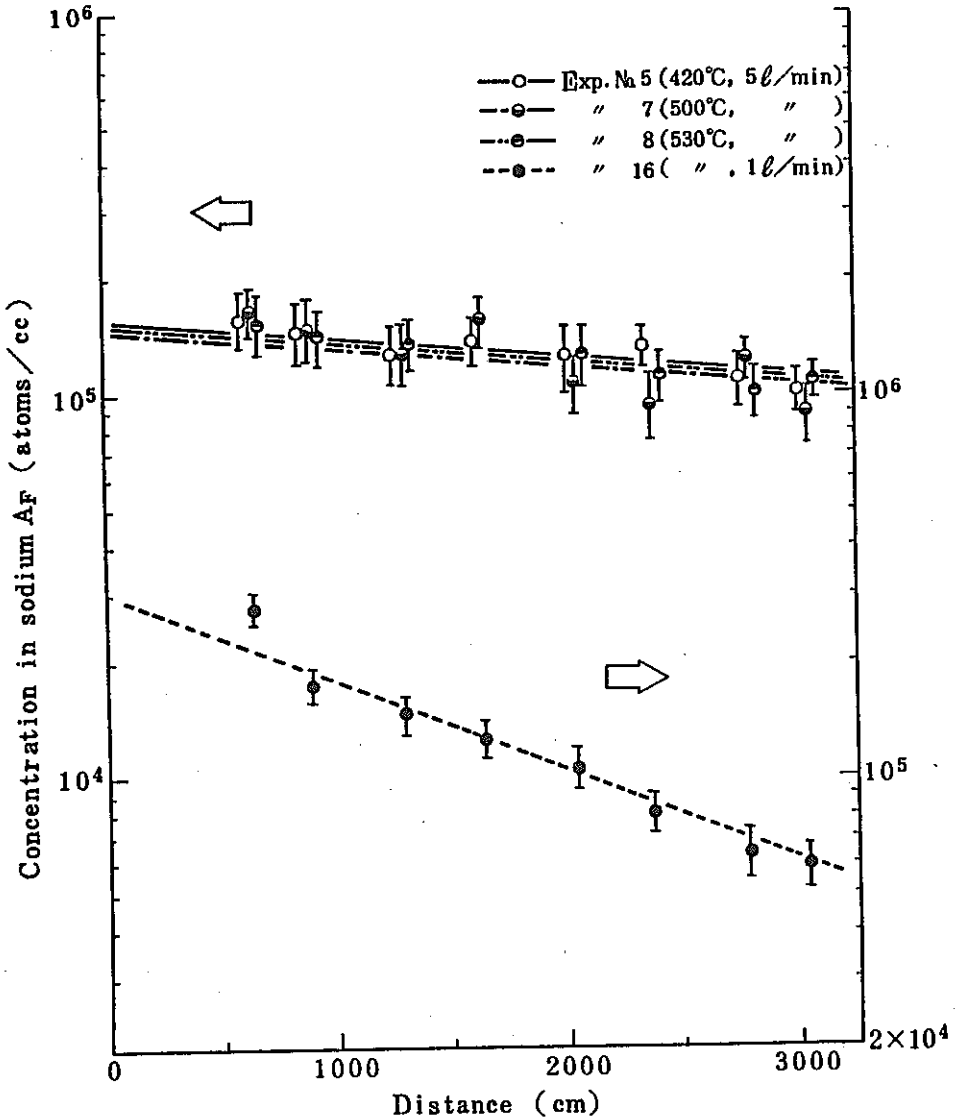

Fig. 6-3 Distribution for Br-86 concentration in sodium along the delay line

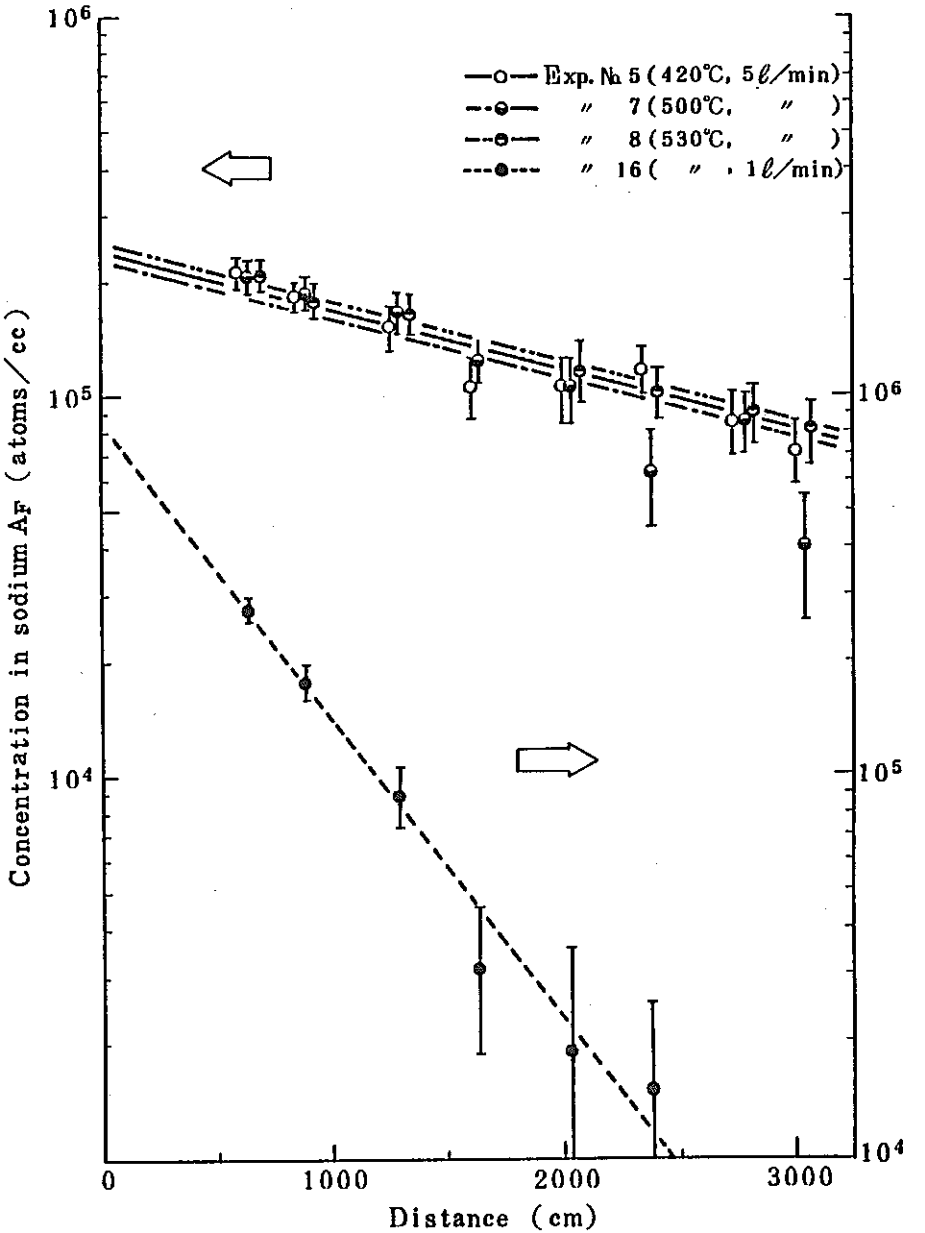

Fig. 6-4 Distribution for Br-88 concentration in sodium along the delay line

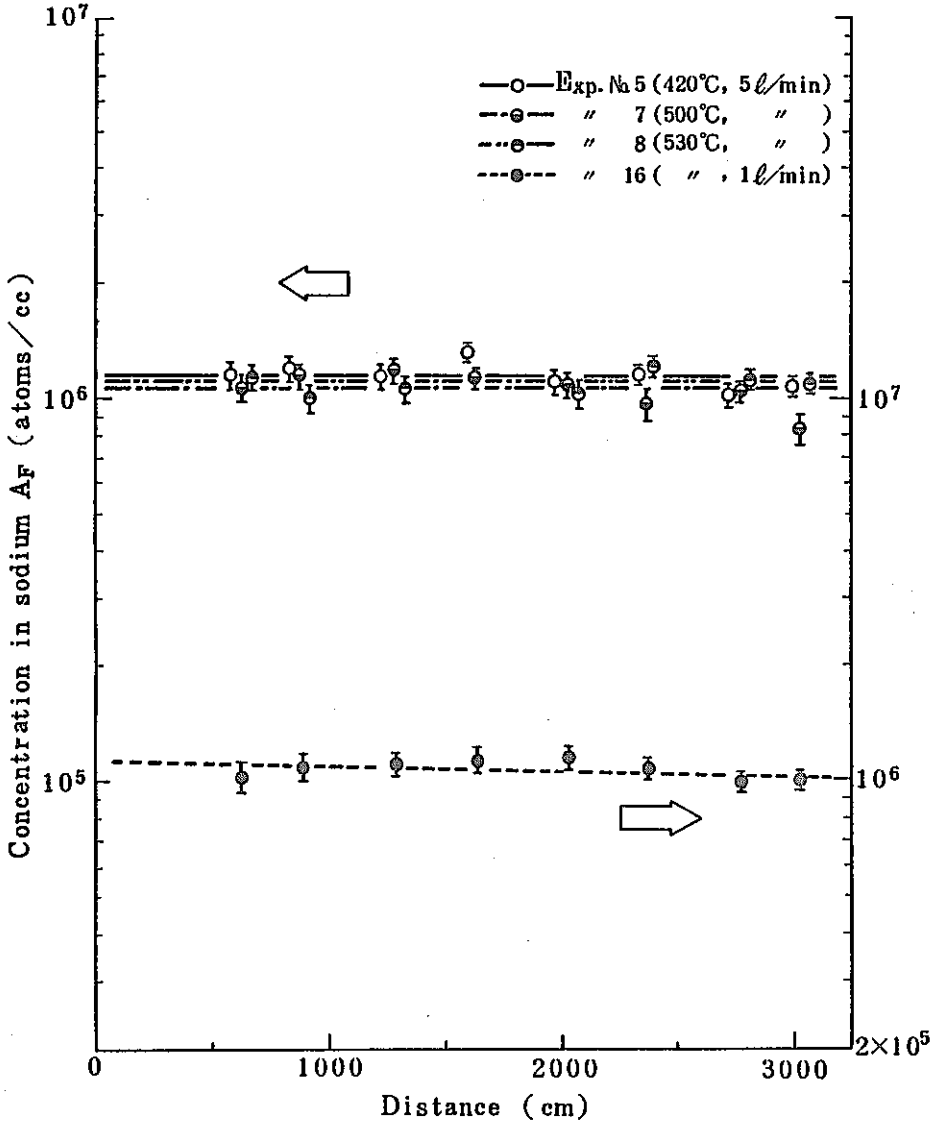

Fig. 6-5 Distribution for Rb-89 concentration in sodium along the delay line

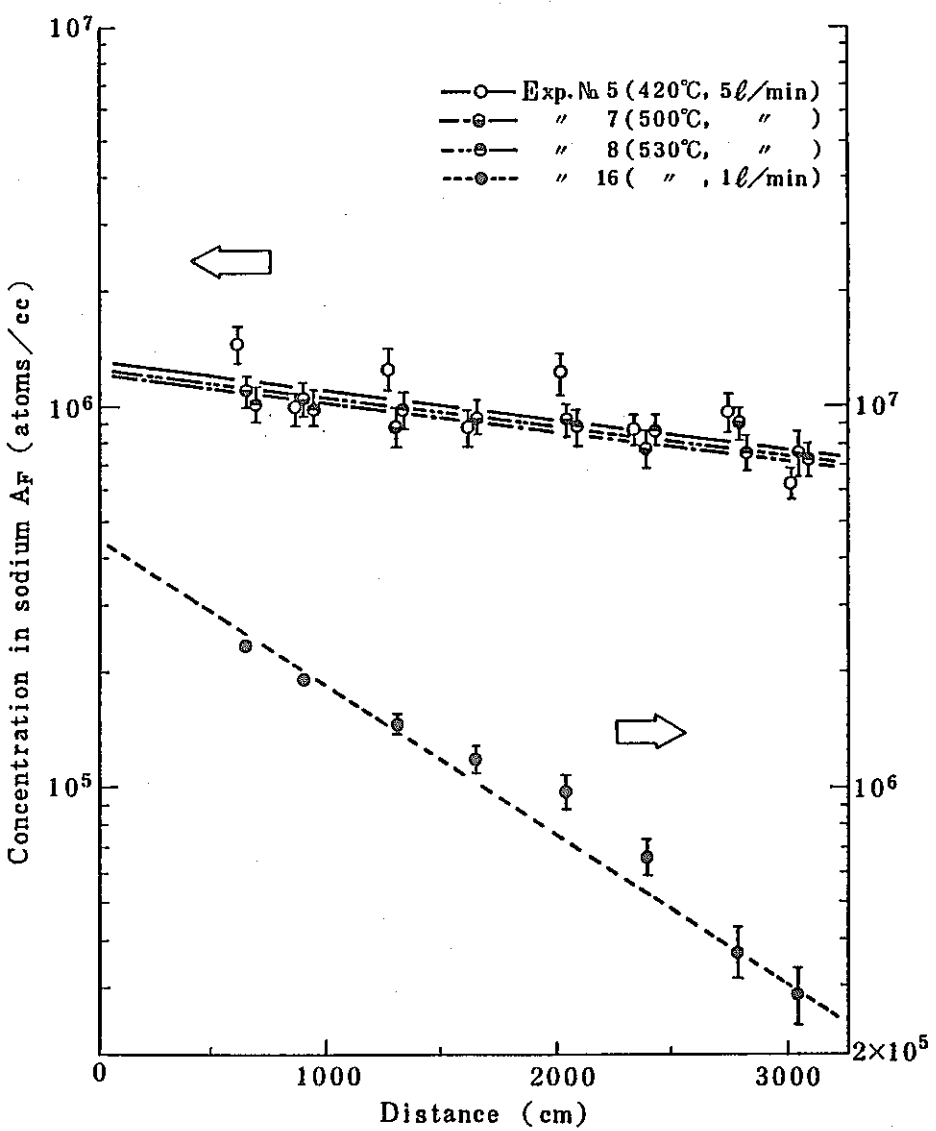

Fig. 6-6 Distribution for Kr-90 concentration in sodium along the delay line

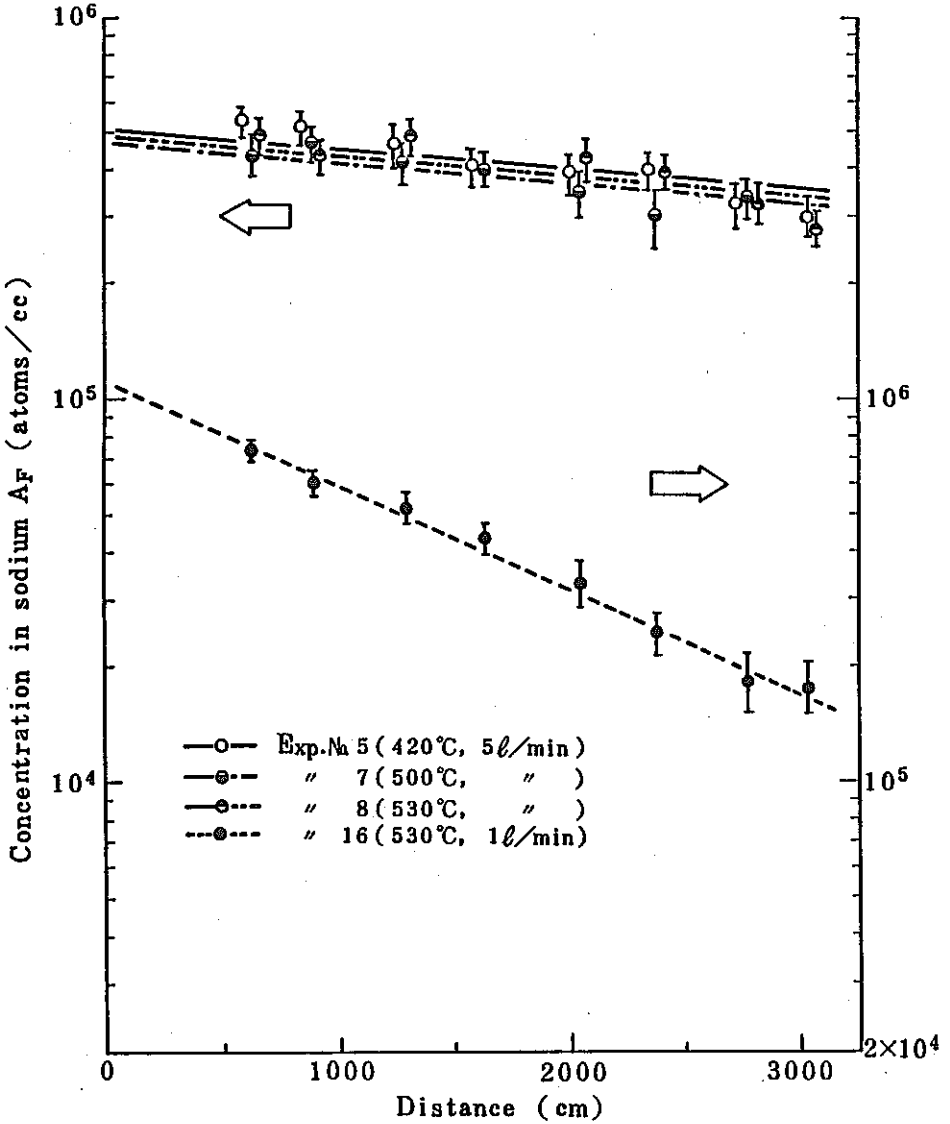

Fig. 6-7 Distribution for I-136m concentration in sodium along the delay line

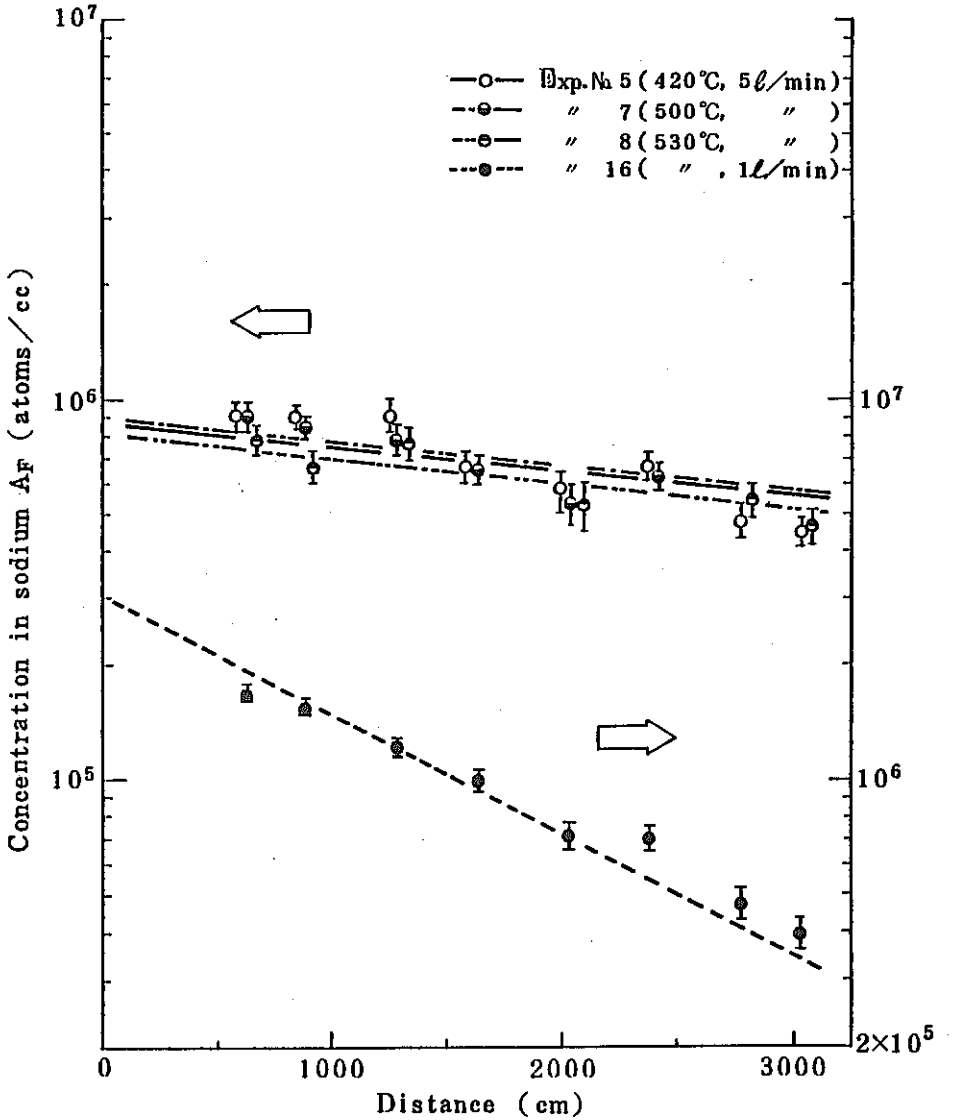

Fig. 6-8 Distribution for Xe-139 concentration in sodium along the delay line

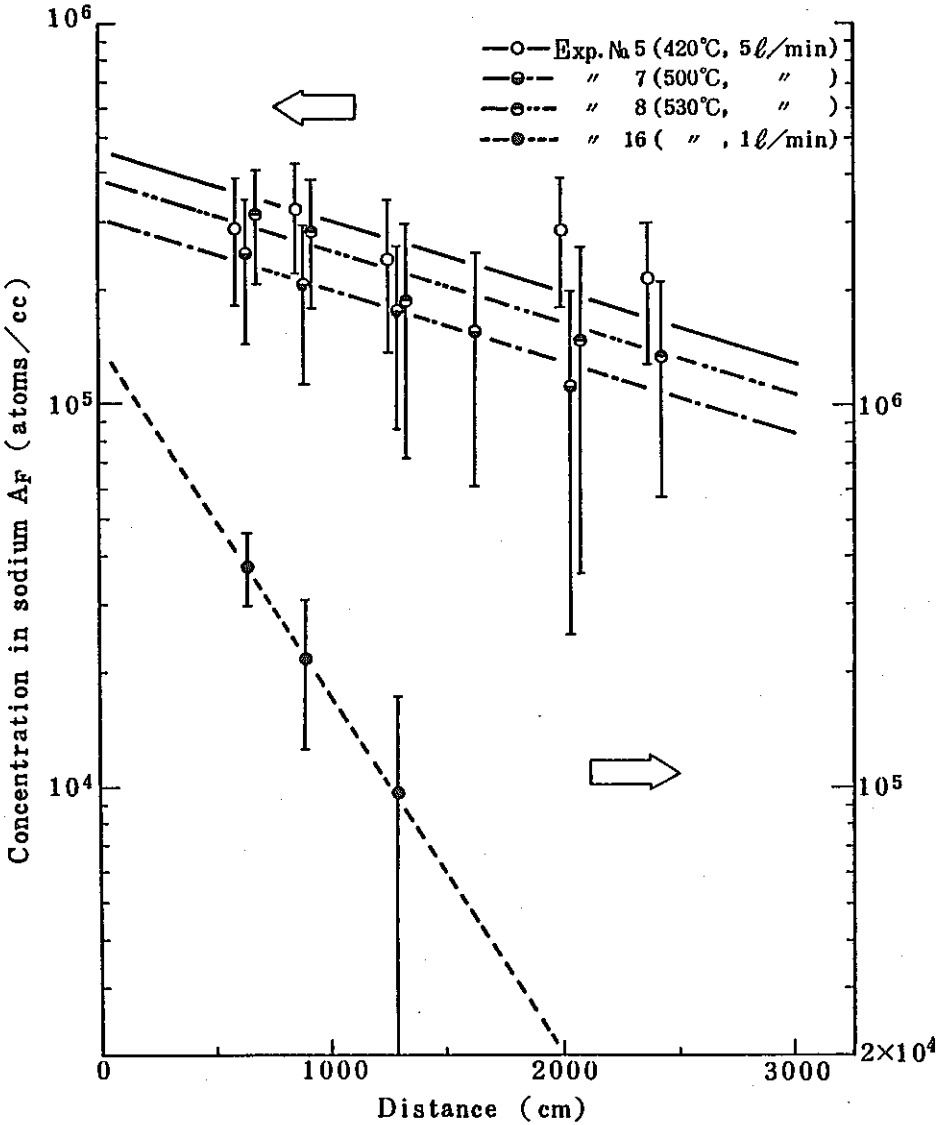

Fig. 6-9 Distribution for Xe-140 concentration in sodium along the delay line

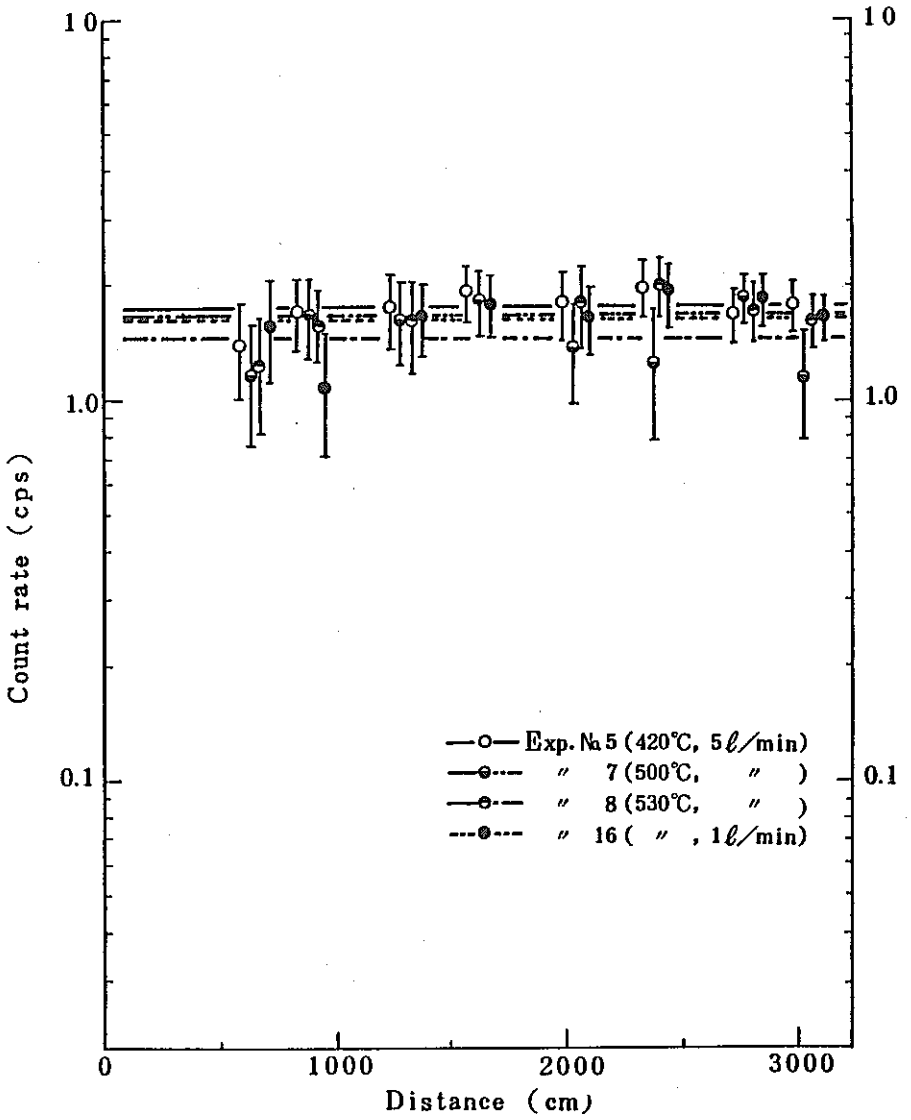

Fig. 6-10 Te-134 distribution along the delay line

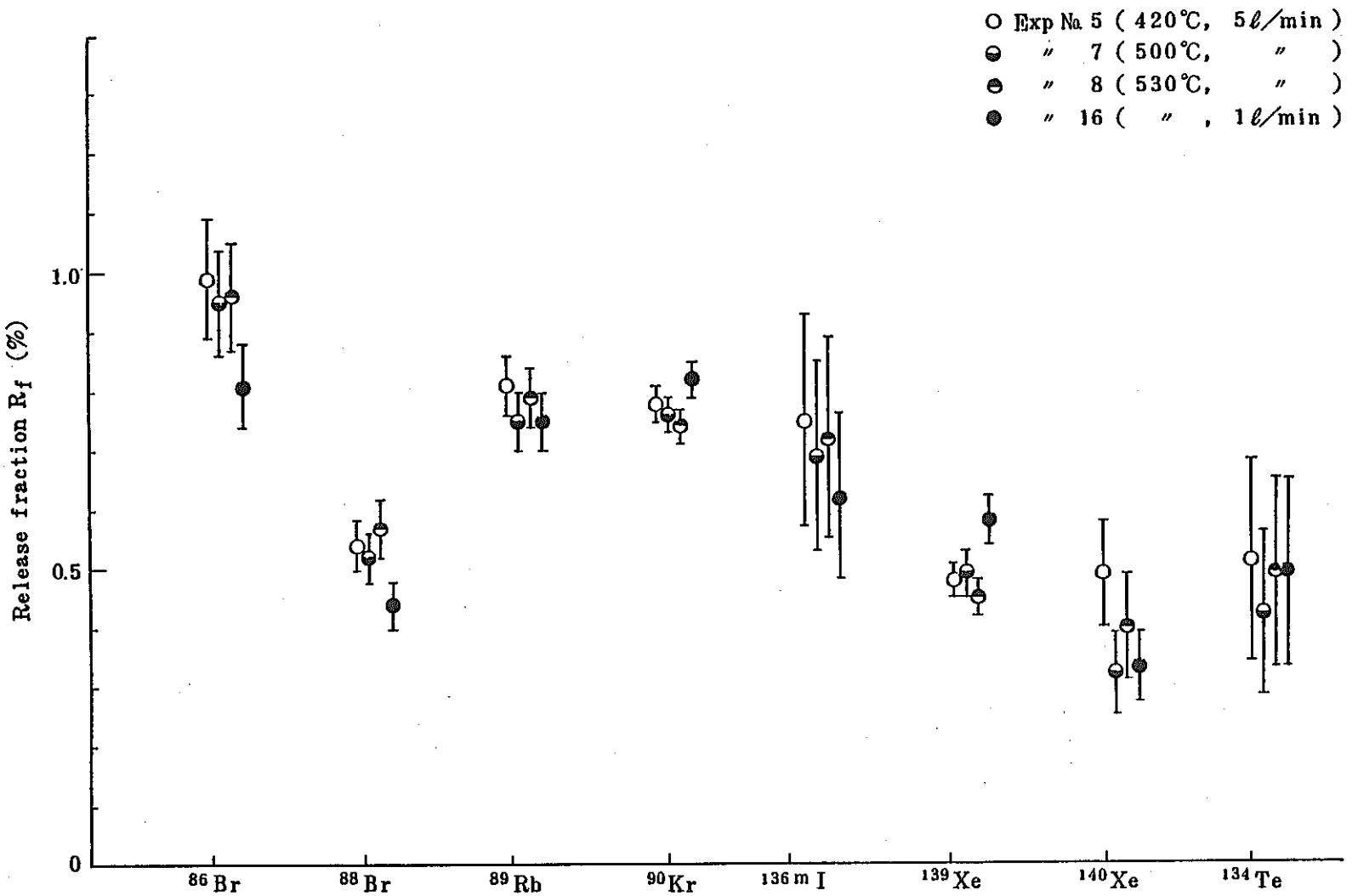

Fig. 6-11 Fission product release fraction for each FP nuclide

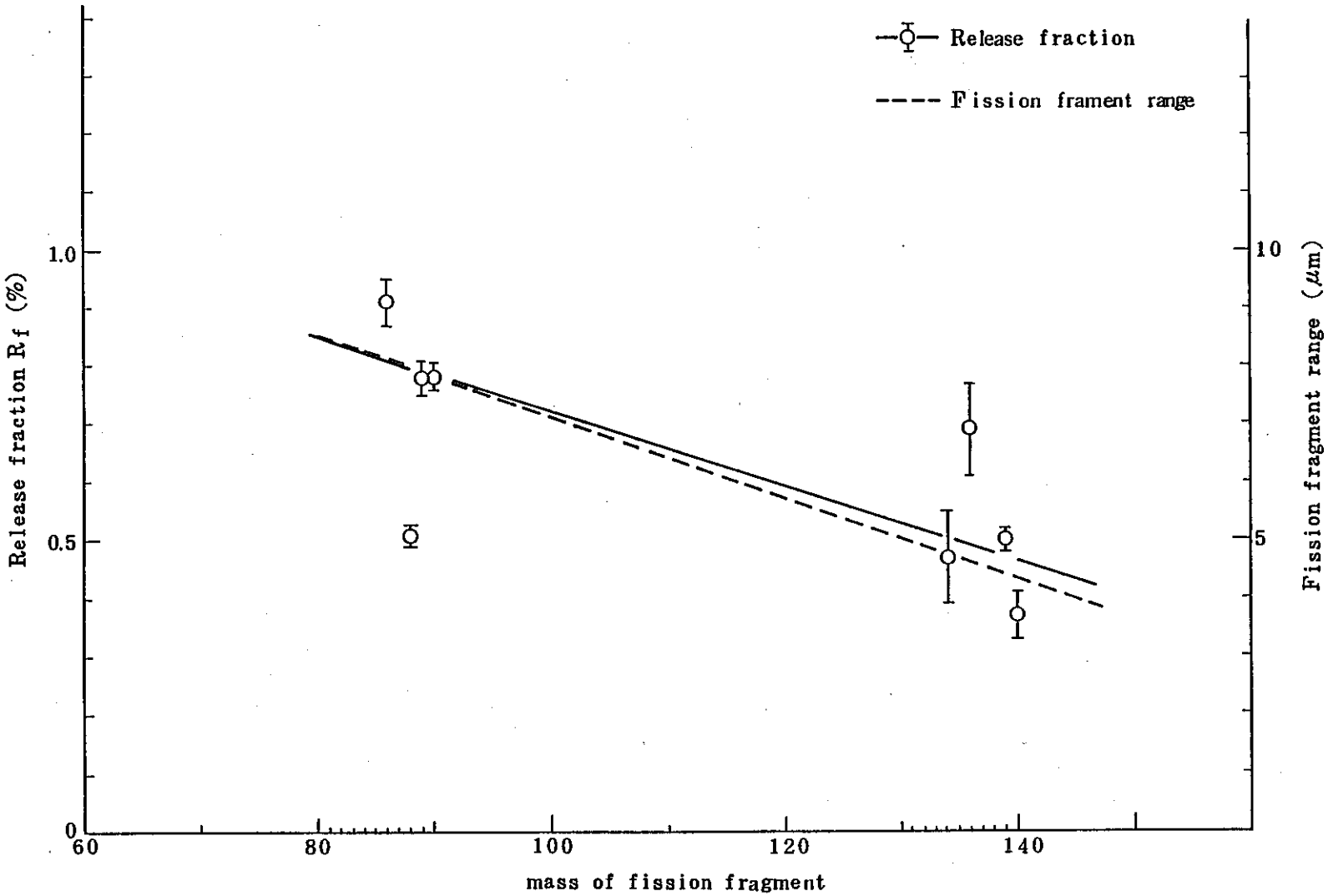

Fig. 6-12 Release fraction and fission fragment range in UO_2 as a function of mass

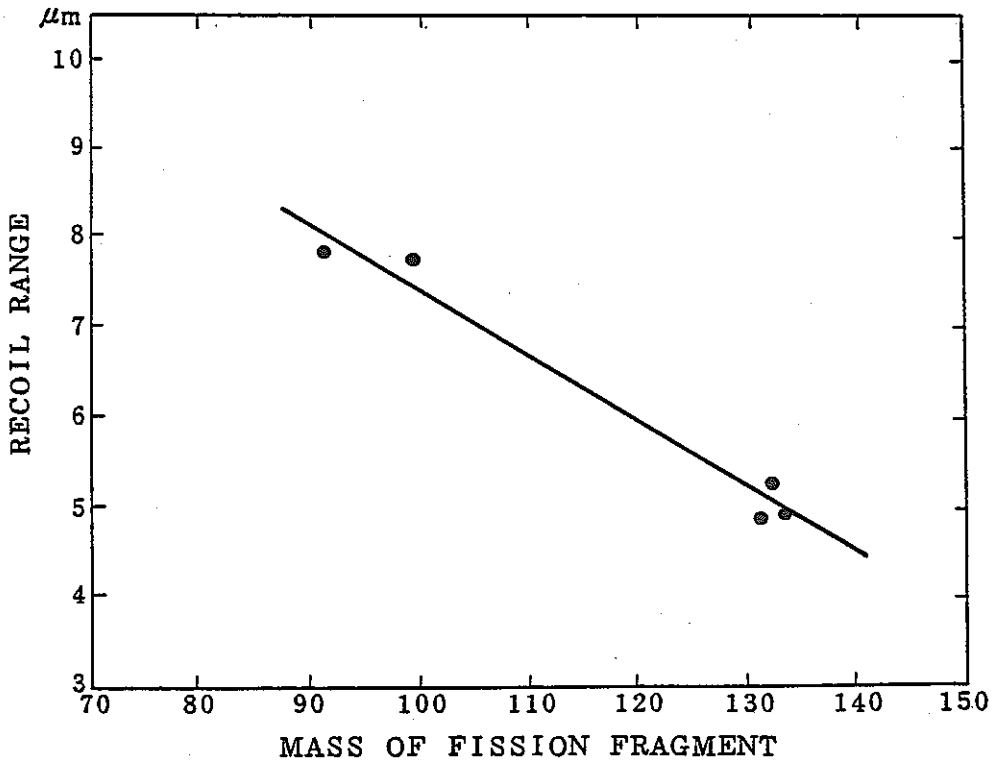

Fig. 6-13 Fission fragment recoil range in UO_2 as a function of mass (12)

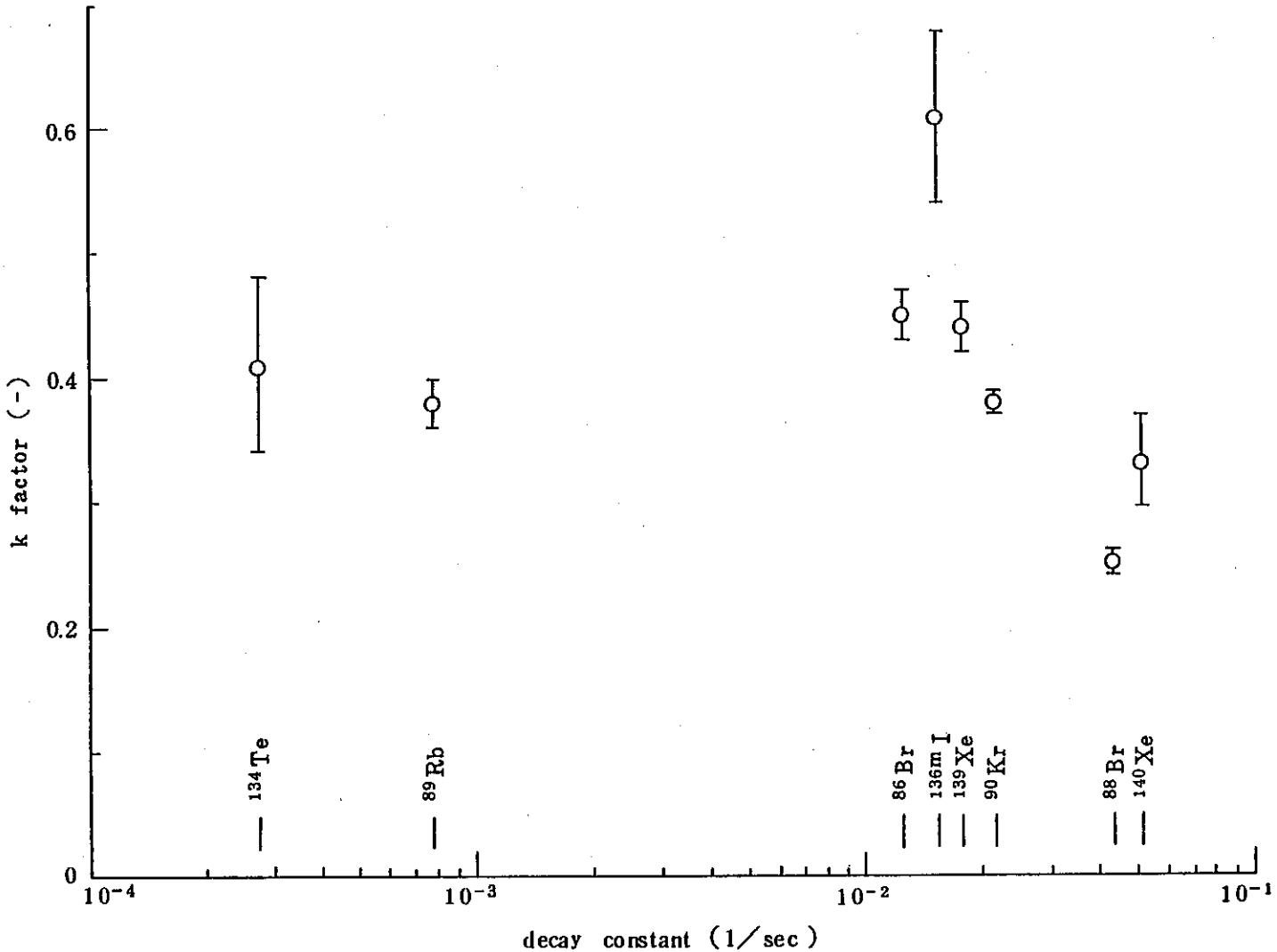

Fig. 6-14 k factor as a function of decay constant

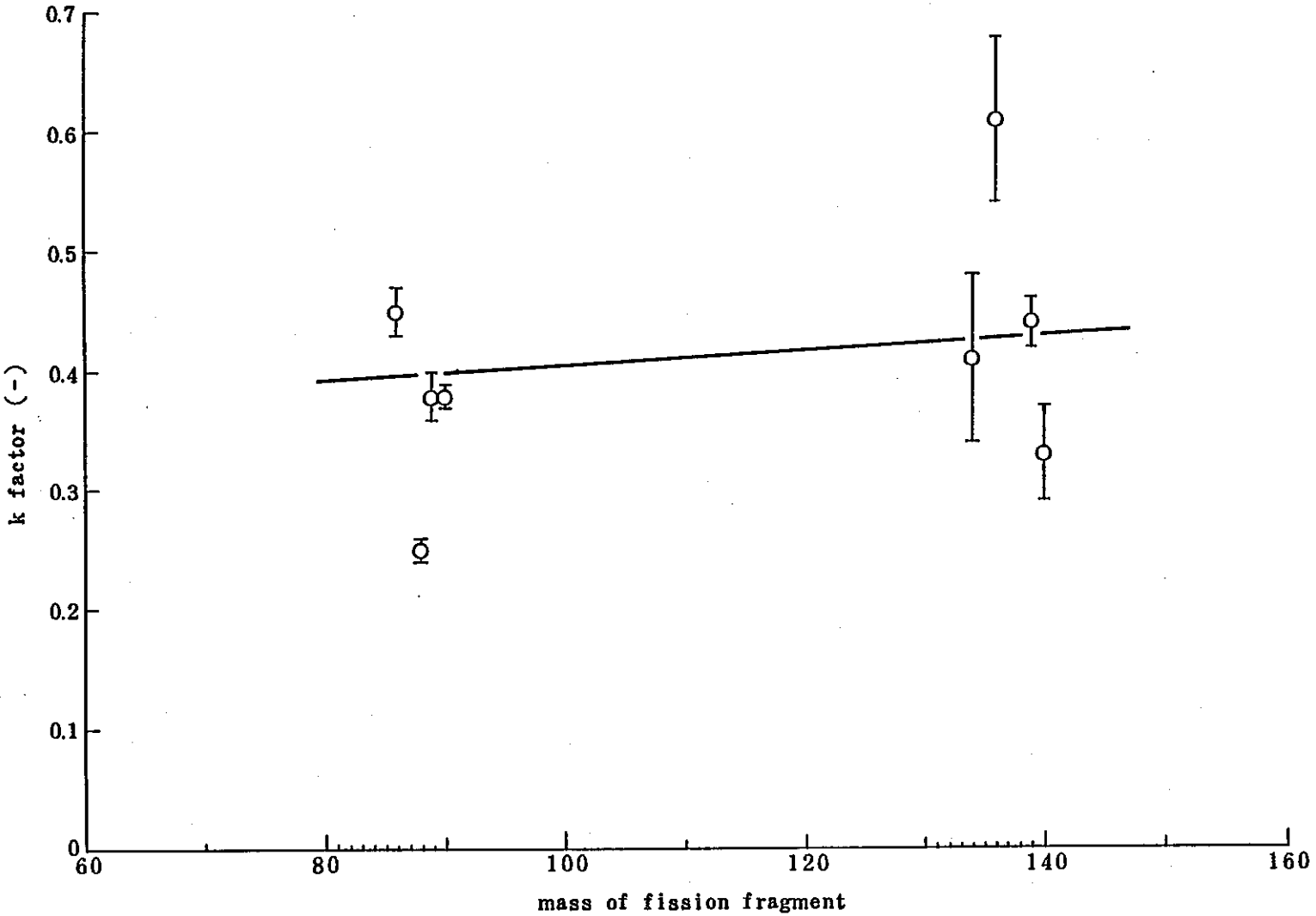

Fig. 6-15 k factor as a function of mass

7. RESULT OF MEASUREMENT OF DELAYED NEUTRON

7.1 Introduction

Transition behavior of delayed neutron (DN) precursor nuclides (hereafter abbreviated as DN nuclides) in sodium is useful for performance evaluation of fuel failure detection system in FBR. Two DN detectors were installed on the delay line of FPL-II, in order to measure DN and to reveal the transfer behavior of DN nuclides in sodium during FPL-II normal operation, during sodium flow change, during no flow and during TTR shut down, similar to the previously performed test. (1)

DN measurements were conducted at 11 irradiation tests (Exp. No. 16, 19 to 28) in this fiscal year, but transfer behavior of DN nuclide was analyzed by using irradiation test data obtained in fiscal year of 1982.

DN nuclides such Br-87, I-137 etc. are classified in 5 groups according to their half life. Names and average half lives of nuclides belong to each group, together with total DN number released from DN nuclides produced by 10^4 fission (14), are indicated in Table 7-1. In general half lives of DN nuclides are short as less than 1 min.

7.2 Result of Measurement at Steady State Operation of the Loop

Detection positions of DN are located at two points of 700 cm and 2848 cm apart from uranium capsule on the delay line. By comparing count rates at the two detection positions at a distance of 2148 cm, adsorption behavior of DN nuclides on stainless steel surface is estimated. Time lags between two positions are 17.9 sec at sodium flow rate 5 ℓ/min, 44.8 sec at 2 ℓ/min and 89.6 sec at 1 ℓ/min.

When the loop is at steady state operation, measured count rates of DND-1 and DND-2 in Exp. No. 16 to 28 are indicated in Table 7-2, where the count rate shows corrected value by neutron

background counts 33.8 cps and 7.3 cps for DND-1 and DND-2, respectively, at 100 kW output of TTR. Here, values indicated in Table 7-2 were corrected by subtracting these background counts. In the case when TTR power was less than 100 kW, values were corrected assuming that back-ground counts were proportional to the power.

In Exp. Nos. 27 and 28, where irradiation tests were conducted at sodium cold trap temperature of 200°C, DN count rates kept same values since start-up of irradiation tests. It is assumed that FP release fraction did not change since start-up of irradiation tests, i.e. no change occurred at the irradiation specimen surface.

As explained in the previous paper (1), DN count rate decreases with decrease in sodium temperature. Temperature dependence of DN count rate at sodium flow rate of 5 ℓ/min is shown in Fig. 7-1. The decrease in count rate is probably due to temperature dependence in DN nuclides release from irradiation specimen and increase in DN nuclide adsorption on the surface of irradiation specimen and piping wall. Ratio of count rates of DND-1 and DND-2 is useful to estimate adsorption behavior of DN nuclides on inner wall of piping, but the variation of the ratio appeared remarkedly only at below 230°C sodium temperature. (ref. Table 7-4 and Exp. No. 9 to 12).

In Exp. No. 23, dependence of DN count rate on TTR power was measured by varying TTR power stepwise from 0.1 kW to 100 kW. The results shown in Fig. 7-2 indicate that DN detection system holds a linearity in wide range of 0.1 to 100 kW of TTR output and it is concluded that the recoil phenomenon is a main mechanism of FP release.

7.3 Result of Measurement During Sodium Flow Stop Test

Following 1982 irradiation tests, in Exp. No. 23, 26 and 28, decays of DN nuclides remained in sodium in the loop piping were measured during sodium flow stop at steady state operation of the loop.

DN count rates of DND-1 and DND-2 were measured alternately for 1 sec with interval of 1 sec using present scalor timer. Results of each experiments are shown in Fig. 7-3, where the ordinate at left hand is for count rate of DND-1 and that at right hand is for DND-2.

In experiments, variation of count rates of DND-1 was measured with starting immediately after sodium flow stop. When initial sodium flow rate is 5.0 ℓ/min, gradient of count rate drop is steep because of decay of nuclides with short half life; on the other hand, in cases that reduced flow rates are set such as 2.5 /min and 1.0 ℓ/min, the gradients become milder because of the decay of FP with short half life before arrival at DND-1 detection position. In Test No. 28, sodium with a high concentration of oxygen (cold trap temperature of sodium was 200°C and oxygen concentration was 12 ppm)[6] was used. However, the test result did not differ significantly from the results of Test Nos. 23 and 26 which used ordinary sodium (cold trap temperature was 120°C and oxygen concentration was 1 ppm). For this reason oxygen concentration of around 12 ppm is not considered to affect the behavior of DN nuclides in the sodium of 500°C.

7.4 Result of Measurement after TTR Power Shut Down (test scram)

In Exp. Nos. 19, 20, 21, 22, 25, 27 and 28, change of DN count rate of DND-1 and DND-2 at TTR test scram during sodium circulation, was measured, with the same method in Sec. 7-3, alternately for 1 sec with interval of 1 sec. The results of each test are shown in Fig. 7-4. Here, in Exp. No. 19, where a special experiment was conducted as described later, DN count rates of DND-1 and DND-2 were measured continuously 0.4 sec interval by using two multichannel scalors (MCS). In Exp. No. 21 only the count rate of DND-1 was recorded, due to the malfunction of printer.

Excluding Exp. No. 19 and No.20, at sodium flow rate 5 ℓ/min, the count rate of DND-1 after 6 sec of test scram and the count rate of DND-2 after 24 sec of test scram started to drop sharply;

at the sodium flow rate of 1 ℓ/min count rates of DND-1 and DND-2 started to drop after 30 sec and 110 sec, respectively. It is explained that steady state of DN nuclides is maintained by release and addition of a certain amount of FP in flowing sodium from/on irradiation specimen, but at test scram, FP release drops to zero resulting in drop of count rates independent of sodium temperature. Changes of DN count rate at TTR test scram in sodium flow rate of 5 ℓ/min, showed almost same trend (in Exp. Nos. 21, 27 and 28) independently of sodium temperature. It concludes that composition of DN nuclides in sodium is almost independent of temperature and the same conclusion (1) was obtained in experiments during sodium flow stop conducted in 1982.

In the measurement of variation at TTR test scram, probability of additional DN counting from other positions than detection positions, is assumed from the following fact: for example in Exp. No. 27, the count rate of DND-2 should keep constant value until abrupt drop of count rate occurs (25 sec after test scram); however, in spite of that count rate of DND-2 commences dropping accompanied with that of DND-1 at 6 sec after test scram (see, Fig. 7-4, 7). In order to clarify this situation, a mock-up test described in Sec. 3.1 was conducted, but mock up test was not sufficient because neutron standard radiation source using in the mock up test has a peak at 700 keV and DN has a different spectrum with peak at 450 keV.

So, in Exp. No. 19, DN response from loop piping was examined again: sodium flow is stopped before 5 min of TTR test scram, and FP is accumulated in uranium capsule, then simultaneously DN nuclides in sodium at loop piping decrease by radiation decay. Time scale in Exp. No. 19 of Fig. 7-4 was expressed from the sodium flow restart as starting point, when sodium flow was resumed after 25 sec from test scram.

The result is similar with that of the mock-up test (cf. Figs. 3-7 and 8), but it showed that the ratio of the highest peak against the second peak is larger for count rate of DND-1 than for that of mock-up test and shielding capability of DN detector is

larger for DN than for neutron released from neutron radiation source used in mock-up test. It is due to difference of neutron spectra, i.e. shielding is easier for DN with lower energy. The result that half value width of peak obtained in this test was larger than that obtained in Fig. 3-7 is probably due to the fact that the sodium mass, containing FP which had flown out from the uranium capsule when sodium circulation was resumed, was not a perfect point-like radiation source but was an extended radiation source.

In the case of count rate of DND-1, a clear peak was detected no longer after 30 sec elapsed, because mixing up with bulk sodium occurred when flowing sodium passed through the electromagnetic pump, the main heater and the uranium capsule etc., resulting in extended sodium region containing FP. Count rate shows minimum value at 50 sec after resumption of sodium flow. That is consistent with one circulation time of sodium flow rate 5 ℓ/min in the loop.

7.5 Result of Measurement During Sodium Drain before TTR Shut Down

In Exp. No. 24 and No. 26, DN count rate from DN nuclides adsorbed on inner wall of piping was measured during sodium drain before TTR shut down, as shown in Fig. 7-5. But due to taking time to drain sodium completely from loop (more than 30 sec) and the incomplete shielding of DN detector system, DN nuclides adsorbed on the piping can not be distinguished from the count rate pattern.

7.6 Analytical Model

In order to evaluate behavior of DN nuclides in sodium quantitatively, modeling of DN nuclide behavior in sodium is necessary.

Hereafter, DN nuclides are expressed by grouping as described above. Concentration of DN nuclides in i-group in sodium $\bar{C}_i$ (atoms/cm^3) is expressed (ref. Appendix C)

$$\bar{C}_i(x) = \bar{C}_{i0} \cdot e^{-\alpha_i \cdot x} \qquad (7\text{-}1)$$

where,

- x : distance from uranium capsule (cm)
- $\bar{C}_{io}$: initial concentration of DN nuclides in i-group at irradiation specimen (atoms/cm^3)

$$\alpha_i = \frac{\lambda_i}{v} \{ K_{ai} \cdot (\ell / a) + 1 \}$$

Concentration at wall surface $C_i^W(x)$ (atoms/cm^2)

$$C_i^W(x) = K_{ai} \cdot \bar{C}_i(x) \qquad (7\text{-}2)$$

where,

- K_{ai}: distribution coefficient of DN nuclides in i-group
- λi : decay constant of DN nuclides in i-group
- v : sodium flow velocity (cm/sec)
- ℓ : circumference of piping ($2\pi r$; cm) (r: inner diameter of piping)
- a : cross-section of piping (πr^2; cm^2)

expresses ratio of concentration on wall surface against that in sodium, as defined in Eq. (7-2)

DN count rate measured at detection position $C_{rj}(x_j)$ (cps)
(j = 1, 2 for DND-1, DND-2)

$$C_{rj}(x_j) = \sum_{i=1}^{5} f_j \cdot \eta_i \cdot \lambda_i \cdot \{ V \cdot \bar{C}_i(x_j) + S \cdot C_i^W(x_j) \} \qquad (7\text{-}3)$$

where,

- x_j : distance to DND-1, DND-2
- V : volume of sodium projected by detector
- S : wall surface area projected by detector
- ℓd : length of piping projected by detector
- f_j : detection efficiency

η_i : DN release fraction

$V = \pi r^2 \ell_d$, $S = 2\pi r \ell_d$ and applying Eqs. (7-1), (7-2) to Eq. (7-3) and using Eq. (C-8) in Appendix C

$$C_{rj}(x_j) = f_j \cdot \pi r \cdot \ell_d \cdot \sum_{i=1}^{5} \frac{\lambda_i \cdot \eta_i \cdot P_i}{F \cdot (1 - e^{-\alpha_i \cdot L})} \cdot e^{-\alpha_i \cdot x_j} \cdot \{ r + 2K_{ai} \} \qquad (7\text{-}4)$$

where,

F : sodium flow rate (cm^3/sec)
L : total length of the loop
P_i : FP release rate (atoms/sec)
R_{fi}: release fraction (dimensionless)
Y_i : fission yield (atoms/fission)
F_r : fission rate (fission/sec)

$$P_i = R_{fi} \cdot Y_i \cdot F_r$$

It can be described as

$$C_{rj}(x_j) = f_{rj} \cdot \sum_i \frac{\lambda_i \cdot Q_i \cdot R_{fi}}{F \cdot (1 - e^{-\alpha_i \cdot L})} \cdot K_{ai}' \cdot e^{-\alpha_i \cdot x_j} \qquad (7\text{-}4a)$$

where, $f_{rj} = f_j \cdot \pi r \cdot \ell_d$, $K_{ai}' = r + 2\,K_{ai}$

$Q_i = \eta_i \cdot Y_i \cdot F_r$ corresponds to the DN emission rate in Table 7-1.

Using these equations, variations of DN count rate during sodium flow stop and at the TTR power shut down (test scram) are expressed as follows:

1) At sodium flow stop

When sodium flow is stoped, DN nuclides in i-group in piping decrease by following decay constant,

$$C_{rj}(x_j, t) = f_{rj} \cdot \sum_i \frac{\lambda_i \cdot Q_i \cdot R_{fi}}{F \cdot (1 - e^{-\alpha_i \cdot L})} \cdot K_{ai}' \cdot e^{-\alpha_i \cdot x_j} \cdot e^{-\lambda_i \cdot t} \quad (7\text{-}5)$$

where t: elapsed time after flow stop

2) At TTR scram

When TTR power shut down, stepwise variation of count rate with time is expected. At the time when TTR scram, because FP release in sodium stops, the concentration of FP at irradiation specimen varies from the initial value C_{io} to $\bar{C}_{io} \cdot e^{-\alpha_i \cdot L}$.

The initial concentration of FP nuclides represents FP survived being subject to the radiation decay after one circulation through the loop in sodium. Therefore, variation of count rate is expressed by putting,

t_1 : one circulation time of flowing sodium through the loop

t_{2j}: time of sodium to arrive at detection position from irradiation specimen ($= x_j/v$)

n : number of circulation,

$$\left.\begin{aligned} C_{rj}(x_j, t) &= f_{rj} \cdot \sum_i \frac{\lambda_i \cdot Q_i \cdot R_{fi}}{F \cdot (1 - e^{-\alpha_i \cdot L})} \cdot K_{ai}' \cdot e^{-\alpha_i \cdot x_j} \quad (0 \leqq t \leqq t_{2j}) \\ C_{rj}(x_j, t) &= f_{rj} \cdot \sum_i \frac{\lambda_i \cdot Q_i \cdot R_{fi}}{F \cdot (1 - e^{-\alpha_i \cdot L})} \cdot K_{ai}' \cdot e^{-\alpha_i \cdot x_j} \cdot e^{-\alpha_i \cdot nL} \\ &\qquad (t_{2j} + (n-1)t_1 \leqq t \leqq t_{2j} + nt_1) \end{aligned}\right\} \quad (7\text{-}6)$$

7.7 Analytical Model in Consideration of Mock-Up Test Result

Analytical model stated above is available only to case when DN nuclide is measured by using ideal detectors with complete

shielding, therefore it is practically not available to the DN detection system in FPL-II. For example, if adsorption of DN nuclides on stainless steel surface at high sodium temperature is negligible, to the state of a stationary flow rate of 5 ℓ/min, the ratio of count rate of DND-1 to that of DND-2 is calculated as 5.96 according to the analytical model mentioned above, however, the experimental value was around 2.1 deviating largely from the analytical result. So, the analytical model should be refined considering mock-up test result.

At the mock-up test described in Paragraph 3.1, the detection efficiency was measured at discrete positions, therefore interpolation between measured values using following exponential function is performed. The detection efficiency of DN detection system at x from uranium capsule is,

$$f_{j,k}(x) = B_{j,k} \cdot e^{\beta_{j,k} \cdot x} \qquad (x_k \leqq x \leqq x_{k+1}) \qquad (7\text{-}7)$$

where j = 1, 2 for DND-1, DND-2, and K means sectional interval.

The release rate dA of DN nuclide in a infinitesimal length dx at distance x is expressed using Eqs. (7-1) and (7-2)

$$dA = \pi r \cdot \sum_i \frac{\lambda_i \cdot Q_i \cdot R_{fi}}{F \cdot (1 - e^{-\alpha_i \cdot L})} \cdot K_{ai}' \cdot e^{-\alpha_i \cdot x} \cdot dx$$

and the count rate is $f_{j,k}(x).dA$

By integration, the count rate of DN nuclide distributed through overall length of the loop is,

$$C_{rj} = \pi r \cdot \sum_i \frac{\lambda_i \cdot Q_i \cdot R_{fi}}{F \cdot (1 - e^{-\alpha_i \cdot L})} \cdot K_{ai}' \cdot \int_0^L f_{j \cdot k}(x) \cdot e^{-\alpha_i \cdot x} dx \qquad (7\text{-}8)$$

For reference, when sodium flow is in steady state at high

temperature, (i.e., adsorption of DN nuclides on inner wall of piping is neglected $K_{ai} = 0$). DN contribution at DN detector from various parts of FPL-II loop piping is indicated in Table 7-3 for various sodium flow rates.

These values are calculated as follows:

count rate $C_{rj,k}$(cps) of each DN detector given from each divided area k ($x_k \leqq x \leqq x_k + 1$)

$$C_{r_{j,k}} = \pi r^2 \cdot \sum_i \frac{\lambda_i \cdot Q_i \cdot R_{fi}}{F \cdot (1-e^{-\alpha_i \cdot L})} \cdot \int_{x_k}^{x_{k+1}} f_{j \cdot k}(x) \cdot e^{-\alpha_i \cdot x} \, dx$$

The contribution ratio is expressed by

$$\frac{C_{r_{j,k}}}{C_{r_j}} = \frac{\sum_i \frac{\lambda_i \cdot Q_i}{(1-e^{-\alpha_i \cdot L})} \int_{x_k}^{x_{k+1}} f_{j,k}(x) \cdot e^{-\alpha_i \cdot x} \, dx}{\sum_i \frac{\lambda_i \cdot Q_i}{(1-e^{-\alpha_i \cdot L})} \int_0^L f_{j,k}(x) \cdot e^{-\alpha_i \cdot x} \, dx}$$

Here, λ_i and Q_i use decay constant and DN release rate in Table 7-1, respectively and L is 5734 cm. $f_{j,k}(x)$ is calculated in mock-up test and used $\alpha_i = \lambda_i / v$, where v is sodium flow rate.

In calculation of contribution ratio, large computer was used. As seen in Table 7-3, the contribution ratio for DND-1 at detection position (DL-A) increases as flow rate decreases, i.e. 59.7% at flow rate 5 ℓ/min, 62% at 2.5 ℓ/min, 66.9% at 1 ℓ/min, 73.5% at 0.5 ℓ/min and the contribution ratio at detection position (DL-B) decreases, i.e. 5.3% at 5 ℓ/min, 3.3% at 0.5 ℓ/min. The contribution ratio at electromagnetic pump is very small, i.e. 6% at 5 ℓ/min and 0.4% at 0.5 ℓ/min.

On the other hand, the contribution ratio for DND-2 at detection position (DL-D) decreases, i.e. 22.1, 21.0, 14.4 and 6.2%

at 5.0, 2.5, 1.0 and 0.5 ℓ/min, respectively. Now, analytical models of count rate variation at sodium flow stop and at TTR test scram will be shown, respectively.

1) At sodium flow stop

Count rate C_{rj} is expressed as a function of time, so from Eq. (7-4).

$$C_{rj}(t) = \pi r \cdot \sum_i \frac{\lambda_i \cdot Q_i \cdot R_{fi}}{F \cdot (1-e^{-\alpha_i \cdot L})} \cdot K_{ai}' \cdot e^{-\lambda_i \cdot t} \int_0^L f_{j,k}(x) \cdot e^{-\alpha_i \cdot x} dx \qquad (7\text{-}9)$$

where t: elapsed time after sodium flow stop (sec)

2) At TTR test scram

From Eq. (7-6), using elapsed time t (sec) after test scram,

$$C_{rj}(t) = \pi r \cdot \sum_i \frac{\lambda_i \cdot Q_i \cdot R_{fi} \cdot K_{ai}'}{F \cdot (1-e^{-\alpha_i \cdot L})} \cdot \left\{ \int_0^{x_t} f_{j \cdot k}(x) \cdot e^{-\alpha_i \cdot (x+(n+1)L)} dx + \int_{x_t}^L f_{j \cdot k}(x) \cdot e^{-\alpha_i \cdot (x+nL)} dx \right\} \qquad (7\text{-}10)$$

X_t: position where DN count rate changes rapidly by the effect of scram

$$X_t = v.t - nL \quad (n = \text{integer } (L/vt))$$

7.8 Comparison of Analytical Model with Experimental Result

1) Comparison with experimental result at steady state loop condition

Ratio of count rate of DND-1 and DND-2 (C_{r1}/C_{r2}) calculated from Eq. (7-8) is indicated in Table 7-4 together with results of irradiation test (Exp. No. 3 to No. 16). The ratio is shown as

$$\frac{C_{r1}}{C_{r2}} = \frac{\sum_i \frac{\lambda_i \cdot Q_i}{(1-e^{-\alpha_i \cdot L})} \cdot \int_0^L f_{1,k}(x) \cdot e^{-\alpha_i \cdot x} dx}{\sum_i \frac{\lambda_i \cdot Q_i}{(1-e^{-\alpha_i \cdot L})} \cdot \int_0^L f_{2,k}(x) \cdot e^{-\alpha_i \cdot x} dx}$$

Here, in the calculation, $K_{ai} = 0$ (adsorption behavior of DN nuclides is neglected) and release fractions of each DN nuclide are all equalized as R_f.

The result of calculation was in reasonably good agreement with experimental result at higher than 270°C. In Exp. No. 10 and No. 13, flow dependence of DN count rate was measured by changing flow rate stepwise from 5.0 to 0.5 ℓ/min at 500°C sodium temperature.

The experimental result is 2.11 to the analytical result is 2.20 at flow rate 5 ℓ/min and the relation between them changes inversely as flow rate decreases, i.e. the experimental result is 4.32 and the analytical result is 3.91 at flow rate 0.5 ℓ/min. Though the reason should be discussed a little more, it was clarified that analytical model taken account of mock-up test result explains well test results.

Test results of flow rate dependence of DND-1 and DND-2 are shown in Fig. 7-6, where experimental values were obtained in Exp. No. 10 and regarding DND-1 values obtained in Exp. No. 13 were also included but regarding DND-2 in Exp. No. 13 were excluded because of extreme low value due to unknown trouble in the test (cf. Table 7-4). Solid lines in the figure indicate flow rate dependences of C_{r1} and C_{r2}, which are calculated from Eq. (7-8), putting $K_{ai} = 0$ and adjusting R_f to equalize C_{r1} as the test result for DND-1 at flow rate of 5 ℓ/min in Exp. No. 10. Test results were in good agreement with analytical results. In more detail these results were checked: experimental values were higher than analytical values for DND-1 at low flow rate, but both of them were in good agreement for DND-2 except at high flow rate where analytical values were higher than experimental values.

2) Result of DN measurement and temperature dependence

DN count rate decreases with decreased sodium temperature, as shown in Fig. 7-1 probably owing to adsorption behavior of DN nuclides. As indicated in Table 7-4, at low flow rate of 5 ℓ/min, the rate of count rate of DND-1 to that of DND-2 was around 2.05 indicating no considerable change between 270 and 500°C, but the change of ratio appeared at lower than 225°C and attained to 2.78 at 225°C. On the other hand, at flow rate of 2 ℓ/min, the ratio was kept around 2.27 down to 270°C but changed to 2.43 and 3.45 at 225°C and 170°C, respectively. Also, the ratio of count rate of DND-1 to that of DND-2 is considered to change, but as indicated in Table 7-4, no remarkable change appeared practically at above 225°C.

3) Comparison with experimental result during flow stop test

Count rates during flow stop test (flow rate: 4.64 ℓ/min $\longrightarrow$ 0) measured in Exp. No. 13 and calculated from analytical model using Eq. (7-9) are shown in Fig. 7-7, where solid line shows calculated value by Eq. (7-9). Here, count rate calculated from Eq. (7-9) putting $K_{ai} = 0$ and $t = 0$ and count rate of DND-1 measured at flow rate in stationary state were equalized by adjusting unknown R_f. (Dotted line shows that by Eq. (7-5). Poor consistency within experimental values.) In the case of DND-1, analytical values were in fairly complete agreement with experimental values. In the case of DND-2, on the other hand, deviation between both values was large immediately after flow stop, but since then good agreement between them was held indicating consistent analytical model with test result.

4) Comparison of experimental result at the TTR test scram

DN count rates at the TTR test scram (flow rate 4.64 ℓ/min) measured in Exp. No. 13 and calculated from analytical model using Eq. (7-10) are shown in Fig. 7-8, where solid line shows calculated value by Eq. (7-10). Here, count rate calculated from Eq. (7-10) putting $K_{ai} = 0$ and $t = 0$ and count rate of

DND-1 measured at flow rate in stationary state were equalized scramby adjusting unknown R_f. (Dotted line shows by that Eq. (7-6). Poor consistency within experimental value.) In the case of DND-1, analytical values were in fairly good agreement with experimental values. In the case of DND-2, on the other hand, deviation between both values was large at several seconds after scram (i.e. within period of time when no influence of test scram appeared at count rate of DND-1), but since then good agreement between them was held indicating consistent analytical model with test result.

In Fig. 7-8, abrupt change in count rate appeared remarkably at the 1st circulation after scram but the change was something blurred after the 2nd circulation after scram. It is owing to the phenomenon that when flowing sodium passes through electromagnetic pump, heater, uranium capsule etc. and enters into the large main piping, it mixes with bulk sodium making turbulence.

7.9 Calculation of k Factor

Up to now, in order to evaluate result of DN measurement, relative comparison of analytical model with experimental result has been mainly performed, but in order to calculate k factor, comparison of analytical model with absolute values of experimental result is necessary.

Comparison of analytical model with absolute values of experimental result is necessary.

$$k_{fi} = R_{fi} / R_{fci}$$

where,

k_{fi} : k factor
R_f : release fraction obtained by experiment
R_{fc} : release fraction obtained by calculation using model

In order to simplify the following calculation, assuming that k_{fi}, k_{fi} and R_{fci} are constant being independent of DN nuclides, suffix i of the above equation is eliminated as follows:

Substituting R_f in Eq. (7-8)

$$C_{rj} = \pi r \cdot \sum_i \frac{\lambda_i \cdot Q_i \cdot R_{fc} \cdot k_f}{F \cdot (1 - e^{-\alpha_i \cdot L})} \cdot K_{ai}' \cdot \int_0^L f_{j,k}(x) \cdot e^{-\alpha_i \cdot x} \, dx$$

Here, considering that the count rate C_{rj} is equal to that obtained for DND-1 and DND-2 in Exp. No. 10, k factor was calculated.

At high sodium temperature, putting $K_{ai} = 0$,

$$\left.\begin{aligned} C_{rj} &= \pi r^2 \cdot \frac{R_{fc} \cdot k_f}{F} \sum_i \frac{\lambda_i \cdot Q_i}{1 - e^{-\alpha_i \cdot L}} \cdot \int_0^L f_{j,k}(x) \cdot e^{-\alpha_i \cdot x} \, dx \\ \alpha_i &= \lambda_i / v \end{aligned}\right\} \qquad (7\text{-}11)$$

where,

r = 0.47 cm and L = 5734 cm

R_{fc} = 0.0159: average value of light and heavy FP

Q_i : emission rate in Table 7-1; to apply values multiplied by 2.05×10^7 (fission / sec)

The calculation was performed using large computer and obtained values of k factor (average 0.59) at various flow rates for DND-1 and DND-2 are indicated in Table 7-5. Here, as explained in Chapter 6, since generally k factor is well known as larger than 1, reasons why k factor of less than 1 was obtained should be studied hereafter. Further study is necessary to clarify why larger value of k factor was obtained compared with that from gamma-ray measurement of volatile FP in Chap. 6. Further study on k factor value is necessary. However, since detection efficiency of DN detection system was obtained by using Am-Be neutron

radiation source that showed different neutron spectrum from DN spectrum, the different spectrum may be responsible for different value of k factor.

7.10 Conclusion

Transition behavior of DN nuclides, that is useful for performance evaluation of fuel failure detection system, was measured by using two detectors installed on the loop. However, it was clarified that DN count rates of the detectors count additionally DN from other than detection positions, such as loop pipings and instrument, owing to their incomplete shielding against neutron.

To estimate DN contribution quantitatively, mock-up test was conducted using neutron standard radiation source. Analytical model in consideration of result of mock-up test was applied to compare each experimental results obtained during steady state of sodium flow, during flow stop test, and at TTR test scram. Also, by applying the analytical model, dependence of DN count rate on sodium flow rate was well explained.

Adsorption behavior of DN nuclides in loop was measured at various sodium temperatures. The result indicates that DN count rate decreases with decreased sodium temperature and the count rate at 500°C decreases to 1/1.7 at 270°C and 1/4.7 at 170°C.

From ratio of count rate of two detectors, adsorption behavior of DN nuclides on stainless steel inner wall surface was estimated. The result indicates that the ratio keeps a constant value at sodium temperature between 500 and 270°C, but increases at 225°C (count rate at downstream side decreases more rapidly) and increases more at 170°C, suggesting that the adsorbed amount on stainless steel at lower than 225°C can not be neglected at lower sodium temperature.

Using analytical model and result of DN measurement, k factor concerned with FP release from irradiation specimen in sodium flow was calculated to average value of 0.59. Though the value is higher than that obtained by gamma-ray measurement of volatile FP, the value is lower than 1. Since k factor is usually believed as higher than 1, further study is necessary to clarify the reason.

Table 7-1 Delayed neutron precursor nuclides[14)]

Group	Half life (Average)	Emission Rate*	Delayed Neutron Precursor Nuclides
1	55.7 sec	5.1	^{87}Br
2	24.6 sec	23.2	^{136}Te, ^{137}I, ^{141}Cs
3	15.9 sec	12.4	^{88}Br
4	5.2 sec	31.4	^{89}Br, ^{93}Rb, ^{138}I, ^{87}Se, ^{137}Te
5	2.2 sec	53.7	^{90}Br, ^{94}Rb, ^{139}I, ^{85}As, ^{135}Sb ^{88}Se

* Emission Rate/10^4 fission

Table 7-2 Steady state count rates for delayed neutrons under constant loop conditions

Exp. No.	Na Temp (°C)	TTR Power (KW)	Na Flow Rate (l/min)	Count rate (CPS)	
				DND-1	DND-2
16	530	5	1.0	77.1	21.7
		100		1527.4	500.3
19	530	5	2.0	115.1	41.9
		100		2145.1	818.6
20	170	5	1.0	7.1	1.3
		100		142.8	32.9
21	170	5	5.0	46.1	13.0
		100		864.5	271.7
22	400	5	1.0	77.2	22.3
		100		1518.5	449.8
23	500	0.1	5.0	3.62	1.36
		0.2		7.39	2.93
		0.5		18.6	7.43
		1		76.8	14.5
		2		73.9	29.1
		5		184.4	73.9
		10		369.2	146.0
		20		734.8	295.0
		50		1784.7	728.9
		70		2467.4	1018.6
		100		3415.9	1456.0
			4.2	3234.1	1353.6
24	270	5	5.0	121.5	54.2
		100		2306.5	1039.7
25	300	5	1.0	56.4	14.4
		100		1093.8	296.3
26	500	5	5.0	179.2	75.3
		100		3385.7	1443.0
			2.5	2369.7	936.2
			1.0	1552.8	435.1
			5.0	3323.2	1419.7
27	500	5	5.0	178.6	77.5
		100		3262.9	1496.6
28	500	5	5.0	181.7	82.5
		100		3420.8	1574.3
				3388.6	1552.1

Table 7-3 Delayed neutron contribution ratio at each delayed neutron detector from the various part of FPL-II loop pipings

Flow Rate / position	5.0 ℓ/min		2.5 ℓ/min		1.0 ℓ/min		0.5 ℓ/min	
	DND-1	DND-2	DND-1	DND-2	DND-1	DND-2	DND-1	DND-2
DL-A(DN1)	59.70%	8.34%	62.03%	9.17%	66.89%	12.18%	73.53%	18.28%
DL-B	5.28	6.90	4.97	6.88	5.07	8.64	3.30	7.66
DL-C	1.91	6.46	1.79	6.43	1.39	6.13	0.58	3.51
DL-D(DN2)	0.61	22.12	0.55	21.04	0.30	14.42	0.10	6.19
DL-E(Heater)	1.39	0.42	0.97	0.31	0.27	0.11	0.05	0.03
EMP	5.96	10.94	4.75	9.35	1.81	4.54	0.44	1.55
Other parts	25.15	44.82	24.94	46.82	24.27	53.98	22.00	12.78
Total	100.0%	100.0%	100.0%	100.0%	100.0%	100.0%	100.0%	100.0%

Table 7-4 Steady state count rates for delayed neutrons under constant loop conditions and calculated data by using analytical model

Exp No.	Sodiam Condition		Count Rates (cps)+)		DND-1/DND-2 Ratio	
	Temp (℃)	Flow Rate (ℓ/min)	DND-1	DND-2*)	Experimental Results	Calculated value
16	530	1.0	1527	500	3.05	2.87
14	〃	1.0 **)	1492	373	4.00	〃
10	500	5.3	3491	1687	2.07	2.19
7	〃	5.0	—	1747	—	2.20
10	〃	〃	3436	1631	2.11	〃
13	〃	〃	3440	1256 ?)	2.74 ?)	〃
13	〃	4.64	3367	1342 ?)	2.51 ?)	2.23
10	〃	4.2	3273	1539	2.13	2.26
13	〃	3.84	3195	1216 ?)	2.63 ?)	2.28
10	〃	3.6	3052	1428	2.14	2.30
13	〃	3.24	2916	1103 ?)	2.64 ?)	2.31
10	〃	2.5	2471	1124	2.20	2.33
13	〃	2.14	2232	810 ?)	2.76 ?)	2.36
10	〃	1.0	1543	508	3.04	2.87
13	〃	0.64	1206	249 ?)	4.84 ?)	3.53
10	〃	0.50	1045	242	4.32	3.91
13	〃	0.14	241	35.4 ?)	6.81 ?)	4.55
5	420	5.0	3444	1672	2.06	2.20
6	〃	〃	3260	1609	2.03	〃
3	350	5.0	3119	1014 ?)	3.08 ?)	2.20
4	〃	〃	2846	—	—	〃
15	300	5.0	2654	1312	2.02	2.20
15	〃	2.0	1586	693	2.29	2.37
11	270	5.0	2054	1010	2.03	2.20
11	〃	2.0	1104	486	2.27	2.37
12	225	5.0	1333	624	2.14	2.20
12	〃	2.0	590	243	2.43	2.37
9	170	5.0	730	263	2.78	2.20
9	〃	2.0	261	75.6	3.45	2.37

+) After correction of neutron background caused by neutron leak from TTR

*) corrected value for detection efficiency

**) Flow rate is smaller than 1.0 ℓ/min

?) DND-2 counter trouble

Table 7-5 k factor calculated by using delayed neutron experimental results (Exp. No. 10) and analytical model

Flow rate	DND-1		DND-2	
	DN count rate	k factor	DN count rate	k factor
5.0 ℓ/min	3436 cps	0.574	1631 cps	0.601
2.5	2471	0.573	1124	0.610
1.0	1543	0.600	508	0.568
0.5	1045	0.637	242	0.578
Average		0.596		0.589

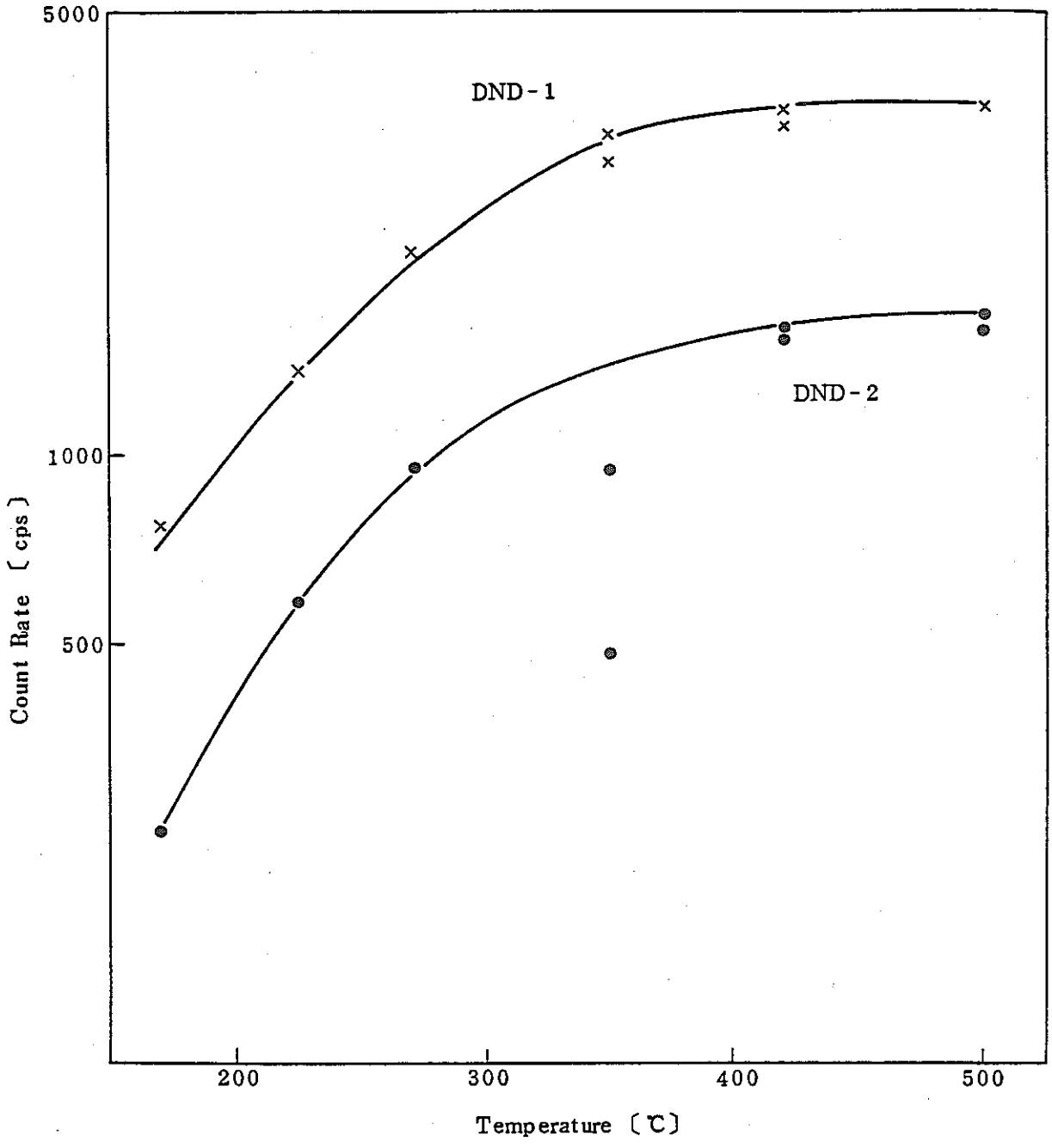

Fig. 7-1 DN-count rate vs. sodium temperature (Sodium flow rate 5 ℓ/min, Data from experiments 3 to 13)

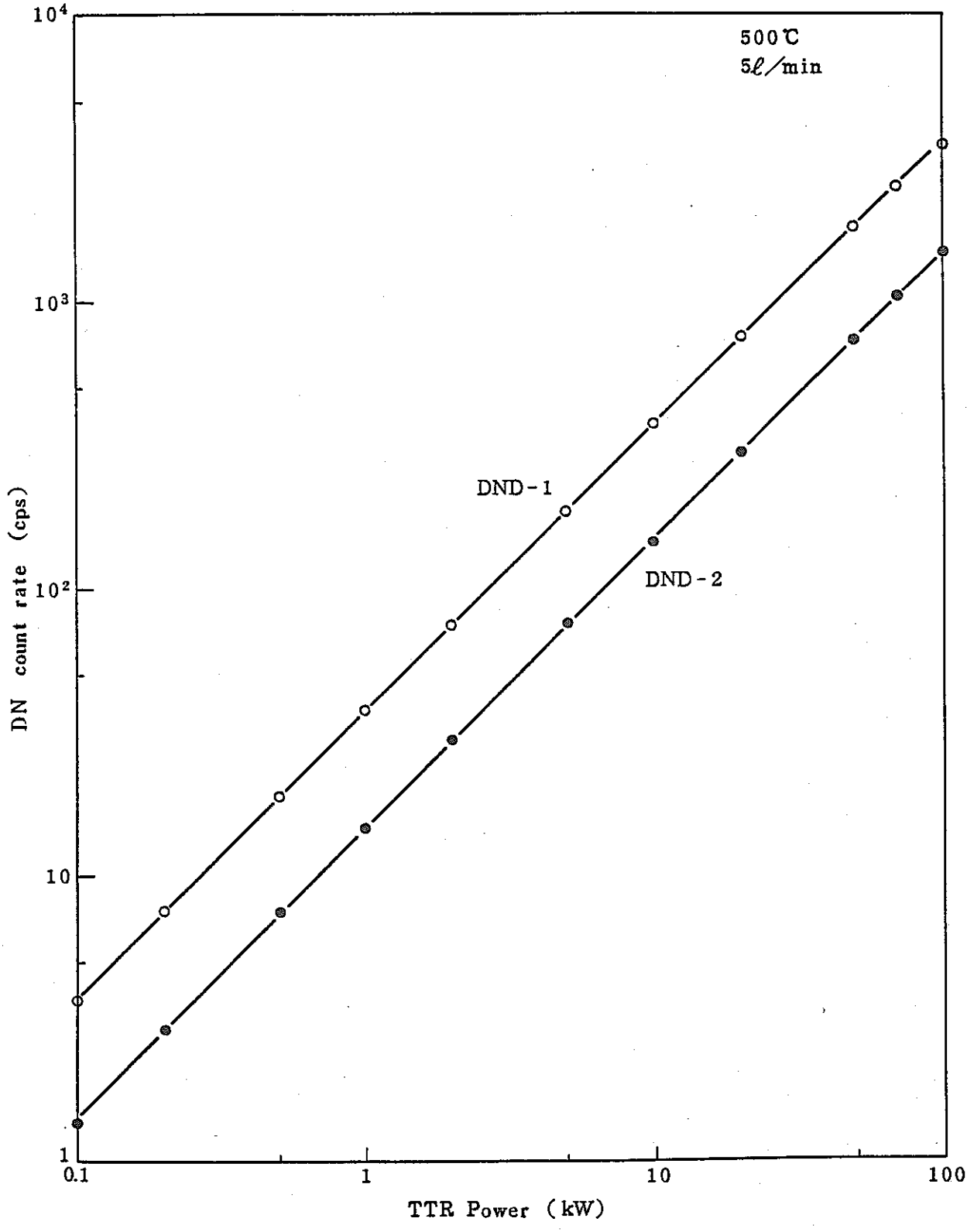

Fig. 7-2 Relationship between delayed neutron count rate and TTR power

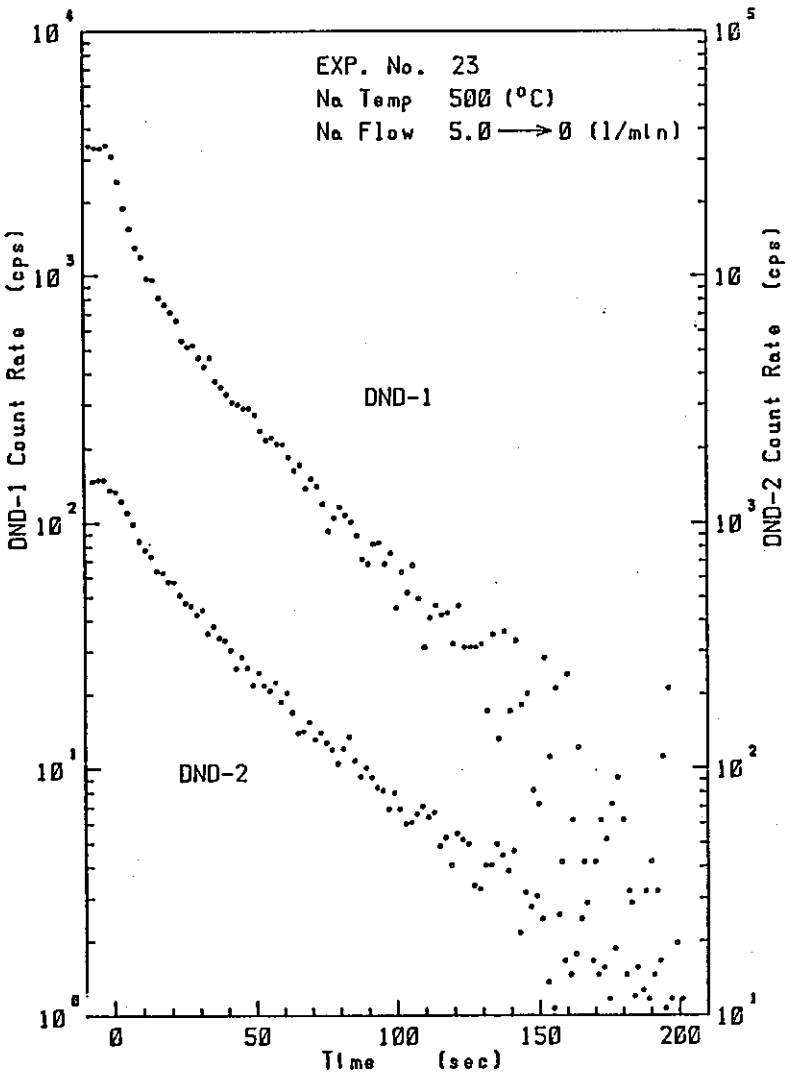

1) Exp. No. 23

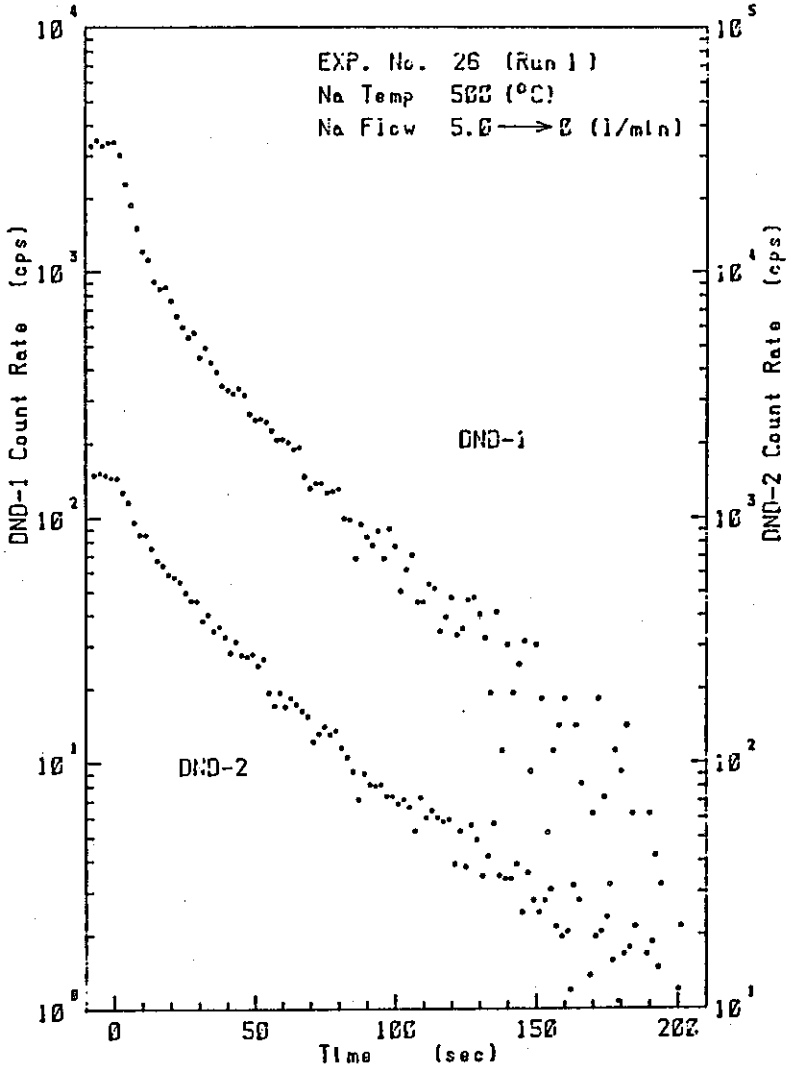

2) Exp. No. 26 (Run 1)

Fig. 7-3 Delayed neutron count rate during flow stop test

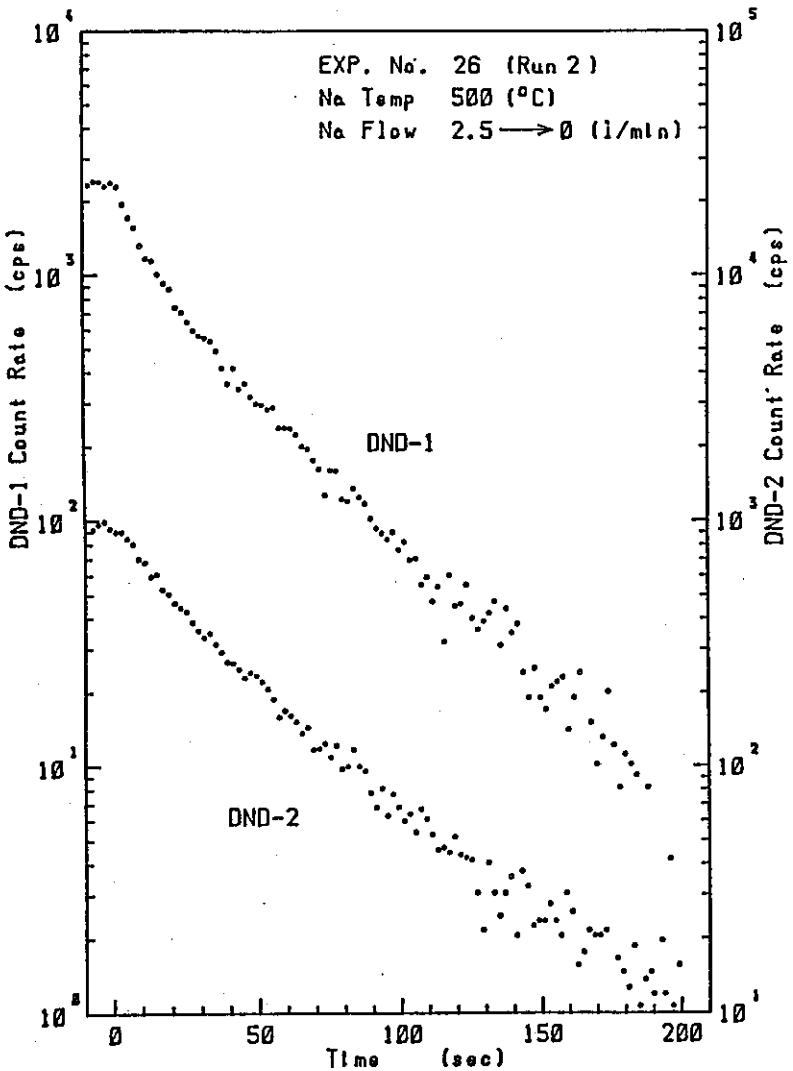

3) Exp. No. 26 (Run 2)

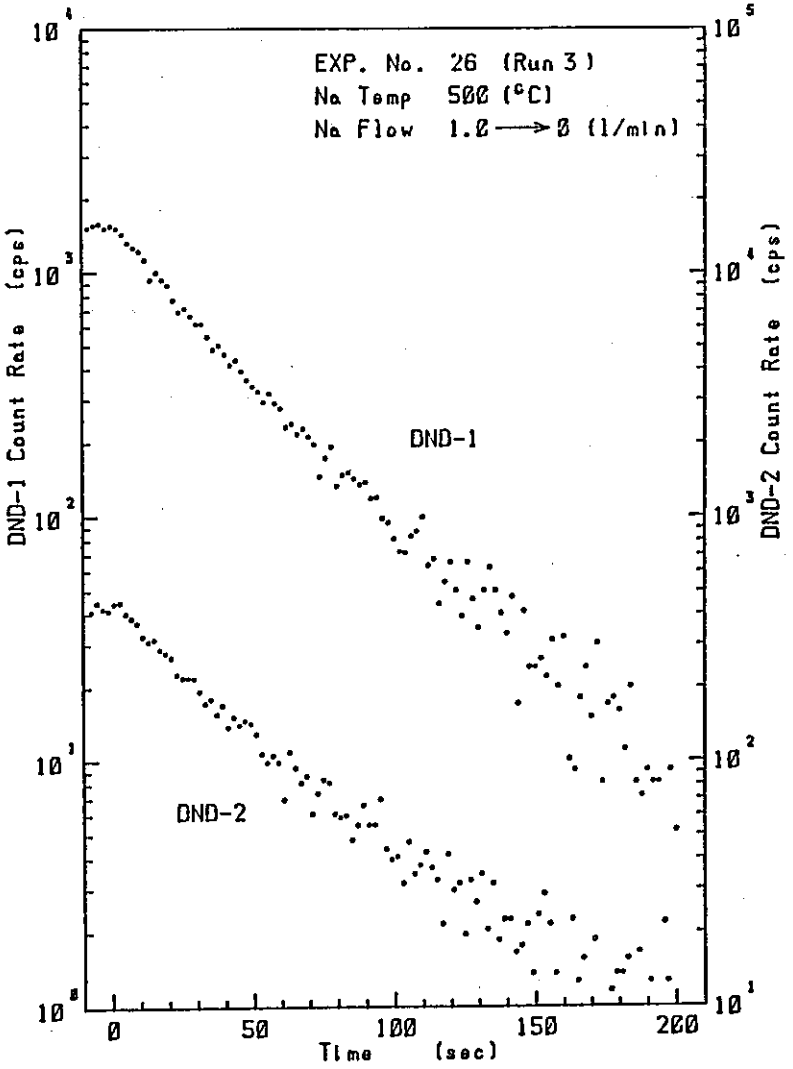

4) Exp. No. 26 (Run 3)

Fig. 7-3 (continued)

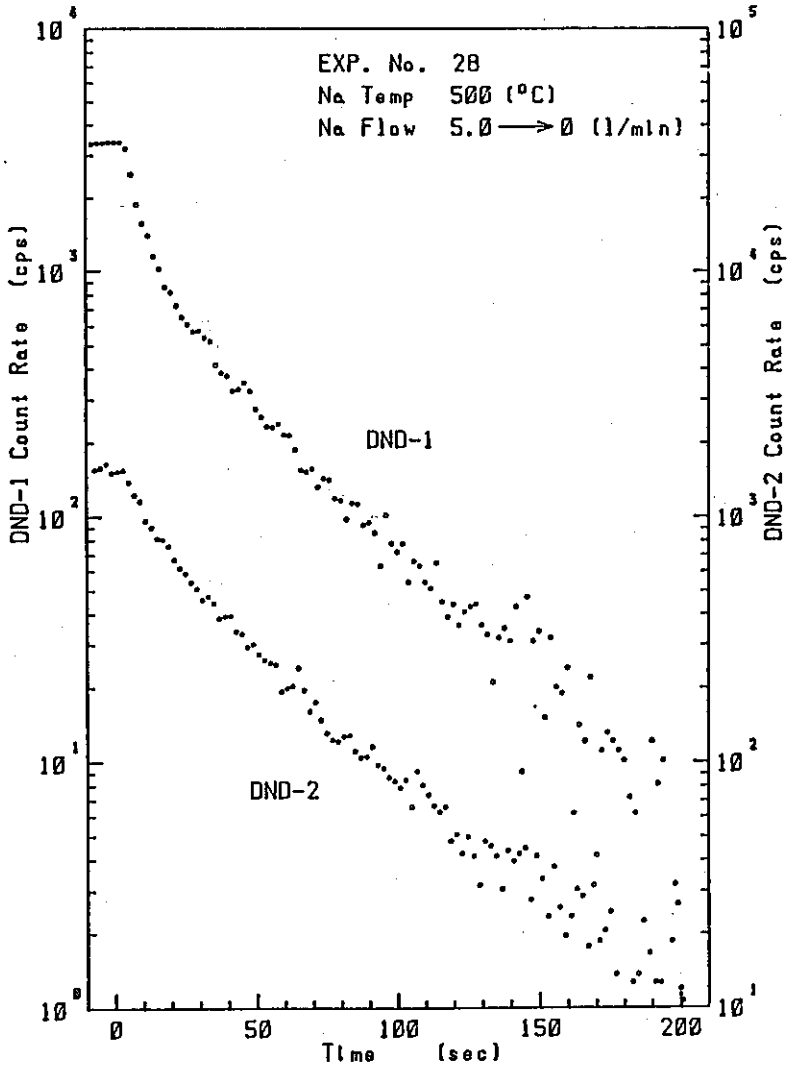

5) Exp. No. 28

Fig. 7-3 (continued)

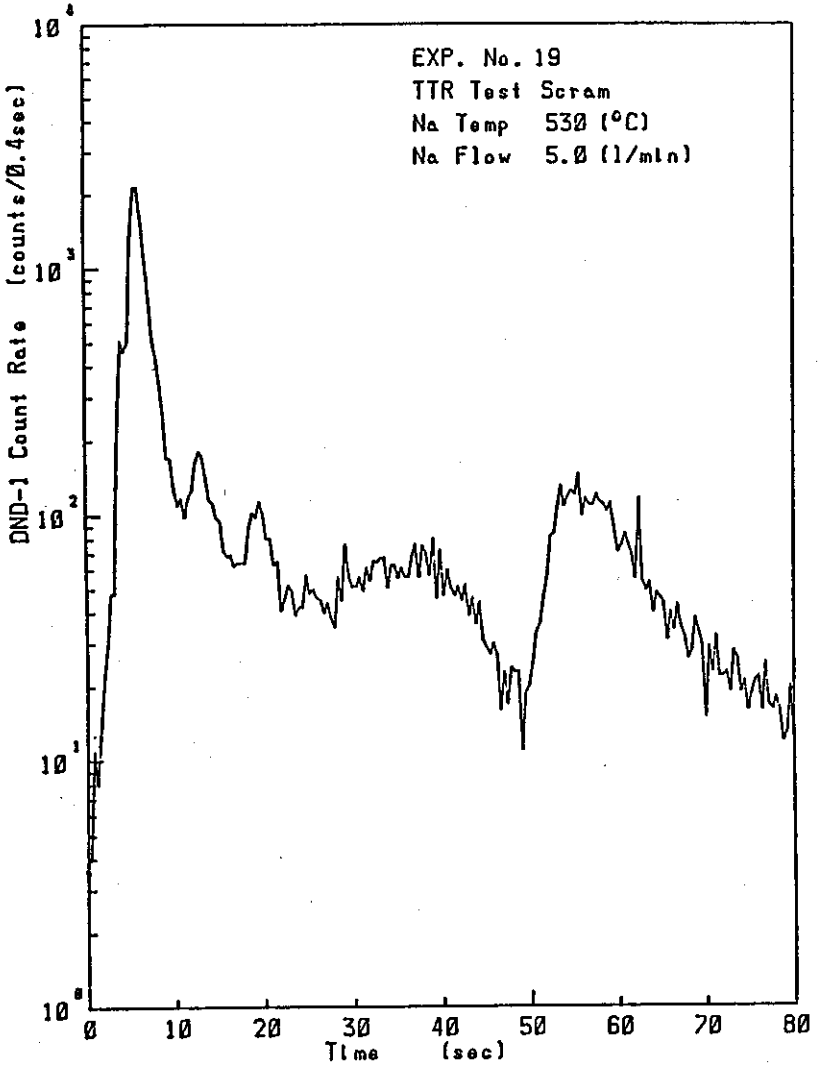

1) Exp. No. 19 (DND-1)

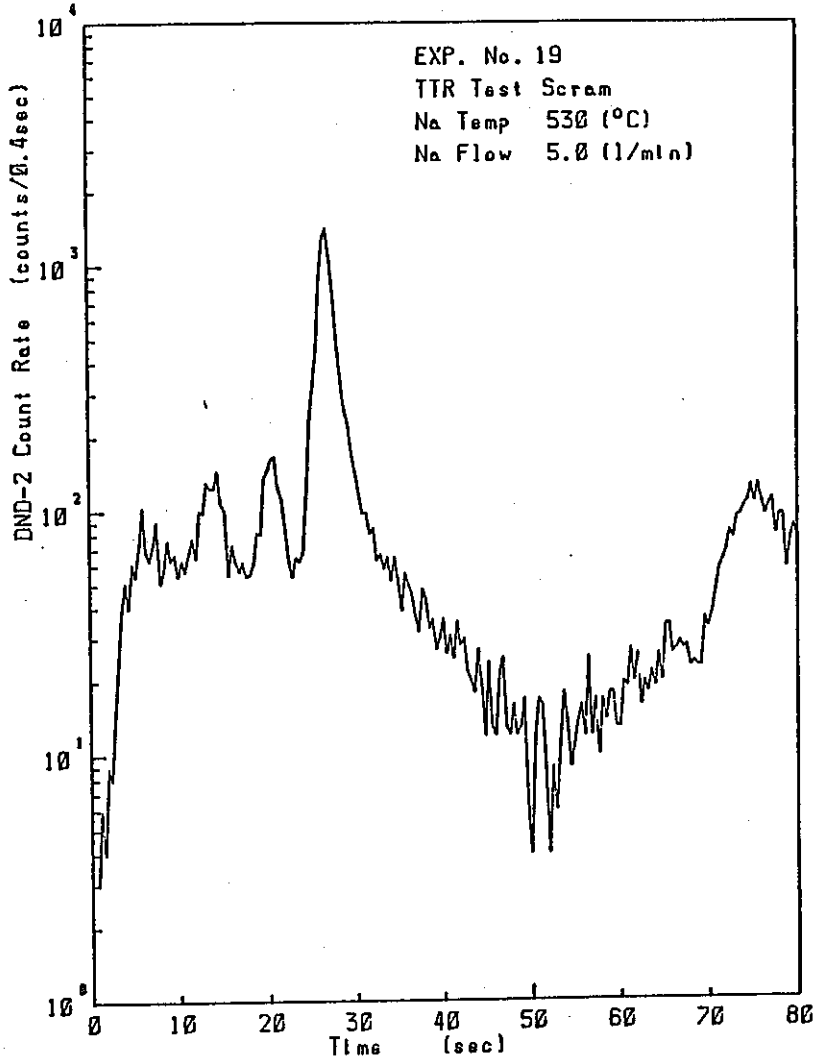

2) Exp. No. 19 (DND-2)

Fig. 7-4 Delayed neutron count rate after TTR test scram

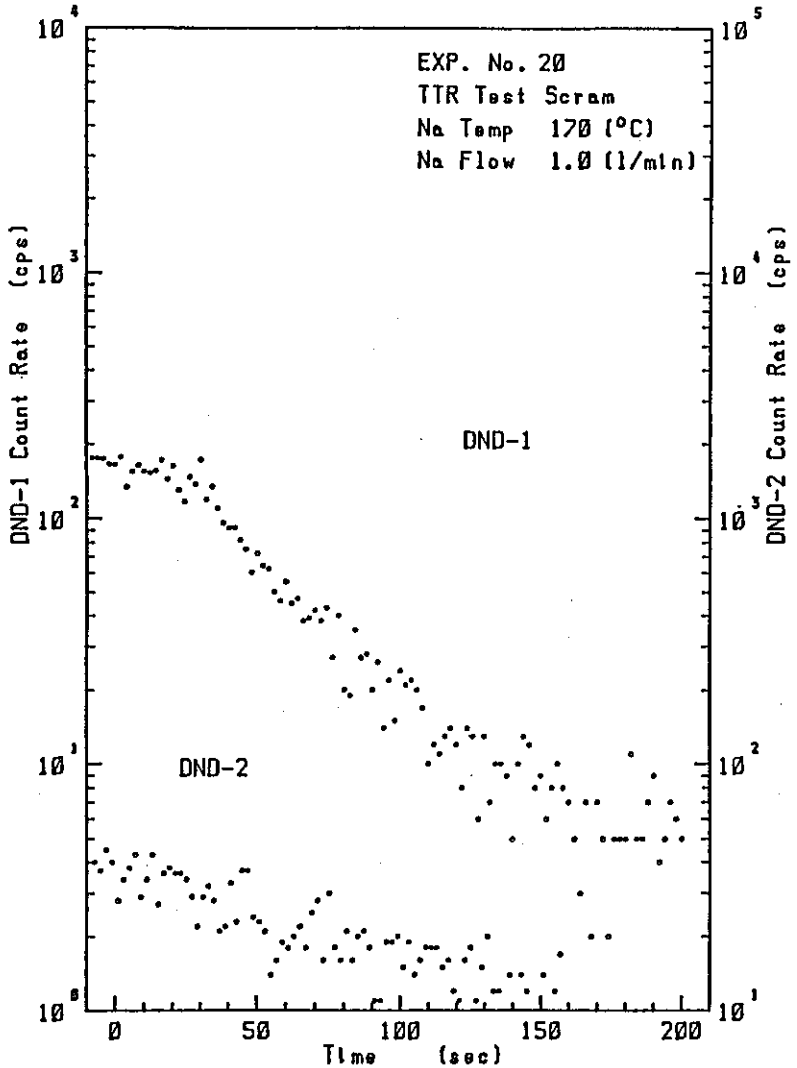

3) Exp. No. 20

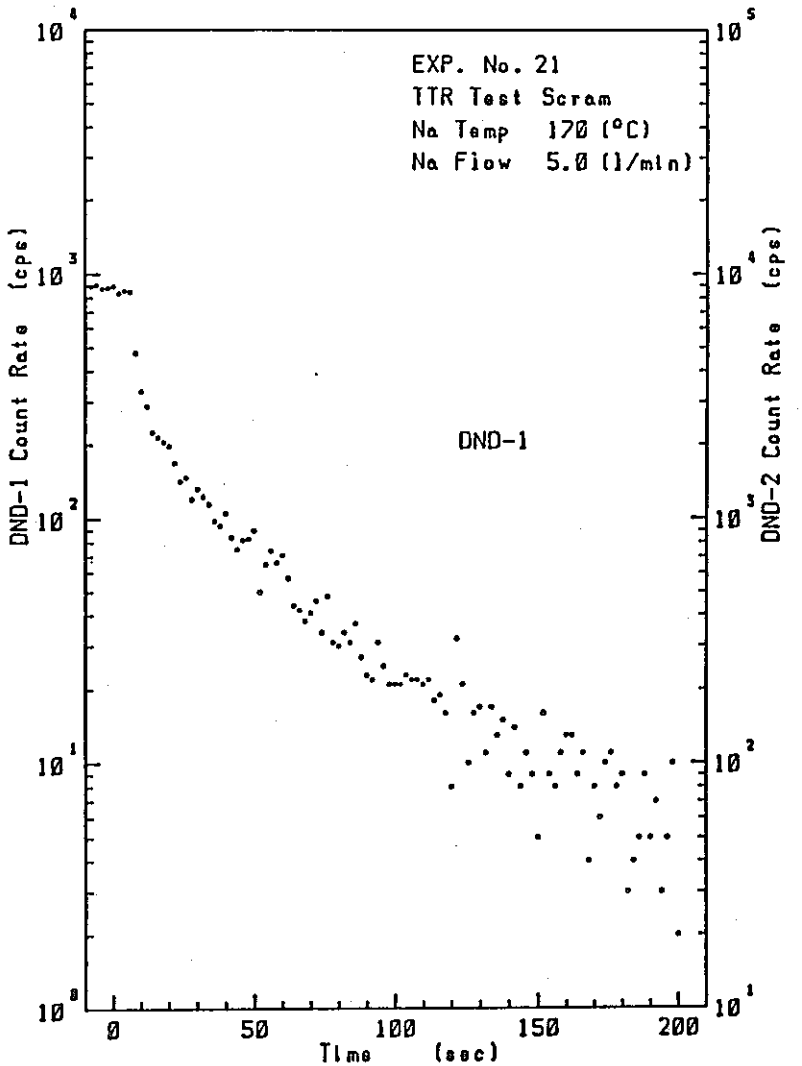

4) Exp. No. 21

Fig. 7-4 (continued)

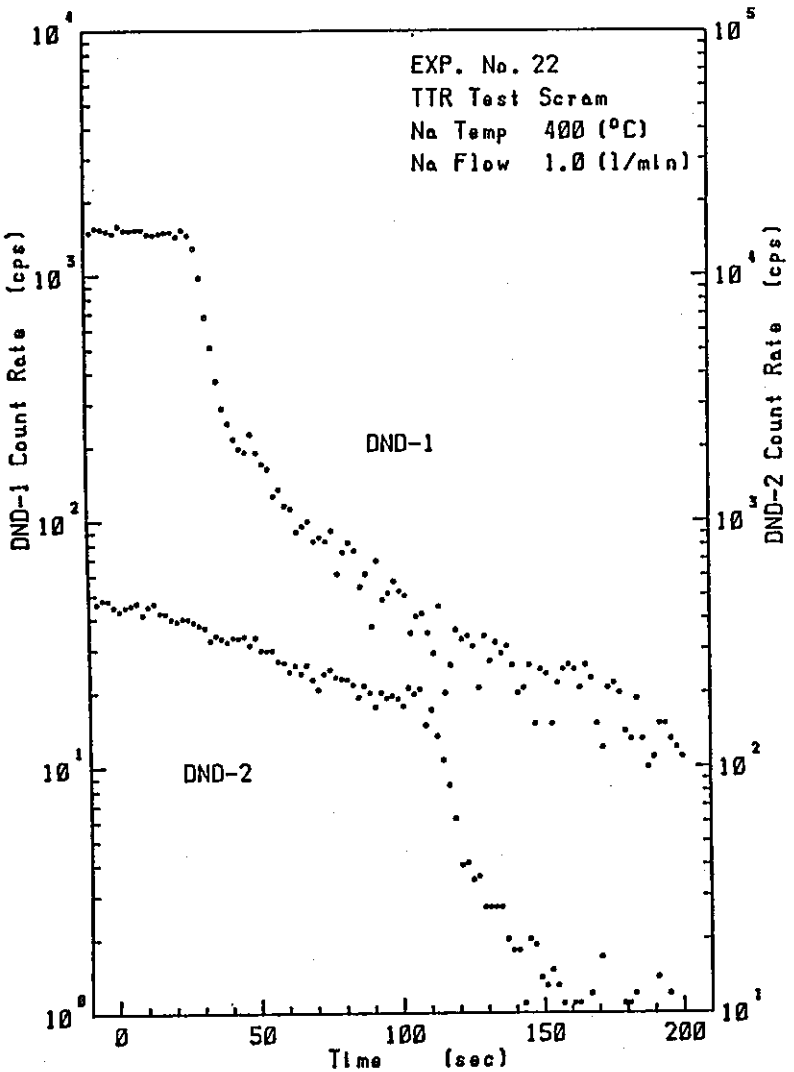

5) Exp. No. 22

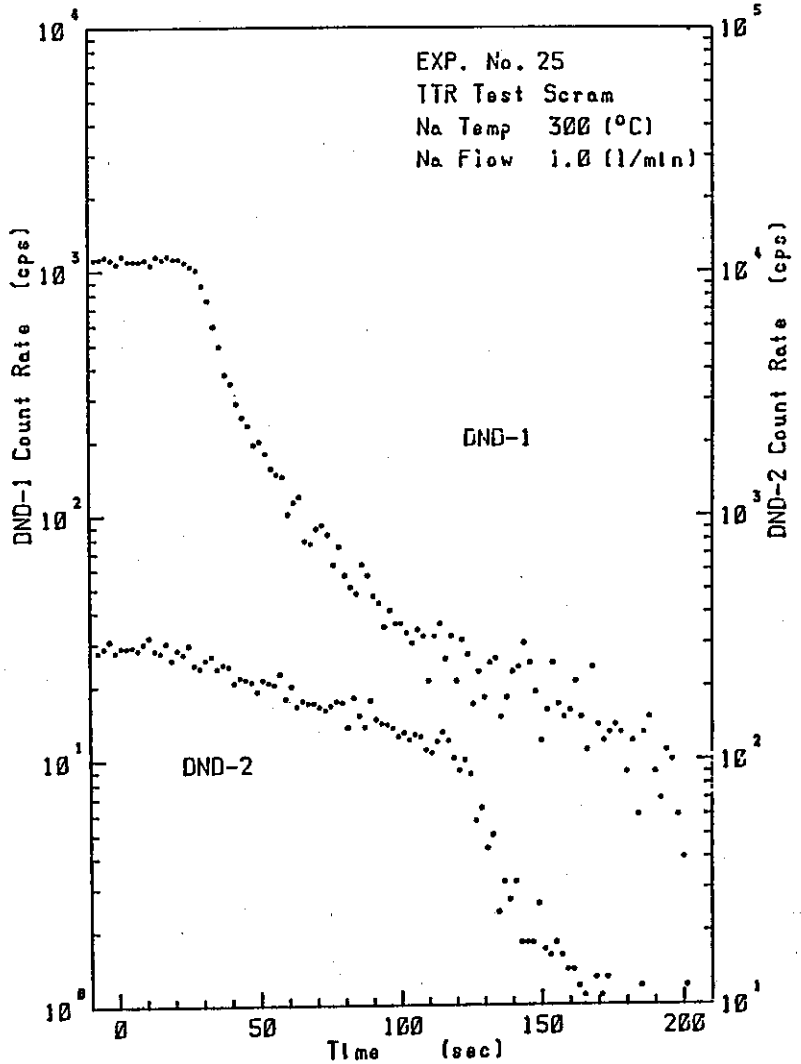

6) Exp. No. 25

Fig. 7-4 (continued)

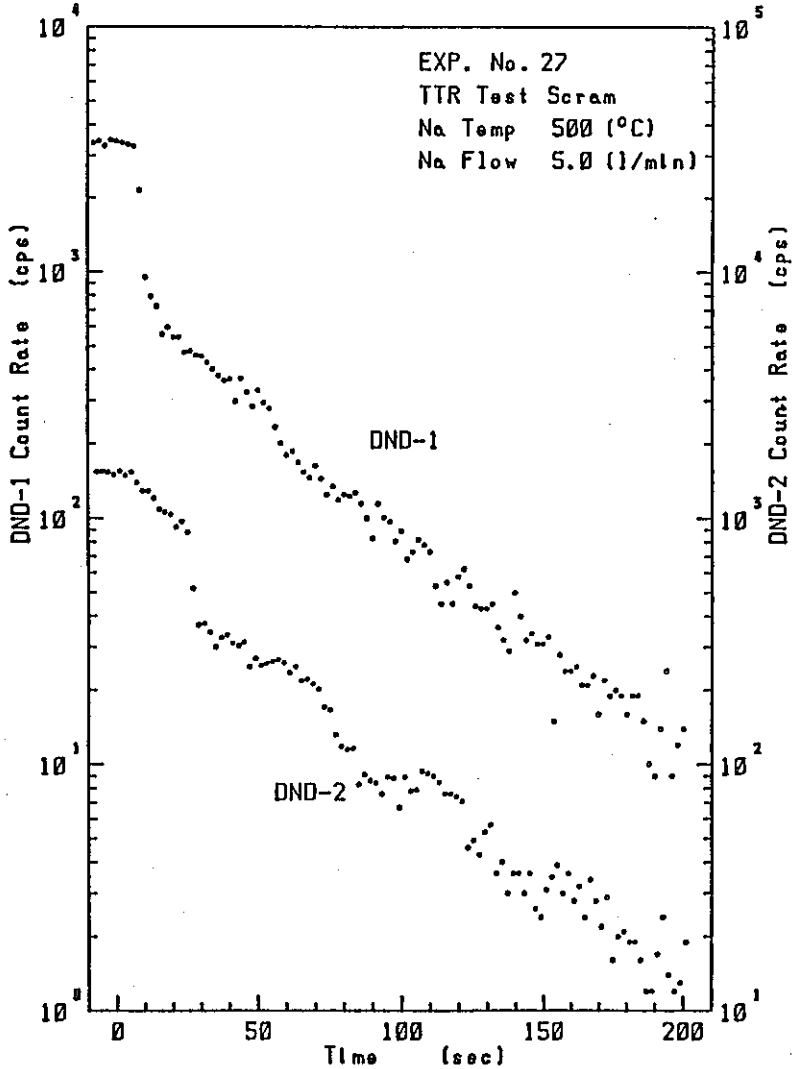

7) Exp. No. 27

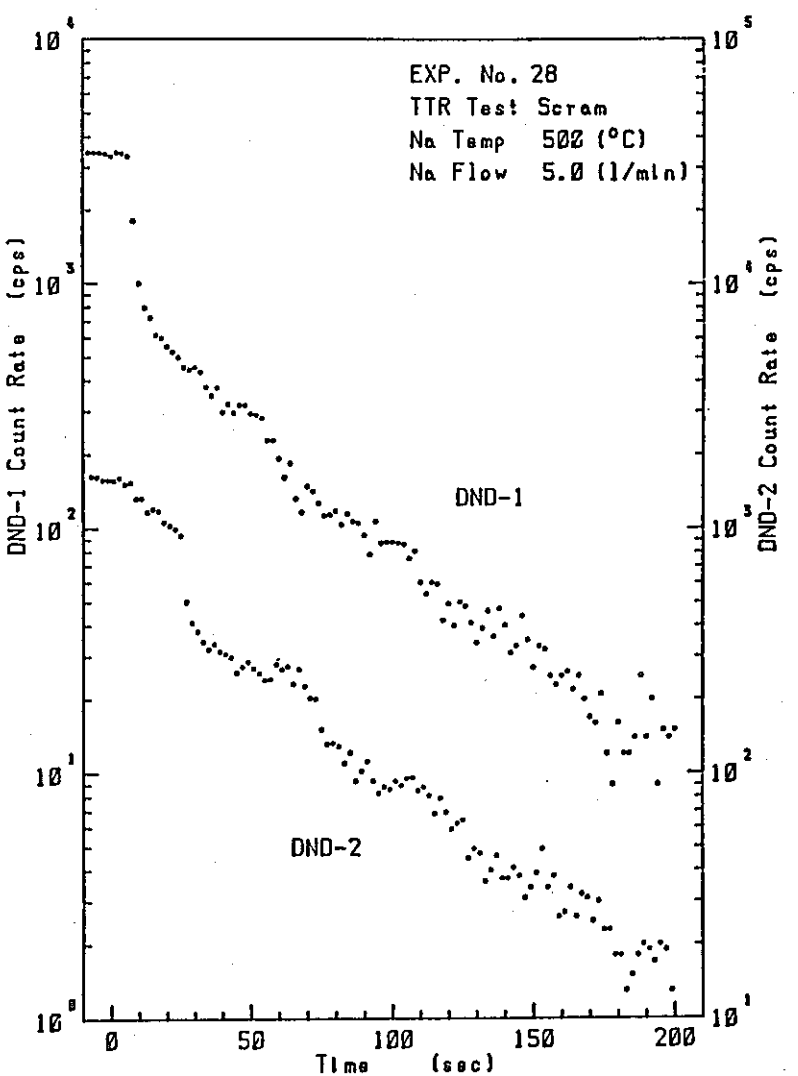

8) Exp. No. 28

Fig. 7-4 (continued)

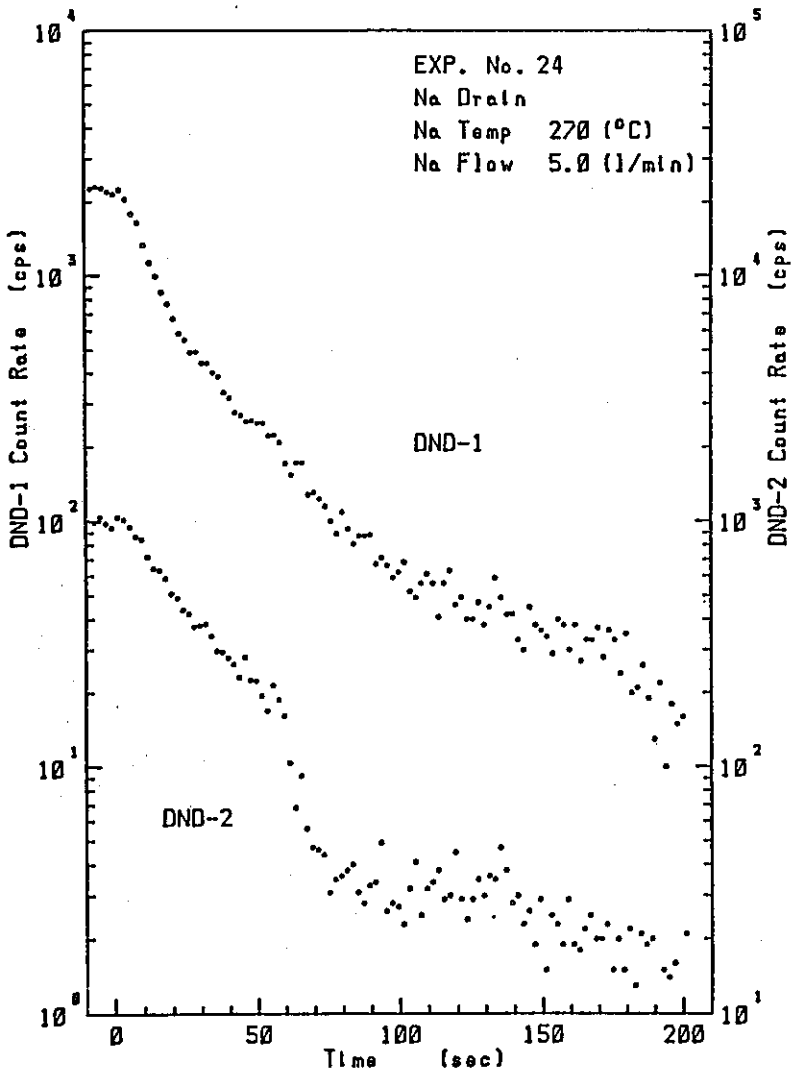

1) Exp. No. 24

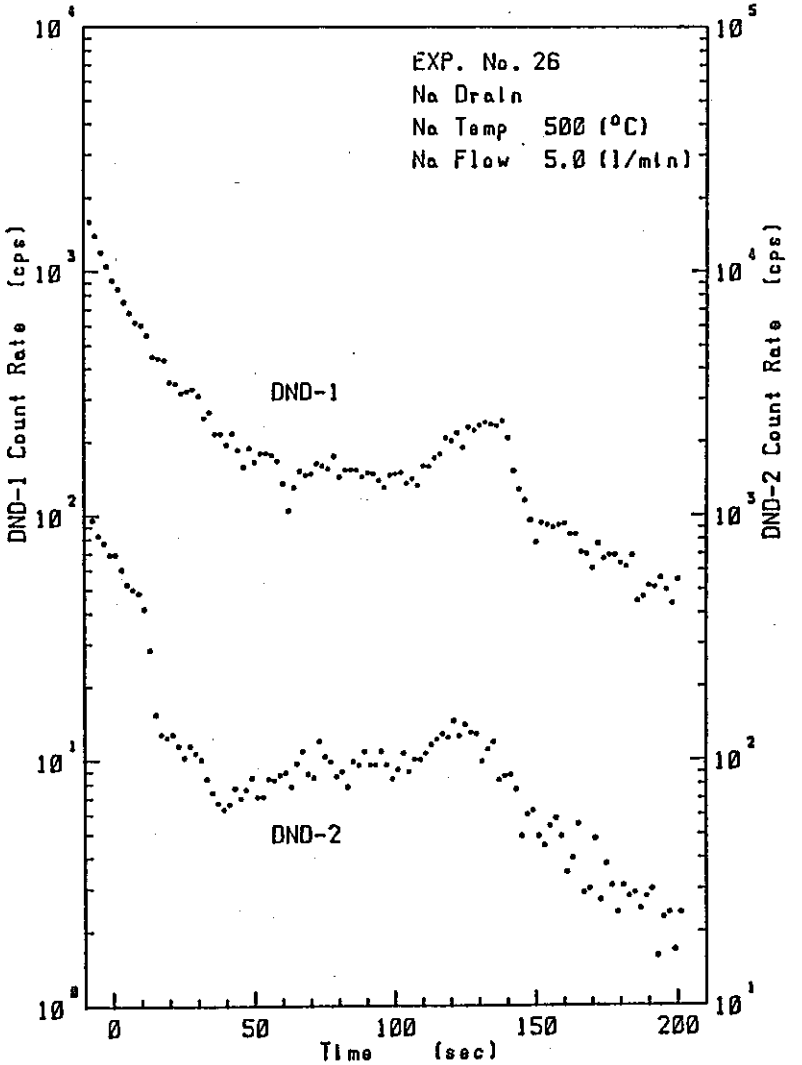

2) Exp. No. 26

Fig. 7-5 Delayed neutron count rate during sodium drain before TTR shut down

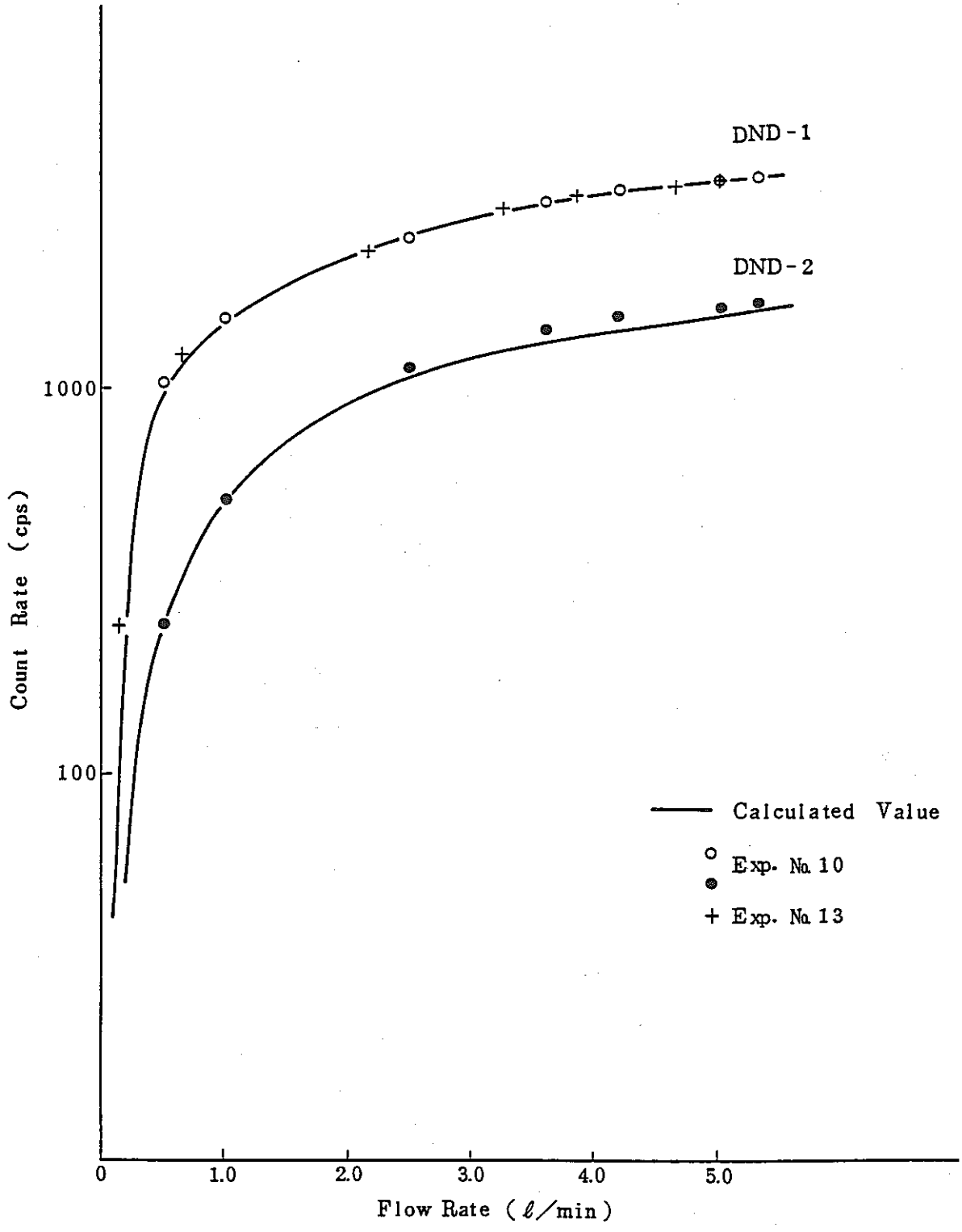

Fig. 7-6 Delayed neutron count rate vs. flow rate for both detectors

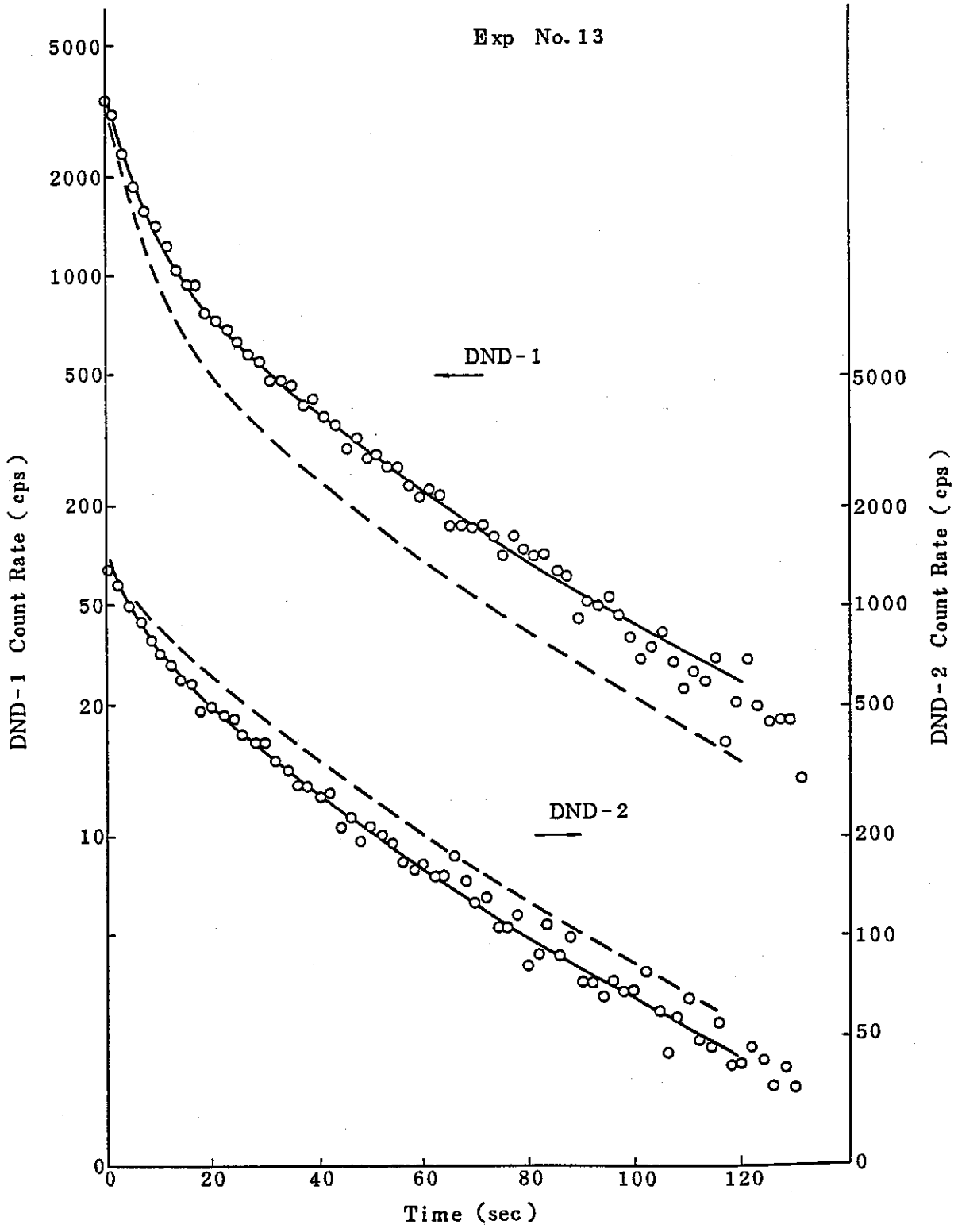

Fig. 7-7 Delayed neutron count rate and calculated value by using analytical model for both detectors during flow stop test

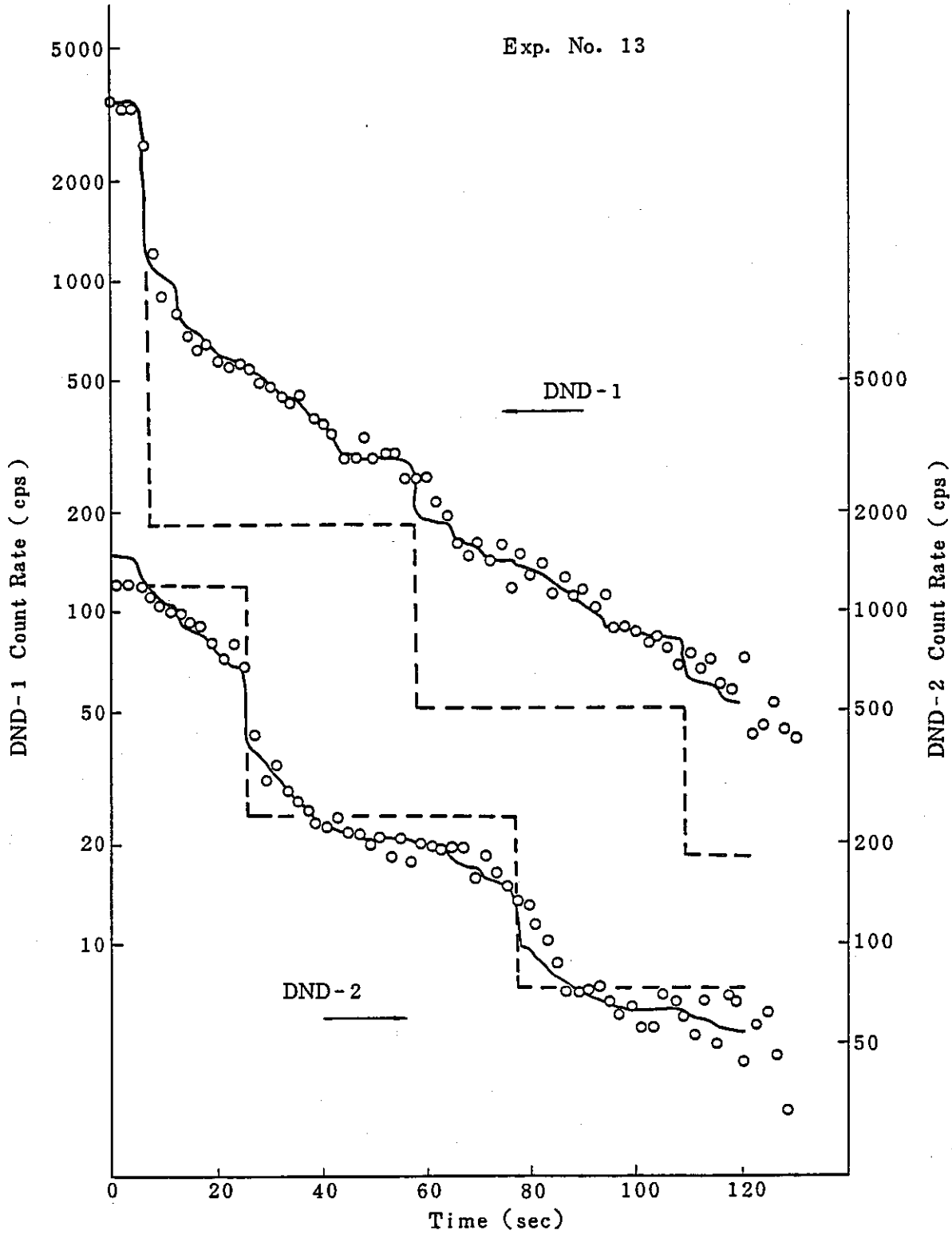

Fig. 7-8 Delayed neutron count rate and calculated value by using analytical model for both detectors after TTR test scram

8. CONCLUSION

Study on behaviors of non-volatile FP and delayed neutron precursor FP in sodium, using inpile fission product behavior test loop (FPL-II) with uranium capsule loading 20% enriched uranium dioxide of 100g, has been performed.

15 irradiation tests in 1982 and 12 tests in 1983 have been conducted collecting irradiation measurement data with parameters of sodium temperature, sodium flow velocity and oxygen concentration in sodium (this fiscal year). From these tests 1500 gamma-ray spectra data with 4K memory were obtained.

In consequence of deposition behavior analyses of non-volatile FP, behaviors of Sr, Y, Zr, Nb, Ba and La in sodium were clarified as follows:

1) Sr nuclides deposition is irreversible and rapid at higher temperatures.

   Deposition rate constants are obtained for Sr-92, Sr-93, and Sr-94 by analyzing deposition distribution patterns. Deposition rate constants of isotope nuclides are consistent and no isotope effect is observed. Activation energy for Sr deposition process is found to be -13 ± 1 (KJ/g-atom) by Arrhenius plot of Sr deposition rate constant. It is concluded that Sr deposition rate is controlled by Sr diffusion through the boundary layer at sodium in the vicinity of inner wall of piping.

2) Y nuclides show similar deposition behavior to Sr nuclides and the deposition rate of Y nuclides is in complete agreement with that for Sr nuclides between 200 and 530°C of sodium temperature.

3) Desorption of Zr nuclides would occur.

Apparent deposition rate constant including desorption phenomenon of Zr nuclides is smaller than Sr deposition rate at high sodium temperatures and shows no dependence on sodium temperature between 200 and 530°C.

4) Nb nuclides show no deposition behavior in sodium at high temperature.

5) The deposition rate for Ba nuclides is almost same at 400°C sodium temperature but shows smaller temperature dependence, compared with Sr deposition rate.

6) La shows almost same deposition behavior with Ba.

As explained above, deposition behaviors of main nuclides of non-volatile FP have been almost clarified.

Further study of deposition behavior in sodium with high oxygen concentration and desorption behavior of FP nuclides once deposit on wall surface is necessary to proceed. By achievement of the study, evaluation of deposition distribution and the radiation intensity etc. of FP in large scale FBR plant will be feasible.

In gamma-ray measurement in FPL-II, many clear gamma-ray peaks of volatile FP nuclides, such as Br, Kr and I etc., besides non-volatile FP nuclides stated above, have been detected.

Among them, 8 nuclides, Br-86, Br-88, Kr-90, Rb-89, Te-134, I-136m, Xe-139 and Xe-140, were selected to obtain the release fraction of FP nuclides from irradiation specimen surface to sodium. Using the release fraction obtained and that calculated from recoil model, k factors which are almost 0.4 value independent of mass number and nuclides are obtained.

Transition behaviors of DN nuclides which are useful for evaluation of fuel failure detection system were measured by using two detectors installed on the loop. From the ratio of DN count rates at two detection positions, transfer behavior of DN nuclides in sodium was estimated.

Little adsorption on stainless steel surface was observed at 270°C sodium temperature, but decrease in count rate appears at the downstream position at 225°C and becomes more distinct at 170°C. It means that adsorption of DN nuclides on stainless steel surface can not be neglected any more at 225°C and increases as temperature decreases.

k factor was calculated by using DN count rate and the value was 0.59 that is higher than k factor of volatile FP obtained by gamma-ray measurement. k factor is usually higher than 1, so it is necessary to examine further.

9. REFERENCES

1) T. Sakai, S. Hara et al:
"Inpile FP behavior test loop experiment (Contract study)", SJ 201 83-05 (1983)

2) N. V. Krasnoyarov et al:
CONF-760503 pp. 30-34 (1976)

3) T. Sakai, K. Ono et al:
"Behavior analysis of SIL radioactive materials (Contract study)", SJ 201 79-06 (1979)

4) M. H. Cooper and G. R. Taylor:
"A transport model for radioactive corrosion product deposition in an LMFBR", Nucl. Eng. Des., 52, 246 (1975)

5) T. Mitsuka et al:
"Inpile fission product behavior test loop", Toshiba Review, Vol. 34, No. 4 (1979)

6) R. L. Eichelberger:
"Solubility of oxygen in liquid sodium: a recommended expression", AI-AEC-12685 (1968)

7) C. M. Lederer et al:
"Table of Isotopes", seventh edition, John willey & sons, inc., New York (1978)

8) R. F. Rider:
"Compilation of fission product yields", NEDO-12154-3(A) (1979)

9) R. E. Treybal:
"Mass transfer operations", MeGraw-Hill, New York (1965)

10) N. H. Nachtrieb:
"Self diffusion in liqind metals", Advan. Phys., 16, 309 (1967)

11) M. H. Cooper and G. R. Taylor:
"Adsorption and diffusion of Ba-137m from Na-^{137}Cs solution", Trans. Am. Nucl. Soc., 12, 57 (1969)

12) B. G. Childs:
"Fission product effects in uranium dioxide", Jour. Nucl. Mat., 9 No.3 (1963)

13) Miyazawa et al:
"Development of failure signal evaluation in fuel failure detection system"

14) T. Izak-Biran and S. Amiel, Nucl. Sci. and Eng., 57, 117 (1975)

Appendix A Calculation of Thermal Neutron Flux in FPL-II

A.1 Introduction

Flowing sodium through the inpile plug of FPL-II is activated by thermal neutron from TTR and Na-24 is produced.

Half life of Na-24 is 15 hrs and is so long enough to sodium circulation time (48 ∿ 480 sec) through the loop that Na-24 distributes homogeneously along the main circulation line. Production rate of Na-24 was obtained from radioactivity measurement in the delay line, and based on the production rate thermal neutron flux in uranium capsule at TTR regular output (100 kW) was calculated as 7.9×10^9 n/cm^2.sec. The value is at the same level of 9.5×10^9 n/cm^2.sec obtained from gamma-ray measurement of irradiated uranium dioxide in FPL-II.

A.2 Calculation of thermal neutron flux

i) Na-24 production rate obtained by irradiation test

In calculation of Na-24 production rate, data of count rates of gamma-ray peak at 1368.5 keV obtained as following were applied:

Exp. No.	Sodium temperature (°C)	flow rate (ℓ/min)
3 & 4	350	5
5 & 6	420	5
7	500	5
8	530	5
14 & 16	530	1

Na-24 count ratios of gamma-ray peak at 1368.5 keV is obtained from gamma-ray spectra measured at the delay line and detection positions D-2 to D-9, where the count rate is corrected by decay at time when 4 hr-irradiation is completed.

Na-24 distribution along the delay line is shown in Figs. A-1 and A-2. Distance expressed in abscissa is that from uranium capsule.

Na-24 production rate is expressed by,

$$Ne = \bar{C}_r \times \frac{3.7 \times 10^4}{f_r \cdot f_e \cdot V} V_T$$

where,

$\bar{C}_r$: average count rate of gamma-ray at 1368.5 keV in the delay line

N_e: Na-24 production rate (dps)

f_r: gamma-ray branch ratio at 1368.5 keV (-)

f_e: detection efficiency of gamma-ray at 1368.5 keV (cps.cm/μCi)

V : sodium volume per unit length delay line (cm^3/cm)

V_T: sodium volume in main circulation loop (cm^3)

By substituting f_r=1.0, f_e=15.64 (*) (cps.cm/μCi), V=0.694 (cm^3/cm) and V_T=3979 (cm^3),

Na-24 production rates were obtained, as indicated in the 6th column of Table A-1. Those obtained in irradiation tests were 3.84×10^8 to 4.63×10^8 (dps).

Note: (*) value obtained by using mock-up test of gamma-ray measurement system and Eu-152 standard radiation source

ii) Calculated Na-24 production rate

Sodium in uranium capsule is irradiated homogeneously by thermal neutron, Na-24 production rate Nc (dps) is

$$Nc = N_0 \cdot \sigma \cdot \phi \ (1 - e^{-\lambda \cdot t})$$

where,

N_o: atomic number of Na-23 irradiated (atoms)
σ : reaction cross-section of Na-23 (n,γ) Na-24 (cm^2)
ϕ : thermal neutron flux ($n/cm^2.sec$)
λ : decay constant of Na-24 (1/sec)
t : irradiation time (sec)

Na-23 atomic number,

$$N_0 = 6.02 \times 10^{23} \frac{\rho \cdot V_I}{M}$$

where,

ρ : sodium density (g/cm^3)
V_I: volume of irradiated sodium (cm^3)
M : molecular weight of sodium (g)

When thermal neutron radiations on sodium were performed for 4 hrs at sodium temperatures 350°C, 420°C, 500°C and 530°C, Na-24 production rate N_c (dps) is, putting thermal neutron flux ϕ as unknown value by substituting,

ρ = 0.864 (350°C), 0.851 (420°C), 0.832 (500°C) and 0.824 (530°C)
V_I = 30
M = 22.99
σ = 5×10^{-25}
λ = 1.283×10^{-5}
t = 1.44×10^4

Then, Nc = $5.75 \times 10^{-2}\phi$ (350°C) to $5.47 \times 10^{-2}\phi$ (530°C)

The results are indicated in the 7th column of Table A-1.

iii) Calculation of thermal neutron flux

Na-24 production rate obtained by irradiation test Ne and that by calculation Nc should be equal, so Ne = Nc.

By putting $Nc = Nc'\phi$, the thermal neutron flux $\phi = Ne/Nc'$ is obtained as indicated in 8th column of Table A-1 and Fig. A-3.

Thermal neutron flux in uranium capsule is,
7.74×10^9 to 7.99×10^9 n/cm^2.sec in Exp. No.4 to No.16,
6.67×10^9 n/cm^2.sec in Exp. No.3, and 7.9×10^9 n/cm^2.sec in average of Exp. No.4 to No.16.

In Na-23 nuclear reaction, resonance peak of (n, γ) reaction locates at 3 keV.*1), in which reaction cross-section is 0.245 barn. The reaction cross-section of (n, γ) for thermal neutron is 0.5 barn.

Neutron spectra in TTR irradiation nozzle are not obtained exactly, but slow-down neutron flux including resonance neutron at 3 keV is ca. 1/4 of thermal neturon flux.*2)

Now, assuming that slow neutron flux is composed of neutron having 3 keV resonance energy, its reaction cross-section is ca. 1/2 of thermal neutron cross-section and, therefore, its contribution of Na-24 production rate is ca. 1/8 of thermal neutron contribution. But (n, γ) nuclear reaction cross-section of slow and fast neutron except neutron having 3 keV resonance energy is limited from several mbarn to 100 mbarn. Therefore, above mentioned value is located at the upper limit. Na-24 production by (n, γ) reaction from Na-23 is mainly due to thermal neutron flux and the production rate due to slow and fast neutron flux is so small as 12% compared to thermal neutron, that its contribution can be neglected.

Na-24 is regarded as totally produced from thermal neutron flux.

Note: *1) D. I. Garber and R. R. Kinsey: "Neutron cross sections", BNL 325 Third Edition, Volume II (1976).

*2) Toshiba Review, Vol. 16, No. 9 (1961).

A.3 Conclusion

Based on Na-24 radioactivity obtained in irradiation tests, thermal neutron flux at uranium capsule in TTR regular output (100 kW) was calculated as 7.9×10^9 n/cm^2.sec. Shape, size and installed position in inpile plug of uranium capsule used for FPL-I and -II are same.

As an example: in order to measure thermal neutron flux at uranium capsule in inpile plug in site,*) before installation and start-up of FPL-II, gamma-ray of uranium dioxide in discarded and disjoined FPL-I was measured and thermal neutron flux of 9.5×10^9 n/cm^2.sec was obtained. Obtained thermal neutron flux in this test indicated a value at the same level.

Note: *) Toshiba internal report

Table A-1 Thermal neutron flux

Exp No.	Na Temp. (℃)	Na Flow (ℓ/min)	Na Dens. ρ(g/cm^3)	Count Rate $\overline{C}_r$ (cps)	Production Rate Ne (dps)	Production Rate Nc (dps)	T. Neutron Flux. ϕ(n/cm^2·sec)
3	350	5	0.864	28.29 ± 0.20	3.84×10^8	$5.75 \times 10^{-2}\phi$	6.67×10^9
4				33.07 ± 0.21	4.49×10^8		7.80×10^9
5	420	5	0.851	33.21 ± 0.19	4.50×10^8	$5.64 \times 10^{-2}\phi$	7.99×10^9
6				33.04 ± 0.18	4.48×10^8		7.94×10^9
7	500	5	0.832	32.00 ± 0.21	4.34×10^8	$5.51 \times 10^{-2}\phi$	7.87×10^9
8	530	5		31.90 ± 0.19	4.33×10^8	$5.47 \times 10^{-2}\phi$	7.92×10^9
14		1	0.824	31.19 ± 0.41	4.23×10^8		7.74×10^9
16				31.50 ± 0.21	4.27×10^8		7.82×10^9

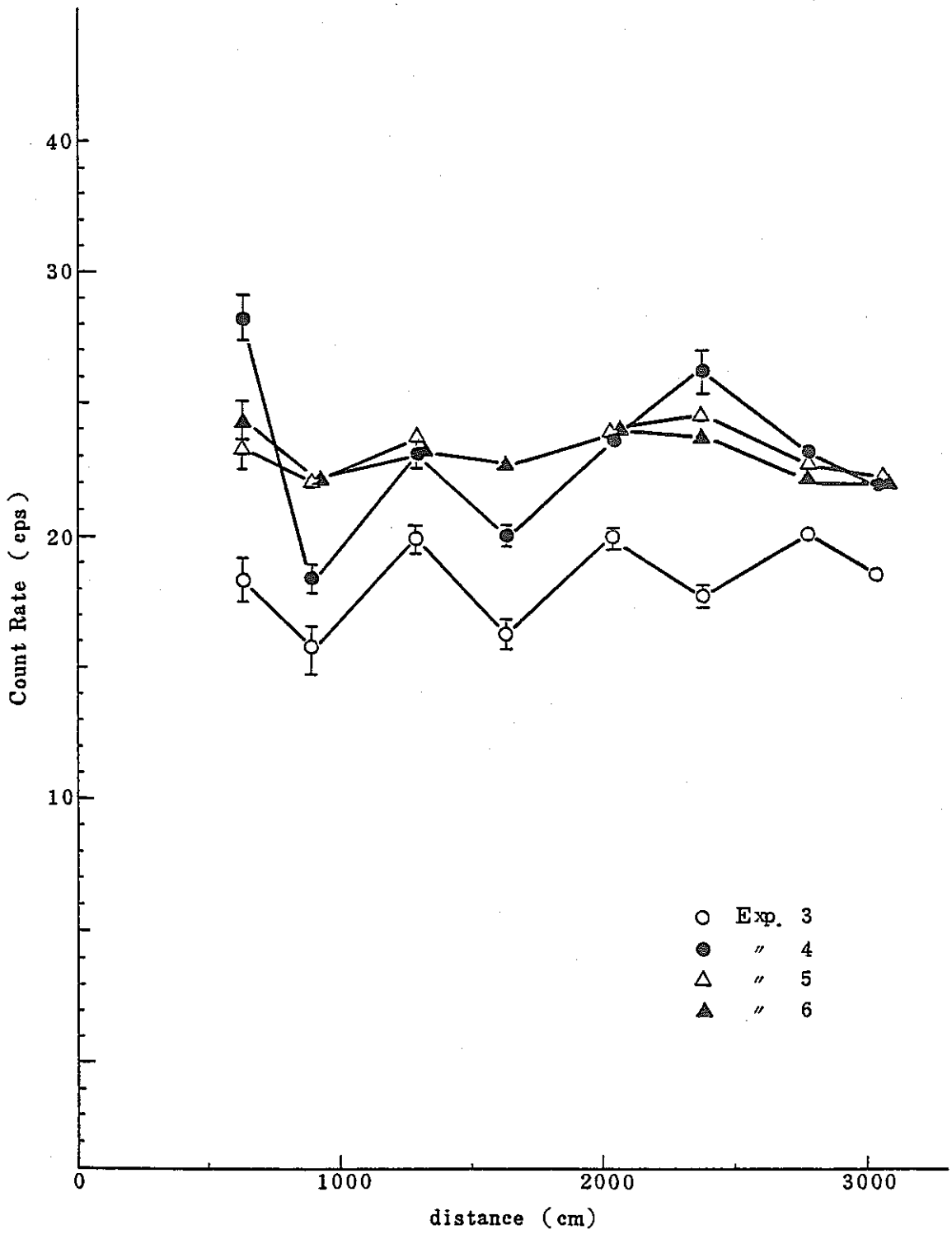

Fig. A-1 Na-24 distribution along the delay line

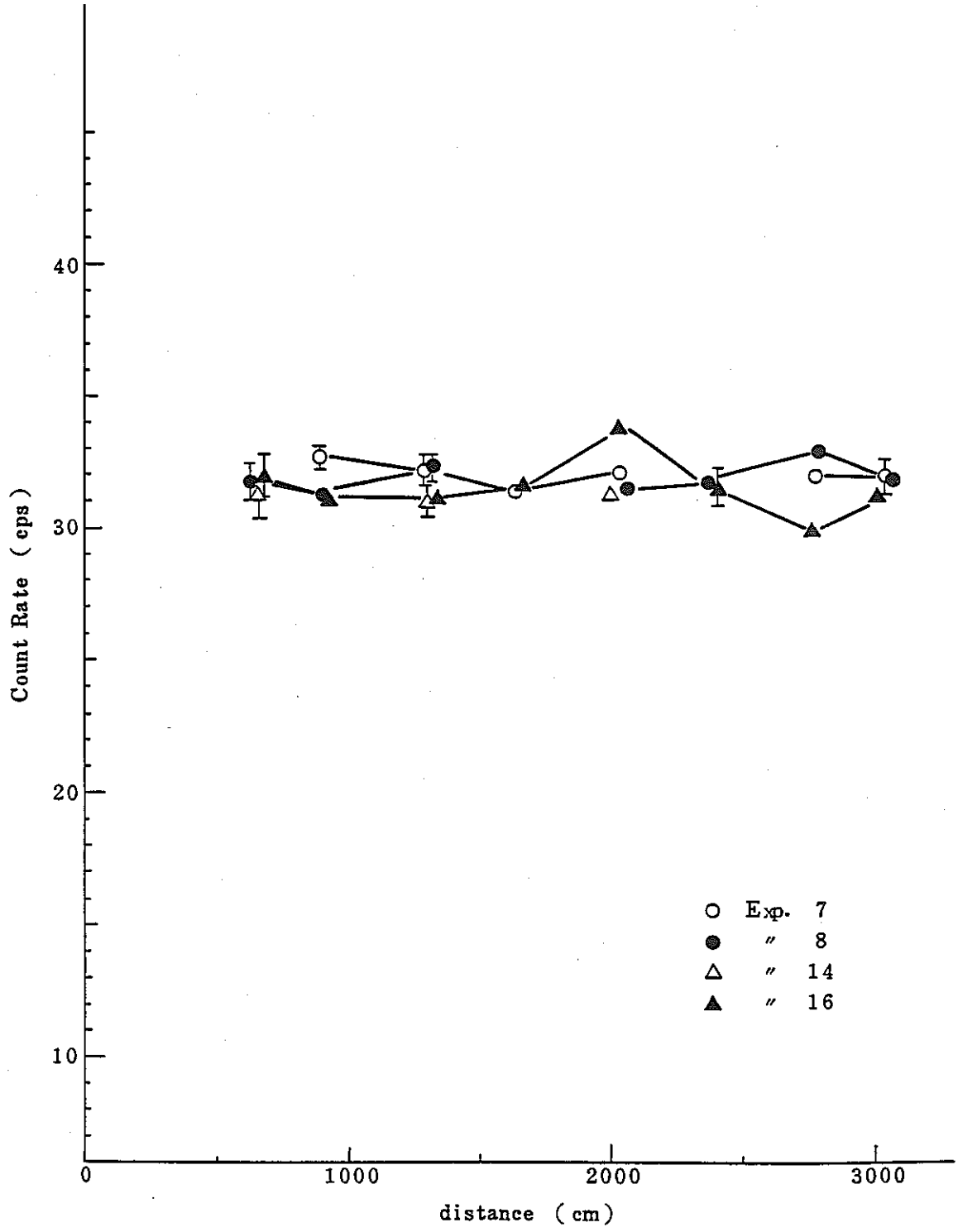

Fig. A-2 Na-24 distribution along the delay line

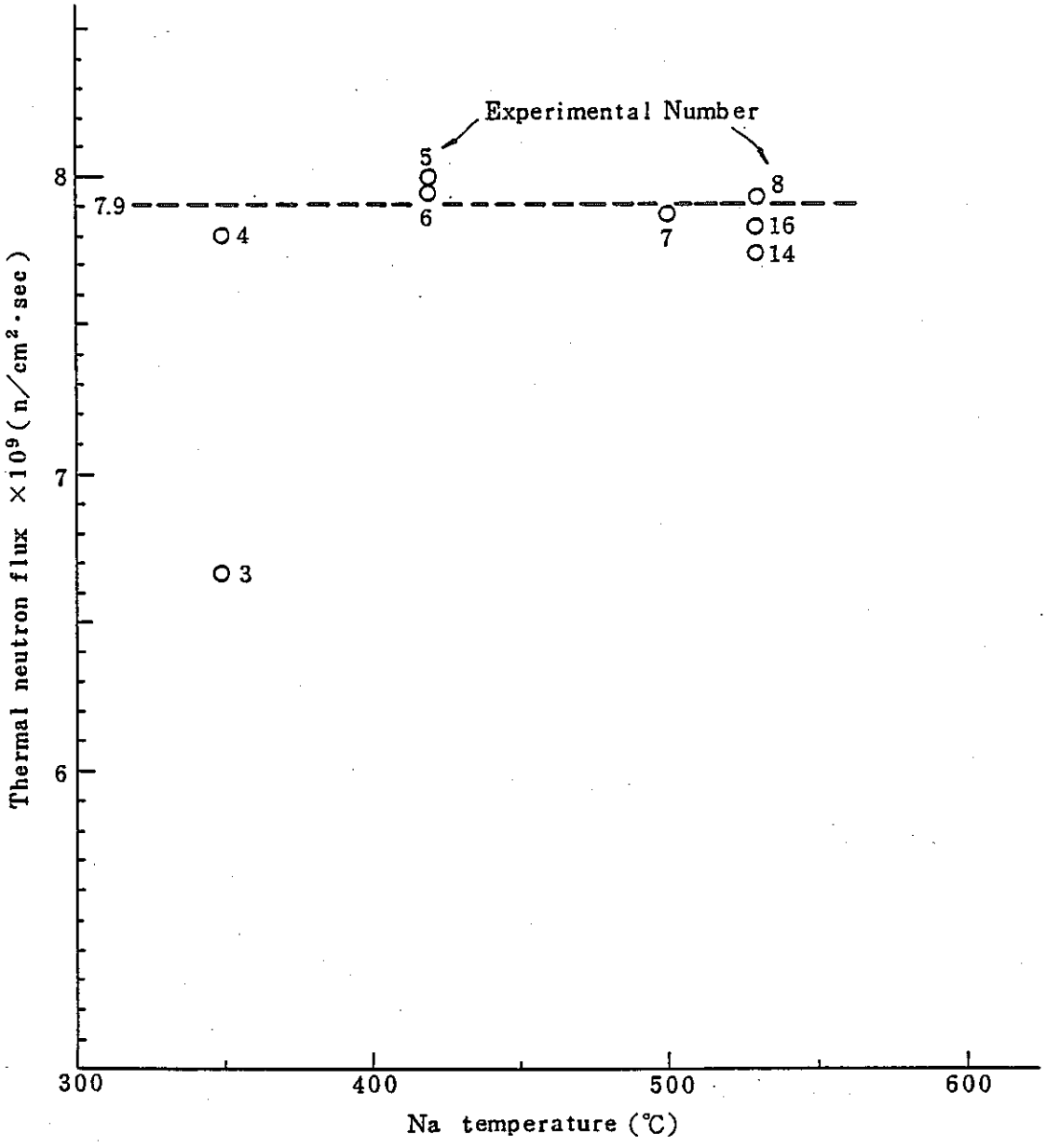

Fig. A-3 Thermal neutron flux calculated by using Na-24 gamma-ray spectra

Appendix B Floppy disk lists

EXP NO. 16 (NA TEMP. 530°C , NA FLOW RATE (LITER/MIN)

DISK NO. 21000

TAG NO.	DATA I.D.	DETECTOR POSITION	DATE	START TIME	COUNT TIME
21000	NA CIRCUL. BEFORE IRR.	D-2	12 APR 83	09:16	5000
21100	NA CIRCUL. BEFORE IRR.	D-7	12 APR 83	09:16	5000
21001	TTR 100KW 530°C 1L/M	D-2	12 APR 83	12:42	300
21101	TTR 100KW 530°C 1L/M	D-7	12 APR 83	12:42	300
21002	TTR 100KW 530°C 1L/M	D-2	12 APR 83	12:51	300
21102	TTR 100KW 530°C 1L/M	D-7	12 APR 83	12:51	300
21003	TTR 100KW 530°C 1L/M	D-2	12 APR 83	12:59	300
21103	TTR 100KW 530°C 1L/M	D-7	12 APR 83	12:59	300
21004	TTR 100KW 530°C 1L/M	D-2	12 APR 83	13:07	600
21104	TTR 100KW 530°C 1L/M	D-7	12 APR 83	13:07	600
21005	TTR 100KW 530°C 1L/M	D-2	12 APR 83	13:21	600
21105	TTR 100KW 530°C 1L/M	D-7	12 APR 83	13:21	600
21006	TTR 100KW 530°C 1L/M	D-2	12 APR 83	13:34	1800
21106	TTR 100KW 530°C 1L/M	D-7	12 APR 83	13:34	1800
21007	TTR 100KW 530°C 1L/M	D-4	12 APR 83	14:09	1800
21107	TTR 100KW 530°C 1L/M	D-9	12 APR 83	14:09	1800
21008	TTR 100KW 530°C 1L/M	D-6	12 APR 83	14:45	1800
21108	TTR 100KW 530°C 1L/M	D-3	12 APR 83	14:45	1800

DISK NO. 21100

TAG NO.	DATA I.D.	DETECTOR POSITION	DATE	START TIME	COUNT TIME
21009	TTR 100KW 530°C 1L/M	D-8	12 APR 83	15:19	1800
21109	TTR 100KW 530°C 1L/M	D-5	12 APR 83	15:19	1800
21010	TTR 100KW 530°C 1L/M	D-2	12 APR 83	15:53	300
21110	TTR 100KW 530°C 1L/M	D-7	12 APR 83	15:53	300
21011	TTR 100KW 530°C 1L/M	D-2	12 APR 83	16:03	300
21111	TTR 100KW 530°C 1L/M	D-7	12 APR 83	16:03	300
21012	TTR STOP 530°C 1L/M	D-2	12 APR 83	16:12	300
21112	TTR STOP 530°C 1L/M	D-7	12 APR 83	16:12	300
21013	TTR STOP 530°C 1L/M	D-2	12 APR 83	16:20	300
21113	TTR STOP 530°C 1L/M	D-7	12 APR 83	16:20	300
21014	TTR STOP 530°C 1L/M	D-2	12 APR 83	16:29	600
21114	TTR STOP 530°C 1L/M	D-7	12 APR 83	16:29	600
21015	TTR STOP 530°C 1L/M	D-2	12 APR 83	16:42	1200
21115	TTR STOP 530°C 1L/M	D-7	12 APR 83	16:42	1200
21016	TTR STOP 530°C 1L/M	D-2	12 APR 83	17:05	1200
21116	TTR STOP 530°C 1L/M	D-7	12 APR 83	17:05	1200
21017	TTR STOP 530°C 1L/M	D-2	12 APR 83	17:29	3600
21117	TTR STOP 530°C 1L/M	D-7	12 APR 83	17:29	3600

DISK NO. 21200

TAG NO.	DATA I.D.	DETECTOR POSITION	DATE	START TIME	COUNT TIME
21018	TTR STOP 530°C 1L/M	D-4	12 APR 83	18:35	3600
21118	TTR STOP 530°C 1L/M	D-9	12 APR 83	18:35	3600
21019	TTR STOP 530°C 1L/M	D-2	12 APR 83	19:42	3600
21119	TTR STOP 530°C 1L/M	D-7	12 APR 83	19:42	3600
21020	TTR STOP 530°C 1L/M	D-4	12 APR 83	20:51	3600
21120	TTR STOP 530°C 1L/M	D-9	12 APR 83	20:51	3600
21021	TTR STOP 530°C 1L/M	D-6	12 APR 83	21:59	3600
21121	TTR STOP 530°C 1L/M	D-3	12 APR 83	21:59	3600
21022	TTR STOP 530°C 1L/M	D-8	13 APR 83	23:10	3600
21122	TTR STOP 530°C 1L/M	D-5	13 APR 83	23:10	3600
21023	TTR STOP 530°C 1L/M	D-2	13 APR 83	00:19	3600
21123	TTR STOP 530°C 1L/M	D-7	13 APR 83	00:19	3600
21024	TTR STOP 530°C 1L/M	D-4	13 APR 83	01:30	3600
21124	TTR STOP 530°C 1L/M	D-9	13 APR 83	01:30	3600
21025	TTR STOP 530°C 1L/M	D-6	13 APR 83	02:52	3600
21125	TTR STOP 530°C 1L/M	D-3	13 APR 83	02:52	3600
21026	TTR STOP 530°C 1L/M	D-8	13 APR 83	03:58	3600
21126	TTR STOP 530°C 1L/M	D-5	13 APR 83	03:58	3600

DISK NO. 21300

TAG NO.	DATA I.D.	DETECTOR POSITION	DATE	START TIME	COUNT TIME
21027	TTR STOP 530°C 1L/M	D-2	13 APR 83	05:05	3600
21127	TTR STOP 530°C 1L/M	D-7	13 APR 83	05:05	3600
21028	TTR STOP 530°C 1L/M	D-4	13 APR 83	06:11	3600
21128	TTR STOP 530°C 1L/M	D-9	13 APR 83	06:11	3600
21029	TTR STOP 530°C 1L/M	D-6	13 APR 83	07:17	3600
21129	TTR STOP 530°C 1L/M	D-3	13 APR 83	07:17	3600
21030	TTR STOP 530°C 1L/M	D-8	13 APR 83	08:27	3600
21130	TTR STOP 530°C 1L/M	D-5	13 APR 83	08:27	3600
21031	TTR STOP 530°C 1L/M	D-2	13 APR 83	09:32	3600
21131	TTR STOP 530°C 1L/M	D-7	13 APR 83	09:32	3600
21032	NA DRAIN	D-2	13 APR 83	10:43	3600
21132	NA DRAIN	D-7	13 APR 83	10:43	3600
21033	NA DRAIN	D-4	13 APR 83	11:51	3600
21133	NA DRAIN	D-9	13 APR 83	11:51	3600
21034	NA DRAIN	D-6	13 APR 83	12:58	3600
21134	NA DRAIN	D-3	13 APR 83	12:58	3600
21035	NA DRAIN	D-8	13 APR 83	14:06	3600
21135	NA DRAIN	D-5	13 APR 83	14:06	3600

DISK NO. 21400

TAG NO.	DATA I.D.	DETECTOR POSITION	DATE	START TIME	COUNT TIME
21036	NA DRAIN	D-2	13 APR 83	15:14	3600
21136	NA DRAIN	D-7	13 APR 83	15:14	3600

Appendix B (continued)

EXP NO. 17 (FPL-2 NO OPERATION)

DISK NO. 22000

TAG NO.	DATA I.D.	DETECTOR POSITION	DATE	START TIME	COUNT TIME
22000	FPL-2 D-3 PGT	D-3	13 JUL 83	15:00	80000
22001	BACK GROUND-1	B-1	14 JUL 83	16:10	70000
22002	FPL-2 D-9 PGT	D-9	15 JUL 83	11:58	80000
22003	BACK GROUND-2	B-2	15 JUL 83	18:33	20000
22004	FPL-2 D-5 PGT	D-5	19 JUL 83	13:27	80000
22005	FPL-2 D-7 PGT	D-7	20 JUL 83	13:27	80000
22006	FPL-2 D-2 PGT	D-2	21 JUL 83	14:00	80000
22007	FPL-2 D-8 PGT	D-8	22 JUL 83	12:35	80000
22008	BACK GROUND-3	B-3	22 JUL 83	11:04	20000
22009	FPL-2 D-6 PGT	D-6	10 AUG 83	12:50	80000
22010	FPL-2 D-4 PGT	D-4	11 AUG 83	11:33	80000
22011	BACK GROUND-4	B-4	12 AUG 83	10:19	80000
22012	FPL-2 D-10 PGT	D-10	12 AUG 83	11:52	19000
22013	FPL-2 D-10 PGT	D-10	17 AUG 83	14:44	00000
22014	FPL-2 D-11 PGT	D-11	19 AUG 83	12:19	80000
22015	BACK GROUND-5	B-5	20 AUG 83	12:02	80000

Appendix B (continued)

EXP NO. 18 (NA TEMP. 280°C , NA FLOW RATE 2-5LITER/MIN)

DISK NO. 23000

TAG NO.	DATA I.D.	DETECTOR POSITION	DATE	START TIME	COUNT TIME
23009	NA CIRCUL. (BYPASS)	D-2	20 SEP 83	12:47	7200
23100	NA CIRCUL. (BYPASS)	D-7	20 SEP 83	12:47	7200
23001	NA CIRCUL. 280°C 2L/M	D-2	20 SEP 83	15:34	600
23101	NA CIRCUL. 280°C 2L/M	D-7	20 SEP 83	15:34	600
23002	280°C 2L/M	D-2	20 SEP 83	15:48	600
23102	280°C 2L/M	D-7	20 SEP 83	15:48	600
23003	280°C 2L/M	D-2	20 SEP 83	16:02	3600
23103	280°C 2L/M	D-7	20 SEP 83	16:02	3600
23004	280°C 2L/M	D-4	20 SEP 83	17:11	3600
23104	280°C 2L/M	D-9	20 SEP 83	17:11	3600
23005	280°C 2L/M	D-6	20 SEP 83	18:16	3600
23105	280°C 2L/M	D-3	20 SEP 83	18:16	3600
23006	280°C 2L/M	D-8	20 SEP 83	19:27	3600
23106	280°C 2L/M	D-5	20 SEP 83	19:27	3600
23007	280°C 2L/M	D-2	20 SEP 83	20:37	3600
23107	280°C 2L/M	D-7	20 SEP 83	20:37	3600
23008	280°C 2L/M	D-4	20 SEP 83	22:47	3600
23108	280°C 2L/M	D-9	20 SEP 83	22:47	3600

DISK NO. 23100

TAG NO.	DATA I.D.	DETECTOR POSITION	DATE	START TIME	COUNT TIME
23009	280°C 2L/M	D-6	21 SEP 83	00:06	3600
23109	280°C 2L/M	D-3	21 SEP 83	00:06	3600
23010	280°C 2L/M	D-8	21 SEP 83	01:22	3600
23110	280°C 2L/M	D-5	21 SEP 83	01:22	3600
23011	280°C 2L/M	D-2	21 SEP 83	04:05	3600
23111	280°C 2L/M	D-7	21 SEP 83	04:05	3600
23012	280°C 2L/M	D-4	21 SEP 83	05:17	3600
23112	280°C 2L/M	D-9	21 SEP 83	05:17	3600
23013	280°C 2L/M	D-6	21 SEP 83	06:29	3600
23113	280°C 2L/M	D-3	21 SEP 83	06:29	3600
23014	280°C 2L/M	D-8	21 SEP 83	07:38	3600
23114	280°C 2L/M	D-5	21 SEP 83	07:38	3600
23015	280°C 2L/M	D-2	21 SEP 83	10:55	3600
23115	280°C 2L/M	D-7	21 SEP 83	10:55	3600
23016	280°C 2L/M	D-4	21 SEP 83	12:01	3600
23116	280°C 2L/M	D-9	21 SEP 83	12:01	3600
23017	280°C 2L/M	D-6	21 SEP 83	13:06	3600
23117	280°C 2L/M	D-3	21 SEP 83	13:06	3600

DISK NO. 23200

TAG NO.	DATA I.D.	DETECTOR POSITION	DATE	START TIME	COUNT TIME
23018	290°C 5L/M	D-8	21 SEP 83	14:18	3600
23118	290°C 5L/M	D-5	21 SEP 83	14:18	3600
23019	290°C 5L/M	D-2	21 SEP 83	15:17	3600
23119	290°C 5L/M	D-7	21 SEP 83	15:17	3600
23020	500°C 5L/M	D-2	21 SEP 83	19:59	3600
23120	500°C 5L/M	D-7	21 SEP 83	09:59	3600
23021	500°C 5L/M	D-4	21 SEP 83	21:11	3600
23121	500°C 5L/M	D-9	21 SEP 83	21:11	3600
23022	500°C 5L/M	D-6	21 SEP 83	22:21	3600
23122	500°C 5L/M	D-3	21 SEP 83	22:21	3600
23023	500°C 5L/M	D-8	21 SEP 83	23:34	3600
23123	500°C 5L/M	D-5	21 SEP 83	23:34	3600
23024	500°C 5L/M	D-2	22 SEP 83	00:44	3600
23124	500°C 5L/M	D-7	22 SEP 83	00:44	3600
23025	500°C 5L/M	D-4	22 SEP 83	01:55	3600
23125	500°C 5L/M	D-9	22 SEP 83	01:55	3600
23026	500°C 5L/M	D-6	22 SEP 83	03:02	3600
23126	500°C 5L/M	D-3	22 SEP 83	03:02	3600

DISK NO. 23300

TAG NO.	DATA I.D.	DETECTOR POSITION	DATE	START TIME	COUNT TIME
23027	500°C 5L/M	D-8	22 SEP 83	04:16	3600
23127	500°C 5L/M	D-5	22 SEP 83	04:16	3600
23028	500°C 5L/M	D-2	22 SEP 83	05:46	3600
23128	500°C 5L/M	D-7	22 SEP 83	05:46	3600
23029	500°C 5L/M	D-4	22 SEP 83	07:04	3600
23129	500°C 5L/M	D-9	22 SEP 83	07:04	3600
23030	500°C 5L/M	D-6	22 SEP 83	09:15	3600
23130	500°C 5L/M	D-3	22 SEP 83	09:15	3600
23031	500°C 5L/M	D-8	22 SEP 83	10:28	3600
23131	500°C 5L/M	D-5	22 SEP 83	10:28	3600
23032	500°C 5L/M	D-2	22 SEP 83	11:33	3600
23132	500°C 5L/M	D-7	22 SEP 83	11:33	3600
23033	500°C 5L/M	D-4	22 SEP 83	12:43	3600
23133	500°C 5L/M	D-9	22 SEP 83	12:43	3600
23034	NA DRAIN	D-2	22 SEP 83	13:47	3600
23134	NA DRAIN	D-7	22 SEP 83	13:47	3600

Appendix B (continued)

EXP NO. 18 (continued)

DISK NO. 23488

TAG NO.	DATA I.D.	DETECTOR POSITION	DATE	START TIME	COUNT TIME
23835	NA DRAIN	D-4	22 SEP 83	14:54	3600
23135	NA DRAIN	D-9	22 SEP 83	14:56	3600
23836	NA DRAIN	D-6	22 SEP 83	16:00	3600
23136	NA DRAIN	D-3	22 SEP 83	16:00	3600
23837	NA DRAIN	D-8	22 SEP 83	17:04	3600
23137	NA DRAIN	D-5	22 SEP 83	17:04	3600
23838	NA DRAIN	D-2	22 SEP 83	18:09	3600
23138	NA DRAIN	D-7	22 SEP 83	18:09	3600

Appendix B (continued)

EXP NO. 19 (NA TEMP. 530°C , NA FLOW RATE 2LITER/MIN)

DISK NO. 24000

TAG NO.	DATA I.D.	DETECTOR POSITION	DATE	START TIME	COUNT TIME
24000	NA CIRCUL. BEFORE IRR.	D-2	18 OCT 83	09:10	2300
24100	NA CIRCUL. BEFORE IRR.	D-7	18 OCT 83	09:10	2300
24001	TTR 100KW 530°C 2L/M	D-2	18 OCT 83	11:10	300
24101	TTR 100KW 530°C 2L/M	D-7	18 OCT 83	11:10	300
24002	TTR 100KW 530°C 2L/M	D-2	18 OCT 83	11:19	300
24102	TTR 100KW 530°C 2L/M	D-7	18 OCT 83	11:19	300
24003	TTR 100KW 530°C 2L/M	D-2	18 OCT 83	11:29	300
24103	TTR 100KW 530°C 2L/M	D-7	18 OCT 83	11:29	300
24004	TTR 100KW 530°C 2L/M	D-2	18 OCT 83	11:36	600
24104	TTR 100KW 530°C 2L/M	D-7	18 OCT 83	11:36	600
24005	TTR 100KW 530°C 2L/M	D-2	18 OCT 83	11:50	600
24105	TTR 100KW 530°C 2L/M	D-7	18 OCT 83	11:50	600
24006	TTR 100KW 530°C 2L/M	D-2	18 OCT 83	12:04	1300
24106	TTR 100KW 530°C 2L/M	D-7	18 OCT 83	12:04	1300
24107	TTR 100KW 530°C 2L/M	D-9	18 OCT 83	12:40	1300
24108	TTR 100KW 530°C 2L/M	D-3	18 OCT 83	13:13	1300
24109	TTR 100KW 530°C 2L/M	D-5	18 OCT 83	13:55	1300
24110	TTR 100KW 530°C 2L/M	D-7	18 OCT 83	14:23	1300

DISK NO. 24100

TAG NO.	DATA I.D.	DETECTOR POSITION	DATE	START TIME	COUNT TIME
24111	TTR STOP 530°C 5L/M	D-7	18 OCT 83	15:11	300
24112	NA DRAIN	D-7	18 OCT 83	15:27	3600
24113	NA DRAIN	D-9	18 OCT 83	16:31	3600
24114	NA DRAIN	D-3	18 OCT 83	17:36	3600
24115	NA DRAIN	D-5	18 OCT 83	18:39	3600
24116	NA DRAIN	D-7	19 OCT 83	10:56	3600
24117	NA DRAIN	D-9	19 OCT 83	11:59	3600
24118	NA DRAIN	D-3	19 OCT 83	13:01	3600
24119	NA DRAIN	D-5	19 OCT 83	14:03	3600
24120	NA DRAIN	D-2	19 OCT 83	15:25	3600
24121	NA DRAIN	D-4	19 OCT 83	16:30	3600

Appendix B (continued)

EXP NO. 20 (NA TEMP. 170°C , NA FLOW RATE. 1LITER/MIN)

DISK NO. 25000

TAG NO.	DATA I.D.	DETECTOR POSITION	DATE	START TIME	COUNT TIME
25000	NA CIRCUL. BEFORE IRR.	D-2	8 NOV 83	09:54	3600
25100	NA CIRCUL. BEFORE IRR.	D-7	8 NOV 83	09:54	3600
25001	TTR 100KW 170°C 1L/M	D-2	8 NOV 83	11:12	300
25101	TTR 100KW 170°C 1L/M	D-7	8 NOV 83	11:12	300
25002	TTR 100KW 170°C 1L/M	D-2	8 NOV 83	11:21	300
25102	TTR 100KW 170°C 1L/M	D-7	8 NOV 83	11:21	300
25003	TTR 100KW 170°C 1L/M	D-2	8 NOV 83	11:29	300
25103	TTR 100KW 170°C 1L/M	D-7	8 NOV 83	11:29	300
25004	TTR 100KW 170°C 1L/M	D-2	8 NOV 83	11:38	600
25104	TTR 100KW 170°C 1L/M	D-7	8 NOV 83	11:38	600
25005	TTR 100KW 170°C 1L/M	D-2	8 NOV 83	11:51	600
25105	TTR 100KW 170°C 1L/M	D-7	8 NOV 83	11:51	600
25006	TTR 100KW 170°C 1L/M	D-2	8 NOV 83	12:03	1800
25106	TTR 100KW 170°C 1L/M	D-7	8 NOV 83	12:03	1800
25007	TTR 100KW 170°C 1L/M	D-4	8 NOV 83	12:38	1800
25107	TTR 100KW 170°C 1L/M	D-9	8 NOV 83	12:38	1800
25008	TTR 100KW 170°C 1L/M	D-6	8 NOV 83	13:11	1800
25108	TTR 100KW 170°C 1L/M	D-3	8 NOV 83	13:11	1800

DISK NO. 25100

TAG NO.	DATA I.D.	DETECTOR POSITION	DATE	START TIME	COUNT TIME
25009	TTR 100KW 170°C 1L/M	D-8	8 NOV 83	13:44	1800
25109	TTR 100KW 170°C 1L/M	D-5	8 NOV 83	13:44	1800
25010	TTR 100KW 170°C 1L/M	D-10	8 NOV 83	14:18	1800
25110	TTR 100KW 170°C 1L/M	D-11	8 NOV 83	14:18	1800
25011	TTR 100KW 170°C 1L/M	D-2	8 NOV 83	14:52	300
25111	TTR 100KW 170°C 1L/M	D-7	8 NOV 83	14:52	300
25012	TTR 100KW 170°C 1L/M	D-2	8 NOV 83	15:01	300
25112	TTR 100KW 170°C 1L/M	D-7	8 NOV 83	15:01	300
25013	TTR STOP 170°C 1L/M	D-2	8 NOV 83	15:12	300
25113	TTR STOP 170°C 1L/M	D-7	8 NOV 83	15:12	300
25014	TTR STOP 170°C 1L/M	D-2	8 NOV 83	15:21	300
25114	TTR STOP 170°C 1L/M	D-7	8 NOV 83	15:21	300
25015	TTR STOP 170°C 1L/M	D-2	8 NOV 83	15:29	600
25115	TTR STOP 170°C 1L/M	D-7	8 NOV 83	15:29	600
25016	TTR STOP 170°C 1L/M	D-2	8 NOV 83	15:42	1800
25116	TTR STOP 170°C 1L/M	D-7	9 NOV 83	15:42	1800
25017	TTR STOP 170°C 1L/M	D-4	8 NOV 83	16:20	1800
25117	TTR STOP 170°C 1L/M	D-9	8 NOV 83	16:20	1800

DISK NO. 25200

TAG NO.	DATA I.D.	DETECTOR POSITION	DATE	START TIME	COUNT TIME
25018	TTR STOP 170°C 1L/M	D-6	8 NOV 83	17:00	1800
25118	TTR STOP 170°C 1L/M	D-3	8 NOV 83	17:00	1800
25019	TTR STOP 170°C 1L/M	D-8	8 NOV 83	17:38	1800
25119	TTR STOP 170°C 1L/M	D-5	8 NOV 83	17:38	1800
25020	TTR STOP 170°C 1L/M	D-10	8 NOV 83	18:14	1800
25120	TTR STOP 170°C 1L/M	D-11	8 NOV 83	18:14	1800
25021	TTR STOP 170°C 1L/M	D-2	8 NOV 83	18:48	3600
25121	TTR STOP 170°C 1L/M	D-7	8 NOV 83	18:48	3600
25022	TTR STOP 170°C 1L/M	D-4	8 NOV 83	19:56	3600
25122	TTR STOP 170°C 1L/M	D-9	8 NOV 83	19:56	3600
25023	TTR STOP 170°C 1L/M	D-6	8 NOV 83	21:05	3600
25123	TTR STOP 170°C 1L/M	D-3	8 NOV 83	21:05	3600
25024	TTR STOP 170°C 1L/M	D-8	8 NOV 83	22:12	3600
25124	TTR STOP 170°C 1L/M	D-5	8 NOV 83	22:12	3600
25025	TTR STOP 170°C 1L/M	D-10	8 NOV 83	23:21	3600
25125	TTR STOP 170°C 1L/M	D-11	8 NOV 83	23:21	3600
25026	TTR STOP 170°C 1L/M	D-2	9 NOV 83	02:30	3600
25126	TTR STOP 170°C 1L/M	D-7	9 NOV 83	02:30	3600

DISK NO. 25300

TAG NO.	DATA I.D.	DETECTOR POSITION	DATE	START TIME	COUNT TIME
25027	TTR STOP 170°C 1L/M	D-4	9 NOV 83	03:38	3600
25127	TTR STOP 170°C 1L/M	D-9	9 NOV 83	03:38	3600
25028	TTR STOP 170°C 1L/M	D-6	9 NOV 83	04:50	3600
25128	TTR STOP 170°C 1L/M	D-3	9 NOV 83	04:50	3600
25029	TTR STOP 170°C 1L/M	D-8	9 NOV 83	06:00	3600
25129	TTR STOP 170°C 1L/M	D-5	9 NOV 83	06:00	3600
25030	TTR STOP 170°C 1L/M	D-10	9 NOV 83	07:10	3600
25130	TTR STOP 170°C 1L/M	D-11	9 NOV 83	07:10	3600
25031	TTR STOP 170°C 1L/M	D-2	9 NOV 83	10:00	3600
25131	TTR STOP 170°C 1L/M	D-7	9 NOV 83	10:00	3600
25032	TTR STOP 170°C 1L/M	D-4	9 NOV 83	11:10	3600
25132	TTR STOP 170°C 1L/M	D-9	9 NOV 83	11:10	3600
25033	TTR STOP 170°C 1L/M	D-6	9 NOV 83	12:36	3600
25133	TTR STOP 170°C 1L/M	D-3	9 NOV 83	12:36	3600
25034	TTR STOP 170°C 1L/M	D-8	9 NOV 83	13:48	3600
25134	TTR STOP 170°C 1L/M	D-5	9 NOV 83	13:48	3600
25035	TTR STOP 170°C 1L/M	D-10	9 NOV 83	15:01	3600
25135	TTR STOP 170°C 1L/M	D-11	9 NOV 83	15:01	3600

Appendix B (continued)

EXP NO. 29 (continued)

DISK NO. 25488

TAG NO.	DATA I.D.	DETECTOR POSITION	DATE	START TIME	COUNT TIME
25036	TTR STOP 170°C 1L/M	D-2	9 NOV 83	17:41	3600
25136	TTR STOP 170°C 1L/M	D-7	9 NOV 83	17:41	3600
25037	TTR STOP 170°C 1L/M	D-4	9 NOV 83	18:51	3600
25137	TTR STOP 170°C 1L/M	D-9	9 NOV 83	18:51	3600
25038	TTR STOP 170°C 1L/M	D-6	9 NOV 83	19:57	3600
25138	TTR STOP 170°C 1L/M	D-3	9 NOV 83	19:57	3600
25039	TTR STOP 170°C 1L/M	D-8	9 NOV 83	21:08	3600
25139	TTR STOP 170°C 1L/M	D-5	9 NOV 83	21:08	3600
25040	TTR STOP 170°C 1L/M	D-10	9 NOV 83	22:14	3600
25140	TTR STOP 170°C 1L/M	D-11	9 NOV 83	22:14	3600
25041	TTR STOP 170°C 1L/M	D-2	10 NOV 83	01:53	3600
25141	TTR STOP 170°C 1L/M	D-7	10 NOV 83	01:53	3600
25042	TTR STOP 170°C 1L/M	D-4	10 NOV 83	03:01	3600
25142	TTR STOP 170°C 1L/M	D-9	10 NOV 83	03:01	3600
25043	TTR STOP 170°C 1L/M	D-6	10 NOV 83	04:08	3600
25143	TTR STOP 170°C 1L/M	D-3	10 NOV 83	04:08	3600
25044	TTR STOP 170°C 1L/M	D-8	10 NOV 83	05:16	3600
25144	TTR STOP 170°C 1L/M	D-5	10 NOV 83	05:16	3600

DISK NO. 25500

TAG NO.	DATA I.D.	DETECTOR POSITION	DATE	START TIME	COUNT TIME
25045	TTR STOP 170°C 1L/M	D-10	10 NOV 83	06:23	3600
25145	TTR STOP 170°C 1L/M	D-11	10 NOV 83	06:23	3600
25046	TTR STOP 170°C 1L/M	D-2	10 NOV 83	08:50	3600
25146	TTR STOP 170°C 1L/M	D-7	10 NOV 83	08:50	3600
25047	NA DRAIN	D-2	10 NOV 83	10:00	3600
25147	NA DRAIN	D-7	10 NOV 83	10:00	3600
25048	NA DRAIN	D-4	10 NOV 83	11:07	3600
25148	NA DRAIN	D-9	10 NOV 83	11:07	3600
25049	NA DRAIN	D-6	10 NOV 83	12:27	3600
25149	NA DRAIN	D-3	10 NOV 83	12:27	3600
25050	NA DRAIN	D-8	10 NOV 83	13:39	3600
25150	NA DRAIN	D-5	10 NOV 83	13:39	3600
25051	NA DRAIN	D-10	10 NOV 83	15:22	3600
25151	NA DRAIN	D-11	10 NOV 83	15:22	3600
25052	NA DRAIN	D-2	10 NOV 83	16:30	3600
25152	NA DRAIN	D-7	10 NOV 83	16:30	3600

Appendix B (continued)

EXP NO. 21 (NA TEMP. 170°C , NA FLOW RATE. 5LITER/MIN)

DISK NO. 25000

TAG NO.	DATA I.D.	DETECTOR POSITION	DATE	START TIME	COUNT TIME
25000	NA CIRCUL. BEFORE IRR.	D-2	29 NOV 83	09:20	6000
25100	NA CIRCUL. BEFORE IRR.	D-7	29 NOV 83	09:20	6000
25001	TTR 100KW 170°C 5L/M	D-2	29 NOV 83	11:12	300
25101	TTR 100KW 170°C 5L/M	D-7	29 NOV 83	11:12	300
25002	TTR 100KW 170°C 5L/M	D-2	29 NOV 83	11:20	300
25102	TTR 100KW 170°C 5L/M	D-7	29 NOV 83	11:20	300
25003	TTR 100KW 170°C 5L/M	D-2	29 NOV 83	11:28	300
25103	TTR 100KW 170°C 5L/M	D-7	29 NOV 83	11:28	300
25004	TTR 100KW 170°C 5L/M	D-2	29 NOV 83	11:38	600
25104	TTR 100KW 170°C 5L/M	D-7	29 NOV 83	11:38	600
25005	TTR 100KW 170°C 5L/M	D-2	29 NOV 83	11:51	600
25105	TTR 100KW 170°C 5L/M	D-7	29 NOV 83	11:51	600
25006	TTR 100KW 170°C 5L/M	D-2	29 NOV 83	12:04	1800
25106	TTR 100KW 170°C 5L/M	D-7	29 NOV 83	12:04	1800
25007	TTR 100KW 170°C 5L/M	D-4	29 NOV 83	12:40	1800
25107	TTR 100KW 170°C 5L/M	D-9	29 NOV 83	12:40	1800
25008	TTR 100KW 170°C 5L/M	D-6	29 NOV 83	13:14	1800
25108	TTR 100KW 170°C 5L/M	D-3	29 NOV 83	13:14	1800

DISK NO. 25100

TAG NO.	DATA I.D.	DETECTOR POSITION	DATE	START TIME	COUNT TIME
25009	TTR 100KW 170°C 5L/M	D-8	29 NOV 83	13:48	1800
25109	TTR 100KW 170°C 5L/M	D-5	29 NOV 83	13:48	1800
25010	TTR 100KW 170°C 5L/M	D-10	29 NOV 83	14:21	1800
25110	TTR 100KW 170°C 5L/M	D-11	29 NOV 83	14:21	1800
25011	TTR 100KW 170°C 5L/M	D-2	29 NOV 83	14:54	300
25111	TTR 100KW 170°C 5L/M	D-7	29 NOV 83	14:54	300
25012	TTR 100KW 170°C 5L/M	D-2	29 NOV 83	15:02	300
25112	TTR 100KW 170°C 5L/M	D-7	29 NOV 83	15:02	300
25013	TTR STOP 170°C 5L/M	D-2	29 NOV 83	15:12	300
25113	TTR STOP 170°C 5L/M	D-7	29 NOV 83	15:12	300
25014	TTR STOP 170°C 5L/M	D-2	29 NOV 83	15:21	300
25114	TTR STOP 170°C 5L/M	D-7	29 NOV 83	15:21	300
25015	TTR STOP 170°C 5L/M	D-2	29 NOV 83	15:29	600
25115	TTR STOP 170°C 5L/M	D-7	29 NOV 83	15:29	600
25016	TTR STOP 170°C 5L/M	D-2	29 NOV 83	15:42	1800
25116	TTR STOP 170°C 5L/M	D-7	29 NOV 83	15:42	1800
25017	TTR STOP 170°C 5L/M	D-4	29 NOV 83	16:20	1800
25117	TTR STOP 170°C 5L/M	D-9	29 NOV 83	16:20	1800

DISK NO. 25200

TAG NO.	DATA I.D.	DETECTOR POSITION	DATE	START TIME	COUNT TIME
25018	TTR STOP 170°C 5L/M	D-6	29 NOV 83	16:57	1800
25118	TTR STOP 170°C 5L/M	D-3	29 NOV 83	16:57	1800
25019	TTR STOP 170°C 5L/M	D-8	29 NOV 83	17:33	1800
25119	TTR STOP 170°C 5L/M	D-5	29 NOV 83	17:33	1800
25020	TTR STOP 170°C 5L/M	D-10	29 NOV 83	18:07	1800
25120	TTR STOP 170°C 5L/M	D-11	29 NOV 83	18:07	1800
25021	TTR STOP 170°C 5L/M	D-2	29 NOV 83	18:40	3600
25121	TTR STOP 170°C 5L/M	D-7	29 NOV 83	18:40	3600
25022	TTR STOP 170°C 5L/M	D-4	29 NOV 83	19:46	3600
25122	TTR STOP 170°C 5L/M	D-9	29 NOV 83	19:46	3600
25023	TTR STOP 170°C 5L/M	D-6	29 NOV 83	20:57	3600
25123	TTR STOP 170°C 5L/M	D-3	29 NOV 83	20:57	3600
25024	TTR STOP 170°C 5L/M	D-8	29 NOV 83	22:04	3600
25124	TTR STOP 170°C 5L/M	D-5	29 NOV 83	22:04	3600
25025	TTR STOP 170°C 5L/M	D-10	29 NOV 83	23:11	3600
25125	TTR STOP 170°C 5L/M	D-11	29 NOV 83	23:11	3600
25026	TTR STOP 170°C 5L/M	D-2	30 NOV 83	00:17	3600
25126	TTR STOP 170°C 5L/M	D-7	30 NOV 83	00:17	3600

DISK NO. 25300

TAG NO.	DATA I.D.	DETECTOR POSITION	DATE	START TIME	COUNT TIME
25027	TTR STOP 170°C 5L/M	D-4	30 NOV 83	01:25	3600
25127	TTR STOP 170°C 5L/M	D-9	30 NOV 83	01:25	3600
25028	TTR STOP 170°C 5L/M	D-6	30 NOV 83	02:32	3600
25128	TTR STOP 170°C 5L/M	D-3	30 NOV 83	02:32	3600
25029	TTR STOP 170°C 5L/M	D-8	30 NOV 83	03:41	3600
25129	TTR STOP 170°C 5L/M	D-5	30 NOV 83	03:41	3600
25030	TTR STOP 170°C 5L/M	D-10	30 NOV 83	05:28	3600
25130	TTR STOP 170°C 5L/M	D-11	30 NOV 83	05:28	3600
25031	TTR STOP 170°C 5L/M	D-2	30 NOV 83	06:52	3600
25131	TTR STOP 170°C 5L/M	D-7	30 NOV 83	06:52	3600
25032	TTR STOP 170°C 5L/M	D-4	30 NOV 83	08:03	3600
25132	TTR STOP 170°C 5L/M	D-9	30 NOV 83	08:03	3600
25033	TTR STOP 170°C 5L/M	D-6	30 NOV 83	09:10	3600
25133	TTR STOP 170°C 5L/M	D-3	30 NOV 83	09:10	3600

Appendix B (continued)

EXP NO. 21 (continued)

DISK NO. 25498

TAG NO.	DATA I.D.	DETECTOR POSITION	DATE	START TIME	COUNT TIME
26034	NA DRAIN	D-2	30 NOV 83	10:21	3600
26134	NA DRAIN	D-7	30 NOV 83	10:21	3600
26035	NA DRAIN	D-4	30 NOV 83	11:31	3600
26135	NA DRAIN	D-9	30 NOV 83	11:31	3600
26036	NA DRAIN	D-6	30 NOV 83	12:37	3600
26136	NA DRAIN	D-3	30 NOV 83	12:37	3600
26037	NA DRAIN	D-8	30 NOV 83	13:44	3600
26137	NA DRAIN	D-5	30 NOV 83	13:44	3600
26038	NA DRAIN	D-10	30 NOV 83	14:58	3600
26138	NA DRAIN	D-11	30 NOV 83	14:58	3600
26039	NA DRAIN	D-2	30 NOV 83	15:58	3600
26139	NA DRAIN	D-7	30 NOV 83	15:58	3600

Appendix B (continued)

EXP NO. 22 (NA TEMP. 400°C , NA FLOW RATE ILITER/MIN)

DISK NO. 27000

TAG NO.	DATA I.D.	DETECTOR POSITION	DATE	START TIME	COUNT TIME
27000	NA CIRCUL. BEFORE IRR.	D-2	13 DEC 83	08:52	7200
27100	NA CIRCUL. BEFORE IRR.	D-7	13 DEC 83	08:52	7200
27001	TTR 100KW 400°C 1L/M	D-2	13 DEC 83	11:12	300
27101	TTR 100KW 400°C 1L/M	D-7	13 DEC 83	11:12	300
27002	TTR 100KW 400°C 1L/M	D-2	13 DEC 83	11:20	300
27102	TTR 100KW 400°C 1L/M	D-7	13 DEC 83	11:20	300
27003	TTR 100KW 400°C 1L/M	D-2	13 DEC 83	11:28	300
27103	TTR 100KW 400°C 1L/M	D-7	13 DEC 83	11:28	300
27004	TTR 100KW 400°C 1L/M	D-2	13 DEC 83	11:36	600
27104	TTR 100KW 400°C 1L/M	D-7	13 DEC 83	11:36	600
27005	TTR 100KW 400°C 1L/M	D-2	13 DEC 83	11:50	600
27105	TTR 100KW 400°C 1L/M	D-7	13 DEC 83	11:50	600
27006	TTR 100KW 400°C 1L/M	D-2	13 DEC 83	12:03	1800
27106	TTR 100KW 400°C 1L/M	D-7	13 DEC 83	12:03	1800
27007	TTR 100KW 400°C 1L/M	D-4	13 DEC 83	12:38	1800
27107	TTR 100KW 400°C 1L/M	D-9	13 DEC 83	12:38	1800
27008	TTR 100KW 400°C 1L/M	D-6	13 DEC 83	13:12	1800
27108	TTR 100KW 400°C 1L/M	D-3	13 DEC 83	13:12	1800

DISK NO. 27200

TAG NO.	DATA I.D.	DETECTOR POSITION	DATE	START TIME	COUNT TIME
27018	TTR STOP 400°C 1L/M	D-6	13 DEC 83	16:47	1800
27118	TTR STOP 400°C 1L/M	D-3	13 DEC 83	16:47	1800
27019	TTR STOP 400°C 1L/M	D-8	13 DEC 83	17:26	1800
27119	TTR STOP 400°C 1L/M	D-5	13 DEC 83	17:26	1800
27020	TTR STOP 400°C 1L/M	D-10	13 DEC 83	17:59	1800
27120	TTR STOP 400°C 1L/M	D-11	13 DEC 83	17:59	1800
27021	TTR STOP 400°C 1L/M	D-2	13 DEC 83	18:37	3600
27121	TTR STOP 400°C 1L/M	D-7	13 DEC 83	18:37	3600
27022	TTR STOP 400°C 1L/M	D-4	13 DEC 83	19:45	3600
27122	TTR STOP 400°C 1L/M	D-9	13 DEC 83	19:45	3600
27023	TTR STOP 400°C 1L/M	D-6	13 DEC 83	20:52	3600
27123	TTR STOP 400°C 1L/M	D-3	13 DEC 83	20:52	3600
27024	TTR STOP 400°C 1L/M	D-8	13 DEC 83	22:02	3600
27124	TTR STOP 400°C 1L/M	D-5	13 DEC 83	22:02	3600
27025	TTR STOP 400°C 1L/M	D-10	13 DEC 83	23:17	3600
27125	TTR STOP 400°C 1L/M	D-11	13 DEC 83	23:17	3600
27026	TTR STOP 400°C 1L/M	D-2	14 DEC 83	02:38	3600
27126	TTR STOP 400°C 1L/M	D-7	14 DEC 83	02:38	3600

DISK NO. 27100

TAG NO.	DATA I.D.	DETECTOR POSITION	DATE	START TIME	COUNT TIME
27009	TTR 100KW 400°C 1L/M	D-8	13 DEC 83	13:46	1800
27109	TTR 100KW 400°C 1L/M	D-5	13 DEC 83	13:46	1800
27010	TTR 100KW 400°C 1L/M	D-10	13 DEC 83	14:20	1800
27110	TTR 100KW 400°C 1L/M	D-11	13 DEC 83	14:20	1800
27011	TTR 100KW 400°C 1L/M	D-2	13 DEC 83	14:53	300
27111	TTR 100KW 400°C 1L/M	D-7	13 DEC 83	14:53	300
27012	TTR 100KW 400°C 1L/M	D-2	13 DEC 83	15:01	300
27112	TTR 100KW 400°C 1L/M	D-7	13 DEC 83	15:01	300
27013	TTR STOP 400°C 1L/M	D-2	13 DEC 83	15:12	300
27113	TTR STOP 400°C 1L/M	D-7	13 DEC 83	15:12	300
27014	TTR STOP 400°C 1L/M	D-2	13 DEC 83	15:20	300
27114	TTR STOP 400°C 1L/M	D-7	13 DEC 83	15:20	300
27015	TTR STOP 400°C 1L/M	D-2	13 DEC 83	15:28	600
27115	TTR STOP 400°C 1L/M	D-7	13 DEC 83	15:28	600
27016	TTR STOP 400°C 1L/M	D-2	13 DEC 83	15:40	1800
27116	TTR STOP 400°C 1L/M	D-7	13 DEC 83	15:40	1800
27017	TTR STOP 400°C 1L/M	D-4	13 DEC 83	16:15	1800
27117	TTR STOP 400°C 1L/M	D-9	13 DEC 83	16:15	1800

DISK NO. 27300

TAG NO.	DATA I.D.	DETECTOR POSITION	DATE	START TIME	COUNT TIME
27027	TTR STOP 400°C 1L/M	D-4	14 DEC 83	03:38	3600
27127	TTR STOP 400°C 1L/M	D-9	14 DEC 83	03:38	3600
27028	TTR STOP 400°C 1L/M	D-6	14 DEC 83	04:46	3600
27128	TTR STOP 400°C 1L/M	D-3	14 DEC 83	04:46	3600
27029	TTR STOP 400°C 1L/M	D-8	14 DEC 83	05:54	3600
27129	TTR STOP 400°C 1L/M	D-5	14 DEC 83	05:54	3600
27030	TTR STOP 400°C 1L/M	D-10	14 DEC 83	07:00	3600
27130	TTR STOP 400°C 1L/M	D-11	14 DEC 83	07:00	3600
27031	TTR STOP 400°C 1L/M	D-2	14 DEC 83	10:00	3600
27131	TTR STOP 400°C 1L/M	D-7	14 DEC 83	10:00	3600
27032	TTR STOP 400°C 1L/M	D-4	14 DEC 83	11:11	3600
27132	TTR STOP 400°C 1L/M	D-9	14 DEC 83	11:11	3600
27033	TTR STOP 400°C 1L/M	D-6	14 DEC 83	12:20	3600
27133	TTR STOP 400°C 1L/M	D-3	14 DEC 83	12:20	3600
27034	TTR STOP 400°C 1L/M	D-8	14 DEC 83	13:27	3600
27134	TTR STOP 400°C 1L/M	D-5	14 DEC 83	13:27	3600
27035	TTR STOP 400°C 1L/M	D-10	14 DEC 83	14:35	3600
27135	TTR STOP 400°C 1L/M	D-11	14 DEC 83	14:35	3600

Appendix B (continued)

EXP NO. 22 (continued)

DISK NO. 27488

TAG NO.	DATA I.D.	DETECTOR POSITION	DATE	START TIME	COUNT TIME
27036	TTR STOP 400°C 1L/M	D-2	14 DEC 83	17:29	3600
27136	TTR STOP 400°C 1L/M	D-7	14 DEC 83	17:29	3600
27037	TTR STOP 400°C 1L/M	D-4	14 DEC 83	18:36	3600
27137	TTR STOP 400°C 1L/M	D-9	14 DEC 83	18:36	3600
27038	TTR STOP 400°C 1L/M	D-6	14 DEC 83	19:43	3600
27138	TTR STOP 400°C 1L/M	D-3	14 DEC 83	19:43	3600
27039	TTR STOP 400°C 1L/M	D-8	14 DEC 83	20:49	3600
27139	TTR STOP 400°C 1L/M	D-5	14 DEC 83	20:49	3600
27040	TTR STOP 400°C 1L/M	D-10	14 DEC 83	22:16	3600
27140	TTR STOP 400°C 1L/M	D-11	14 DEC 83	22:16	3600
27041	TTR STOP 400°C 1L/M	D-2	15 DEC 83	01:10	3600
27141	TTR STOP 400°C 1L/M	D-7	15 DEC 83	01:10	3600
27042	TTR STOP 400°C 1L/M	D-4	15 DEC 83	02:17	3600
27142	TTR STOP 400°C 1L/M	D-9	15 DEC 83	02:17	3600
27043	TTR STOP 400°C 1L/M	D-6	15 DEC 83	03:24	3600
27143	TTR STOP 400°C 1L/M	D-3	15 DEC 83	03:24	3600
27044	TTR STOP 400°C 1L/M	D-8	15 DEC 83	04:30	3600
27144	TTR STOP 400°C 1L/M	D-5	15 DEC 83	04:30	3600

DISK NO. 27500

TAG NO.	DATA I.D.	DETECTOR POSITION	DATE	START TIME	COUNT TIME
27045	TTR STOP 400°C 1L/M	D-10	15 DEC 83	05:38	3600
27145	TTR STOP 400°C 1L/M	D-11	15 DEC 83	05:38	3600
27046	TTR STOP 400°C 1L/M	D-2	15 DEC 83	06:44	3600
27146	TTR STOP 400°C 1L/M	D-7	15 DEC 83	06:44	3600

Appendix B (continued)

EXP NO. 23 (NA TEMP. 500°C , NA FLOW RATE 0-5LITER/MIN)

DISK NO. 28000

TAG NO.	DATA I.D.	DETECTOR POSITION	DATE	START TIME	COUNT TIME
28000	500°C 5L/M BEFORE IRR.	D-2	15 DEC 83	08:50	3600
28100	500°C 5L/M BEFORE IRR.	D-9	15 DEC 83	08:50	3600
28001	TTR 100KW 500°C 5L/M	D-2	15 DEC 83	12:07	600
28101	TTR 100KW 500°C 5L/M	D-9	15 DEC 83	12:07	600
28002	TTR 100KW 500°C 5L/M	D-2	15 DEC 83	12:20	600
28102	TTR 100KW 500°C 5L/M	D-9	15 DEC 83	12:20	600
28003	TTR 100KW 500°C 4.2L/M	D-2	15 DEC 83	12:41	600
28103	TTR 100KW 500°C 4.2L/M	D-9	15 DEC 83	12:41	600
28004	TTR 100KW 500°C 4.2L/M	D-2	15 DEC 83	12:53	600
28104	TTR 100KW 500°C 4.2L/M	D-9	15 DEC 83	12:53	600
28005	TTR 100KW NA DRAIN	D-2	15 DEC 83	13:21	600
28105	TTR 100KW NA DRAIN	D-9	15 DEC 83	13:21	600
28006	TTR 100KW NA DRAIN	D-2	15 DEC 83	13:34	600
28106	TTR 100KW NA DRAIN	D-9	15 DEC 83	13:34	600
28007	TTR STOP NA DRAIN	D-2	15 DEC 83	14:05	600
28107	TTR STOP NA DRAIN	D-9	15 DEC 83	14:05	600
28008	TTR STOP NA DRAIN	D-2	15 DEC 83	14:18	600
28108	TTR STOP NA DRAIN	D-9	15 DEC 83	14:18	600

Appendix B (continued)

EXP NO. 24 (NA TEMP. 270°C , NA FLOW RATE. 5LITER/MIN)

DISK NO. 29000

TAG NO.	DATA I.D.	DETECTOR POSITION	DATE	START TIME	COUNT TIME
29000	270°C 5L/M BEFORE IRR.	D-2	25 JAN 84	09:40	3600
29100	270°C 5L/M BEFORE IRR.	D-7	25 JAN 84	09:40	3600
29001	TTR 100KW 270°C 5L/M	D-2	25 JAN 84	11:10	300
29101	TTR 100KW 270°C 5L/M	D-7	25 JAN 84	11:10	300
29002	TTR 100KW 270°C 5L/M	D-2	25 JAN 84	11:18	300
29102	TTR 100KW 270°C 5L/M	D-7	25 JAN 84	11:18	300
29003	TTR 100KW 270°C 5L/M	D-2	25 JAN 84	11:25	300
29103	TTR 100KW 270°C 5L/M	D-7	25 JAN 84	11:25	300
29004	TTR 100KW 270°C 5L/M	D-2	25 JAN 84	11:34	600
29104	TTR 100KW 270°C 5L/M	D-7	26 JAN 84	11:34	600
29005	TTR 100KW 270°C 5L/M	D-2	25 JAN 84	11:47	600
29105	TTR 100KW 270°C 5L/M	D-7	25 JAN 84	11:47	600
29006	TTR 100KW 270°C 5L/M	D-2	25 JAN 84	12:00	1800
29106	TTR 100KW 270°C 5L/M	D-7	25 JAN 84	12:00	1800
29007	TTR 100KW 270°C 5L/M	D-4	25 JAN 84	12:36	1800
29107	TTR 100KW 270°C 5L/M	D-9	25 JAN 84	12:36	1800
29008	TTR 100KW 270°C 5L/M	D-6	26 JAN 84	13:10	1800
29108	TTR 100KW 270°C 5L/M	D-3	25 JAN 84	13:10	1800

DISK NO. 29100

TAG NO.	DATA I.D.	DETECTOR POSITION	DATE	START TIME	COUNT TIME
29009	TTR 100KW 270°C 5L/M	D-8	26 JAN 84	13:44	1800
29109	TTR 100KW 270°C 5L/M	D-5	25 JAN 84	13:44	1800
29010	TTR 100KW 270°C 5L/M	D-10	26 JAN 84	14:19	1800
29110	TTR 100KW 270°C 5L/M	D-11	25 JAN 84	14:19	1800
29011	TTR 100KW 270°C 5L/M	D-2	25 JAN 84	15:03	301
29111	TTR 100KW 270°C 5L/M	D-5	26 JAN 84	15:03	301
29012	NA DRAIN 270°C 5L/M	D-2	25 JAN 84	15:12	60
29112	NA DRAIN 270°C 5L/M	D-5	25 JAN 84	15:12	60
29013	NA DRAIN 270°C 5L/M	D-2	25 JAN 84	15:13	60
29113	NA DRAIN 270°C 5L/M	D-5	25 JAN 84	15:13	60
29014	NA DRAIN	D-2	26 JAN 84	15:17	300
29114	NA DRAIN	D-5	26 JAN 84	15:17	300
29015	NA DRAIN	D-2	25 JAN 84	15:26	300
29115	NA DRAIN	D-5	26 JAN 84	15:26	300
29016	NA DRAIN	D-10	25 JAN 84	15:34	600
29116	NA DRAIN	D-11	26 JAN 84	15:34	600
29017	NA DRAIN	D-2	25 JAN 84	15:51	600
29117	NA DRAIN	D-7	25 JAN 84	15:51	600
29018	NA DRAIN	D-4	25 JAN 84	16:10	600
29118	NA DRAIN	D-9	25 JAN 84	16:10	600

DISK NO. 29200

TAG NO.	DATA I.D.	DETECTOR POSITION	DATE	START TIME	COUNT TIME
29019	NA DRAIN	D-6	25 JAN 84	16:25	600
29119	NA DRAIN	D-3	26 JAN 84	16:25	600
29020	NA DRAIN	D-8	25 JAN 84	16:43	600
29120	NA DRAIN	D-5	26 JAN 84	16:43	600
29021	NA DRAIN	D-2	25 JAN 84	16:56	2400
29121	NA DRAIN	D-7	26 JAN 84	16:56	2400
29022	NA DRAIN	D-4	25 JAN 84	17:41	2400
29122	NA DRAIN	D-9	26 JAN 84	17:41	2400
29023	NA DRAIN	D-6	25 JAN 84	18:24	2400
29123	NA DRAIN	D-3	25 JAN 84	18:24	2400
29024	NA DRAIN	D-8	25 JAN 84	19:08	2400
29124	NA DRAIN	D-5	25 JAN 84	19:08	2400
29025	NA DRAIN	D-2	27 JAN 84	09:35	3600
29125	NA DRAIN	D-7	27 JAN 84	09:35	3600
29026	NA DRAIN	D-4	27 JAN 84	10:41	3600
29126	NA DRAIN	D-9	27 JAN 84	10:41	3600
29027	NA DRAIN	D-6	27 JAN 84	11:47	3600
29127	NA DRAIN	D-3	27 JAN 84	11:49	3600

DISK NO. 29300

TAG NO.	DATA I.D.	DETECTOR POSITION	DATE	START TIME	COUNT TIME
29028	NA DRAIN	D-8	27 JAN 84	13:01	3600
29128	NA DRAIN	D-5	27 JAN 84	13:01	3600
29029	NA DRAIN	D-10	27 JAN 84	14:12	3600
29129	NA DRAIN	D-11	27 JAN 84	14:12	3600

Appendix B (continued)

EXP NO. 25 (NA TEMP. 300°C , NA FLOW RATE. 1LITER/MIN)

DISK NO. 30000

TAG NO.	DATA I.D.	DETECTOR POSITION	DATE	START TIME	COUNT TIME
30000	300°C 1L/M BEFORE IRR.	D-2	31 JAN 84	10:47	1251
30100	300°C 1L/M BEFORE IRR.	D-7	31 JAN 84	10:47	1251
30001	TTR 100KW 300°C 1L/M	D-2	31 JAN 84	11:15	300
30101	TTR 100KW 300°C 1L/M	D-7	31 JAN 84	11:15	300
30002	TTR 100KW 300°C 1L/M	D-2	31 JAN 84	11:23	300
30102	TTR 100KW 300°C 1L/M	D-7	31 JAN 84	11:23	300
30003	TTR 100KW 300°C 1L/M	D-2	31 JAN 84	11:31	300
30103	TTR 100KW 300°C 1L/M	D-7	31 JAN 84	11:31	300
30004	TTR 100KW 300°C 1L/M	D-2	31 JAN 84	11:40	600
30104	TTR 100KW 300°C 1L/M	D-7	31 JAN 84	11:40	600
30005	TTR 100KW 300°C 1L/M	D-2	31 JAN 84	11:53	600
30105	TTR 100KW 300°C 1L/M	D-7	31 JAN 84	11:53	600
30006	TTR 100KW 300°C 1L/M	D-2	31 JAN 84	12:07	1800
30106	TTR 100KW 300°C 1L/M	D-7	31 JAN 84	12:07	1800
30007	TTR 100KW 300°C 1L/M	D-4	31 JAN 84	12:44	1800
30107	TTR 100KW 300°C 1L/M	D-9	31 JAN 84	12:44	1800
30008	TTR 100KW 300°C 1L/M	D-6	31 JAN 84	13:18	1800
30108	TTR 100KW 300°C 1L/M	D-3	31 JAN 84	13:18	1800

DISK NO. 30100

TAG NO.	DATA I.D.	DETECTOR POSITION	DATE	START TIME	COUNT TIME
30009	TTR 100KW 300°C 1L/M	D-8	31 JAN 84	13:53	1800
30109	TTR 100KW 300°C 1L/M	D-5	31 JAN 84	13:53	1800
30010	TTR 100KW 300°C 1L/M	D-10	31 JAN 84	14:26	1800
30110	TTR 100KW 300°C 1L/M	D-11	31 JAN 84	14:26	1800
30011	TTR 100KW 300°C 1L/M	D-2	31 JAN 84	14:59	300
30111	TTR 100KW 300°C 1L/M	D-7	31 JAN 84	14:59	300
30012	TTR 100KW 300°C 1L/M	D-2	31 JAN 84	15:08	300
30112	TTR 100KW 300°C 1L/M	D-7	31 JAN 84	15:08	300
30013	TTR STOP 300°C 1L/M	D-2	31 JAN 84	15:16	300
30113	TTR STOP 300°C 1L/M	D-7	31 JAN 84	15:16	300
30014	TTR STOP 300°C 1L/M	D-2	31 JAN 84	15:24	300
30114	TTR STOP 300°C 1L/M	D-7	31 JAN 84	15:24	300
30015	TTR STOP 300°C 1L/M	D-2	31 JAN 84	15:31	600
30115	TTR STOP 300°C 1L/M	D-7	31 JAN 84	15:31	600
30016	TTR STOP 300°C 1L/M	D-2	31 JAN 84	15:44	1800
30116	TTR STOP 300°C 1L/M	D-7	31 JAN 84	15:44	1800
30017	TTR STOP 300°C 1L/M	D-4	31 JAN 84	16:20	1800
30117	TTR STOP 300°C 1L/M	D-9	31 JAN 84	16:20	1800

DISK NO. 30200

TAG NO.	DATA I.D.	DETECTOR POSITION	DATE	START TIME	COUNT TIME
30018	TTR STOP 300°C 1L/M	D-2	31 JAN 84	18:50	3600
30118	TTR STOP 300°C 1L/M	D-7	31 JAN 84	18:50	3600
30019	TTR STOP 300°C 1L/M	D-4	31 JAN 84	19:57	3600
30119	TTR STOP 300°C 1L/M	D-9	31 JAN 84	19:57	3600
30020	TTR STOP 300°C 1L/M	D-6	31 JAN 84	21:05	3600
30120	TTR STOP 300°C 1L/M	D-3	31 JAN 84	21:05	3600
30021	TTR STOP 300°C 1L/M	D-8	31 JAN 84	22:12	3600
30121	TTR STOP 300°C 1L/M	D-5	31 JAN 84	22:12	3600
30022	TTR STOP 300°C 1L/M	D-10	31 JAN 84	23:18	3600
30122	TTR STOP 300°C 1L/M	D-11	31 JAN 84	23:18	3600
30023	TTR STOP 300°C 1L/M	D-2	1 FEB 84	00:27	10800
30123	TTR STOP 300°C 1L/M	D-7	1 FEB 84	00:27	10800
30024	TTR STOP 300°C 1L/M	D-4	1 FEB 84	03:37	3600
30124	TTR STOP 300°C 1L/M	D-9	1 FEB 84	03:37	3600
30025	TTR STOP 300°C 1L/M	D-6	1 FEB 84	04:50	3600
30125	TTR STOP 300°C 1L/M	D-3	1 FEB 84	04:50	3600
30026	TTR STOP 300°C 1L/M	D-8	1 FEB 84	06:00	3600
30126	TTR STOP 300°C 1L/M	D-5	1 FEB 84	06:00	3600

DISK NO. 30300

TAG NO.	DATA I.D.	DETECTOR POSITION	DATE	START TIME	COUNT TIME
30027	TTR STOP 300°C 1L/M	D-10	1 FEB 84	07:06	3600
30127	TTR STOP 300°C 1L/M	D-11	1 FEB 84	07:06	3600
30028	FROM 300°C TO 500°C 5L/M	D-2	1 FEB 84	08:13	7200
30128	FROM 300°C TO 500°C 5L/M	D-7	1 FEB 84	08:13	7200

Appendix B (continued)

EXP NO. 26 (NA TEMP. 500°C , NA FLOW RATE. 1-5LITER/MIN)

DISK NO. 31000

TAG NO.	DATA I.D.	DETECTOR POSITION	DATE	START TIME	COUNT TIME
31000	500°C 5L/M BEFORE IRR.	D-2	1 FEB 84	10:26	1900
31100	500°C 5L/M BEFORE IRR.	D-7	1 FEB 84	10:26	1800
31001	NA DRAIN	D-2	1 FEB 84	15:10	1800
30101	NA DRAIN	D-5	1 FEB 84	15:10	1000
30002	NA DRAIN	D-2	1 FEB 84	15:40	1000
30102	NA DRAIN	D-5	1 FEB 84	15:40	1000
30003	NA DRAIN	D-2	1 FEB 84	16:16	1000
30103	NA DRAIN	D-5	1 FEB 84	16:16	1000

EXP NO. 27 (NA TEMP. 500°C , NA FLOW RATE. 5LITER/MIN)

DISK NO. 32000

TAG NO.	DATA I.D.	DETECTOR POSITION	DATE	START TIME	COUNT TIME
32000	TTR 100KV 500°C 5L/M	D-2	14 FEB 84	14:35	1799
32100	TTR 100KV 500°C 5L/M	D-7	14 FEB 84	14:35	1799
32001	TTR STOP 500°C 5L/M	D-2	14 FEB 84	15:11	300
32101	TTR STOP 500°C 5L/M	D-7	14 FEB 84	15:11	300
32002	NA DRAIN	D-2	14 FEB 84	15:20	300
32102	NA DRAIN	D-7	14 FEB 84	15:20	300
32003	NA DRAIN	D-2	14 FEB 84	15:30	600
32103	NA DRAIN	D-7	14 FEB 84	15:30	600
32004	NA DRAIN	D-4	14 FEB 84	15:44	600
32104	NA DRAIN	D-9	14 FEB 84	15:44	600
32005	NA DRAIN	D-6	14 FEB 84	15:59	600
32105	NA DRAIN	D-3	14 FEB 84	15:59	600
32006	NA DRAIN	D-8	14 FEB 84	16:13	600
32106	NA DRAIN	D-5	14 FEB 84	16:13	600
32007	NA DRAIN	D-2	14 FEB 84	16:27	3000
32107	NA DRAIN	D-7	14 FEB 84	16:27	3000
32008	NA DRAIN	D-4	14 FEB 84	17:22	3000
32108	NA DRAIN	D-9	14 FEB 84	17:22	3000

DISK NO. 32100

TAG NO.	DATA I.D.	DETECTOR POSITION	DATE	START TIME	COUNT TIME
32009	NA DRAIN	D-6	14 FEB 84	18:15	3000
32109	NA DRAIN	D-3	14 FEB 84	18:15	3000
32010	NA DRAIN	D-8	14 FEB 84	19:08	3000
32110	NA DRAIN	D-5	14 FEB 84	19:08	3000
32011	NA DRAIN	D-2	15 FEB 84	09:08	7200
32111	NA DRAIN	D-7	15 FEB 84	09:08	7200
32012	NA DRAIN	D-4	15 FEB 84	11:12	7200
32112	NA DRAIN	D-9	15 FEB 84	11:12	7200
32013	NA DRAIN	D-6	15 FEB 84	13:16	7200
32113	NA DRAIN	D-3	15 FEB 84	13:16	7200
32014	NA DRAIN	D-8	15 FEB 84	15:24	7200
32114	NA DRAIN	D-5	15 FEB 84	15:24	7200
32015	NA DRAIN	D-10	15 FEB 84	17:27	3600
32115	NA DRAIN	D-11	15 FEB 84	17:27	3600

Appendix B (continued)

EXP NO. 28 (NA TEMP. 500°C , NA FLOW RATE 5LITER/MIN)

DISK NO. 33000

TAG NO.	DATA I.D.	DETECTOR POSITION	DATE	START TIME	COUNT TIME
33000	500°C 5L/M BEFORE IRR.	D-2	28 FEB 84	08:52	7200
33100	500°C 5L/M BEFORE IRR.	D-7	28 FEB 84	08:52	7200
33001	TTR 100KW 500°C 5L/M	D-2	28 FEB 84	11:18	300
33101	TTR 100KW 500°C 5L/M	D-7	28 FEB 84	11:18	300
33002	TTR 100KW 500°C 5L/M	D-2	28 FEB 84	11:24	300
33102	TTR 100KW 500°C 5L/M	D-7	28 FEB 84	11:24	300
33003	TTR 100KW 500°C 5L/M	D-2	28 FEB 84	11:33	300
33103	TTR 100KW 500°C 5L/M	D-7	28 FEB 84	11:33	300
33004	TTR 100KW 500°C 5L/M	D-2	28 FEB 84	11:41	600
33104	TTR 100KW 500°C 5L/M	D-7	28 FEB 84	11:41	600
33005	TTR 100KW 500°C 5L/M	D-2	28 FEB 84	11:54	1800
33105	TTR 100KW 500°C 5L/M	D-7	28 FEB 84	11:54	1800
33006	TTR 100KW 500°C 5L/M	D-4	28 FEB 84	12:31	1800
33106	TTR 100KW 500°C 5L/M	D-9	28 FEB 84	12:31	1800
33007	TTR 100KW 500°C 5L/M	D-6	28 FEB 84	13:04	1800
33107	TTR 100KW 500°C 5L/M	D-3	28 FEB 84	13:04	1800
33008	TTR 100KW 500°C 5L/M	D-8	28 FEB 84	13:37	1800
33108	TTR 100KW 500°C 5L/M	D-5	28 FEB 84	13:37	1800

DISK NO. 33100

TAG NO.	DATA I.D.	DETECTOR POSITION	DATE	START TIME	COUNT TIME
33009	TTR 100KW 500°C 5L/M	D-10	28 FEB 84	14:11	1800
33109	TTR 100KW 500°C 5L/M	D-11	28 FEB 84	14:11	1800
33010	TTR 100KW 500°C 0L/M	D-2	28 FEB 84	14:45	300
33110	TTR 100KW 500°C 0L/M	D-7	28 FEB 84	14:45	300
33011	TTR 100KW 500°C 0L/M	D-2	28 FEB 84	14:52	300
33111	TTR 100KW 500°C 0L/M	D-7	28 FEB 84	14:52	300
33012	TTR 100KW 500°C 5L/M	D-2	28 FEB 84	15:05	300
33112	TTR 100KW 500°C 5L/M	D-7	28 FEB 84	15:05	300
33013	TTR STOP 500°C 5L/M	D-2	28 FEB 84	15:18	300
33113	TTR STOP 500°C 5L/M	D-7	28 FEB 84	15:18	300
33014	TTR STOP 500°C 5L/M	D-2	28 FEB 84	15:26	600
33114	TTR STOP 500°C 5L/M	D-7	28 FEB 84	15:26	600
33015	TTR STOP 500°C 5L/M	D-2	28 FEB 84	15:38	1800
33115	TTR STOP 500°C 5L/M	D-7	28 FEB 84	15:38	1800
33016	TTR STOP 500°C 5L/M	D-4	28 FEB 84	16:13	1800
33116	TTR STOP 500°C 5L/M	D-9	28 FEB 84	16:13	1800
33017	TTR STOP 500°C 5L/M	D-6	28 FEB 84	16:46	1800
33117	TTR STOP 500°C 5L/M	D-3	28 FEB 84	16:46	1800

DISK NO. 33200

TAG NO.	DATA I.D.	DETECTOR POSITION	DATE	START TIME	COUNT TIME
33018	TTR STOP 500°C 5L/M	D-8	28 FEB 84	17:58	1800
33118	TTR STOP 500°C 5L/M	D-5	28 FEB 84	17:58	1800
33019	TTR STOP 500°C 5L/M	D-10	28 FEB 84	18:30	1800
33119	TTR STOP 500°C 5L/M	D-11	28 FEB 84	18:30	1800
33020	TTR STOP 500°C 5L/M	D-2	28 FEB 84	19:03	3600
33120	TTR STOP 500°C 5L/M	D-7	28 FEB 84	19:05	3600
33021	TTR STOP 500°C 5L/M	D-4	28 FEB 84	20:11	3600
33121	TTR STOP 500°C 5L/M	D-9	28 FEB 84	20:11	3600
33022	TTR STOP 500°C 5L/M	D-6	28 FEB 84	21:18	3600
33122	TTR STOP 500°C 5L/M	D-3	28 FEB 84	21:18	3600
33023	TTR STOP 500°C 5L/M	D-9	28 FEB 84	22:23	3600
33123	TTR STOP 500°C 5L/M	D-5	28 FEB 84	22:23	3600
33024	TTR STOP 500°C 5L/M	D-10	28 FEB 84	23:28	10800
33124	TTR STOP 500°C 5L/M	D-11	28 FEB 84	23:28	10800
33025	TTR STOP 500°C 5L/M	D-2	29 FEB 84	02:52	3600
33125	TTR STOP 500°C 5L/M	D-7	29 FEB 84	02:52	3600
33026	TTR STOP 500°C 5L/M	D-4	29 FEB 84	03:59	3600
33126	TTR STOP 500°C 5L/M	D-9	29 FEB 84	03:59	3600

DISK NO. 33300

TAG NO.	DATA I.D.	DETECTOR POSITION	DATE	START TIME	COUNT TIME
33027	TTR STOP 500°C 5L/M	D-6	29 FEB 84	05:06	3600
33127	TTR STOP 500°C 5L/M	D-3	29 FEB 84	05:06	3600
33028	TTR STOP 500°C 5L/M	D-8	29 FEB 84	07:01	3600
33128	TTR STOP 500°C 5L/M	D-5	29 FEB 84	07:01	3600
33029	TTR STOP 500°C 5L/M	D-10	29 FEB 84	08:14	3600
33129	TTR STOP 500°C 5L/M	D-11	29 FEB 84	08:14	3600
33030	TTR STOP 500°C 5L/M	D-2	29 FEB 84	09:21	7200
33130	TTR STOP 500°C 5L/M	D-7	29 FEB 84	09:21	7200
33031	TTR STOP 500°C 5L/M	D-4	29 FEB 84	11:31	3600
33131	TTR STOP 500°C 5L/M	D-9	29 FEB 84	11:31	3600
33032	TTR STOP 500°C 5L/M	D-6	29 FEB 84	12:37	3600
33132	TTR STOP 500°C 5L/M	D-3	29 FEB 84	12:37	3600
33033	TTR STOP 500°C 5L/M	D-8	29 FEB 84	13:46	3600
33133	TTR STOP 500°C 5L/M	D-5	29 FEB 84	13:46	3600
33034	TTR STOP 500°C 5L/M	D-10	29 FEB 84	14:56	3600
33134	TTR STOP 500°C 5L/M	D-11	29 FEB 84	14:56	3600
33035	TTR STOP 500°C 5L/M	D-2	29 FEB 84	17:00	3600
33135	TTR STOP 500°C 5L/M	D-7	29 FEB 84	17:00	3600

Appendix B (continued)

EXP NO. 28 (continued)

DISK NO. 33488

TAG NO.	DATA I.D.	DETECTOR POSITION	DATE	START TIME	COUNT TIME
33036	TTR STOP 500°C 5L/M	D-4	29 FEB 84	18:06	3600
33136	TTR STOP 500°C 5L/M	D-9	29 FEB 84	18:06	3600
33037	TTR STOP 500°C 5L/M	D-6	29 FEB 84	19:16	3600
33137	TTR STOP 500°C 5L/M	D-3	29 FEB 84	19:16	3600
33038	TTR STOP 500°C 5L/M	D-8	29 FEB 84	20:21	3600
33138	TTR STOP 500°C 5L/M	D-5	29 FEB 84	20:21	3600
33039	TTR STOP 500°C 5L/M	D-10	29 FEB 84	21:26	3600
33139	TTR STOP 500°C 5L/M	D-11	29 FEB 84	21:26	3600
33040	TTR STOP 500°C 5L/M	D-2	29 FEB 84	22:32	3600
33140	TTR STOP 500°C 5L/M	D-7	29 FEB 84	22:32	3600
33041	TTR STOP 500°C 5L/M	D-4	29 FEB 84	23:48	3600
33141	TTR STOP 500°C 5L/M	D-9	29 FEB 84	23:48	3600
33042	TTR STOP 500°C 5L/M	D-6	1 MAR 84	00:56	3600
33142	TTR STOP 500°C 5L/M	D-3	1 MAR 84	00:56	3600
33043	TTR STOP 500°C 5L/M	D-8	1 MAR 84	02:03	3600
33143	TTR STOP 500°C 5L/M	D-5	1 MAR 84	02:03	3600
33044	TTR STOP 500°C 5L/M	D-10	1 MAR 84	03:09	3600
33144	TTR STOP 500°C 5L/M	D-11	1 MAR 84	03:09	3600

DISK NO. 33588

TAG NO.	DATA I.D.	DETECTOR POSITION	DATE	START TIME	COUNT TIME
33045	NA DRAIN	D-2	1 MAR 84	04:48	7200
33145	NA DRAIN	D-7	1 MAR 84	04:48	7200
33046	NA DRAIN	D-4	1 MAR 84	06:47	7200
33146	NA DRAIN	D-9	1 MAR 84	06:47	7200
33047	NA DRAIN	D-6	1 MAR 84	08:53	7200
33147	NA DRAIN	D-3	1 MAR 84	08:53	7200
33048	NA DRAIN	D-8	1 MAR 84	11:00	7200
33148	NA DRAIN	D-5	1 MAR 84	11:00	7200
33049	NA DRAIN	D-10	1 MAR 84	13:17	7200
33149	NA DRAIN	D-11	1 MAR 84	13:17	7200
33050	NA DRAIN	D-2	1 MAR 84	15:25	7200
33150	NA DRAIN	D-7	1 MAR 84	15:25	7200

Appendix C Mass Transfer Model

In order to evaluate behavior of DN nuclides in sodium quantitatively, modeling of DN nuclide behavior in sodium is done. In general, FP nuclides are classified into gaseous FP (kr, Xe), volatile FP (Br, Rb, Te, I, Cs etc.) and non-volatile FP (Zr, Ba, La, Ce etc.), according to their behaviors in sodium.

Now, modeling of volatile FP behavior will be done as follows.

C.1 Mass transfer model

Behavior of FP in sodium is controlled by mass transfer of rate-determining diffusion, i.e. FP nuclides are released in sodium transfer diffusing through boundary layer which exists between sodium bulk flow and the wall surface of piping and arrive at wall surface. Rate of mass transfer by diffusion increases with increase in flow velocity, and it increases with increased difference between FP concentration in bulk sodium and that in sodium close to wall surface.

Transfer rate of FP nuclide per unit area, j (atoms/cm^2/sec), is expressed by analogy of heat transfer as,

$$j = k_L \cdot (\bar{C} - C_s) \qquad \text{(C-1)}$$

where,

- $\bar{C}$: concentration of FP nuclides in sodium bulk flow (atoms/cm^3)
- C_s: concentration of FP nuclides in sodium close to wall surface (atoms/cm^3)
- K_L: mass transfer coefficient (cm/sec)

According to Treybal[9]

$$k_L = 0.023 \cdot Re^{0.83} \cdot Sc^{0.33} \cdot D/d \qquad \text{(C-2)}$$

where, $Re = \frac{v \cdot d}{\mu / \rho}$

Re, Sc: Reynolds number, Schmidt number (-)

D : diffusion coefficient of FP nuclide in sodium (cm^2/sec)

d : diameter of cylindrical tube

Re and Sc are expressed as follows.

$$Sc = \frac{\mu}{\rho \cdot D}$$

where, v: flow velocity of sodium.

C.2 Transfer model of volatile FP in sodium

Adsorption and desorption of volatile FP on wall surface occur reversibly depending on sodium temperature. The phenomenon is introduced into the mass transfer model.

Processes of adsorption and desorption are shown in Fig. C-1. A curve shown in the figure indicates FP concentration in sodium distributed in vertical direction of sodium flow in the cylindrical tube. j, $\bar{C}$, C_s are defined parameters in Eq. (C-1).

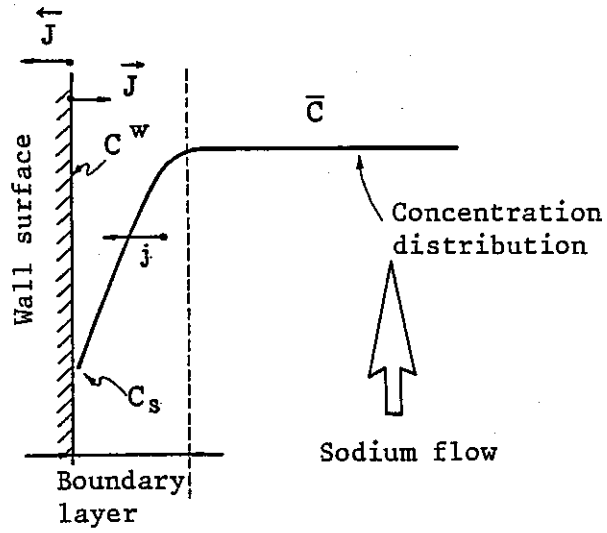

Absorption velocity and desorption velocity of FP on wall surface are written as follows.

$$\overleftarrow{J} = \overleftarrow{k} \cdot C_S \tag{C-3}$$

where,

$$\overrightarrow{J} = \overrightarrow{k} \cdot C^W \tag{C-4}$$

$\overleftarrow{j}$: adsorption rate of FP on wall surface (atoms/cm^2/sec)
$\overrightarrow{j}$: desorption rate of FP on wall surface (atoms/cm^2/sec)
$\overleftarrow{k}$: adsorption rate coefficient (cm/sec)
$\overrightarrow{k}$: desorption rate coefficient (ℓ/sec)
C^W : FP concentration at wall surface (atoms/cm^2)

$$j = \overleftarrow{J} - \overrightarrow{J} \tag{C-5}$$

Applying transfer phenomenon of FP in sodium

$$\frac{d\overline{C}}{dt} = -\frac{\ell}{a} j - \lambda \cdot \overline{C} \tag{C-6}$$

where,

$\ell = 2\pi r$, $a = \pi r^2$ (r: radius of cylindrical tube)
λ : decay constant of FP nuclide (ℓ/sec)

Variation of concentration C along the loop occurs only in the direction of flowing sodium, so by putting the direction as X, Eq. (C-6) is

$$\frac{d\overline{C}(x, t)}{dt} = \frac{\partial \overline{C}(x, t)}{\partial t} + \frac{\partial \overline{C}(x, t)}{\partial x} \cdot \frac{dx}{dt} \tag{C-7}$$

Assuming that FP has short half life, then radioactivity attains a saturation level soon:

$$\frac{d\overline{C}(x)}{dx} = -\frac{\ell}{av} j - \frac{\lambda}{v}\overline{C}(x), \quad \left(\frac{dx}{dt} = v\right) \tag{C-8}$$

On the other hand,

$$\frac{\partial C^W(x, t)}{\partial t} = j - \lambda \cdot C^W(x, t)$$

The concentration at wall surface attains a saturation level soon:

$$j = \lambda \cdot C^W(x) \tag{C-9}$$

Introducing Eqs. (C-3) and (C-4) into Eq. (C-5) and combine Eq. (C-9),

$$C^W(x) = \{ \overleftarrow{k} / (\lambda + \overrightarrow{k}) \} \cdot C_s(x) = K^W \cdot C_s(x) \tag{C-10}$$

From Eqs. (C-1), (C-8) and (C-10) erasing Cs(x),

$$\frac{d\overline{C}(x)}{dx} = -\frac{\lambda}{v} \{ \frac{k_L \cdot K^W}{\lambda \cdot K^W + k_L} \cdot (\ell / a) + 1 \} \overline{C}(x) \tag{C-11}$$

where,

$$\alpha = \frac{\lambda}{v} \{ \frac{k_L \cdot K^W}{\lambda \cdot K^W + k_L} \cdot (\ell / a) + 1 \} \tag{C-12}$$

Eq. (C-11) becomes,

$$\frac{d\bar{C}(x)}{dx} = -\alpha \cdot \bar{C}(x)$$

Using $\bar{C}_o$: initial concentration at x = 0 (fuel) (atoms/cm^3)

$$\bar{C}(x) = \bar{C}_0 \cdot e^{-\alpha \cdot x} \qquad \text{(C-13)}$$

It means that FP concentration in sodium shows exponential function along the loop.

Concentration at the wall area is,

$$C^W(x) = \frac{k_L \cdot K^W}{\lambda \cdot K^W + k_L} \cdot \bar{C}(x) \qquad \text{(C-14)}$$

where Ka: partition coefficient (cm),

$$C^W(x) = K_a \cdot \bar{C}(x) \qquad \text{(C-15)}$$

Eq. (C-12) is simplified as,

$$\alpha = \frac{\lambda}{v} \{ K_a \cdot (\ell/a) + 1 \} \qquad \text{(C-16)}$$

Since the initial concentration $\bar{C}o$ is expressed by sum of released-FP from fuel and introduced-FP from loop to fuel.

$$\bar{C}_0 = \bar{C}(L) + P/F \qquad \text{(C-17)}$$

where,

L: total length of loop

P: release velocity of FP (atoms/sec)

F: flow rate (cm^3/sec)

Introducing Eq.(C-13) of X=L into Fq.(C-17)

$$\overline{C}_0 = P/F \cdot (1 - e^{-\alpha \cdot L}) \qquad \text{(C-18)}$$